

May 2021

## Investigating Mechanisms of Nanotoxicity of a Next-Generation Lithium Cobalt Oxide Nanomaterial

Nicholas Joseph Niemuth  
*University of Wisconsin-Milwaukee*

Follow this and additional works at: <https://dc.uwm.edu/etd>



Part of the [Aquaculture and Fisheries Commons](#), [Nanoscience and Nanotechnology Commons](#), and the [Toxicology Commons](#)

---

### Recommended Citation

Niemuth, Nicholas Joseph, "Investigating Mechanisms of Nanotoxicity of a Next-Generation Lithium Cobalt Oxide Nanomaterial" (2021). *Theses and Dissertations*. 2705.  
<https://dc.uwm.edu/etd/2705>

This Dissertation is brought to you for free and open access by UWM Digital Commons. It has been accepted for inclusion in Theses and Dissertations by an authorized administrator of UWM Digital Commons. For more information, please contact [scholarlycommunicationteam-group@uwm.edu](mailto:scholarlycommunicationteam-group@uwm.edu).

INVESTIGATING MECHANISMS OF NANOTOXICITY OF A NEXT-GENERATION  
LITHIUM COBALT OXIDE NANOMATERIAL

by

Nicholas Niemuth

A Dissertation Submitted in  
Partial Fulfillment of the  
Requirements for the Degree of

Doctor of Philosophy  
in Freshwater Sciences

at

The University of Wisconsin-Milwaukee

May 2021

## ABSTRACT

### INVESTIGATING MECHANISMS OF NANOTOXICITY OF A NEXT-GENERATION LITHIUM COBALT OXIDE NANOMATERIAL

by

Nicholas Niemuth

The University of Wisconsin-Milwaukee, 2021  
Under the Supervision of Professor Rebecca Klaper

Commercial use of engineered nanomaterials (ENMs; materials in the range of 1-100 nm) has grown dramatically since the discovery of the means to observe, characterize, and controllably synthesize these materials at the end of the 20<sup>th</sup> century. Today, ENMs represent a global market valued in the trillions of dollars, incorporated into products because of the unique properties they confer, including increased strength, catalytic activity, and interactions with light. In this time, ENMs have also grown from relatively simple first-generation materials, such as Au, Ag, and carbon ENMs, to complex next-generation materials incorporating numerous elements into materials with complex secondary structures, such as the lithium intercalating complex metal oxide cathode materials used in lithium-ion batteries (LIBs). The commercial use of ENMs results in ENM waste on the order of hundreds of thousands to millions of tons annually, enough that ENM waste represents an emerging environmental concern. LIB cathode waste alone amounts to hundreds of thousands of tons annually, with little of this recycled. As the development and use of ENMs has grown, alongside it has grown the field of nanotoxicology, determined to understand if the same properties, such as size, core material, surface area, and surface chemistry, that confer useful properties to ENMs also imbue them with toxicity toward biological systems. However, while the diversity of ENMs has grown, the field of

nanotoxicology has focused to a large extent on examining the toxicity of first-generation materials (*e.g.*, Au and Ag) and on oxidative stress as the mechanism of nanotoxicity. Oxidative stress as a mechanism of nanotoxicity is understood as a general mechanism of cellular damage by reactive oxygen species (ROS). However, simple observation of ROS is not explanatory of ENM toxicity, as ROS are not only damaging molecules, but are involved in regulation of critical cellular processes including metabolism, growth, and differentiation. Therefore, the presence of redox-sensitive components in these pathways makes them susceptible to specific interactions with redox-active ENMs or ROS even at sublethal, physiologically relevant concentrations. Environmental nanotoxicology has also focused to a large degree on the aquatic invertebrate *Daphnia magna*, whose wide use in the field of toxicology more generally makes it a broadly applicable model. However, *D. magna* reside in the water column, while many ENMs are expected to settle in the aquatic environment and concentrate in the sediment, making testing on sediment-dwelling organisms such as the invertebrate midge species *Chironomus riparius* important for understanding the potential environmental impacts of ENMs. Overcoming these limitations of nanotoxicology requires testing of next-generation ENMs, including on sediment-dwelling organisms, and the exploration of mechanisms of nanotoxicology at the molecular level, beyond simple oxidative stress. A useful framework to guide the elucidation of this molecular-level understanding is the adverse outcome pathway (AOP). In this framework, the interaction of a toxicant such as an ENM with a biological system is understood from the standpoint of a molecular interaction between the toxicant and a biological component (called the molecular initiating event; MIE), which results in a series of key events (KEs) that occur in the biological system in response to this impact, and ultimately causes an adverse outcome (AO) for the biological system, such as the death of an organism or cell. By using molecular tools to

interrogate ENM impacts at each stage of this process, it is possible to trace observed AOs through their series of associated KEs and ultimately down to the specific MIE(s). This thesis sought to address the shortcomings of current nanotoxicology by using molecular methods to inform an AOP for the toxicity of the next-generation complex metal oxide LIB cathode material lithium cobalt oxide (LCO) in sediment-dwelling *Chironomus riparius* and in *Daphnia magna*. Results of these investigations demonstrate oxidation of the Fe-S center of energy metabolism enzyme aconitase as an MIE of LCO toxicity, disrupted heme synthesis and energy metabolism as KEs by targeted and global gene expression analysis, KEs of altered metabolic gene expression and metabolite levels toward energy production by combined global gene expression and non-targeted metabolomics, and AOs of reduced growth and delayed development. This work thus demonstrates the paradigm by which ENM toxicity can be understood at the molecular level, including the interconnections of the MIE, KEs, and AOs for LCO within the AOP framework. Furthermore, this AOP, placed in the context of the literature, suggest a general AOP for toxicity of metal oxide ENMs in which the redox chemistry of a metal oxide ENM causes oxidation of redox-sensitive biological components, such as proteins and cofactors involved in energy metabolism, disrupting critical processes including energy metabolism, and ultimately disrupting growth and development at the organism level. Further exploration of the details of this AOP represent an exciting future direction for the investigation of the interaction of metal oxide ENMs with biological systems.

© Copyright by Nicholas Niemuth, 2021  
All Rights Reserved

In appreciation of those in history  
who have fought for  
a scientific understanding of our world.

## TABLE OF CONTENTS

List of figures.....	x
List of Tables.....	xi
List of Abbreviations .....	xii
Acknowledgements .....	xiv

Chapter	Page
<b>I. INTRODUCTION.....</b>	<b>1</b>
The history and environmental implications of nanomaterials.....	1
Current state of nanotoxicology and its limitations .....	3
The Adverse Outcome Pathway, molecular mechanisms and tools for nanotoxicology.....	5
Indications of energy metabolism as a target of metal oxide ENM toxicity .....	6
Environmental fate of nanomaterials and choice of model organisms .....	7
Aims, research strategy, and significance.....	8
References.....	12
<b>II. NEXT-GENERATION COMPLEX METAL OXIDE NANOMATERIALS</b>	
<b>    NEGATIVELY IMPACT GROWTH AND DEVELOPMENT IN THE BENTHIC</b>	
<b>    INVERTEBRATE <i>CHIRONOMUS RIPARIUS</i> UPON SETTLING.....</b>	<b>25</b>
Abstract.....	26
Introduction.....	27
Materials and Methods.....	30
Results and Discussion .....	36
Acknowledgments.....	45

References.....	46
Figures.....	58
Supporting information.....	62
Supporting references .....	69
Supporting Tables .....	73
Supporting Figures.....	74
<b>III. PROTEIN FE-S CENTERS AS A MOLECULAR TARGET OF TOXICITY OF A COMPLEX TRANSITION METAL OXIDE NANOMATERIAL WITH DOWNSTREAM IMPACTS ON METABOLISM AND GROWTH .....</b>	<b>79</b>
Abstract.....	80
Introduction.....	81
Materials and Methods.....	84
Results and Discussion .....	91
Acknowledgement .....	98
References.....	99
Tables .....	112
Figures.....	113
Supporting information.....	118
Supporting tables .....	119
Supporting figures.....	154
<b>IV. ENERGY STARVATION IN <i>DAPHNIA MAGNA</i> FROM EXPOSURE TO A LITHIUM COBALT OXIDE NANOMATERIAL .....</b>	<b>163</b>
Abstract.....	164

Introduction.....	165
Materials and Methods.....	168
Results and Discussion .....	176
Acknowledgement .....	185
References.....	187
Tables .....	195
Figures.....	199
Supporting information.....	203
Supporting tables .....	204
Supporting figures.....	212
<b>V. DISCUSSION AND CONCLUSIONS .....</b>	<b>216</b>
Evidence of LCO nanotoxicity and development of an AOP.....	217
Proposed mechanism and implications for AOP across metal oxide ENMs .....	222
Environmental implications of proposed AOP .....	224
Future directions .....	226
Conclusion .....	228
References.....	229
<b>VI. CURRICULUM VITAE .....</b>	<b>237</b>

## LIST OF FIGURES

Figure II-1. Differences in <i>C. riparius</i> larval size and Hb after 7 d exposure .....	58
Figure II-2. Differences in <i>C. riparius</i> time to emergence as adult flies .....	59
Figure II-3. Differences in <i>C. riparius</i> larval gene expression after 7 day exposure .....	60
Figure II-4. Proposed adverse outcome pathway for <i>C. riparius</i> LCO and NMC exposure .....	61
Figure III-1. Electron paramagnetic resonance spectroscopy of intact larvae shows changes in Fe-S centers from LCO exposure.....	113
Figure III-2. Aconitase activity of larval protein is negatively impacted by LCO .....	114
Figure III-3. Significantly enriched molecular functions and pathways show importance of metabolism and Fe-S centers in LCO impacts .....	115
Figure III-4. Differentially expressed metabolic gene pathways indicate shift toward energy production in LCO-exposed larvae .....	116
Figure III-5. Proposed adverse outcome pathway showing observed LCO impacts from molecular initiating event through adverse outcomes.....	117
Figure IV-1. Diagram of oxidative phosphorylation showing genes differentially expressed between LCO 1 mg/L and control.....	199
Figure IV-2. Pathway for valine, leucine, and isoleucine degradation showing differential compounds and genes between LCO 1 mg/L and control .....	201

## LIST OF TABLES

Table III-1. Differentially expressed Fe-S protein genes by function .....	112
Table IV-1. Selected DAVID enrichment terms for differentially expressed genes between LCO 1 mg/L and control.....	195
Table IV-2. MetaboAnalyst enriched KEGG pathways for differential metabolites between LCO 1 mg/L and control.....	196
Table IV-3. Differential sugars in Starch, Sucrose, and Galactose metabolism identified by Metaboanalyst between LCO 1 mg/L and control.....	198

## LIST OF ABBREVIATIONS

ANOVA	Analysis of variance
AO	Adverse outcome
AOP	Adverse outcome pathway
ATP	Adenosine triphosphate
BET	Brunauer–Emmett–Teller adsorption
BLAST	Basic local alignment search tool
<i>C. riparius</i>	<i>Chironomus riparius</i>
cDNA	Complementary deoxyribonucleic acid
<i>D. magna</i>	<i>Daphnia magna</i>
DAVID	Database for Annotation, Visualization, and Integrated Discovery
DIMS	Direct injection mass spectrometry
DNA	Deoxyribonucleic acid
ENM	Engineered nanomaterial
EPR	Electron paramagnetic resonance
ETC	Electron transport chain
FDR	False discovery rate
GO	Gene ontology
Hb	Hemoglobin
HPLC	High-performance liquid chromatography
ICP-MS	Inductively coupled plasma mass spectrometry
ICP-OES	Inductively coupled plasma optical emission spectroscopy
KE	Key event

KEGG	Kyoto Encyclopedia of Genes and Genomes
KO	KEGG orthology
LCO	Lithium cobalt oxide nanosheets
LIB	Lithium ion battery
MHRW	Moderately hard water
MIE	Molecular initiating event
mRNA	Messenger ribonucleic acid
NADH	Nicotinamide adenine dinucleotide hydride
NCBI	National Center for Biotechnology Information
NIST	National Institute of Standards and Technology
NMC	Lithium nickel manganese cobalt oxide nanosheets
NP	Nanoparticle
qPCR	Quantitative polymerase chain reaction
RNA	Ribonucleic acid
RNA-seq	Ribonucleic acid sequencing
ROS	Reactive oxygen species
SEM	Scanning electron microscopy
SIM	Selected ion monitoring
SPSS	Statistical package for the social sciences
TCA	Tricarboxylic acid
TMO	Transition metal oxide
US EPA	United States Environmental Protection Agency
XRD	X-ray powder diffraction

## ACKNOWLEDGEMENTS

I must first express my deep appreciation for the encouragement and support of my mentor Dr Rebecca Klaper. None of this would have been possible without her. I must also acknowledge the important support, both financial and professional, of the NSF Center for Sustainable Nanotechnology (CSN). In particular, thank you to our CSN collaborators Dr Robert Hamers at the University of Wisconsin – Madison and his students Kelly Zhang and Liz Laudadio. Thanks also to our collaborators outside of the CSN: Dr Aurash Mohaimani and Angela Schmoltdt of the Great Lakes Genomic Center at the University of Wisconsin – Milwaukee and Dr Mark Viant and his student Jelena Sostare at the University of Birmingham in the UK. Thank you also to members of the Klaper lab Becky Curtis and Nicklaus Neureuther.

Thank to my committee for their service: Dr Michael Carvan, Dr Ryan Newton, Dr Hongbo Ma, and Dr Galya Orr. Thank you also to the staff of the School of Freshwater Sciences at the University of Wisconsin – Milwaukee for their assistance throughout my time here, in particular Linda Horbinski and Nina Ottman.

I would also like to acknowledge the part played in my education as a researcher by my Master's advisor Dr Ursula Jakob and her student Daniela Knoefler at the University of Michigan and by my undergraduate research advisor Dr Leonard Levin and his technician Chris Lieven at the University of Wisconsin - Madison. I also could not have reached this point in my career without the solid knowledge of the fundamentals of writing, mathematics, science, and logic imparted to me by my high school teachers: Veronica Crane, Michelle Jungbauer, Dr Wayne Mannebach, Jim Murphy, Mark Stano, and Jean Zuliger.

Of course, I would not be here without the encouragement and support of my education at all its stages by my parents Joe and Gemma Niemuth. I would also like to thank my wife Katrin for her support and encouragement during my PhD.

Finally, I would like to acknowledge the role of Gene Roddenberry's *Star Trek* in inspiring my passion for science and my pursuit of science as a career. Live long and prosper.

## CHAPTER I:

### INTRODUCTION

#### **The history and environmental implications of nanomaterials**

A nanomaterial is defined as any material having at least one dimension being in the range of 1-100 nm.<sup>1,2</sup> Interest in nanomaterials has grown substantially since tools were invented that allowed their direct observation at the end of the 20<sup>th</sup> century, with useful material properties resulting from the inclusion of nanoscale components including: increased strength, catalytic activity, and quantum interactions with light.<sup>1</sup> Unknowingly, materials on this scale have been used since antiquity by civilizations around the world, including the forging of Damascus steel swords—given their strength by the unknowing inclusion of carbon nanotubes in the alloy—by the Romans circa 300 AD and the creation of an environmentally stable azure pigment with indigo-containing clay nanopores by the Mayans circa 800 AD.<sup>1,3,4</sup> Humans have also unknowingly produced nanomaterials through our interactions with the environment, particularly as byproducts of mining and of combustion of biomass and fossil fuels.<sup>5</sup> In addition to these unintentional, human-made nanomaterials, nanoscale materials also exist in nature,<sup>2,6</sup> including in biological nanostructures such as proteins (on the scale of a few nm to tens of nm)<sup>7</sup> and viruses (tens of nm up to 100 nm),<sup>2,8</sup> as well as geochemically derived nanomaterials that result from weathering and volcanic activity.<sup>5</sup>

This first scientifically reported synthesis of a nanomaterial is credited to Michael Faraday, who synthesized Au nanoparticles in the 1850s.<sup>1,6</sup> However, Faraday could only speculate as to the

relationship between the size of his colloidal Au particles and the color of the colloidal solution (light scattering due the Faraday-Tyndall effect), since the means to actually observe objects at the atomic scale would not exist until the invention of the scanning tunneling electron microscope (STM) in the 1980s.<sup>1</sup> In the intervening decades, developments in chemistry allowed the synthesis of materials at the nanoscale—although these still were not understood to be nanomaterials—including anodized aluminum in the 1930s,<sup>2</sup> silica nanoparticles in the 1940s,<sup>1</sup> metal powders in the 1950s,<sup>9</sup> and nanoscale semiconductors and carbon materials in the 1970s.<sup>9</sup> The invention of the STM in the 1980s, along with the development of the atomic force microscope (AFM), finally allowed materials to be observed and characterized at the atomic scale.<sup>2</sup> The coalescence of these analytical techniques and new methods of chemical synthesis lead to rapid development of nanomaterials throughout the 1990s, including metal, semiconductor, and carbon materials, intentionally engineered and characterized as materials at the nanoscale.<sup>1,2</sup> In the United States, this decade of rapid progress culminated in the foundation of the National Nanotechnology Initiative in the year 2000, meant to coordinate research and development of engineered nanomaterials (ENMs) at the Federal level.<sup>2</sup>

In the more than two decades since the founding of the NNI, the worldwide market for ENMs has grown from approximately \$40 billion in 2000 to \$250 billion in 2010, \$1 trillion in 2015, and an estimated \$3 trillion by 2020.<sup>10,11</sup> Production of ENMs on this scale equated to an estimated 318,000 tons of ENM waste generated annually by 2010,<sup>12</sup> a mass of material that could have multiplied twelve-fold by 2020.<sup>10</sup> At the same time, the types of ENMs produced have expanded from the first-generation carbon, metal, and semiconductor materials to more complex next-generation materials incorporating multiple materials into complex

nanostructures.<sup>13</sup> Products using first-generation ENMs include: nano-TiO<sub>2</sub> in paints and sunscreens,<sup>14</sup> nano-Ag in clothing and personal care products,<sup>14</sup> semiconductor quantum dots in displays (*e.g.*, televisions),<sup>15</sup> and carbon nanotubes used in composites.<sup>13,16</sup> Of next-generation ENMs, an important category from the standpoint of production and waste are the lithium intercalating cathode materials used in lithium ion batteries (LIBs): lithium cobalt oxide (LCO) and lithium nickel manganese cobalt oxide (NMC).<sup>13,17</sup> Production of these materials, employed in LIBs for commercial electronics and electric vehicles, has been estimated at 200,000 tons annually in 2020 and is expected to grow to 380,000 tons annually by 2025.<sup>17</sup> Less than 5% of LIB waste is recycled,<sup>17</sup> and the amount of LIB waste produced is expected to reach 200,000 tons annually by 2025.<sup>18</sup> Thus, as a result of the large volumes of ENMs being produced, their accumulation as waste, and the unique properties of these materials, ENMs are now recognized as a growing environmental concern.<sup>13</sup>

### **Current state of nanotoxicology and its limitations**

As the production and use of ENMs increased at the beginning of the 21<sup>st</sup> century, concerns grew within the toxicology community that the same unique properties that made ENMs useful might also confer particular toxicity to these materials.<sup>19</sup> As a result, the field of nanotoxicology grew from around 150 publications in the year 2000 to an estimated 4,500 publications annually by 2018.<sup>20,21</sup> Over this time, the field has come to recognize the importance of ENM properties such as size, surface chemistry, and core composition in determining the impacts of these materials on biological systems.<sup>13</sup> Some examples from the literature are: size dependent toxicity of ENMs, including Au and Ag, with smaller particles generally being more toxic in cells and animals;<sup>22–25</sup> positively charged ENMs being orders of magnitude more toxic than their negatively charged

counterparts, including for Au and Ag ENMs in animals and bacteria;<sup>26–28</sup> and core composition being determinant of toxicity, with metal composition of complex metal oxide ENMs determining toxicity in aquatic invertebrate *Daphnia magna* and bacteria *Shewanella oneidensis*<sup>29–31</sup> and Ag particles being more toxic than Au particles in *D. magna*.<sup>32</sup> By providing an understanding of the role of ENM properties in toxicity, nanotoxicology can inform material redesign or use of alternative materials in order to reduce ENM impacts on human health and the environment.

However, as is evident from the given examples, most nanotoxicology studies to date have focused on first-generation materials—Ag and Au ENMs in particular.<sup>13</sup> Given the increasing production of next-generation materials (*e.g.*, LIB cathode materials), expansion of the nanotoxicology literature to include a wider range of ENMs is imperative. Another shortcoming of the literature has been in the mechanisms of nanotoxicity proposed. Despite the wide variety of differences in materials studied, including differences in surface chemistry, size, and core composition, the near universal mechanism cited for nanotoxicity is oxidative stress, making it the most common mechanism of nanotoxicity proposed.<sup>21</sup> More than 7000 studies cite oxidative stress as the mechanism of toxicity for ENMs as diverse as Au, Ag, TiO<sub>2</sub>, FeO, CeO<sub>2</sub>, ZnO, SiO<sub>2</sub>, carbon nanotubes, and ceramic nanoparticles.<sup>33–36</sup> Oxidative stress is generally understood as the production of reactive oxygen species (ROS) that damage proteins, lipids, and DNA.<sup>34</sup> However, the proposal of this mechanism does not take in to account evidence that ROS are produced under normal physiological conditions as signaling molecules,<sup>37,38</sup> regulating processes including metabolism, growth, differentiation, autophagy, and apoptosis.<sup>37–41</sup> Thus, observation

of ROS can potentially indicate any number of impacts, even at sublethal, physiological levels, making oxidative stress a non-specific and perhaps misleading “mechanism.”

### **The Adverse Outcome Pathway, molecular mechanisms and tools for nanotoxicology**

Characterization of the mechanisms of ENM nanotoxicity requires a molecular-level understanding of ENM impacts on biological systems. One toxicology concept that incorporates the elements required for such an understanding is the Adverse Outcome Pathway (AOP).<sup>42</sup> In this framework, a molecular initiating event (MIE)—usually an interaction between a compound and a specific enzyme or cellular component—is translated through a series of key events (KEs) that result in the adverse outcome (AO) of observable toxicity (*e.g.*, cell death, mortality, lowered reproduction).<sup>42,43</sup> The application of the AOP to nanotoxicology requires an understanding of the molecular-level impact of an ENM on a specific cellular component (the MIE) and the tracing of this impact through the series of changes in the cell or organism (the KEs) that lead to observable toxicity (the AO). The MIEs for ENMs would be expected to correspond to material properties such as size, surface chemistry, and core composition. Moreover, in the context of ROS as a signaling molecule,<sup>37</sup> observed ROS could represent KEs in toxicity, rather than the MIE itself. Identifying ROS as the molecular initiator of ENM toxicity requires identifying the specific molecular interaction by which ROS can cause observed adverse outcomes.

To achieve this requires moving beyond phenomenological observations of toxicity or ROS in response to ENM exposure. To do this, we must employ molecular tools to both gain a picture of the global response of biological systems to ENM exposure and to test hypotheses about specific

molecular targets. In this way we can capture the key events leading to observed toxicity, trace the events to their source(s), and test the specific molecular event(s) posited to initiate these changes. To this end, a number of molecular, biochemistry, and chemistry tools can be employed, including: monitoring of gene expression, either with targeted techniques like qPCR or through global gene expression by RNA-seq;<sup>44-46</sup> observation of changes in proteins, which can be achieved in biological samples by measuring absorbance of cofactors such as heme,<sup>47,48</sup> by measuring activity of enzymes,<sup>49,50</sup> or by looking at abundance of protein metal centers through techniques such as electron paramagnetic resonance;<sup>51</sup> and determining changes in levels of metabolites, which can be ascertained using mass spectrometric techniques, *i.e.* non-targeted metabolomics.<sup>52</sup> These and other molecular techniques (*e.g.*, proteomics)<sup>50</sup> make possible a more sophisticated understanding of ENM toxicity by providing mechanistic information at the molecular level.

### **Indications of energy metabolism as a target of metal oxide ENM toxicity**

The resort to oxidative stress also ignores recent evidence pointing to a specific molecular mechanism by which metal oxide ENMs in particular may be interacting with biological systems: by engaging in redox chemistry at the ENM surface that interferes with biological redox processes.<sup>53</sup> Critical components of energy metabolism that are conserved across species—specifically the tricarboxylic acid (TCA) cycle and oxidative phosphorylation (*i.e.*, the electron transport chain; ETC)—rely on redox processes to transfer electrons from sugars, fats, and amino acids to oxygen in order to produce the proton gradient that allows production of large amounts of ATP by mitochondria.<sup>54-57</sup> Specifically, the Fe-S center of aconitase—the critical second enzyme in the TCA cycle, which converts citrate to isocitrate—has been proposed to be redox

regulated in response to ROS produced by the ETC.<sup>58</sup> Aconitase and its Fe-S center also regulate Fe homeostasis and heme synthesis (critical cofactors for numerous metabolic enzymes) through aconitase's role as the iron-responsive protein.<sup>59–62</sup> Complexes I and II of the ETC also contain Fe-S centers,<sup>60,63–66</sup> and cytochrome c, which transfers electrons between Complexes III and IV of the ETC via a heme cofactor,<sup>55</sup> was shown to be oxidized by metal oxide ENMs *in vitro*.<sup>53</sup> The central role of redox chemistry in these widely conserved processes of energy metabolism<sup>56</sup>—and the potential for metal oxide ENMs to interact with redox processes<sup>53</sup>—indicate that components of the TCA cycle and the ETC could be important molecular targets of metal oxide ENM toxicity.

### **Environmental fate of nanomaterials and choice of model organisms**

An estimated 22% of ENM waste (69,200 tons) was estimated to have reached the aquatic environment in 2010,<sup>12</sup> and this mass of material may have been as much as 12 times greater in 2020.<sup>10</sup> In this context, aquatic toxicity testing of ENMs is imperative.<sup>75</sup> In aquatic toxicology, *Daphnia magna* has been well-established as a widely-used, sensitive model, which is used for screening of material toxicity across species.<sup>76</sup> *D. magna* are also important in the food webs of many freshwater ecosystems,<sup>29</sup> and the extensive use of *D. magna* as a model in aquatic toxicology and toxicology more generally brings a broad relevance to its use in nanotoxicology.<sup>11</sup> In fact, most studies of ENM toxicity have been done using this organism, making it a useful model as a benchmark for comparative nanotoxicity.<sup>11</sup>

However, *D. magna* reside largely throughout water column,<sup>77</sup> and while they would be expected to be exposed to ENMs as they enter the aquatic environment, many ENMs are expected to settle

out in the aqueous environment over time and concentrate in the sediment,<sup>78,79</sup> with greater than 98% of ENMs expected to be retained in lake sediments due to settling.<sup>80</sup> Therefore, it is important to test the impacts of ENMs on sediment-dwelling model organisms, as organisms residing in this environmental compartment would be expected to be exposed to particularly high concentrations of released ENMs.<sup>75,81</sup>

*Chironomus riparius* is a sediment-dwelling midge species and an important component of both aquatic and terrestrial food webs, with larval stages that reside in the sediment consuming detritus from silt and an adult stage as a fly.<sup>82</sup> *C. riparius* is sensitive to pollutants, with toxicology exposure protocols developed by the United States Environmental Protection Agency (USEPA),<sup>83</sup> and it has been used in a number of studies to ascertain ENM toxicity.<sup>84-88</sup> *C. riparius* also has a sequenced genome, making it amenable to molecular studies by qPCR and RNA-Seq.<sup>89</sup> Thus, *C. riparius* represents a model well-suited to the testing of impacts of settled ENMs on sediment-dwelling species.

### **Aims, research strategy, and significance**

This dissertation aims toward addressing some of the shortcomings of current nanotoxicology research by including the following components: expansion of the scope of materials investigated by studying the commercially important, next-generation, LIB transition metal oxide cathode material LCO; investigation of mechanisms of nanotoxicology at a molecular level, through the use of a suite of molecular tools; and use of environmentally relevant animal models that dwell in both the water column and the sediment.

To address these critical aspects, the specific aims to be included in this dissertation are:

**1. Test the hypothesis that settled LCO negatively impacts sediment-dwelling organism *C. riparius*.**

- a. Establish changes in larval growth and time to adult emergence.
- b. Ascertain changes in larval hemoglobin expression and expression of genes related to stress and heme synthesis.

**2. Test the hypothesis that LCO disrupts *C. riparius* Fe-S centers, causing negative impacts on metabolism.**

- a. Probe status of larval Fe-S centers using aconitase enzyme assay and electron paramagnetic resonance.
- b. Interrogate changes in expression of Fe-S and metabolic genes using RNA-Seq.

**3. Test the hypothesis that metabolic impacts of LCO are conserved across species and observable by metabolomics.**

- a. Investigate global gene expression changes in *Daphnia magna* by RNA-seq.
- b. Determine changes in metabolite levels by non-targeted metabolomics.

The studies addressing these aims (**Aim 1, Chapter II; Aim2, Chapter III; Aim 3, Chapter IV**) lay the basis for a molecular-level understanding of the nanotoxicity of LCO. Initial studies on benthic midge *C. riparius* (**Aim 1, Chapter II**) examined impacts of LCO on growth, adult emergence, hemoglobin (Hb) levels, and expression of genes involved in heme synthesis, demonstrating negative impacts on these endpoints that could be the result of dysregulated heme synthesis. These results led to the hypothesis that LCO could negatively impact the Fe-S center of the iron-responsive protein (IRP), which would disrupt heme synthesis and cause broader metabolic disruptions because of IRP's role as an aconitase in the TCA cycle. Aconitase enzyme activity assays and electron paramagnetic resonance were used to probe the status of the IRP Fe-S center in *C. riparius* larvae exposed to LCO (**Aim 2a, Chapter III**), demonstrating negative impacts on this key Fe-S center from LCO exposure. RNA-Seq experiments were used to examine global gene expression changes resulting from LCO exposure (**Aim 2b, Chapter III**), revealing widespread metabolic disruption in LCO-exposed larvae and changes in expression of Fe-S proteins including key metabolic enzymes. Finally, building on these results, impacts of LCO on *D. magna* were explored by RNA-seq and non-targeted metabolomics (**Aim 3, Chapter IV**), showing that impacts on energy metabolism are a conserved mechanism of LCO toxicity, evident at both the level of gene expression and in changes in levels of metabolites.

The experiments included in this thesis, thus, represent an innovative approach that provides evidence to inform a potential AOP for LCO toxicity: a molecular initiating event of oxidation of the aconitase Fe-S center, key events resulting from this involving changes in heme and energy metabolism, and adverse outcomes of reduced growth and development as a result of metabolic impacts. The combination of advanced techniques employed in this series of studies provide

highly needed molecular-level insight into ENM-biological interactions. By establishing an AOP for metal oxide ENM toxicity that points to impacts on redox components of energy metabolism as an important mechanism of nanotoxicity, this work provides a paradigm for the field of nanotoxicology to move it in the direction of a mechanistic understanding of ENM-biological interactions beyond simple “oxidative stress.” As such, this work offers necessary direction and insight that can begin to establish new AOPs for nanotoxicity and push nanotoxicology toward a molecular level understanding of ENM toxicity.

## References

- (1) Sudha, P. N.; Sangeetha, K.; Vijayalakshmi, K.; Barhoum, A. Nanomaterials History, Classification, Unique Properties, Production and Market. In *Emerging Applications of Nanoparticles and Architecture Nanostructures*; Elsevier, 2018; pp 341–384.  
<https://doi.org/10.1016/B978-0-323-51254-1.00012-9>.
- (2) Kumar, N.; Kumbhat, S. *Essentials in Nanoscience and Nanotechnology*; Wiley, 2016.  
<https://doi.org/10.1002/9781119096122>.
- (3) Arnold, D. E. Maya Blue and Palygorskite: a Second Possible Pre-Columbian Source. *Anc. Mesoamerica* **2005**, *16* (1), 51–62. <https://doi.org/10.1017/S0956536105050078>.
- (4) Reibold, M.; Pätzke, N.; Levin, A. A.; Kochmann, W.; Shakhverdova, I. P.; Paufler, P.; Meyer, D. C. Structure of Several Historic Blades at Nanoscale. *Cryst. Res. Technol.* **2009**, *44* (10), 1139–1146. <https://doi.org/10.1002/crat.200900445>.
- (5) Hochella, M. F.; Mogk, D. W.; Ranville, J.; Allen, I. C.; Luther, G. W.; Marr, L. C.; McGrail, B. P.; Murayama, M.; Qafoku, N. P.; Rosso, K. M.; et al. Natural, Incidental, and Engineered Nanomaterials and Their Impacts on the Earth System. *Science (80-. )*. **2019**, *363* (6434), eaau8299. <https://doi.org/10.1126/science.aau8299>.
- (6) Heiligtag, F. J.; Niederberger, M. The Fascinating World of Nanoparticle Research. *Mater. Today* **2013**, *16* (7–8), 262–271. <https://doi.org/10.1016/j.mattod.2013.07.004>.
- (7) Erickson, H. P. Size and Shape of Protein Molecules at the Nanometer Level Determined by Sedimentation, Gel Filtration, and Electron Microscopy. *Biol. Proced. Online* **2009**, *11* (1), 32–51. <https://doi.org/10.1007/s12575-009-9008-x>.
- (8) Douglas, T.; Young, M. Virus Particles as Templates for Materials Synthesis. *Adv. Mater.* **1999**, *11* (8), 679–681. [https://doi.org/10.1002/\(SICI\)1521-4095\(199906\)11:8<679::AID-](https://doi.org/10.1002/(SICI)1521-4095(199906)11:8<679::AID-)

ADMA679>3.0.CO;2-J.

- (9) Terekhov, A. I. Nanotechnologies and Nanomaterials in the Modern World. *Her. Russ. Acad. Sci.* **2009**, *79* (5), 412–419. <https://doi.org/10.1134/S1019331609050025>.
- (10) Roco, M. C. The Long View of Nanotechnology Development: The National Nanotechnology Initiative at 10 Years. *J. Nanoparticle Res.* **2011**, *13* (2), 427–445. <https://doi.org/10.1007/s11051-010-0192-z>.
- (11) Walters, C.; Pool, E.; Somerset, V. Nanotoxicology: A Review. In *Toxicology - New Aspects to This Scientific Conundrum*; InTech, 2016. <https://doi.org/10.5772/64754>.
- (12) Keller, A. A.; Lazareva, A. Predicted Releases of Engineered Nanomaterials: From Global to Regional to Local. *Environ. Sci. Technol. Lett.* **2014**, *1* (1), 65–70. <https://doi.org/10.1021/ez400106t>.
- (13) Klaper, R. D. The Known and Unknown about the Environmental Safety of Nanomaterials in Commerce. *Small* **2020**, 2000690. <https://doi.org/10.1002/sml.202000690>.
- (14) Lehutso, R. F.; Tancu, Y.; Maity, A.; Thwala, M. Characterisation of Engineered Nanomaterials in Nano-Enabled Products Exhibiting Priority Environmental Exposure. *Molecules* **2021**, *26* (5), 1370. <https://doi.org/10.3390/molecules26051370>.
- (15) Wang, Y.; Nowack, B. Dynamic Probabilistic Material Flow Analysis of Nano-SiO<sub>2</sub>, Nano Iron Oxides, Nano-CeO<sub>2</sub>, Nano-Al<sub>2</sub>O<sub>3</sub>, and Quantum Dots in Seven European Regions. *Environ. Pollut.* **2018**, *235*, 589–601. <https://doi.org/10.1016/j.envpol.2018.01.004>.
- (16) Temizel-Sekeryan, S.; Wu, F.; Hicks, A. L. Global Scale Life Cycle Environmental Impacts of Single- and Multi-Walled Carbon Nanotube Synthesis Processes. *Int. J. Life*

- Cycle Assess.* **2021**. <https://doi.org/10.1007/s11367-020-01862-1>.
- (17) Hamers, R. J. Energy Storage Materials as Emerging Nano-Contaminants. *Chem. Res. Toxicol.* **2020**, *acs.chemrestox.0c00080*. <https://doi.org/10.1021/acs.chemrestox.0c00080>.
- (18) Winslow, K. M.; Laux, S. J.; Townsend, T. G. A Review on the Growing Concern and Potential Management Strategies of Waste Lithium-Ion Batteries. *Resources, Conservation and Recycling*. Elsevier 2018, pp 263–277.  
<https://doi.org/10.1016/j.resconrec.2017.11.001>.
- (19) Santamaria, A. Historical Overview of Nanotechnology and Nanotoxicology; 2012; pp 1–12. [https://doi.org/10.1007/978-1-62703-002-1\\_1](https://doi.org/10.1007/978-1-62703-002-1_1).
- (20) Ostrowski, A. D.; Martin, T.; Conti, J.; Hurt, I.; Harthorn, B. H. Nanotoxicology: Characterizing the Scientific Literature, 2000–2007. *J. Nanoparticle Res.* **2009**, *11* (2), 251–257. <https://doi.org/10.1007/s11051-008-9579-5>.
- (21) Chen, X. Mapping the Decadal (2009–2018) Research Landscape of Nanotoxicity: Insights from a Bibliometric Study. *Nanosci. Nanotechnol. Lett.* **2019**, *11* (10), 1327–1337. <https://doi.org/10.1166/nnl.2019.3015>.
- (22) Kim, T.-H.; Kim, M.; Park, H.-S.; Shin, U. S.; Gong, M.-S.; Kim, H.-W. Size-Dependent Cellular Toxicity of Silver Nanoparticles. *J. Biomed. Mater. Res. Part A* **2012**, *100A* (4), 1033–1043. <https://doi.org/10.1002/jbm.a.34053>.
- (23) Pan, Y.; Neuss, S.; Leifert, A.; Fischler, M.; Wen, F.; Simon, U.; Schmid, G.; Brandau, W.; Jahnke-Dechent, W. Size-Dependent Cytotoxicity of Gold Nanoparticles. *Small* **2007**, *3* (11), 1941–1949. <https://doi.org/10.1002/sml.200700378>.
- (24) Cho, Y.-M.; Mizuta, Y.; Akagi, J.; Toyoda, T.; Sone, M.; Ogawa, K. Size-Dependent Acute Toxicity of Silver Nanoparticles in Mice. *J. Toxicol. Pathol.* **2018**, *31* (1), 73–80.

- <https://doi.org/10.1293/tox.2017-0043>.
- (25) Coradeghini, R.; Gioria, S.; García, C. P.; Nativo, P.; Franchini, F.; Gilliland, D.; Ponti, J.; Rossi, F. Size-Dependent Toxicity and Cell Interaction Mechanisms of Gold Nanoparticles on Mouse Fibroblasts. *Toxicol. Lett.* **2013**, *217* (3), 205–216.  
<https://doi.org/10.1016/j.toxlet.2012.11.022>.
- (26) Bozich, J. S.; Lohse, S. E.; Torelli, M. D.; Murphy, C. J.; Hamers, R. J.; Klaper, R. D. Surface Chemistry, Charge and Ligand Type Impact the Toxicity of Gold Nanoparticles to *Daphnia Magna*. *Environ. Sci. Nano* **2014**, *1* (3), 260–270.  
<https://doi.org/10.1039/C4EN00006D>.
- (27) El Badawy, A. M.; Silva, R. G.; Morris, B.; Scheckel, K. G.; Suidan, M. T.; Tolaymat, T. M. Surface Charge-Dependent Toxicity of Silver Nanoparticles. *Environ. Sci. Technol.* **2011**, *45* (1), 283–287. <https://doi.org/10.1021/es1034188>.
- (28) Nasser, F.; Davis, A.; Valsami-Jones, E.; Lynch, I. Shape and Charge of Gold Nanomaterials Influence Survivorship, Oxidative Stress and Moulting of *Daphnia Magna*. *Nanomaterials* **2016**, *6* (12), 222. <https://doi.org/10.3390/nano6120222>.
- (29) Bozich, J.; Hang, M.; Hamers, R.; Klaper, R. Core Chemistry Influences the Toxicity of Multicomponent Metal Oxide Nanomaterials, Lithium Nickel Manganese Cobalt Oxide, and Lithium Cobalt Oxide to *Daphnia Magna*. *Environ. Toxicol. Chem.* **2017**, *36* (9), 2493–2502. <https://doi.org/10.1002/etc.3791>.
- (30) Gunsolus, I. L.; Hang, M. N.; Hudson-Smith, N. V.; Buchman, J. T.; Bennett, J. W.; Conroy, D.; Mason, S. E.; Hamers, R. J.; Haynes, C. L. Influence of Nickel Manganese Cobalt Oxide Nanoparticle Composition on Toxicity toward *Shewanella Oneidensis* MR-1: Redesigning for Reduced Biological Impact. *Environ. Sci. Nano* **2017**, *4* (3), 636–646.

<https://doi.org/10.1039/C6EN00453A>.

- (31) Buchman, J. T.; Bennett, E. A.; Wang, C.; Abbaspour Tamijani, A.; Bennett, J. W.; Hudson, B. G.; Green, C. M.; Clement, P. L.; Zhi, B.; Henke, A. H.; et al. Nickel Enrichment of Next-Generation NMC Nanomaterials Alters Material Stability, Causing Unexpected Dissolution Behavior and Observed Toxicity to *S. Oneidensis* MR-1 and *D. Magna*. *Environ. Sci. Nano* **2020**, *7* (2), 571–587. <https://doi.org/10.1039/C9EN01074B>.
- (32) Li, T.; Albee, B.; Alemayehu, M.; Diaz, R.; Ingham, L.; Kamal, S.; Rodriguez, M.; Whaley Bishnoi, S. Comparative Toxicity Study of Ag, Au, and Ag–Au Bimetallic Nanoparticles on *Daphnia Magna*. *Anal. Bioanal. Chem.* **2010**, *398* (2), 689–700. <https://doi.org/10.1007/s00216-010-3915-1>.
- (33) Murphy, C. J.; Vartanian, A. M.; Geiger, F. M.; Hamers, R. J.; Pedersen, J.; Cui, Q.; Haynes, C. L.; Carlson, E. E.; Hernandez, R.; Klaper, R. D.; et al. Biological Responses to Engineered Nanomaterials: Needs for the Next Decade. *ACS Cent. Sci.* **2015**, *1* (3), 117–123. <https://doi.org/10.1021/acscentsci.5b00182>.
- (34) Lujan, H.; Sayes, C. M. Cytotoxicological Pathways Induced after Nanoparticle Exposure: Studies of Oxidative Stress at the ‘Nano–Bio’ Interface. *Toxicol. Res. (Camb)*. **2017**, *6* (5), 580–594. <https://doi.org/10.1039/C7TX00119C>.
- (35) Khanna, P.; Ong, C.; Bay, B. H.; Baeg, G. H.; Khanna, P.; Ong, C.; Bay, B. H.; Baeg, G. H. Nanotoxicity: An Interplay of Oxidative Stress, Inflammation and Cell Death. *Nanomaterials* **2015**, *5* (3), 1163–1180. <https://doi.org/10.3390/nano5031163>.
- (36) Abdal Dayem, A.; Hossain, M.; Lee, S.; Kim, K.; Saha, S.; Yang, G.-M.; Choi, H.; Cho, S.-G. The Role of Reactive Oxygen Species (ROS) in the Biological Activities of Metallic Nanoparticles. *Int. J. Mol. Sci.* **2017**, *18* (1), 120. <https://doi.org/10.3390/ijms18010120>.

- (37) Ray, P. D.; Huang, B.-W.; Tsuji, Y. Reactive Oxygen Species (ROS) Homeostasis and Redox Regulation in Cellular Signaling. *Cell. Signal.* **2012**, *24* (5), 981–990.  
<https://doi.org/10.1016/J.CELLSIG.2012.01.008>.
- (38) Ushio-Fukai, M. Compartmentalization of Redox Signaling through NADPH Oxidase-Derived ROS. *Antioxid. Redox Signal.* **2009**, *11* (6), 1289–1299.  
<https://doi.org/10.1089/ars.2008.2333>.
- (39) Wen, X.; Wu, J.; Wang, F.; Liu, B.; Huang, C.; Wei, Y. Deconvoluting the Role of Reactive Oxygen Species and Autophagy in Human Diseases. *Free Radic. Biol. Med.* **2013**, *65*, 402–410. <https://doi.org/10.1016/J.FREERADBIOMED.2013.07.013>.
- (40) Atashi, F.; Modarressi, A.; Pepper, M. S. The Role of Reactive Oxygen Species in Mesenchymal Stem Cell Adipogenic and Osteogenic Differentiation: A Review. *Stem Cells Dev.* **2015**, *24* (10), 1150–1163. <https://doi.org/10.1089/scd.2014.0484>.
- (41) Redza-Dutordoir, M.; Averill-Bates, D. A. Activation of Apoptosis Signalling Pathways by Reactive Oxygen Species. *Biochim. Biophys. Acta - Mol. Cell Res.* **2016**, *1863* (12), 2977–2992. <https://doi.org/10.1016/J.BBAMCR.2016.09.012>.
- (42) Leist, M.; Ghallab, A.; Graepel, R.; Marchan, R.; Hassan, R.; Bennekou, S. H.; Limonciel, A.; Vinken, M.; Schildknecht, S.; Waldmann, T.; et al. Adverse Outcome Pathways: Opportunities, Limitations and Open Questions. *Arch. Toxicol.* **2017**, *91* (11), 3477–3505.  
<https://doi.org/10.1007/s00204-017-2045-3>.
- (43) Ankley, G. T.; Bennett, R. S.; Erickson, R. J.; Hoff, D. J.; Hornung, M. W.; Johnson, R. D.; Mount, D. R.; Nichols, J. W.; Russom, C. L.; Schmieder, P. K.; et al. Adverse Outcome Pathways: A Conceptual Framework to Support Ecotoxicology Research and Risk Assessment. *Environ. Toxicol. Chem.* **2010**, *29* (3), 730–741.

- <https://doi.org/10.1002/etc.34>.
- (44) Livak, K. J.; Schmittgen, T. D. Analysis of Relative Gene Expression Data Using Real-Time Quantitative PCR and the  $2^{-\Delta\Delta CT}$  Method. *Methods* **2001**, *25* (4), 402–408.  
<https://doi.org/10.1006/meth.2001.1262>.
- (45) Martin, M. Cutadapt Removes Adapter Sequences from High-Throughput Sequencing Reads. *EMBnet.journal* **2011**, *17* (1), 10. <https://doi.org/10.14806/ej.17.1.200>.
- (46) Grabherr, M. G.; Haas, B. J.; Yassour, M.; Levin, J. Z.; Thompson, D. A.; Amit, I.; Adiconis, X.; Fan, L.; Raychowdhury, R.; Zeng, Q.; et al. Full-Length Transcriptome Assembly from RNA-Seq Data without a Reference Genome. *Nat. Biotechnol.* **2011**, *29* (7), 644–652. <https://doi.org/10.1038/nbt.1883>.
- (47) Ha, M. H.; Choi, J. Effects of Environmental Contaminants on Hemoglobin of Larvae of Aquatic Midge, *Chironomus Riparius* (Diptera: Chironomidae): A Potential Biomarker for Ecotoxicity Monitoring. *Chemosphere* **2008**, *71* (10), 1928–1936.  
<https://doi.org/10.1016/j.chemosphere.2008.01.018>.
- (48) Panis, L. I.; Goddeeris, B.; Verheyen, R. The Hemoglobin Concentration Of *Chironomus Cf. Plumosus* L. (Diptera: Chironomidae) Larvae from Two Lentic Habitats. *Netherlands J. Aquat. Ecol.* **1995**, *29* (1), 1–4. <https://doi.org/10.1007/BF02061785>.
- (49) Quirós, P. M. Determination of Aconitase Activity: A Substrate of the Mitochondrial Lon Protease; 2018; pp 49–56. [https://doi.org/10.1007/978-1-4939-7595-2\\_5](https://doi.org/10.1007/978-1-4939-7595-2_5).
- (50) Niu, L.; Xu, X.; Liu, H.; Wu, X.; Wang, W. On the Promising Role of Enzyme Activity Assay in Interpreting Comparative Proteomic Data in Plants. *Proteomics* **2018**, *18* (20), 1800234. <https://doi.org/10.1002/pmic.201800234>.
- (51) Kalyanaraman, B.; Cheng, G.; Zielonka, J.; Bennett, B. Low-Temperature EPR

- Spectroscopy as a Probe-Free Technique for Monitoring Oxidants Formed in Tumor Cells and Tissues: Implications in Drug Resistance and OXPHOS-Targeted Therapies. *Cell Biochem. Biophys.* **2019**, *77* (1), 89–98. <https://doi.org/10.1007/s12013-018-0858-1>.
- (52) Southam, A. D.; Weber, R. J. M.; Engel, J.; Jones, M. R.; Viant, M. R. A Complete Workflow for High-Resolution Spectral-Stitching Nanoelectrospray Direct-Infusion Mass-Spectrometry-Based Metabolomics and Lipidomics. *Nat. Protoc.* **2017**, *12* (2), 255–273. <https://doi.org/10.1038/nprot.2016.156>.
- (53) Zhang, H.; Ji, Z.; Xia, T.; Meng, H.; Low-Kam, C.; Liu, R.; Pokhrel, S.; Lin, S.; Wang, X.; Liao, Y.-P.; et al. Use of Metal Oxide Nanoparticle Band Gap To Develop a Predictive Paradigm for Oxidative Stress and Acute Pulmonary Inflammation. *ACS Nano* **2012**, *6* (5), 4349–4368. <https://doi.org/10.1021/nn3010087>.
- (54) Peregrín-Alvarez, J. M.; Sanford, C.; Parkinson, J. The Conservation and Evolutionary Modularity of Metabolism. *Genome Biol.* **2009**, *10* (6), R63. <https://doi.org/10.1186/gb-2009-10-6-r63>.
- (55) Chaban, Y.; Boekema, E. J.; Dudkina, N. V. Structures of Mitochondrial Oxidative Phosphorylation Supercomplexes and Mechanisms for Their Stabilisation. *Biochim. Biophys. Acta - Bioenerg.* **2014**, *1837* (4), 418–426. <https://doi.org/10.1016/j.bbabi.2013.10.004>.
- (56) Griffiths, H. R.; Gao, D.; Pararasa, C. Redox Regulation in Metabolic Programming and Inflammation. *Redox Biol.* **2017**, *12*, 50–57. <https://doi.org/10.1016/j.redox.2017.01.023>.
- (57) Polyzos, A. A.; McMurray, C. T. The Chicken or the Egg: Mitochondrial Dysfunction as a Cause or Consequence of Toxicity in Huntington’s Disease. *Mech. Ageing Dev.* **2017**, *161*, 181–197. <https://doi.org/10.1016/j.mad.2016.09.003>.

- (58) Armstrong, J. S.; Whiteman, M.; Yang, H.; Jones, D. P. The Redox Regulation of Intermediary Metabolism by a Superoxide-Aconitase Rheostat. *BioEssays* **2004**, *26* (8), 894–900. <https://doi.org/10.1002/bies.20071>.
- (59) Beinert, H. Iron-Sulfur Proteins: Ancient Structures, Still Full of Surprises. *Journal of Biological Inorganic Chemistry*. Springer-Verlag February 2000, pp 2–15. <https://doi.org/10.1007/s007750050002>.
- (60) Castello, A.; Hentze, M. W.; Preiss, T. Metabolic Enzymes Enjoying New Partnerships as RNA-Binding Proteins. *Trends Endocrinol. Metab.* **2015**, *26* (12), 746–757. <https://doi.org/10.1016/j.tem.2015.09.012>.
- (61) Resch, V.; Hanefeld, U. The Selective Addition of Water. *Catal. Sci. Technol.* **2015**, *5* (3), 1385–1399. <https://doi.org/10.1039/C4CY00692E>.
- (62) Tong, J.; Feinberg, B. A. Direct Square-Wave Voltammetry of Superoxidized [4Fe-4S]<sup>3+</sup> Aconitase and Associated 3Fe/4Fe Cluster Interconversions. *J. Biol. Chem.* **1994**, *269* (40), 24920–24927.
- (63) Sazanov, L. A. A Giant Molecular Proton Pump: Structure and Mechanism of Respiratory Complex I. *Nat. Rev. Mol. Cell Biol.* **2015**, *16* (6), 375–388. <https://doi.org/10.1038/nrm3997>.
- (64) Van Vranken, J. G.; Na, U.; Winge, D. R.; Rutter, J. Protein-Mediated Assembly of Succinate Dehydrogenase and Its Cofactors. *Crit. Rev. Biochem. Mol. Biol.* **2015**, *50* (2), 168–180. <https://doi.org/10.3109/10409238.2014.990556>.
- (65) Barras, F.; Fontecave, M. Cobalt Stress in Escherichia Coli and Salmonella Enterica: Molecular Bases for Toxicity and Resistance. *Metallomics* **2011**, *3* (11), 1130–1134. <https://doi.org/10.1039/c1mt00099c>.

- (66) Lill, R.; Mühlhoff, U. Iron–Sulfur-Protein Biogenesis in Eukaryotes. *Trends Biochem. Sci.* **2005**, *30* (3), 133–141. <https://doi.org/10.1016/j.tibs.2005.01.006>.
- (67) Filippi, C.; Pryde, A.; Cowan, P.; Lee, T.; Hayes, P.; Donaldson, K.; Plevris, J.; Stone, V. Toxicology of ZnO and TiO<sub>2</sub> Nanoparticles on Hepatocytes: Impact on Metabolism and Bioenergetics. *Nanotoxicology* **2015**, *9* (1), 126–134. <https://doi.org/10.3109/17435390.2014.895437>.
- (68) Cardinale, B. J.; Bier, R.; Kwan, C. Effects of TiO<sub>2</sub> Nanoparticles on the Growth and Metabolism of Three Species of Freshwater Algae. *J. Nanoparticle Res.* **2012**, *14* (8), 913. <https://doi.org/10.1007/s11051-012-0913-6>.
- (69) Dieni, C. A.; Callaghan, N. I.; Gormley, P. T.; Butler, K. M. A.; MacCormack, T. J. Physiological Hepatic Response to Zinc Oxide Nanoparticle Exposure in the White Sucker, *Catostomus Commersonii*. *Comp. Biochem. Physiol. Part C Toxicol. Pharmacol.* **2014**, *162*, 51–61. <https://doi.org/10.1016/j.cbpc.2014.03.009>.
- (70) Guo, J.; Gao, S.-H.; Lu, J.; Bond, P. L.; Verstraete, W.; Yuan, Z. Copper Oxide Nanoparticles Induce Lysogenic Bacteriophage and Metal-Resistance Genes in *Pseudomonas Aeruginosa* PAO1. *ACS Appl. Mater. Interfaces* **2017**, *9* (27), 22298–22307. <https://doi.org/10.1021/acsami.7b06433>.
- (71) Yan, G.; Huang, Y.; Bu, Q.; Lv, L.; Deng, P.; Zhou, J.; Wang, Y.; Yang, Y.; Liu, Q.; Cen, X.; et al. Zinc Oxide Nanoparticles Cause Nephrotoxicity and Kidney Metabolism Alterations in Rats. *J. Environ. Sci. Heal. Part A* **2012**, *47* (4), 577–588. <https://doi.org/10.1080/10934529.2012.650576>.
- (72) Ratnasekhar, C.; Sonane, M.; Satish, A.; Mudiam, M. K. R. Metabolomics Reveals the Perturbations in the Metabolome of *Caenorhabditis Elegans* Exposed to Titanium Dioxide

- Nanoparticles. *Nanotoxicology* **2015**, 9 (8), 994–1004.  
<https://doi.org/10.3109/17435390.2014.993345>.
- (73) Jayaram, D. T.; Kumar, A.; Kippner, L. E.; Ho, P.-Y.; Kemp, M. L.; Fan, Y.; Payne, C. K. TiO<sub>2</sub> Nanoparticles Generate Superoxide and Alter Gene Expression in Human Lung Cells. *RSC Adv.* **2019**, 9 (43), 25039–25047. <https://doi.org/10.1039/C9RA04037D>.
- (74) Tedesco, S.; Bayat, N.; Danielsson, G.; Buque, X.; Aspichueta, P.; Fresnedo, O.; Cristobal, S. Proteomic and Lipidomic Analysis of Primary Mouse Hepatocytes Exposed to Metal and Metal Oxide Nanoparticles. *J. Integr. OMICS* **2015**, 5 (1).  
<https://doi.org/10.5584/jiomics.v5i1.184>.
- (75) Koelmans, A. A.; Diepens, N. J.; Velzeboer, I.; Besseling, E.; Quik, J. T. K.; van de Meent, D. Guidance for the Prognostic Risk Assessment of Nanomaterials in Aquatic Ecosystems. *Sci. Total Environ.* **2015**, 535, 141–149.  
<https://doi.org/10.1016/j.scitotenv.2015.02.032>.
- (76) Martins, J.; Oliva Teles, L.; Vasconcelos, V. Assays with *Daphnia Magna* and *Danio Rerio* as Alert Systems in Aquatic Toxicology. *Environ. Int.* **2007**, 33 (3), 414–425.  
<https://doi.org/10.1016/j.envint.2006.12.006>.
- (77) Ranta, E.; Nuutinen, V. *Daphnia* Exhibit Diurnal Vertical Migration in Shallow Rock-Pools. *Hydrobiologia* **1985**, 127 (3), 253–256. <https://doi.org/10.1007/BF00024229>.
- (78) Petosa, A. R.; Jaisi, D. P.; Quevedo, I. R.; Elimelech, M.; Tufenkji, N. Aggregation and Deposition of Engineered Nanomaterials in Aquatic Environments: Role of Physicochemical Interactions. *Environ. Sci. Technol.* **2010**, 44 (17), 6532–6549.  
<https://doi.org/10.1021/es100598h>.
- (79) Peijnenburg, W. J. G. M.; Baalousha, M.; Chen, J.; Chaudry, Q.; Von Der Kammer, F.;

- Kuhlbusch, T. A. J.; Lead, J.; Nickel, C.; Quik, J. T. K.; Renker, M.; et al. A Review of the Properties and Processes Determining the Fate of Engineered Nanomaterials in the Aquatic Environment. *Crit. Rev. Environ. Sci. Technol.* **2015**, *45* (19), 2084–2134.  
<https://doi.org/10.1080/10643389.2015.1010430>.
- (80) Koelmans, A. A.; Quik, J. T. K.; Velzeboer, I. Lake Retention of Manufactured Nanoparticles. *Environ. Pollut.* **2015**, *196*, 171–175.  
<https://doi.org/10.1016/j.envpol.2014.09.025>.
- (81) Jennings, V.; Goodhead, R.; Tyler, C. R. Ecotoxicology of Nanomaterials in Aquatic Systems. In *Characterization of Nanomaterials in Complex Environmental and Biological Media*; Baalousha, M., Lead, J. R., Eds.; Elsevier, 2015; pp 25–32.
- (82) Armitage, P. D.; Cranston, P. S.; Pinder, L. C. V. *The Chironomidae : Biology and Ecology of Non-Biting Midges*, 1st ed.; Chapman & Hall, 1995.
- (83) Besten, P. J. den.; Munawar, M. *Ecotoxicological Testing of Marine and Freshwater Ecosystems : Emerging Techniques, Trends, and Strategies*; Taylor & Francis, 2005.
- (84) Park, S.-Y.; Chung, J.; Colman, B. P.; Matson, C. W.; Kim, Y.; Lee, B.-C.; Kim, P.-J.; Choi, K.; Choi, J. Ecotoxicity of Bare and Coated Silver Nanoparticles in the Aquatic Midge, *Chironomus Riparius*. *Environ. Toxicol. Chem.* **2015**, *34* (9), 2023–2032.  
<https://doi.org/10.1002/etc.3019>.
- (85) Gopalakrishnan Nair, P. M.; Chung, I. M. Alteration in the Expression of Antioxidant and Detoxification Genes in *Chironomus Riparius* Exposed to Zinc Oxide Nanoparticles. *Comp. Biochem. Physiol. Part B Biochem. Mol. Biol.* **2015**, *190*, 1–7.  
<https://doi.org/10.1016/j.cbpb.2015.08.004>.
- (86) Waissi-Leinonen, G. C.; Petersen, E. J.; Pakarinen, K.; Akkanen, J.; Leppänen, M. T.;

- Kukkonen, J. V. K. Toxicity of Fullerene (C60) to Sediment-Dwelling Invertebrate Chironomus Riparius Larvae. *Environ. Toxicol. Chem.* **2012**, *31* (9), 2108–2116. <https://doi.org/10.1002/etc.1926>.
- (87) Nair, P. M. G.; Park, S. Y.; Lee, S.-W.; Choi, J. Differential Expression of Ribosomal Protein Gene, Gonadotrophin Releasing Hormone Gene and Balbiani Ring Protein Gene in Silver Nanoparticles Exposed Chironomus Riparius. *Aquat. Toxicol.* **2011**, *101* (1), 31–37. <https://doi.org/10.1016/j.aquatox.2010.08.013>.
- (88) Lee, S.-W.; Kim, S.-M.; Choi, J. Genotoxicity and Ecotoxicity Assays Using the Freshwater Crustacean Daphnia Magna and the Larva of the Aquatic Midge Chironomus Riparius to Screen the Ecological Risks of Nanoparticle Exposure. *Environ. Toxicol. Pharmacol.* **2009**, *28* (1), 86–91. <https://doi.org/10.1016/j.etap.2009.03.001>.
- (89) Oppold, A. M.; Schmidt, H.; Rose, M.; Hellmann, S. L.; Dolze, F.; Ripp, F.; Weich, B.; Schmidt-Ott, U.; Schmidt, E.; Kofler, R.; et al. Chironomus Riparius (Diptera) Genome Sequencing Reveals the Impact of Minisatellite Transposable Elements on Population Divergence. *Mol. Ecol.* **2017**, *26* (12), 3256–3275. <https://doi.org/10.1111/mec.14111>.

## CHAPTER II:

# NEXT-GENERATION COMPLEX METAL OXIDE NANOMATERIALS NEGATIVELY IMPACT GROWTH AND DEVELOPMENT IN THE BENTHIC INVERTEBRATE *CHIRONOMUS RIPARIUS* UPON SETTLING

### Published in:

American Chemical Society, *Environmental Science & Technology*

DOI: 10.1021/acs.est.8b06804

Nicholas J. Niemuth<sup>1</sup>, Becky J. Curtis<sup>1</sup>, Mimi N. Hang<sup>2</sup>, Miranda J. Gallagher<sup>3</sup>, D. Howard Fairbrother<sup>3</sup>, Robert J. Hamers<sup>2</sup>, Rebecca D. Klaper<sup>1\*</sup>

<sup>1</sup> School of Freshwater Sciences, University of Wisconsin-Milwaukee, 600 E Greenfield Ave., Milwaukee, WI 53204

<sup>2</sup>Department of Chemistry, University of Wisconsin-Madison, 1101 University Ave., Madison, WI 53706

<sup>3</sup>Department of Chemistry, Johns Hopkins University, 3400 North Charles St., Baltimore, MD 21218

\*Corresponding Author

[rklaper@uwm.edu](mailto:rklaper@uwm.edu), Phone: 414-382-1713, Fax: 414-382-1705

(Received 3 December 2018, Accepted 14 March 2019)

## Abstract

Most studies of nanomaterial environmental impacts have focused on relatively simple first-generation nanomaterials, including metals or metal oxides (e.g. Ag, ZnO) for which dissolution largely accounts for toxicity. Few studies have considered nanomaterials with more complex compositions, such as complex metal oxides, which represent an emerging class of next-generation nanomaterials used in commercial products at large scales. In addition, many nanomaterials are not colloidally stable in aqueous environments and will aggregate and settle, yet most studies use pelagic rather than benthic-dwelling organisms. Here we show that lithium cobalt oxide ( $\text{Li}_x\text{Co}_{1-x}\text{O}_2$ , LCO) and lithium nickel manganese cobalt oxide ( $\text{Li}_x\text{Ni}_y\text{Mn}_z\text{Co}_{1-y-z}\text{O}_2$ , NMC) exposure of the model benthic species *Chironomus riparius* at 10 and 100  $\text{mg}\cdot\text{L}^{-1}$  caused 30-60% declines in larval growth, and a delay of 7-25 d in adult emergence. A correlated 41-48% decline in larval hemoglobin concentration and related gene expression changes suggest a potential adverse outcome pathway. Metal ions released from nanoparticles do not cause equivalent impacts, indicating a nano-specific effect. Nanomaterials settled within 2 days and indicate higher cumulative exposures to sediment organisms than those in the water column, making this a potentially realistic environmental exposure. Differences in toxicity between NMC and LCO indicate compositional tuning may reduce material impact.

## Introduction

Standard aquatic toxicity assays using pelagic organisms (*e.g.*, *Daphnia magna*, *Danio rerio*) have demonstrated a range of potential environmental impacts depending on the types of engineered nanomaterials (ENMs) considered, with some being toxic at low concentrations when considered over a chronic exposure but many not toxic until very high unrealistic concentrations.<sup>1</sup> However, most pristine ENMs are not stable in aqueous exposure conditions,<sup>2</sup> and thus many studies on pelagic organisms largely assume exposure to the stable fraction of ENMs left behind in the water column after a majority settles out.<sup>2,3</sup> Testing for impacts of ENMs on benthic organisms is therefore extremely important, in certain cases perhaps more important than impacts on pelagic organisms, as many ENMs are expected to settle and concentrate to higher exposure concentrations in sediment.<sup>3,4</sup> Despite this, the preponderance of aquatic nanotoxicology research has focused on exposures to pelagic organisms.<sup>3</sup>

Most ENM toxicity studies have also focused on first-generation materials, including metal nanoparticles, Au and Ag, and metal oxide nanoparticles, TiO<sub>2</sub>, ZnO, and CeO<sub>2</sub>,<sup>5</sup> as they have demonstrated potential for the highest use. For these materials, dissolution is often identified as the main source of toxicity.<sup>6</sup> However, we have comparatively little information on more complex next-generation ENMs that are now coming to use in the marketplace. The complex metal oxides lithium cobalt oxide (Li<sub>x</sub>Co<sub>1-x</sub>O<sub>2</sub>, LCO) and lithium nickel manganese cobalt oxide (Li<sub>x</sub>Ni<sub>y</sub>Mn<sub>z</sub>Co<sub>1-y-z</sub>O<sub>2</sub>, NMC) and other related complex metal oxides are examples of next-generation materials that are increasing dramatically in the marketplace due to their use as electrode materials in lithium ion batteries (LIBs)<sup>7-10</sup> and lower-volume applications such as catalysts for solar fuel production.<sup>11</sup> NMC is an alternative to LCO that has the same crystal

structure, but partial substitution of Co with Ni and Mn lowers cost and can increase performance.<sup>12</sup> A typical electric vehicle contains approximately 35-90 kg of metal oxide particles, with rapid increases in electric vehicle production leading to predicted global production of 300-800 kilotons of Co and Ni annually by 2025,<sup>13</sup> and LIB waste by 2025 estimated to reach 200 kilotons from EVs alone.<sup>14</sup> Present-generation batteries frequently use particle sizes in the micron range, but smaller particles in the nanometer size regime achieve fast recharge times and are also formed *in situ* by mechanical fracturing of larger particles during use.<sup>12</sup> Because lithium-ion batteries are not generally recycled due to the low cost of Ni and Mn,<sup>13,15</sup> potential release of cathode materials in micron- and nano-particle form into the aquatic environment from battery waste is a legitimate concern.<sup>16,17</sup>

Previous research has demonstrated that the complex metal oxides NMC and LCO do not behave or cause toxicity in the same manner as their simple metal oxide counterparts.<sup>18,19</sup> For example, density functional calculations and experimental measurements showed that NMC dissolves incongruently, with Ni released more rapidly in aqueous media compared with Co and Mn.<sup>18</sup> Material dissolution is also impacted by properties of the media such as pH.<sup>18</sup> A consequence of incongruent dissolution is that the ions released and ENM composition change over the course of the exposure. Ni and Co are both toxic to pelagic and benthic organisms,<sup>20-23</sup> while Mn is relatively non-toxic.<sup>24,25</sup> Our previous study showed that concentrations of LCO and NMC as low as 0.25 mg·L<sup>-1</sup> have significant negative impacts on survival and reproduction in *Daphnia magna* that are not accounted for by particle dissolution.<sup>19</sup> This work also showed that NMC exposure produced lower daphnid toxicity compared to LCO, indicating a difference due to ENM composition.<sup>19</sup>

Metal oxide nanoparticles including TiO<sub>2</sub>, ZnO, and CeO<sub>2</sub> have been shown to settle over time in aqueous media at ambient pH.<sup>26–28</sup> We previously showed both LCO and NMC nanoparticles settle substantially within 24 hours in aqueous media: 66 and 33% settling in 22.5 h respectively.<sup>19</sup> Thus, testing for impacts of these materials on benthic organisms is warranted.

For this study, impacts of ENMs entering the environment were investigated using freshwater midge *Chironomus riparius*, a model species for testing effects of chemical exposures on benthic organisms. This organism is a keystone species and an important food source in both aquatic and terrestrial environments.<sup>29</sup> It has been shown to be sensitive to pollutants, and protocols for exposure and culturing have been established by the American Society for Testing and Materials and U.S. Environmental Protection Agency.<sup>30</sup> The *C. riparius* genome is sequenced,<sup>31</sup> and large mRNA and expressed sequence tag (EST) databases exist for *C. riparius*, including genes relevant to stress and the response to chemical exposures. *C. riparius* have also been used rarely but successfully in ENM toxicity exposures,<sup>32–36</sup> though only one study (of fullerene ENMs) has explicitly looked at impacts of material settling.<sup>34</sup> In the current study, *C. riparius* larvae were exposed to LCO and NMC at 1, 10, and 100 mg·L<sup>-1</sup> as well as ion controls from 5 days post-hatch until adult emergence and organisms were evaluated for changes in size, coloration, and gene expression at 7 d and adult emergence up to 50 d. Results indicate significant negative impacts on all of these endpoints from LCO and NMC exposure, which are not replicated by ion controls. Implications of these effects in the context of the expected volume of LIB waste and settling of these materials in the environment are discussed, with compositional tuning indicated as a potential means of mitigating environmental impacts. This study demonstrates the

importance of using sediment species for testing environmental impacts, reveals a nano-specific impact of complex nanoparticles, and indicates a potential adverse outcome pathway for metal oxide NPs.

## **Materials and methods**

### ***Synthesis of LCO and NMC nanosheets***

Synthesis of LCO and NMC nanosheets was carried out using methods described in <sup>37,38</sup> and consists of two steps. All reagents used for synthesis were purchased from Sigma Aldrich and only ultrapure water was used. To specifically make LCO nanosheets, cobalt hydroxide nanosheets were first synthesized using a precipitation method where in 1 M cobalt (II) nitrate was added dropwise into a 0.1 M LiOH solution under magnetic stirring. The resulting precipitate was then cleaned using repeated cycles (3X) of centrifugation and resuspension in ultrapure water (18 M $\Omega$  cm resistivity) followed by repeated cycles (2X) of centrifugation and resuspension in methanol. The precipitate (200 mg) was then dried under a continual flow of nitrogen gas and subsequently was added to a 10 g mixture of molten lithium salt consisting of a molar ratio of 6:4 LiOH: LiNO<sub>3</sub> (205 °C, under magnetic stirring) in a poly(tetrafluorethylene) vessel. After 1 h, the reaction was carefully quenched with ultrapure water and the LCO precipitate was purified using repeated cycles of centrifugation and resuspension in ultrapure water (2X) and methanol (3X) before drying under a flow of nitrogen gas. All centrifugation was completed using the Thermo Scientific Sorvall Legend X1R Centrifuge with a Thermo TX-400 rotor at 4696 g. To synthesize NMC nanosheet, an identical method was used with the exception that in the precipitation step, a ratio of 1:1:1 of Ni:Co:Mn salts (0.1 M nickel (II) acetate, 0.1 M cobalt (II) acetate, and 0.1 M manganese (II) acetate) were used instead. The degree of lithiation

was not directly controlled for using this synthetic method. Characterization of nanosheet stoichiometry, crystal phase, and size and morphology from XRD, ICP-OES and SEM are included in the Supporting Information.

### *C. riparius larval exposure*

#### *ENM stock suspension*

Stock solutions of LCO and NMC ( $200 \text{ mg}\cdot\text{L}^{-1}$ ) were prepared by adding 40 mg of ENM powder to 200 mL of Milli-Q<sup>®</sup> water and sonicating at 100% power for 20 minutes in a Branson 2800 ultrasonic bath (Emerson Electric Co, St Louis, MO). Dilutions to 20 and  $2 \text{ mg}\cdot\text{L}^{-1}$  were made in Milli-Q<sup>®</sup> and sonicated for an additional 10 min immediately before dosing. Zeta potential of ENMs at final concentrations in 1x Moderately Hard Reconstituted Water (MHRW)<sup>19</sup> were characterized using a Zetasizer Nano ZS (Malvern Instruments, Westborough, MA, USA).

#### *Exposure beaker preparation and maintenance*

Exposure beakers were prepared by adding 15 g of 140-270 mesh silica sand (AGSCO Corp) to 100 mL beakers and autoclaving to sterilize. Sand was then rinsed 3x with 80 mL Milli-Q<sup>®</sup>.

Control beakers were prepared by adding 20 mL of Milli-Q<sup>®</sup> and 20 mL of 2x MHRW.

Treatment beakers (1, 10, and  $100 \text{ mg}\cdot\text{L}^{-1}$ ) were prepared by adding 20 mL of 2x MHRW and 20 mL of the appropriate 2x nanoparticle stock. Five *C. riparius* larvae (5 days post-hatch) were added to each replicate control and exposure beaker.

Beakers were covered with plastic wrap and incubated at 20 °C with a 16:8 light:dark photoperiod. A 50% water exchange was carried out three times per week. For exposure beakers,

new ENMs were not added, as ENMs had settled by this time. Animals were fed ground TetraMin<sup>®</sup> flakes (20 g·L<sup>-1</sup> in Milli-Q<sup>®</sup>) daily, 125 uL per beaker.

### *ENM exposures*

An initial LCO exposure was conducted with 10 replicate beakers per condition (5 larvae per beaker) each for control, 1, 10 and 100 mg·L<sup>-1</sup>. A second round of experiments was carried out with 10 replicate beakers per condition to compare LCO to NMC, exposing larvae to LCO at 1, 10, and 100 mg·L<sup>-1</sup>; NMC at 1, 10, and 100 mg·L<sup>-1</sup>; and control. For both sets of experiments, larvae were harvested from 5 beakers per condition on exposure day 7 and frozen for gene expression analysis. The remaining 5 beakers per condition were maintained until exposure day 50 for adult fly emergence.

Having observed changes in size and coloration of ENM-exposed larvae, a third experiment was conducted with 5 replicate beakers per condition, exposing larvae to LCO at 1, 10, and 100 mg·L<sup>-1</sup>; NMC at 1, 10, and 100 mg·L<sup>-1</sup>; and control. Larvae from all 5 beakers were harvested on exposure day 7, flash frozen in liquid nitrogen, and stored at – 80 °C for imaging for size and coloration analysis.

### *Ion control exposures*

Data from ICP-MS analysis (see *ICP-MS analysis of released ions* below) were used to determine the concentrations for 2x stocks of metal salts to yield exposure concentrations reflective of ion concentrations found in the supernatants of 10 and 100 mg·L<sup>-1</sup> LCO and NMC exposure media samples. We chose to test whether the ions observed released from the particles

were by themselves sufficient to cause any observed toxicity, as metal dissolution from NPs is indicated as a major cause of toxicity in other studies. If not, then the portion of settled particles, by concentrating material in the sand, are the cause of toxicity: either by direct nano-toxic effects of the particles themselves or by acting as a vector to bring particles with high concentrations of metals into the feeding environment of the larvae. Animals were dosed with Li, Ni, Mn, and Co ions at the highest concentration observed over 7 d. For LCO, dosed ions were 1000  $\mu\text{g}\cdot\text{L}^{-1}$  Li and 400  $\mu\text{g}\cdot\text{L}^{-1}$  Co for 10  $\text{mg}\cdot\text{L}^{-1}$  and 4200  $\mu\text{g}\cdot\text{L}^{-1}$  Li and 900  $\mu\text{g}\cdot\text{L}^{-1}$  Co for 100  $\text{mg}\cdot\text{L}^{-1}$ . For NMC, dosed ions were 710  $\mu\text{g}\cdot\text{L}^{-1}$  Li, 360  $\mu\text{g}\cdot\text{L}^{-1}$  Ni, 270  $\mu\text{g}\cdot\text{L}^{-1}$  Mn, and 160  $\mu\text{g}\cdot\text{L}^{-1}$  Co for 10  $\text{mg}\cdot\text{L}^{-1}$  and 7000  $\mu\text{g}\cdot\text{L}^{-1}$  Li, 2000  $\mu\text{g}\cdot\text{L}^{-1}$  Ni, 300  $\mu\text{g}\cdot\text{L}^{-1}$  Mn, and 600  $\mu\text{g}\cdot\text{L}^{-1}$  Co for 100  $\text{mg}\cdot\text{L}^{-1}$ . An ion control exposure was conducted with 10 replicate beakers per condition: control, LCO 10 and 100  $\text{mg}\cdot\text{L}^{-1}$  ion equivalents, and NMC 10 and 100  $\text{mg}\cdot\text{L}^{-1}$  ion equivalents. At water changes, 20 mL of exposure media was removed and replaced with 20 mL of 1x ion solution to maintain ion concentrations throughout the exposure. Larvae were harvested from 6 beakers per condition on exposure day 7: 3 beakers per condition for gene expression analysis were frozen and 3 beakers per condition for imaging and size measurement were preserved in 70% ethanol. The remaining 4 beakers per condition were maintained until exposure day 50 for adult fly emergence.

### ***ICP-MS analysis of released ions***

Inductively coupled plasma mass spectrometry (ICP-MS) was conducted on exposure media at all concentrations to determine the level of metal dissolution into exposure media after 2, 4, and 7 d, sampling exposure beakers before each water change over the first seven days of the experiment. Supernatant of centrifuged samples were acidified to 2% wt nitric acid and analyzed

with an Elan DRC II ICP-MS (Perkin Elmer). 10 to 150-fold dilutions were carried out on supernatants containing ions at concentrations above 100 ppb to ensure analyte concentrations fell within the detection range of the instrument. The calibration curve was prepared from serial dilutions of  $1003 \pm 5$ ppb Ni,  $1007 \pm 4$ ppb Mn,  $996 \pm 3$ ppb Co, and  $1006 \pm 2$ ppb Li NIST Traceable standards (Inorganic Ventures). Full details for sampling and quantification are included in the Supporting Information.

### ***ENM sedimentation behavior***

We previously showed that LCO and NMC settle out in MHRW.<sup>19</sup> To determine the extent of particle settling in this study, we sampled exposure treatments of 1, 10, and 100 mg·L<sup>-1</sup> of LCO or NMC particles in 1x MHRW on exposure days 0, 2, 4, and 7. Absorbance values of sampled supernatants were measured at 600 nm using a Synergy H4 plate reader (Biotek Instruments, Winooski, VT).

### ***Imaging and measurement***

#### *Size*

Flash frozen and alcohol-preserved larvae were imaged using a Motic SMZ-168 TL stereomicroscope with an attached MotiCam 2, 2.0 MP CMOS camera (Motic, Hong Kong). Images were recorded using Motic Images Plus 2.0 software, and the included measurement tool used to determine animal size metrics. Measurements were calibrated with a Leica 50 mm metric stage micrometer (Leica Camera AG, Wetzlar, Germany).

### *Animal coloration (Hemoglobin absorbance)*

The green channel from an RGB (red-green-blue) image was isolated and pixel intensity used to measure the absorbance of hemoglobin (Hb) in *C. riparius* larvae on day 7. Hb absorbance analysis was only carried out on flash-frozen larvae, as those preserved in ethanol did not retain intact Hb. Detailed information on image processing is included in the Supporting Information.

### *Gene expression analysis*

Total RNA was extracted from flash-frozen 7 d exposure samples and 100 ng of total RNA transcribed into complementary deoxyribonucleic acid (cDNA). Gene expression analysis was carried out on a variety of genes associated with metal, oxidative, protein, and general stress responses. The following were analyzed for gene expression: ribosomal protein *RPL13* (housekeeping gene); metal stress gene metallothionein (*MTT*), as metal exposure is hypothesized to be a major source of toxicity; oxidative stress genes: catalase (*CAT*), gamma-glutamylcystein synthase (*GCS*), glutathione s-transferase (*GST*), and two different superoxide dismutases (*Cu-ZnSOD* and *MnSOD*), as oxidative stress is hypothesized to be a main cause of damage by nanoparticle exposures; heat shock protein *HSP27*, important for protecting protein folding after exposure to toxins; stress-responsive regulatory kinase *p38*; developmental regulator ecdysone receptor (*EcR*), to measure changes in developmental pathways as a result of exposure; and genes related to heme synthesis, added as we found an indication in the change of heme production in exposed organisms: aminolevulinic acid synthase (*ALAS*), porphobilinogen synthase (*PBGS*), and heme oxygenase (*HO*) (Table S1).

Relative gene expression was quantified using the iTaq Universal SYBR Green Supermix (Bio-Rad, Hercules, CA) for 20  $\mu$ L reactions and the  $2^{-\Delta\Delta C_t}$  method.<sup>39</sup> For detailed information on extraction, cDNA creation, primer design, and qPCR, see the Supporting Methods.

### ***Statistical analysis***

Statistical analyses were performed using SPSS version 22 for Mac (IBM). Statistical tests for each dataset were chosen based on data normality determined by the Shapiro-Wilk test and equality of variance using Levene's test. Normally distributed data with equal variance (width, Hb concentration) were compared using a one-way ANOVA with Tukey post-hoc comparisons. Data with normal distributions but unequal variances (gene expression) were compared using a Welch one-way ANOVA with Dennett's T3 post-hoc comparisons. Non-normal data were compared using Kruskal-Wallis (length, head capsule length) or Kaplan-Meier (time to emergence) non-parametric tests. Significance for all statistics was set at  $p < 0.05$ . Datasets with a nested design (size, Hb, emergence) were tested for any replicate effect; no replicate effects were detected for any dataset ( $p > 0.05$ ).

### **Results and Discussion**

Our results show that next-generation complex metal oxide ENMs LCO and NMC settle in aqueous media and cause significant, negative, nano-specific effects on the keystone benthic species *C. riparius*, impacting their size, time to emergence, Hb levels, and expression of stress and heme-metabolism genes. Impacts of these ENMs are nano-specific, as the effects of ENM exposure exceed or are absent in equivalent ion exposures. Effects are much greater for LCO than the alternative NMC materials providing an indication that using NMC may cause less

environmental impact. Impacts on Hb levels and gene expression may point to the molecular mechanism underlying these effects in chironomids.

### ***LCO and NMC aggregate and settle***

LCO and NMC both settled substantially over the course of the experiment: more than 90% of material within 2 d for 100 mg·L<sup>-1</sup> exposures, and more than 70% of material within 2 d at 10 mg·L<sup>-1</sup> (Fig S3). Settling is more rapid for higher concentrations, as has been observed for other ENMs including CeO<sub>2</sub>, TiO<sub>2</sub>, and iron oxides.<sup>40-42</sup> Zeta-potential data point to an explanation for this concentration-dependent settling. Zeta-potential values for LCO and NMC at their moment of addition are highly negatively charged in 1 mg·L<sup>-1</sup> exposures (-16.33 and -17.73 mV respectively), while 10 mg·L<sup>-1</sup> exposures are slightly less negative (-7.74 and -6.07 mV), and values approach neutral to slightly positive at 100 mg·L<sup>-1</sup> (0.52 and 1.59 mV) (Table S2). Electrostatic repulsion is one of the primary sources of ENM stability in aqueous media.<sup>43</sup> Thus, increased settling at higher LCO and NMC exposure concentrations is likely due to an increased propensity for particles to aggregate due to lower electrostatic repulsion.

Aggregation of LCO and NMC at higher concentrations likely underlies observed concentration-dependent declines in material dissolution. For both materials all intercalated Li left the material by the 2 d time point, but even at high concentrations lithium is not considered toxic to these organisms (Fig S4d).<sup>19</sup> For LCO, ICP-MS results showed that dissolution of Co ions from the material did not scale linearly with exposure concentration, but rather proportionally to the log<sub>10</sub> of the exposure concentration. That is, dissolved Co for 100 mg·L<sup>-1</sup> LCO was only 2-3x the dissolved Co for 10 mg·L<sup>-1</sup>, which was only 2-3x the dissolved Co for 1 mg·L<sup>-1</sup>, rather than the

10x that might be expected (Fig S4c). Only a portion of Co from the material dissolved over the course of 7 d, although relatively more Co dissolved as ions at 1 mg·L<sup>-1</sup> (39%) than at 10 mg·L<sup>-1</sup> (14%) or 100 mg·L<sup>-1</sup> (5%) (Fig S5c). For NMC particles, ICP-MS results indicated dissolution of Ni, Mn, and Co from the material over the course of 7 d, with most dissolution for these metals occurring by day 2 for 1 and 10 mg·L<sup>-1</sup> exposures (Fig S4). Dissolved ion concentration for Ni, Mn, and Co was proportional to the log<sub>10</sub> of exposure concentration over 7 d, similar to Co for LCO (Fig S4). Only a fraction of Ni, Mn, or Co dissolved from the material over 7 d, with relatively more metal dissolving as ions at lower exposure concentrations: 1 mg·L<sup>-1</sup> – 67% of Ni, 55% of Mn, and 49% of Co; 10 mg·L<sup>-1</sup> - 30, 24, and 25% respectively; 100 mg·L<sup>-1</sup> – 9, 6, and 12% respectively (Fig S5).

Thus, more metal as a percent of total material mass dissolved at lower concentrations than at higher concentrations: about 50% at 1 mg·L<sup>-1</sup>, about 25% at 10 mg·L<sup>-1</sup>, and only about 10% at 100 mg·L<sup>-1</sup> (Fig S5). The lower surface-area-to-volume ratio of aggregated particles formed at high concentrations likely reduces ion dissolution from the material, as has been shown for NMC with different surface-area-to-volume ratios.<sup>12</sup> Since only a small percentage of ions dissolve from the material, particularly at higher concentrations, particle exposures, by concentrating large amounts of settled material in surface sand, have impacts of a much higher degree than — or are unobservable in — ion exposures.

### ***LCO and NMC impact C. riparius growth and adult emergence***

Particle exposure causes significant, dose-dependent effects on the development of *C. riparius* larvae not explicable by ion dissolution into the media, retarding growth and delaying emergence

of adult flies. Larvae in exposures were 30% (LCO and NMC 10 mg·L<sup>-1</sup>) to 60% (100 mg·L<sup>-1</sup> LCO) smaller than controls (Fig 1a, c, and e; e.g. lengths of 3.2 ± 0.8 mm for LCO 10 mg·L<sup>-1</sup> and 1.8 ± 0.2 mm for LCO 100 mg·L<sup>-1</sup> versus 4.5 ± 0.2 mm for control). Ion exposures only caused a 20% decrease in size and at the highest concentration, representative of 100 mg·L<sup>-1</sup> NMC (Fig 1b and d). Emergence was also significantly delayed for particle-exposed animals at 10 and 100 mg·L<sup>-1</sup> for LCO and at 100 mg·L<sup>-1</sup> for NMC (Fig 2a). Ion exposures showed no impact on emergence (Fig 2b), demonstrating the importance of settled nanomaterials for these impacts. Toxicity of Ni to *C. riparius* has been fairly well studied in the literature. Accounting for the amount of Co and Ni in added LCO and NMC, impacts on *C. riparius* larval growth were seen at concentrations 10-30 fold lower than that seen in the literature for Ni-spiked sediment: 11-16 mg·kg<sup>-1</sup> for 10 mg·L<sup>-1</sup> NMC and LCO, respectively, versus 146-358 mg·kg<sup>-1</sup> in Ni-spiked sediment.<sup>21,44</sup> No impacts were seen on emergence from Ni-spiked sediments even up to 7990 mg·kg<sup>-1</sup>,<sup>21</sup> whereas impacts were observed from LCO at 16 mg·kg<sup>-1</sup> (10 mg·L<sup>-1</sup> exposure) and NMC at 112 mg kg<sup>-1</sup> (100 mg·L<sup>-1</sup> exposure). Thus, toxicity from settled ENM exceeds that expected from sediment-spiked ions based on the literature. The concentration of metal particles at the sediment surface and *C. riparius* feeding behavior may account for increased toxicity from ENMs, as discussed below.

### ***Metal-specific differences in ENM toxicity***

Importantly, LCO 10 mg·L<sup>-1</sup> exposures caused a significant delay in emergence at a concentration an order of magnitude lower than seen in NMC (100 mg·L<sup>-1</sup>). Larvae from 100 mg·L<sup>-1</sup> LCO exposures did not emerge even up to exposure day 50, more than double the emergence time of controls, despite being visible in disturbed sand.

Differences in response between NMC and LCO may be related to compositional differences between the two ENMs. While the amount of settled material was similar for both materials, not all metals in these materials are expected to elicit the same toxicity. Ni and Co are both toxic metals. On a per mass basis, LCO has 50% more toxic metal than NMC, as it contains only cobalt, while NMC includes Mn in addition to Ni. Cobalt has been shown to cause oxidative stress by depleting reduced thiols from cells.<sup>45</sup> Nickel is also known to cause oxidative stress,<sup>46</sup> and may cause oxidative damage that would elicit a response similar to Co. Both  $\text{Co}_3\text{O}_4$  and NiO ENMs have been shown to cause oxidative stress *in vitro*.<sup>47,48</sup> Manganese, however, has been shown to have antioxidant properties in rats, counteracting the oxidative impacts of other heavy metals,<sup>49</sup> and  $\text{MnO}_2$  ENMs have been shown to scavenge ROS *in vitro*.<sup>50</sup>

Differing gene expression patterns between LCO and NMC may be related to these compositional differences. *MTT* gene expression, related to metal ion exposure and toxicity, declined significantly and in a dose-dependent manner with increasing LCO exposure while NMC had no impact on its expression (Fig 3c). For *CAT* and *HSP27*, 1  $\text{mg}\cdot\text{L}^{-1}$  NMC had the opposite effect of LCO at 100  $\text{mg}\cdot\text{L}^{-1}$ , with expression moving in parallel as dose increased (Fig 3a and b). Manganese has been shown to decrease expression of *EcR* in the amphipod *T. japonicas*,<sup>51</sup> which may explain reduced *EcR* expression in NMC-exposed larvae (Fig 3d). The antioxidant properties of Mn, and the overwhelming of this antioxidant effect with increasing Co and Ni, may explain observed gene expression patterns and account for the lower observed impact of NMC compared to LCO in this study and in our previous work.<sup>19</sup> Thus, tuning of material composition may be a means of mitigating material impact.

***Impact of cobalt on heme synthesis as a potential mechanism of toxicity and adverse outcome pathway***

Larvae exposed to LCO and NMC showed significantly reduced levels of Hb beginning at 10 mg·L<sup>-1</sup> exposure (Fig 1g). This paralleled cobalt disruption of heme synthesis enzymes observed in other organism such as avian and rat liver cells.<sup>52,53</sup> Bacterial and animal studies suggest that the mechanism of cobalt interference with heme biosynthesis is perhaps through substituting cobalt for iron.<sup>54</sup>

Increased expression of *ALAS* and decreased expression of *PBGS* observed in this study (Figs 3e and f) are indicative of inhibition of heme synthesis by Co.<sup>52</sup> *ALAS* expression was up significantly at NMC 100 mg·L<sup>-1</sup> (Fig 3e). *PBGS* expression appeared to decline with dose, particularly for LCO exposure, being significantly down-regulated for both LCO and NMC at 100 mg·L<sup>-1</sup> (Fig 3f). Dose-dependent reductions in expression of *CAT*, an oxidative stress gene that requires heme, in LCO-exposed larvae at 10 and 100 mg·L<sup>-1</sup> (Fig 3a) may also point to disruption of heme synthesis by Co as a mechanism of toxicity. Cobalt exposure has been shown to have a strong negative impact on catalase expression in liver of rats<sup>55</sup> and goldfish.<sup>56</sup>

Both Hb levels and *PBGS* expression correlated inversely with the log<sub>10</sub> of Co settled in LCO and NMC (Hb: R<sup>2</sup> = 0.848, β = -2.25, p < 0.001; *PBGS*: R<sup>2</sup> = 0.681, β = -0.314, p < 0.05).

Inhibition of Hb in *Tanytarsus* chironomids by carbon-monoxide was previously shown to reduce chironomid metabolism and increase larval mortality.<sup>57</sup> The importance of functional Hb for normal chironomid metabolism thus suggests that inhibition of heme synthesis by cobalt may

underlie the developmental impacts of LCO and NMC exposure. A proposed adverse outcome pathway summarizing this is presented in Fig 4.

### ***Benthic organisms are susceptible to settled ENMs***

Settling in aqueous environments is characteristic of many ENMs.<sup>2,58</sup> This settling will cause their accumulation in the sediment and an increase in accumulation over time with continual introduction, which may impact benthic organisms. ENMs in sediment could have a particular impact on deposit feeders that uptake sediment particles like *C. riparius* larvae, which feed primarily on detritus < 250  $\mu\text{m}$ <sup>59</sup> and accumulate small silt particles in their gut.<sup>60</sup> Settled fullerene nanoparticles pack the *C. riparius* larval gut after exposure.<sup>61</sup> Thus, their mode of feeding may create particularly high environmental exposures for *C. riparius* larvae and other deposit feeders from settled ENMs. We posit that the nano-specific impacts observed in this study are the result of the concentration of ENMs in surface sand due to settling, with the likely mode of exposure being ingestion due to *C. riparius* deposit feeding. Whether observed impacts are the result of LCO and NMC exposure directly or the result of material dissolution in the gut or in cellular compartments such as the lysosome (where low pH would be predicted to enhance dissolution)<sup>18</sup> is beyond the scope of this study. Future studies using x-ray computed tomography and x-ray fluorescence techniques to determine the distribution of particles and ions in the organism<sup>62,63</sup> could be informative.

Bioavailability of aggregated ENMs in the benthos may depend on their interaction with sediment particles.<sup>64</sup> Most studies have examined interactions of ENMs with soils rather than sediments,<sup>64</sup> but soil studies have observed that Ag ENMs bind more tightly to clay particles than

to sand.<sup>65</sup> Thus, our use of sand as a model sediment in this study may mean that settled LCO and NMC are more bioavailable than they might be in sediments with high clay content.

Impacts on *C. riparius* development and emergence observed in this study would be expected to negatively impact reproductive success,<sup>66</sup> which could impact higher trophic levels due to their position as a keystone species in aquatic and terrestrial environments.<sup>67</sup> ENM ingestion could also result in trophic transfer of ENMs as they are a primary food resource for many fish species.<sup>68</sup> Bioaccumulation of ENMs in chironomids has been shown for Ag and CeO<sub>2</sub> ENMs.<sup>68,69</sup> CeO<sub>2</sub> ENMs were shown to transfer from chironomids to amphibian larvae, where they accumulated and caused genotoxicity.<sup>68</sup> Thus benthic organisms such as *C. riparius* may act as important vectors for ENMs to enter the aquatic food chain, even when these particles are not stable in the water column.

Modeling studies have shown that for large lakes with long residence times, upwards of 98% of input ENMs can be anticipated to be retained within the lake system due to settling.<sup>70</sup> This means that reaching the sediment concentration found to cause impacts in this study — 23 µg·cm<sup>-2</sup> for 10 mg·L<sup>-1</sup> exposures — would only require a detectable steady-state ENM concentration of 50 ng·L<sup>-1</sup> in surface water. TiO<sub>2</sub> ENMs were detectable in a European lake at 1.4 µg·L<sup>-1</sup>.<sup>71</sup> No study has yet been done to model or measure amounts of LCO or NMC in the environment. The most likely source of LCO or NMC in the environment would be as leachate from LIB waste in landfills, as LIBs are generally not recycled.<sup>14,17</sup> Co leached from LIBs in standard tests was found to be on the order of 164,000 mg Co per kg of battery.<sup>14</sup> Hendren et al. have proposed that production volume may be an indicator of likely exposure risk,<sup>72</sup> and production does correlate

to some degree with modeled and measured environmental concentrations of ENMs.<sup>73</sup> The total mass of LIBs used globally in 2016 was estimated at 374,000 metric tons.<sup>14</sup> Depending on battery life expectancy, this same mass of batteries can be expected to be discarded as waste within years.<sup>14</sup> Given the amount of Co leached from batteries, 60,000 metric tons annually of Co waste will be emitted from LIBs. In this case metal oxide battery waste will be on the same order of magnitude as annual US production estimated for TiO<sub>2</sub> (38,000 tons).<sup>72</sup> Given that TiO<sub>2</sub> has been modeled<sup>74</sup> and measured<sup>71</sup> to be present in surface waters at around 1 µg·L<sup>-1</sup>, a significant amount of LCO and NMC may be expected to be found in the environment based on the expected mass of LIB waste. The 50 ng·L<sup>-1</sup> steady-state estimate corresponding to our 10 mg·L<sup>-1</sup> exposure may not be unrealistic in such a scenario.

### ***Implications***

The expected increase in use of battery cathode materials such as LCO and NMC in the next decade and the lack of material recycling means that environmental release due to disposal may be expected.<sup>16,17</sup> Exposure to LCO and NMC caused significant impacts on the growth and development of *C. riparius* through stress pathways and inhibition of heme synthesis. Settling of nanomaterials creates the potential for small amounts of complex metal oxides and other ENMs to accumulate in the benthos of aquatic systems at concentrations that may cause adverse impacts. Reduced impact of NMC versus LCO points to tuning of material composition as a means of limiting environmental effects of material release.

## **Acknowledgements**

This work was supported by National Science Foundation under the Center for Sustainable Nanotechnology (CSN), CHE-1503408. The CSN is part of the Centers for Chemical Innovation Program. Gene expression work was conducted at the Great Lakes Genomics Center at UW-Milwaukee. The authors acknowledge Nicklaus Neureuther and Dylan Olson for help with culture maintenance and exposure takedowns. Thank you to the Johns Hopkins Department of Environmental Health and Engineering for use of their equipment.

## **Disclosure of interests**

The authors declare no competing financial interest.

## References

- (1) Lin, S.; Wang, H.; Yu, T. A Promising Trend for Nano-EHS Research — Integrating Fate and Transport Analysis with Safety Assessment Using Model Organisms. *NanoImpact* **2017**, *7*, 1–6. <https://doi.org/10.1016/j.impact.2016.09.007>.
- (2) Petosa, A. R.; Jaisi, D. P.; Quevedo, I. R.; Elimelech, M.; Tufenkji, N. Aggregation and Deposition of Engineered Nanomaterials in Aquatic Environments: Role of Physicochemical Interactions. *Environ. Sci. Technol.* **2010**, *44* (17), 6532–6549. <https://doi.org/10.1021/es100598h>.
- (3) Koelmans, A. A.; Diepens, N. J.; Velzeboer, I.; Besseling, E.; Quik, J. T. K.; van de Meent, D. Guidance for the Prognostic Risk Assessment of Nanomaterials in Aquatic Ecosystems. *Sci. Total Environ.* **2015**, *535*, 141–149. <https://doi.org/10.1016/j.scitotenv.2015.02.032>.
- (4) Jennings, V.; Goodhead, R.; Tyler, C. R. Ecotoxicology of Nanomaterials in Aquatic Systems. In *Characterization of Nanomaterials in Complex Environmental and Biological Media*; Baalousha, M., Lead, J. R., Eds.; Elsevier, 2015; pp 25–32.
- (5) Maynard, A. D.; Warheit, D. B.; Philbert, M. A. The New Toxicology of Sophisticated Materials: Nanotoxicology and Beyond. *Toxicol. Sci.* **2011**, *120* (Supplement 1), S109–S129. <https://doi.org/10.1093/toxsci/kfq372>.
- (6) Bondarenko, O.; Juganson, K.; Ivask, A.; Kasemets, K.; Mortimer, M.; Kahru, A. Toxicity of Ag, CuO and ZnO Nanoparticles to Selected Environmentally Relevant Test Organisms and Mammalian Cells in Vitro: A Critical Review. *Arch. Toxicol.* **2013**, *87* (7), 1181–1200. <https://doi.org/10.1007/s00204-013-1079-4>.

- (7) Brodd, R. J. *Batteries for Sustainability : Selected Entries from the Encyclopedia of Sustainability Science and Technology*; Springer, 2012.
- (8) Grey, C. P.; Ceder, G.; Kang, K.; Meng, Y. S.; Bre, J. Electrodes with High Power and High Capacity for Rechargeable Lithium Batteries. *Science*. **2005**, *311* (December), 1–5. <https://doi.org/10.1126/science.1122152>.
- (9) Pollet, B. G.; Staffell, I.; Shang, J. L. Current Status of Hybrid, Battery and Fuel Cell Electric Vehicles: From Electrochemistry to Market Prospects. *Electrochim. Acta* **2012**, *84*, 235–249. <https://doi.org/10.1016/j.electacta.2012.03.172>.
- (10) Wang, Y.; Yu, Y.; Huang, K.; Chen, B.; Deng, W.; Yao, Y. Quantifying the Environmental Impact of a Li-Rich High-Capacity Cathode Material in Electric Vehicles via Life Cycle Assessment. *Environ. Sci. Pollut. Res.* **2017**, *24* (2), 1251–1260. <https://doi.org/10.1007/s11356-016-7849-9>.
- (11) Liu, H.; Zhou, Y.; Moré, R.; Müller, R.; Fox, T.; Patzke, G. R. Correlations among Structure, Electronic Properties, and Photochemical Water Oxidation: A Case Study on Lithium Cobalt Oxides. *ACS Catal.* **2015**, *5* (6), 3791–3800. <https://doi.org/10.1021/acscatal.5b00078>.
- (12) Hang, M. N.; Hudson-Smith, N. V.; Clement, P. L.; Zhang, Y.; Wang, C.; Haynes, C. L.; Hamers, R. J. Influence of Nanoparticle Morphology on Ion Release and Biological Impact of Nickel Manganese Cobalt Oxide (NMC) Complex Oxide Nanomaterials. *ACS Appl. Nano Mater.* **2018**, *1* (4), 1721–1730. <https://doi.org/10.1021/acsanm.8b00187>.
- (13) Olivetti, E. A.; Ceder, G.; Gaustad, G. G.; Fu, X. Lithium-Ion Battery Supply Chain Considerations: Analysis of Potential Bottlenecks in Critical Metals. *Joule* **2017**, *1* (2), 229–243. <https://doi.org/10.1016/j.joule.2017.08.019>.

- (14) Winslow, K. M.; Laux, S. J.; Townsend, T. G. A Review on the Growing Concern and Potential Management Strategies of Waste Lithium-Ion Batteries. *Resources, Conservation and Recycling*. Elsevier 2018, pp 263–277.  
<https://doi.org/10.1016/j.resconrec.2017.11.001>.
- (15) Zou, H.; Gratz, E.; Apelian, D.; Wang, Y. A Novel Method to Recycle Mixed Cathode Materials for Lithium Ion Batteries. *Green Chem.* **2013**, *15* (5), 1183.  
<https://doi.org/10.1039/c3gc40182k>.
- (16) Kang, D. H. P.; Chen, M.; Ogunseitan, O. A. Potential Environmental and Human Health Impacts of Rechargeable Lithium Batteries in Electronic Waste. *Environ. Sci. Technol.* **2013**, *47* (10), 5495–5503. <https://doi.org/10.1021/es400614y>.
- (17) Hamers, R. J. Nanomaterials and Global Sustainability. *Acc. Chem. Res.* **2017**, *50* (3), 633–637. <https://doi.org/10.1021/acs.accounts.6b00634>.
- (18) Bennett, J. W.; Jones, D.; Huang, X.; Hamers, R. J.; Mason, S. E. Dissolution of Complex Metal Oxides from First-Principles and Thermodynamics: Cation Removal from the (001) Surface of  $\text{Li}(\text{Ni} \frac{1}{3} \text{Mn} \frac{1}{3} \text{Co} \frac{1}{3})\text{O}_2$ . *Environ. Sci. Technol.* **2018**, *52* (10), 5792–5802. <https://doi.org/10.1021/acs.est.8b00054>.
- (19) Bozich, J.; Hang, M.; Hamers, R.; Klaper, R. Core Chemistry Influences the Toxicity of Multicomponent Metal Oxide Nanomaterials, Lithium Nickel Manganese Cobalt Oxide, and Lithium Cobalt Oxide to *Daphnia Magna*. *Environ. Toxicol. Chem.* **2017**, *36* (9), 2493–2502. <https://doi.org/10.1002/etc.3791>.
- (20) Béchard, K. M.; Gillis, P. L.; Wood, C. M. Acute Toxicity of Waterborne Cd, Cu, Pb, Ni, and Zn to First-Instar *Chironomus Riparius* Larvae. *Arch. Environ. Contam. Toxicol.* **2008**, *54* (3), 454–459. <https://doi.org/10.1007/s00244-007-9048-7>.

- (21) Besser, J. M.; Brumbaugh, W. G.; Ingersoll, C. G.; Ivey, C. D.; Kunz, J. L.; Kemble, N. E.; Schlekot, C. E.; Garman, E. R. Chronic Toxicity of Nickel-Spiked Freshwater Sediments: Variation in Toxicity among Eight Invertebrate Taxa and Eight Sediments. *Environ. Toxicol. Chem.* **2013**, *32* (11), n/a-n/a. <https://doi.org/10.1002/etc.2271>.
- (22) Khangarot, B. S.; Ray, P. K. Sensitivity of Midge Larvae Of *Chironomus Tentans* Fabricius (Diptera Chironomidae) to Heavy Metals. *Bull. Environ. Contam. Toxicol.* **1989**, *42* (3), 325–330. <https://doi.org/10.1007/BF01699956>.
- (23) Münzinger, A. Effects of Nickel on *Daphnia Magna* during Chronic Exposure and Alterations in the Toxicity to Generations Pre-Exposed to Nickel. *Water Res.* **1990**, *24* (7), 845–852. [https://doi.org/10.1016/0043-1354\(90\)90134-R](https://doi.org/10.1016/0043-1354(90)90134-R).
- (24) Subba Rao, D.; Saxena, A. B. Research Report: Acute Toxicity of Mercury, Zinc, Lead, Cadmium, Manganese to the *Chironomus* Sp. *Int. J. Environ. Stud.* **1981**, *16* (3–4), 225–226. <https://doi.org/10.1080/00207238108709874>.
- (25) Fjällborg, B.; Li, B.; Nilsson, E.; Dave, G. Toxicity Identification Evaluation of Five Metals Performed with Two Organisms (*Daphnia Magna* and *Lactuca Sativa*). *Arch. Environ. Contam. Toxicol.* **2006**, *50* (2), 196–204. <https://doi.org/10.1007/s00244-005-7017-6>.
- (26) Van Koetsem, F.; Verstraete, S.; Van der Meeren, P.; Du Laing, G. Stability of Engineered Nanomaterials in Complex Aqueous Matrices: Settling Behaviour of CeO<sub>2</sub> Nanoparticles in Natural Surface Waters. *Environ. Res.* **2015**, *142*, 207–214. <https://doi.org/10.1016/j.envres.2015.06.028>.

- (27) Zhang, Y.; Chen, Y.; Westerhoff, P.; Hristovski, K.; Crittenden, J. C. Stability of Commercial Metal Oxide Nanoparticles in Water. *Water Res.* **2008**, *42* (8–9), 2204–2212. <https://doi.org/10.1016/j.watres.2007.11.036>.
- (28) Velzeboer, I.; Hendriks, A. J.; Ragas, A. M. J.; van de Meent, D. Aquatic Ecotoxicity Test of Some Nanomaterials. *Environ. Toxicol. Chem.* **2008**, *27* (9), 1942. <https://doi.org/10.1897/07-509.1>.
- (29) Armitage, P. D.; Cranston, P. S.; Pinder, L. C. V. *The Chironomidae : Biology and Ecology of Non-Biting Midges*, 1st ed.; Chapman & Hall, 1995.
- (30) Besten, P. J. den.; Munawar, M. *Ecotoxicological Testing of Marine and Freshwater Ecosystems : Emerging Techniques, Trends, and Strategies*; Taylor & Francis, 2005.
- (31) Oppold, A. M.; Schmidt, H.; Rose, M.; Hellmann, S. L.; Dolze, F.; Ripp, F.; Weich, B.; Schmidt-Ott, U.; Schmidt, E.; Kofler, R.; Hankeln, T., Pfenninger, M. Chironomus Riparius (Diptera) Genome Sequencing Reveals the Impact of Minisatellite Transposable Elements on Population Divergence. *Mol. Ecol.* **2017**, *26* (12), 3256–3275. <https://doi.org/10.1111/mec.14111>.
- (32) Park, S.-Y.; Chung, J.; Colman, B. P.; Matson, C. W.; Kim, Y.; Lee, B.-C.; Kim, P.-J.; Choi, K.; Choi, J. Ecotoxicity of Bare and Coated Silver Nanoparticles in the Aquatic Midge, Chironomus Riparius. *Environ. Toxicol. Chem.* **2015**, *34* (9), 2023–2032. <https://doi.org/10.1002/etc.3019>.
- (33) Gopalakrishnan Nair, P. M.; Chung, I. M. Alteration in the Expression of Antioxidant and Detoxification Genes in Chironomus Riparius Exposed to Zinc Oxide Nanoparticles. *Comp. Biochem. Physiol. Part B Biochem. Mol. Biol.* **2015**, *190*, 1–7. <https://doi.org/10.1016/j.cbpb.2015.08.004>.

- (34) Waissi-Leinonen, G. C.; Petersen, E. J.; Pakarinen, K.; Akkanen, J.; Leppänen, M. T.; Kukkonen, J. V. K. Toxicity of Fullerene (C60) to Sediment-Dwelling Invertebrate *Chironomus Riparius* Larvae. *Environ. Toxicol. Chem.* **2012**, *31* (9), 2108–2116. <https://doi.org/10.1002/etc.1926>.
- (35) Nair, P. M. G.; Park, S. Y.; Lee, S.-W.; Choi, J. Differential Expression of Ribosomal Protein Gene, Gonadotrophin Releasing Hormone Gene and Balbiani Ring Protein Gene in Silver Nanoparticles Exposed *Chironomus Riparius*. *Aquat. Toxicol.* **2011**, *101* (1), 31–37. <https://doi.org/10.1016/j.aquatox.2010.08.013>.
- (36) Lee, S.-W.; Kim, S.-M.; Choi, J. Genotoxicity and Ecotoxicity Assays Using the Freshwater Crustacean *Daphnia Magna* and the Larva of the Aquatic Midge *Chironomus Riparius* to Screen the Ecological Risks of Nanoparticle Exposure. *Environ. Toxicol. Pharmacol.* **2009**, *28* (1), 86–91. <https://doi.org/10.1016/j.etap.2009.03.001>.
- (37) Doiangün, M.; Hang, M. N.; Troiano, J. M.; McGeachy, A. C.; Melby, E. S.; Pedersen, J. A.; Hamers, R. J.; Geiger, F. M. Alteration of Membrane Compositional Asymmetry by  $\text{LiCoO}_2$  Nanosheets. *ACS Nano* **2015**, *9* (9), 8755–8765. <https://doi.org/10.1021/acsnano.5b01440>.
- (38) Hang, M. N.; Gunsolus, I. L.; Wayland, H.; Melby, E. S.; Mensch, A. C.; Hurley, K. R.; Pedersen, J. A.; Haynes, C. L.; Hamers, R. J. Impact of Nanoscale Lithium Nickel Manganese Cobalt Oxide (NMC) on the Bacterium *Shewanella Oneidensis* MR-1. *Chem. Mater.* **2016**, *28* (4), 1092–1100. <https://doi.org/10.1021/acs.chemmater.5b04505>.
- (39) Livak, K. J.; Schmittgen, T. D. Analysis of Relative Gene Expression Data Using Real-Time Quantitative PCR and the  $2^{-\Delta\Delta\text{CT}}$  Method. *Methods* **2001**, *25* (4), 402–408. <https://doi.org/10.1006/meth.2001.1262>.

- (40) Markus, A. A.; Parsons, J. R.; Roex, E. W. M.; de Voogt, P.; Laane, R. W. P. M. Modeling Aggregation and Sedimentation of Nanoparticles in the Aquatic Environment. *Sci. Total Environ.* **2015**, 506–507, 323–329. <https://doi.org/10.1016/J.SCITOTENV.2014.11.056>.
- (41) Brunelli, A.; Pojana, G.; Callegaro, S.; Marcomini, A. Agglomeration and Sedimentation of Titanium Dioxide Nanoparticles (n-TiO<sub>2</sub>) in Synthetic and Real Waters. *J. Nanoparticle Res.* **2013**, 15 (6), 1684. <https://doi.org/10.1007/s11051-013-1684-4>.
- (42) Baalousha, M. Aggregation and Disaggregation of Iron Oxide Nanoparticles: Influence of Particle Concentration, PH and Natural Organic Matter. *Sci. Total Environ.* **2009**, 407 (6), 2093–2101. <https://doi.org/10.1016/J.SCITOTENV.2008.11.022>.
- (43) Baalousha, M. Effect of Nanomaterial and Media Physicochemical Properties on Nanomaterial Aggregation Kinetics. *NanoImpact* **2017**, 6, 55–68. <https://doi.org/10.1016/J.IMPACT.2016.10.005>.
- (44) Milani, D.; Reynoldson, T. B.; Borgmann, U.; Kolasa, J. The Relative Sensitivity of Four Benthic Invertebrates to Metals in Spiked-Sediment Exposures and Application to Contaminated Field Sediment. In *Environmental Toxicology and Chemistry*; John Wiley & Sons, Ltd, 2003; Vol. 22, pp 845–854. [https://doi.org/10.1897/1551-5028\(2003\)022<0845:TRSOFB>2.0.CO;2](https://doi.org/10.1897/1551-5028(2003)022<0845:TRSOFB>2.0.CO;2).
- (45) Thorgersen, M. P.; Downs, D. M. Cobalt Targets Multiple Metabolic Processes in Salmonella Enterica. *J. Bacteriol.* **2007**, 189 (21), 7774–7781. <https://doi.org/10.1128/JB.00962-07>.

- (46) Misra, M.; Rodriguez, R. E.; Kasprzak, K. S. Nickel Induced Lipid Peroxidation in the Rat: Correlation with Nickel Effect on Antioxidant Defense Systems. *Toxicology* **1990**, *64* (1), 1–17. [https://doi.org/10.1016/0300-483X\(90\)90095-X](https://doi.org/10.1016/0300-483X(90)90095-X).
- (47) Alarifi, S.; Ali, D.; Y, A. O. S.; Ahamed, M.; Siddiqui, M. A.; Al-Khedhairi, A. A. Oxidative Stress Contributes to Cobalt Oxide Nanoparticles-Induced Cytotoxicity and DNA Damage in Human Hepatocarcinoma Cells. *Int. J. Nanomedicine* **2013**, *8*, 189–199. <https://doi.org/10.2147/IJN.S37924>.
- (48) Ahamed, M.; Ali, D.; Alhadlaq, H. A.; Akhtar, M. J. Nickel Oxide Nanoparticles Exert Cytotoxicity via Oxidative Stress and Induce Apoptotic Response in Human Liver Cells (HepG2). *Chemosphere* **2013**, *93* (10), 2514–2522. <https://doi.org/10.1016/j.chemosphere.2013.09.047>.
- (49) Casalino, E.; Calzaretti, G.; Sblano, C.; Landriscina, C. Molecular Inhibitory Mechanisms of Antioxidant Enzymes in Rat Liver and Kidney by Cadmium. *Toxicology* **2002**, *179* (1–2), 37–50. [https://doi.org/10.1016/S0300-483X\(02\)00245-7](https://doi.org/10.1016/S0300-483X(02)00245-7).
- (50) Covaliu, C. I.; Matei, C.; Litescu, S.; Eremia, S. A.-M.; Stanica, N.; Diamandescu, L.; Ianculescu, A.; Jitaru, I.; Berger, D. Radical Scavenger Properties of Oxide Nanoparticles Stabilized with Biopolymer Matrix. *Mater. Plast.* **2010**, *47* (1).
- (51) Kim, B. M.; Choi, B. S.; Lee, K. W.; Ki, J. S.; Kim, I. C.; Choi, I. Y.; Rhee, J. S.; Lee, J. S. Expression Profile Analysis of Antioxidative Stress and Developmental Pathway Genes in the Manganese-Exposed Intertidal Copepod *Tigriopus Japonicus* with 6K Oligochip. *Chemosphere* **2013**, *92* (9), 1214–1223. <https://doi.org/10.1016/j.chemosphere.2013.04.047>.

- (52) Maines, M. D. Evidence for the Catabolism of Polychlorinated Biphenyl-Induced Cytochrome P-448 by Microsomal Heme Oxygenase, and the Inhibition of Delta-Aminolevulinate Dehydratase by Polychlorinated Biphenyls. *J. Exp. Med.* **1976**, *144* (6), 1509–1519.
- (53) Maines, M. D.; Sinclair, P. Cobalt Regulation of Heme Synthesis and Degradation in Avian Embryo Liver Cell Culture. *J. Biol. Chem.* **1977**, *252* (1), 219–223.
- (54) Ranquet, C.; Ollagnier-de-Choudens, S.; Loiseau, L.; Barras, F.; Fontecave, M. Cobalt Stress in Escherichia Coli. The Effect on the Iron-Sulfur Proteins. *J. Biol. Chem.* **2007**, *282* (42), 30442–30451. <https://doi.org/10.1074/jbc.M702519200>.
- (55) Yasukochi, Y.; Nakamura, M.; Minakami, S. Effect of Cobalt on the Synthesis and Degradation of Hepatic Catalase in Vivo. *Biochem. J.* **1974**, *144* (3), 455–464.
- (56) Kubrak, O. I.; Husak, V. V.; Rovenko, B. M.; Storey, J. M.; Storey, K. B.; Lushchak, V. I. Cobalt-Induced Oxidative Stress in Brain, Liver and Kidney of Goldfish Carassius Auratus. *Chemosphere* **2011**, *85* (6), 983–989. <https://doi.org/10.1016/j.chemosphere.2011.06.078>.
- (57) Walshe, B. Y. B. M. THE FUNCTION OF HAEMOGLOBIN IN TANYTARSUS (CHIRONOMIDAE). *J. Exp. Biol.* **1947**, *24* (3–4), 343–351.
- (58) Peijnenburg, W. J. G. M.; Baalousha, M.; Chen, J.; Chaudry, Q.; Von Der Kammer, F.; Kuhlbusch, T. A. J.; Lead, J.; Nickel, C.; Quik, J. T. K.; Renker, M.; et al. A Review of the Properties and Processes Determining the Fate of Engineered Nanomaterials in the Aquatic Environment. *Crit. Rev. Environ. Sci. Technol.* **2015**, *45* (19), 2084–2134. <https://doi.org/10.1080/10643389.2015.1010430>.

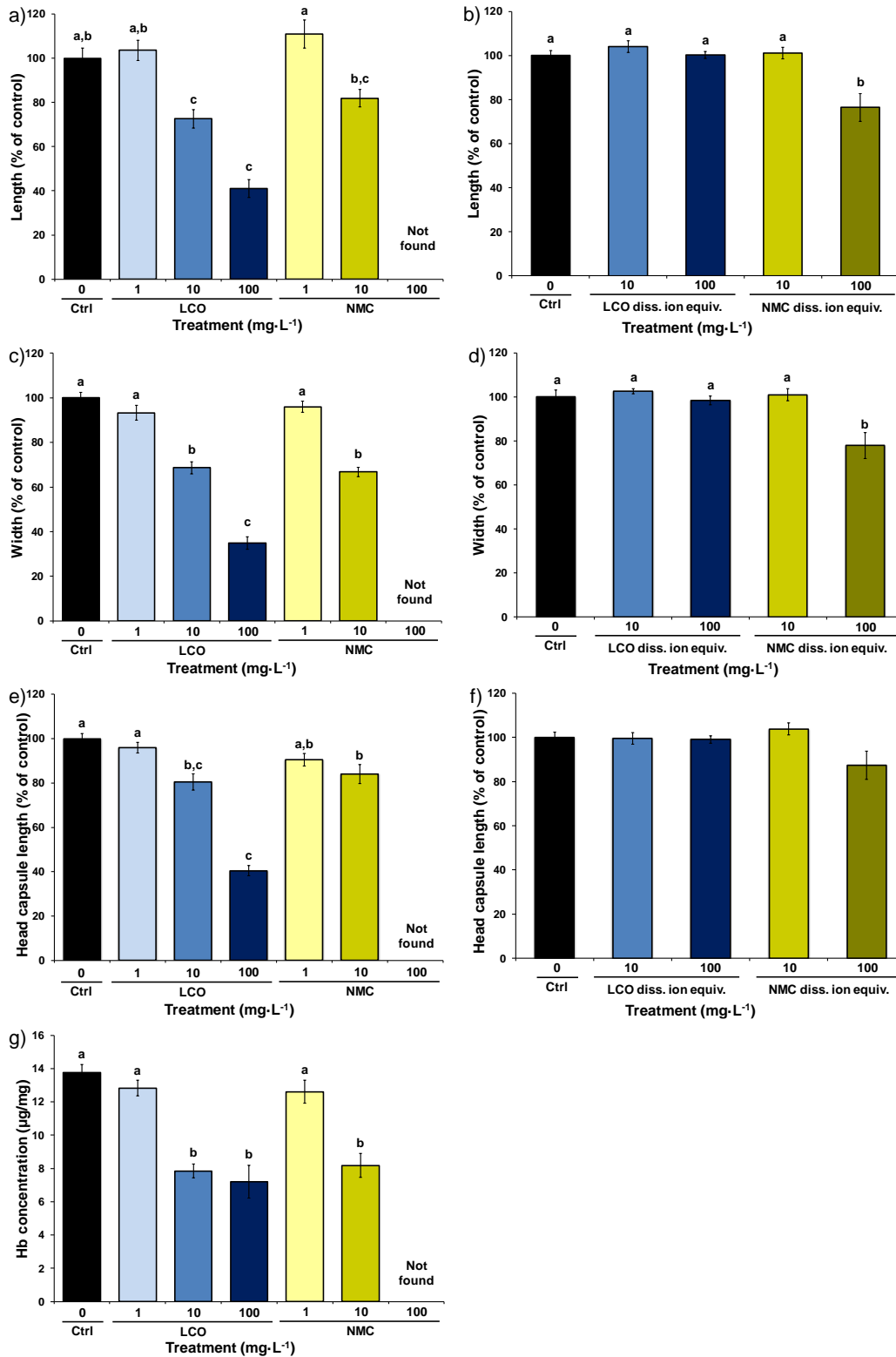
- (59) Ptatscheck, C.; Putzki, H.; Traunspurger, W. Impact of Deposit-Feeding Chironomid Larvae ( *Chironomus Riparius* ) on Meiofauna and Protozoans. *Freshw. Sci.* **2017**, *36* (4), 796–804. <https://doi.org/10.1086/694461>.
- (60) Rasmussen, J. B. Comparison of Gut Contents and Assimilation Efficiency of Fourth Instar Larvae of Two Coexisting Chironomids, *Chironomus Riparius* Meigen and *Glyptotendipes Paripes* (Edwards). *Can. J. Zool.* **1984**, *62* (6), 1022–1026. <https://doi.org/10.1139/z84-145>.
- (61) Waissi, G. C.; Bold, S.; Pakarinen, K.; Akkanen, J.; Leppänen, M. T.; Petersen, E. J.; Kukkonen, J. V. K. *Chironomus Riparius* Exposure to Fullerene-Contaminated Sediment Results in Oxidative Stress and May Impact Life Cycle Parameters. *J. Hazard. Mater.* **2017**, *322*, 301–309. <https://doi.org/10.1016/j.jhazmat.2016.04.015>.
- (62) Chaurand, P.; Liu, W.; Borschneck, D.; Levard, C.; Auffan, M.; Paul, E.; Collin, B.; Kieffer, I.; Lanone, S.; Rose, J.; et al. Multi-Scale X-Ray Computed Tomography to Detect and Localize Metal-Based Nanomaterials in Lung Tissues of in Vivo Exposed Mice. *Sci. Rep.* **2018**, *8* (1), 4408. <https://doi.org/10.1038/s41598-018-21862-4>.
- (63) Cagno, S.; Brede, D. A.; Nuyts, G.; Vanmeert, F.; Pacureanu, A.; Tucoulou, R.; Cloetens, P.; Falkenberg, G.; Janssens, K.; Salbu, B.; et al. Combined Computed Nanotomography and Nanoscopic X-Ray Fluorescence Imaging of Cobalt Nanoparticles in *Caenorhabditis Elegans*. *Anal. Chem.* **2017**, *89* (21), 11435–11442. <https://doi.org/10.1021/acs.analchem.7b02554>.
- (64) Cross, R. K.; Tyler, C.; Galloway, T. S. Transformations That Affect Fate, Form and Bioavailability of Inorganic Nanoparticles in Aquatic Sediments. *Environ. Chem.* **2015**, *12* (6), 627. <https://doi.org/10.1071/EN14273>.

- (65) Cornelis, G.; Pang, L.; Doolette, C.; Kirby, J. K.; McLaughlin, M. J. Transport of Silver Nanoparticles in Saturated Columns of Natural Soils. *Sci. Total Environ.* **2013**, *463–464*, 120–130. <https://doi.org/10.1016/J.SCITOTENV.2013.05.089>.
- (66) Péry, A. R. R.; Mons, R.; Flammarion, P.; Lagadic, L.; Garric, J. A Modeling Approach to Link Food Availability, Growth, Emergence, and Reproduction for the Midge *Chironomus Riparius*. *Environ. Toxicol. Chem.* **2002**, *21* (11), 2507–2513. <https://doi.org/10.1002/etc.5620211133>.
- (67) Azevedo-Pereira, H. M. V. S.; Soares, A. M. V. M. Effects of Mercury on Growth, Emergence, and Behavior of *Chironomus Riparius* Meigen (Diptera: Chironomidae). *Arch. Environ. Contam. Toxicol.* **2010**, *59* (2), 216–224. <https://doi.org/10.1007/s00244-010-9482-9>.
- (68) Bour, A.; Mouchet, F.; Cadarsi, S.; Silvestre, J.; Baqué, D.; Gauthier, L.; Pinelli, E. CeO<sub>2</sub> Nanoparticle Fate in Environmental Conditions and Toxicity on a Freshwater Predator Species: A Microcosm Study. *Environ. Sci. Pollut. Res.* **2017**, *24* (20), 17081–17089. <https://doi.org/10.1007/s11356-017-9346-1>.
- (69) Lowry, G. V.; Espinasse, B. P.; Badireddy, A. R.; Richardson, C. J.; Reinsch, B. C.; Bryant, L. D.; Bone, A. J.; Deonarine, A.; Chae, S.; Therezien, M.; et al. Long-Term Transformation and Fate of Manufactured Ag Nanoparticles in a Simulated Large Scale Freshwater Emergent Wetland. *Environ. Sci. Technol.* **2012**, *46* (13), 7027–7036. <https://doi.org/10.1021/es204608d>.
- (70) Koelmans, A. A.; Quik, J. T. K.; Velzeboer, I. Lake Retention of Manufactured Nanoparticles. *Environ. Pollut.* **2015**, *196*, 171–175. <https://doi.org/10.1016/j.envpol.2014.09.025>.

- (71) Gondikas, A. P.; Kammer, F. von der; Reed, R. B.; Wagner, S.; Ranville, J. F.; Hofmann, T. Release of TiO<sub>2</sub> Nanoparticles from Sunscreens into Surface Waters: A One-Year Survey at the Old Danube Recreational Lake. *Environ. Sci. Technol.* **2014**, *48* (10), 5415–5422. <https://doi.org/10.1021/es405596y>.
- (72) Hendren, C. O.; Mesnard, X.; Dröge, J.; Wiesner, M. R. Estimating Production Data for Five Engineered Nanomaterials as a Basis for Exposure Assessment. *Environ. Sci. Technol.* **2011**, *45* (7), 2562–2569. <https://doi.org/10.1021/es103300g>.
- (73) Gottschalk, F.; Sun, T.; Nowack, B. Environmental Concentrations of Engineered Nanomaterials: Review of Modeling and Analytical Studies. *Environ. Pollut.* **2013**, *181*, 287–300. <https://doi.org/10.1016/j.envpol.2013.06.003>.
- (74) Gottschalk, F.; Sun, T.; Nowack, B. Environmental Concentrations of Engineered Nanomaterials: Review of Modeling and Analytical Studies. *Environ. Pollut.* **2013**, *181*, 287–300. <https://doi.org/10.1016/j.envpol.2013.06.003>.

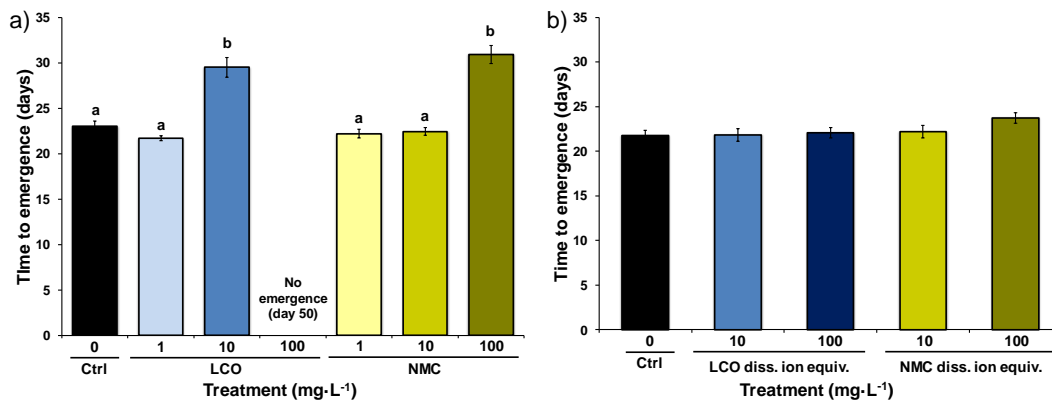
## Figures

Figure 1. Differences in *C. riparius* larval size and Hb after 7 d exposure



**Figure 1. Differences in *C. riparius* larval size and Hb after 7 d exposure.** LCO and NMC particle exposure induces significant impacts on larval size and Hb levels on exposure day 7. Size data (percent of control) for particle and ion exposed larvae. a) Particle-exposed larvae lengths, b) ion-exposed larvae lengths, c) particle-exposed larvae width, d) ion-exposed larvae width, e) particle-exposed larvae head capsule length, f) ion-exposed larvae head capsule length. Columns with different letters differ significantly ( $p < 0.05$ ) by Kruskal-Wallis (panels a, b, e, f) or one-way nested ANOVA with Tukey post-hoc tests (panels c and d). g) Hb concentration calculated from green absorbance for all larvae harvested a day 7. Columns with different letters indicate a significant difference ( $p < 0.05$ ) by one-way nested ANOVA with Tukey post-hoc tests. Error bars represent SEM.

**Figure 2. Differences in *C. riparius* time to emergence as adult flies**



**Figure 2. Differences in *C. riparius* time to emergence as adult flies.** Time to emergence for a) control and LCO and NMC particle-exposed and b) control and LCO and NMC ion exposed animals. Columns with different letters differ significantly ( $p < 0.05$ ) by Kaplan-Meier non-parametric analysis. Error bars represent SEM.

**Figure 3. Differences in *C. riparius* larval gene expression after 7 day exposure**

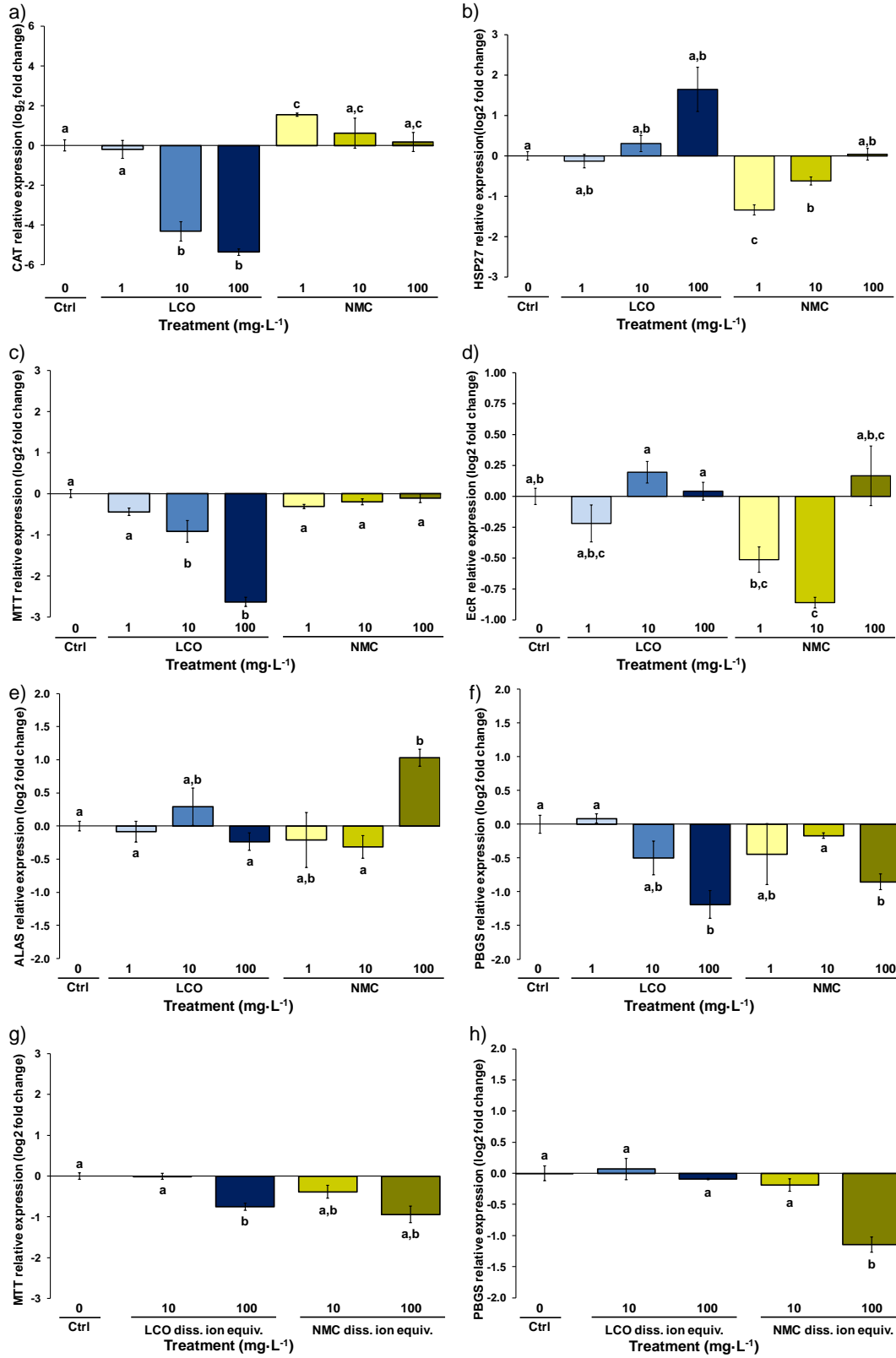


**Figure 3.** Differences in *C. riparius* larval gene expression after 7 d exposure. Log<sub>2</sub> fold change values for LCO and NMC particle-exposed larvae harvested at day 7. Results are shown for a) *CAT*, b) *HSP27*, c) *MTT*, d) *EcR*, e) *ALAS*, and f) *PBGS*. Results for ion-exposed animals are also shown for g) *MTT* and h) *PBGS*. Columns with different letters differ significantly ( $p < 0.05$ ) by one-way Welch ANOVA with Dunnett's T3 post-hoc comparisons. Error bars represent SEM.

**Figure 4. Proposed adverse outcome pathway for *C. riparius* LCO and NMC exposure**

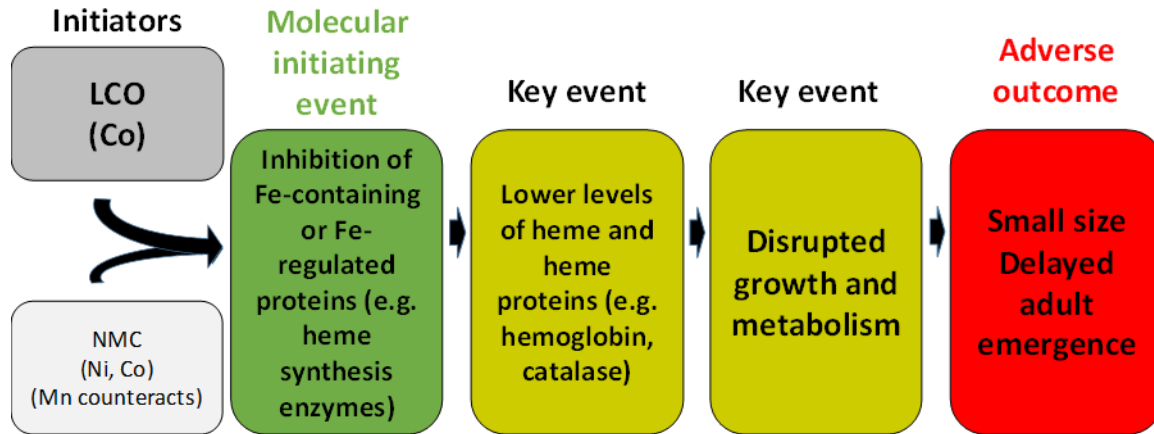


**Figure 4. Proposed adverse outcome pathway for *C. riparius* LCO and NMC exposure.** A proposed adverse outcome pathway for *C. riparius* larval exposure to LCO and NMC showing inhibition of iron-containing or iron-regulated proteins by cobalt as the molecular initiating event, resulting in lowered levels of heme and heme proteins, which in turn causes disruption to normal growth and metabolism, culminating in the adverse outcome of smaller size and delayed emergence as adult flies.

## SUPPORTING INFORMATION

### Supporting Information for:

Settling of next-generation complex metal oxide nanomaterials causes significant impacts on growth and development in model benthic invertebrate *Chironomus riparius*

Nicholas J. Niemuth, Becky J. Curtis, Mimi N. Hang, Miranda J. Gallagher, D. Howard Fairbrother, Robert J. Hamers, Rebecca D. Klaper\*

Pages: 19

Tables: 2

Figures: 6

### Supporting Methods

#### *LCO and NMC stoichiometry characterization*

To characterize the stoichiometry of these materials, a PerkinElmer 4300 Dual View Inductively Coupled Plasma Optical Emission Spectrometer (ICP-OES) was used for elemental analysis. The synthesized nanomaterials were dissolved in freshly prepared *aqua regia* (3:1 v/v mixture consisting of 37% v/v HCl and 70% v/v HNO<sub>3</sub>) for 2 h and diluted with ultrapure water before analysis. All standards were prepared using certified reference materials from Sigma Aldrich. The ion concentrations were measured using three analytical replicates to give LCO with Li/Co =  $1.41 \pm 0.03$  and NMC with Li/Ni =  $1.37 \pm 0.01$ , Ni/Mn =  $0.95 \pm 0.01$ , Ni/Co =  $0.99 \pm 0.01$ . This indicates that LCO is over lithiated by approximately 41%. NMC is partially lithiated to an

extent of ~45 % and the ratio of Ni:Co:Mn is approximately 1:1:1. As previously mentioned, the degree of lithiation is not controlled for using the flux growth method. Moreover, lithium is not known to be particularly toxic to organisms.<sup>1,2</sup>

### ***LCO and NMC crystal phase characterization***

A Bruker D8 Advance Powder X-ray Diffractometer (P-XRD) with a Cu K $\alpha$  source was used to analyze the crystal phase of LCO and NMC nanomaterials. First, the synthesized powder (~15 mg) was deposited onto a zero diffraction plate (SiO<sub>2</sub> from MTI Corp) and then smoothed out with a spatula. No other attempt was made to lower the background to prevent loss of material during this characterization step. The resulting spectra of LCO and NMC nanomaterials (Fig S1) show that both materials can be roughly indexed to a R-3m space group.<sup>3,4</sup> Broad reflections can be attributed to residual disorder of the nanomaterials due to its synthesis at low temperatures and due to the small thickness of the nanosheets.

### ***LCO and NMC morphology characterization***

To assess the morphology of the synthesized materials, a Leo Supra55 VP scanning electron microscope (SEM) was used. A methanolic solution of LCO or NMC was prepared and dropcast onto boron-doped silicon wafers. Samples were imaged using a standard in-lens detector and 1kV incident electron energy. Figure S2a and S2b are SEM images of the synthesized material. A large field-of-view was selected to show the overall morphological appearance of the particles. The SEM images reveal ensembles of nanomaterials clustered in different directions together due to drying effects. The clustering shows particles stacked in ways which reveal their edge and basal dimensions. SEM images here (Fig S2) and in previous studies<sup>5</sup> show LCO and NMC

nanosheets with diameters < 100 nm and thickness < 5nm. Previous characterization of similar particles using transmission electron microscopy further shows that these particles are flake-like in nature.<sup>1,6</sup>

### ***ICP-MS analysis of released ions***

At 2, 4, and 7 d time points, 20 mL of media was drawn carefully from the water column in control and exposure beakers during routine water exchanges (N=3 for each datapoint). To remove suspended nanoparticles, a series of centrifugation steps were carried out. First, 14 ml of media from each control and exposure beaker was centrifuged at 5000 g and 4 °C for 30 minutes. Second, 8 ml of the resulting supernatant was spun at 50,000 RPM and 4 °C for 2 hours in a Beckman-Coulter ultracentrifuge using a 70.1 Ti fixed angle rotor. Finally, 7 ml of the supernatant was removed from each ultracentrifuge tube and split into aliquots of 3.5 ml in two acid washed conical tubes for ICP-MS analysis.

### ***Hemoglobin absorbance measurement***

As hemoglobin (Hb) exhibits strong absorption specifically in the green portion of the visible spectrum (495-570 nm), it is possible to use green light absorbance as an approximation of the relative amount of Hb present, as previously demonstrated in chironomids.<sup>7,8</sup>

Images of flash-frozen larvae were processed using the Fiji ImageJ processing package<sup>9</sup> and split into red, blue, and green components using the Split Channels option under Color in the Image menu. The Polygon selection tool was then used to outline the organism or a background

reference in the green image, and the average pixel intensity determined using the Measure option under the Analyze menu.

Relative Hb concentration was determined from absorbance values using the Beer-Lambert equation:

$$A = -\log_{10}(I/I_0) = \varepsilon \cdot c \cdot L \quad (\text{S1})$$

$$\frac{\log_{10}(I_0/I)}{L} = \varepsilon \cdot c \quad (\text{S2})$$

$$\frac{\log_{10}(I_0/I)}{L \cdot \varepsilon} = c \quad (\text{S3})$$

Where A is absorbance,  $I_0$  is the incident light through the slide (i.e. background pixel intensity),  $I$  is the light transmitted through the organism (pixel intensity of the outlined organism), L is the path length (in this case the width of the organism),  $\varepsilon$  is the molar extinction coefficient for Hb, and c is the Hb concentration. The average  $\varepsilon$  for Hb in the green portion of the spectrum is on the order of  $4 \times 10^4 \text{ cm}^{-1} \text{ M}^{-1}$ .<sup>10</sup> The molecular weight of Hb used was  $64500 \text{ g mole}^{-1}$ .<sup>10</sup>

### ***Gene expression analysis***

Total RNA was extracted using the Direct-zol™ RNA MiniPrep kit (Zymo Research, Irvine, CA) following kit instructions for extraction with 200  $\mu\text{L}$  of Trizol reagent (Thermo Fisher Scientific, Waltham, MA) with on-column DNase treatment. The purity and quantity of isolated RNA for each sample was determined using a NanoDrop ND-1000 spectrophotometer (Thermo Fisher Scientific, Waltham, MA). For each sample, 100 ng of total RNA was transcribed into cDNA using the Applied Biosystems™ High-Capacity cDNA Reverse Transcription Kit (Thermo Fisher Scientific, Waltham, MA) 20  $\mu\text{L}$  reaction according to kit instructions.

### *Gene selection*

Metallothionein (*MTT*), was chosen for its ability to bind and sequester metals, and its role in promoting metal homeostasis and tolerance at the cellular level.<sup>11,12</sup> Genes chosen for their association with cellular activities that respond to and protect against oxidative stress include catalase (*CAT*), copper-zinc superoxide dismutase (*Cu-ZnSOD*), gamma-glutamylcystein synthase (*GCS*), glutathione s-transferase (*GST*), and manganese superoxide dismutase (*MnSOD*).<sup>13-17</sup> Genes associated with general stressors, including heat shock and xenobiotic response, were also analyzed. Playing a vital role in the assurance of proper protein folding, heat shock protein 27 (*HSP27*) is one of a family of small HSPs regulated by environmental stressors including heat and cold shock as well as pollution.<sup>18</sup> Mitogen-activated protein kinase 38 (*p38*) is a signaling protein that plays a role in cellular responses to various environmental stressors.<sup>19,20</sup> Finally, ecdysone receptor (*EcR*), a nuclear receptor for ecdysteroids, was analyzed due to its importance in supporting normal growth, development, and larval molting.<sup>21</sup>

During the experiment, the color of larvae exposed to the nanomaterials changed from their normal red color to clear. Cobalt, present in both LCO and NMC, has been demonstrated to impact heme biosynthesis in avian liver cells.<sup>22,23</sup> *C. riparius* larvae contain substantial concentrations of heme-containing hemoglobin (Hb)<sup>7</sup>. For this reason, genes related to heme biosynthesis were selected for expression analysis based on their demonstrated response to cobalt exposure, as cobalt is a major component of both LCO and NMC. Aminolevulinic acid synthase (ALAS) catalyzes the first and rate-limiting enzymatic step in the synthesis of heme and other tetrapyrroles and has been shown to be inhibited by Co<sup>2+</sup> exposure in avian liver cells.<sup>23</sup>

Porphobilinogen synthase (PBGS) catalyzes the second step of tetrapyrrole synthesis, condensing two molecules of aminolevulinic acid into porphobilinogen, and has been shown to be inhibited by cobalt treatment in rat liver.<sup>22</sup> Heme oxygenase (HO) catalyzes the breakdown of heme into bilirubin and has been shown to be induced by cobalt exposure in rat liver.<sup>22</sup> In addition to gene expression analysis, Hb in larvae was measured colorimetrically to determine any inhibitory impact of ENM exposure on levels of this protein in larvae.

### *Primer design*

All primers were designed using the online PrimerQuest tool from Integrated DNA Technologies (IDT, Coralville, IA) selecting primers designed for qPCR with intercalating dyes. Primers were designed against mRNA sequences for genes available for *C. riparius* in the NCBI nucleotide database: *RPL13*, *EcR*, *MTT*, *CAT*, *Cu-ZnSOD*, *GCS*, *GST*, *MnSOD*, *HSP27*, *p38*.

For genes that were not annotated in the nucleotide database (*ALAS*, *PBGS*, *HO*), mRNA sequences for primer design were retrieved from the *C. riparius* transcriptome shotgun assembly (TSA) database by querying the TSA database with annotated protein sequences for each gene from other species using tblastn. For *ALAS*, the protein sequences for *ALAS* from *Gallus gallus*, *Dictyostelium discoideum*, *Mus musculus*, and *Homo sapiens* (NCBI Reference Sequences: CAA27223.1, XP\_641014.1, NP\_033783.1, NP\_001033057.1) were queried against the *C. riparius* TSA database, and all returned the *Chironomus riparius* CripIT02626 mRNA sequence (GenBank ID: KA177338.1) with 50 - 60% identity (68 – 76% similarity, e-values  $\leq 4e-123$ ). For *PBGS*, the protein sequences for *PBGS* from *Gallus gallus*, *Aedes aegypti*, and *Drosophila melanogaster* (NCBI Reference Sequences: NP\_001278335.1, XP\_001661237.1, NP\_648564.1)

were queried against the *C. riparius* TSA database, and all returned the *Chironomus riparius* CripIT11611 mRNA sequence (GenBank ID: KA186315.1) with 56 - 70% identity (71 – 83% similarity, e-values  $\leq 7e-137$ ). For *HO*, the protein sequences for HO from *Culex quinquefasciatus*, *Drosophila melanogaster*, and *Aedes albopictus* (NCBI Reference Sequences: XP\_001848782.1, NP\_524321.1, JAC09384.1) were queried against the *C. riparius* TSA database, and all returned the *Chironomus riparius* CripIT10970 mRNA sequence (GenBank ID: KA185674.1) with 50 - 58% identity (70 – 73% similarity, e-values  $\leq 1e-41$ ).

#### *qPCR assays*

Relative gene expression was quantified on an Applied Biosystems StepOne Plus RT-PCR machine (Thermo Fisher Scientific, Waltham, MA) using the iTaq Universal SYBR Green Supermix (Bio-Rad, Hercules, CA) for 20  $\mu$ L reactions. Samples were run in duplicate for each primer set. Fold change relative to control was calculated for each sample using the  $2^{-\Delta\Delta C_t}$  method<sup>24</sup> using RPL13 as housekeeping reference gene. Ribosomal protein L13 (RPL13) was chosen as a housekeeping gene as it had previously been demonstrated to be suitable for use as a housekeeping gene for *C. riparius* toxicity exposures.<sup>25</sup>

## Supporting References

- (1) Hang, M. N.; Gunsolus, I. L.; Wayland, H.; Melby, E. S.; Mensch, A. C.; Hurley, K. R.; Pedersen, J. A.; Haynes, C. L.; Hamers, R. J. Impact of Nanoscale Lithium Nickel Manganese Cobalt Oxide (NMC) on the Bacterium *Shewanella Oneidensis* MR-1. *Chem. Mater.* **2016**, *28* (4), 1092–1100. <https://doi.org/10.1021/acs.chemmater.5b04505>.
- (2) Emery, R.; Klopfer, D. C.; Skalski, J. R. *Incipient Toxicity of Lithium to Freshwater Organisms Representing a Salmonid Habitat*; Richland, WA (United States), 1981. <https://doi.org/10.2172/6453668>.
- (3) Okubo, M.; Hosono, E.; Kim, J.; Enomoto, M.; Kojima, N.; Kudo, T.; Zhou, H.; Honma, I. Nanosize Effect on High-Rate Li-Ion Intercalation in LiCoO<sub>2</sub> Electrode. *J. Am. Chem. Soc.* **2007**, *129* (23), 7444–7452. <https://doi.org/10.1021/ja0681927>.
- (4) Lu, Z.; MacNeil, D. D.; Dahn, J. R. Layered LiNi<sub>x</sub>Co<sub>1-2x</sub>Mn<sub>x</sub>O<sub>2</sub> Cathode Materials for Lithium-Ion Batteries. *Electrochem. Solid-State Lett.* **2001**, *4* (12), A200. <https://doi.org/10.1149/1.1413182>.
- (5) Bozich, J.; Hang, M.; Hamers, R.; Klaper, R. Core Chemistry Influences the Toxicity of Multicomponent Metal Oxide Nanomaterials, Lithium Nickel Manganese Cobalt Oxide, and Lithium Cobalt Oxide to *Daphnia Magna*. *Environ. Toxicol. Chem.* **2017**, *36* (9), 2493–2502. <https://doi.org/10.1002/etc.3791>.
- (6) Dołangün, M.; Hang, M. N.; Troiano, J. M.; McGeachy, A. C.; Melby, E. S.; Pedersen, J. A.; Hamers, R. J.; Geiger, F. M. Alteration of Membrane Compositional Asymmetry by LiCoO<sub>2</sub> Nanosheets. *ACS Nano* **2015**, *9* (9), 8755–8765. <https://doi.org/10.1021/acs.nano.5b01440>.

- (7) Ha, M. H.; Choi, J. Effects of Environmental Contaminants on Hemoglobin of Larvae of Aquatic Midge, *Chironomus Riparius* (Diptera: Chironomidae): A Potential Biomarker for Ecotoxicity Monitoring. *Chemosphere* **2008**, *71* (10), 1928–1936.  
<https://doi.org/10.1016/j.chemosphere.2008.01.018>.
- (8) Panis, L. I.; Goddeeris, B.; Verheyen, R. The Hemoglobin Concentration Of *Chironomus Cf. Plumosus* L. (Diptera: Chironomidae) Larvae from Two Lentic Habitats. *Netherlands J. Aquat. Ecol.* **1995**, *29* (1), 1–4. <https://doi.org/10.1007/BF02061785>.
- (9) Schindelin, J.; Arganda-Carreras, I.; Frise, E.; Kaynig, V.; Longair, M.; Pietzsch, T.; Preibisch, S.; Rueden, C.; Saalfeld, S.; Schmid, B.; et al. Fiji: An Open-Source Platform for Biological-Image Analysis. *Nat. Methods* **2012**, *9*, 676.
- (10) Robles, F. E.; Chowdhury, S.; Wax, A. Assessing Hemoglobin Concentration Using Spectroscopic Optical Coherence Tomography for Feasibility of Tissue Diagnostics. *Biomed. Opt. Express* **2010**, *1* (1), 310–317. <https://doi.org/10.1364/boe.1.000310/>.
- (11) Amiard, J. C.; Amiard-Triquet, C.; Barka, S.; Pellerin, J.; Rainbow, P. S. Metallothioneins in Aquatic Invertebrates: Their Role in Metal Detoxification and Their Use as Biomarkers. *Aquat. Toxicol.* **2006**, *76* (2), 160–202.  
<https://doi.org/10.1016/j.aquatox.2005.08.015>.
- (12) Oberdörster, G.; Kane, A. B.; Klaper, R. D.; Hurt, R. H. Nanotoxicology. *Casarett Doull's Toxicol. Basic Sci. Poisons. McGraw-Hill, New York* **2013**, 1189–1229.
- (13) Gopalakrishnan Nair, P. M.; Park, S. Y.; Choi, J. Expression of Catalase and Glutathione S-Transferase Genes in *Chironomus Riparius* on Exposure to Cadmium and Nonylphenol. **2011**. <https://doi.org/10.1016/j.cbpc.2011.07.008>.

- (14) Nair, P. M. G.; Park, S. Y.; Choi, J. Chemosphere Evaluation of the Effect of Silver Nanoparticles and Silver Ions Using Stress Responsive Gene Expression in *Chironomus Riparius*. *Chemosphere* **2013**, *92* (5), 592–599.  
<https://doi.org/10.1016/j.chemosphere.2013.03.060>.
- (15) Forcella, M.; Berra, E.; Giacchini, R.; Parenti, P. Antioxidant Defenses Preserve Membrane Transport Activity In *Chironomus Riparius* Larvae Exposed to Anoxia. *Arch. Insect Biochem. Physiol.* **2007**, *65* (4), 181–194. <https://doi.org/10.1002/arch.20197>.
- (16) Nair, P. M. G.; Choi, J. Identification, Characterization and Expression Profiles of *Chironomus Riparius* Glutathione S-Transferase (GST) Genes in Response to Cadmium and Silver Nanoparticles Exposure. *Aquat. Toxicol.* **2011**, *101* (3–4), 550–560.  
<https://doi.org/10.1016/j.aquatox.2010.12.006>.
- (17) Park, S.; Nair, P. M. G.; Choi, J. Comparative Biochemistry and Physiology , Part C Characterization and Expression of Superoxide Dismutase Genes in *Chironomus Riparius* ( Diptera , Chironomidae ) Larvae as a Potential Biomarker of Ecotoxicity. *Comp. Biochem. Physiol. Part C* **2012**, *156* (3–4), 187–194.  
<https://doi.org/10.1016/j.cbpc.2012.06.003>.
- (18) Martínez-paz, P.; Morales, M.; Martín, R. Characterization of the Small Heat Shock Protein Hsp27 Gene in *Chironomus Riparius* ( Diptera ) and Its Expression Profile in Response to Temperature Changes and Xenobiotic Exposures. **2014**, 529–540.  
<https://doi.org/10.1007/s12192-013-0479-y>.
- (19) Son, Y.; Cheong, Y.-K.; Kim, N.-H.; Chung, H.-T.; Kang, D. G.; Pae, H.-O. Mitogen-Activated Protein Kinases and Reactive Oxygen Species: How Can ROS Activate MAPK

- Pathways? *J. Signal Transduct.* **2011**, 2011, 792639.  
<https://doi.org/10.1155/2011/792639>.
- (20) Park, S.; Choi, J. Molecular Characterization and Expression Analysis of P38 MAPK Gene and Protein in Aquatic Midge , *Chironomus Riparius* ( Diptera : Chironomidae ), Exposed to Environmental Contaminants. *Arch. Environ. Contam. Toxicol.* **2017**, 72 (3), 428–438. <https://doi.org/10.1007/s00244-017-0366-0>.
- (21) Park, K.; Kwak, I. S. The Effect of Temperature Gradients on Endocrine Signaling and Antioxidant Gene Expression during *Chironomus Riparius* Development. *Sci. Total Environ.* **2014**, 470–471, 1003–1011. <https://doi.org/10.1016/j.scitotenv.2013.10.052>.
- (22) Maines, M. D. Evidence for the Catabolism of Polychlorinated Biphenyl-Induced Cytochrome P-448 by Microsomal Heme Oxygenase, and the Inhibition of Delta-Aminolevulinate Dehydratase by Polychlorinated Biphenyls. *J. Exp. Med.* **1976**, 144 (6), 1509–1519.
- (23) Maines, M. D.; Sinclair, P. Cobalt Regulation of Heme Synthesis and Degradation in Avian Embryo Liver Cell Culture. *J. Biol. Chem.* **1977**, 252 (1), 219–223.
- (24) Livak, K. J.; Schmittgen, T. D. Analysis of Relative Gene Expression Data Using Real-Time Quantitative PCR and the  $2^{-\Delta\Delta CT}$  Method. *Methods* **2001**, 25 (4), 402–408.  
<https://doi.org/10.1006/meth.2001.1262>.
- (25) Martínez-Guitarte, J. L.; Planelló, R.; Morcillo, G. Characterization and Expression during Development and under Environmental Stress of the Genes Encoding Ribosomal Proteins L11 and L13 in *Chironomus Riparius*. *Comp. Biochem. Physiol. - B Biochem. Mol. Biol.* **2007**, 147 (4), 590–596. <https://doi.org/10.1016/j.cbpb.2007.03.015>.

## Supporting Tables

Table S1.

Gene (Abbreviation)	Function	GenBank Accession #	Forward and Reverse Primer Sequences 5' => 3'
<b>Ribosomal protein L13 (RPL13)</b>	Ribosomal protein, Housekeeping gene	EF179386.1	Fwd CCG TTC AAT CAC AGA AGA CGA Rev AGC AGT ACG AGC AGC AAT AC
<b>Ecdysone receptor (EcR)</b>	Normal growth, development, molting	JX034568.1	Fwd GGT ATC AAG ACG GTT ACG AAC A Rev GAA ATT TGC CTC GTG CTC TTG
<b>Metallothionein (MTT)</b>	Cellular metal homeostasis and tolerance	HQ260607.1	Fwd AGG ATC AAT CTT GCG GTC AA Rev CAG CAT TCA TCC TTG CTT CC
<b>Catalase (CAT)</b>	Oxidative damage protection	JL641904.1	Fwd ACG TGA CTT ACA AGG ACC ATA C Rev AAA GAC GGC TGC TTG ACT AA
<b>Copper-zinc superoxide dismutase (Cu-ZnSOD)</b>	Transform ROS, oxidative stress protection	JQ342170.1	Fwd GAT GTG CAG ATA AGT GAG GTA GAT Rev CGC TTC TGT CAC TAC TGG ATA C
<b>Gamma-glutamylcystein synthase (GCS)</b>	Oxidative damage protection	JQ762262.1	Fwd GGC GCA ACA TAT TGC TCA TTT A Rev GAT CGG TCT CTT CCT CAT CAT TT
<b>Glutathione s-transferase (GST)</b>	Oxidative stress management and detoxification	EZ966129.1	Fwd TGT GCT GAC GGA ATC AAG AG Rev TCA ACA AGG GCA CGT TTC T
<b>Manganese superoxide dismutase (MnSOD)</b>	Transform ROS, oxidative stress protection	JQ342169.1	Fwd CAT CCG TTC GCA CTA AGG TAA Rev GCT CCA TGA TTT CAC GAC AAA C
<b>Heat shock protein 27 (HSP27)</b>	Heat and cold shock protection	KC495957.1	Fwd TCC TAC TTT GTG GAG AGA CAT AGA Rev GTC GTC GCC ATG AAG GAA TTA
<b>Mitogen-activated protein kinase p38 (p38)</b>	Heat and osmotic shock protection	JX512644.1	Fwd GAC ACA ACG ACT GAC TGA TGA A Rev TAT GAA TGA CTC CAG CGG AAT G
<b>Aminolevulinic acid synthase (ALAS)</b>	Tetrapyrrole precursor synthesis	KA177338.1	Fwd CTC ACT TAC GCG AAC TCA TCT C Rev GAC AGA CAG CAG CAG TCA TAC
<b>Porphobilinogen synthase (PGBS)</b>	Tetrapyrrole precursor synthesis	KA186315.1	Fwd TGG CCA TTG TGG GAT CAT T Rev GTG CTC CAT GAC GGA CAT ATT
<b>Heme oxygenase (HO)</b>	Heme degradation	KA185674.1	Fwd AGA GAA TGT GCC AGC ATC AG Rev CTT TCT CGA GGC TTA TAC GTC TTT

**Table S2.**

ENM	$\zeta$ -potential (mV)	Electrophoretic mobility ( $\mu\text{m}\cdot\text{cm}\cdot\text{Vs}^{-1}$ )
LCO (1 mg·L <sup>-1</sup> )	-16.33 ± 1.46	-1.28 ± 0.11
LCO (10 mg·L <sup>-1</sup> )	-7.74 ± 1.10	-0.61 ± 0.09
LCO (100 mg·L <sup>-1</sup> )	0.52 ± 0.17	0.04 ± 0.01
NMC (1 mg·L <sup>-1</sup> )	-17.73 ± 0.93	-1.39 ± 0.07
NMC (10 mg·L <sup>-1</sup> )	-6.07 ± 0.89	-0.48 ± 0.07
NMC (100 mg·L <sup>-1</sup> )	1.59 ± 0.17	0.12 ± 0.01

## Supporting Figures

**Figure S1: XRD of LCO and NMC**

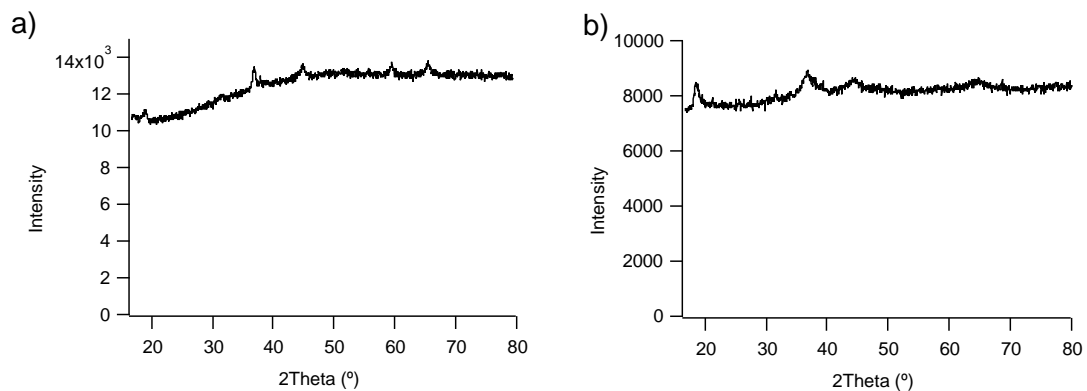


**Fig S1:** XRD of a) LCO and b) NMC.

**Figure S2: SEM of LCO and NMC**

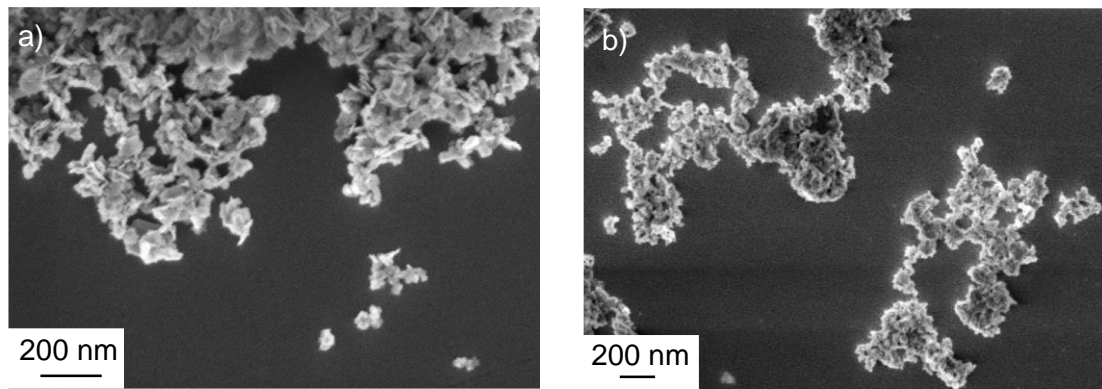


**Fig S2:** SEM of a) LCO and b) NMC.

**Figure S3. Disappearance of LCO and NMC from water column over 7 d**

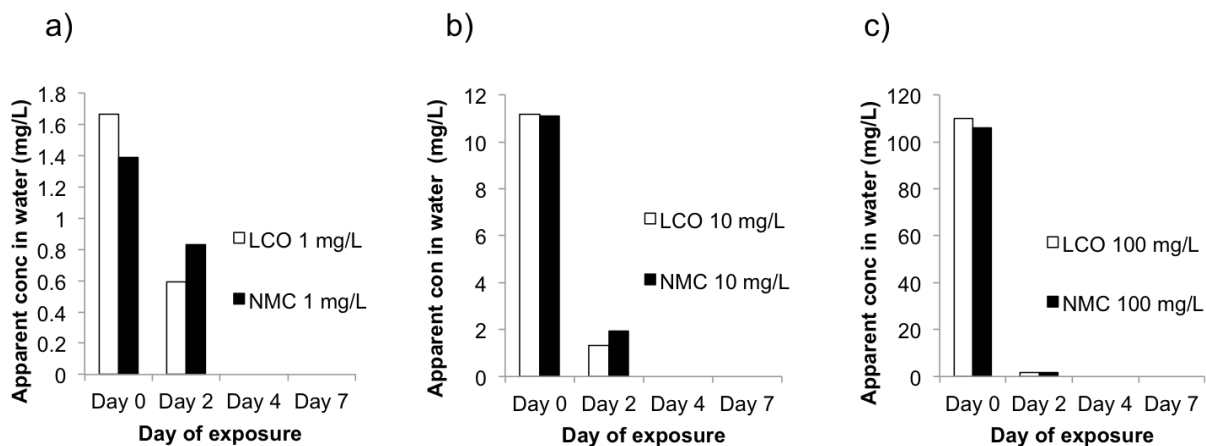


**Fig S3. Disappearance of LCO and NMC from water column over 7 d.** LCO (white bars) and NMC (black bars) as measured by absorbance at 600 nm at initial dosing, 2, 4, and 7 d for a) 1  $\text{mg}\cdot\text{L}^{-1}$ , b) 10  $\text{mg}\cdot\text{L}^{-1}$ , and c) 100  $\text{mg}\cdot\text{L}^{-1}$  exposure concentrations.

**Figure S4. ICP-MS quantification of ions released into media**

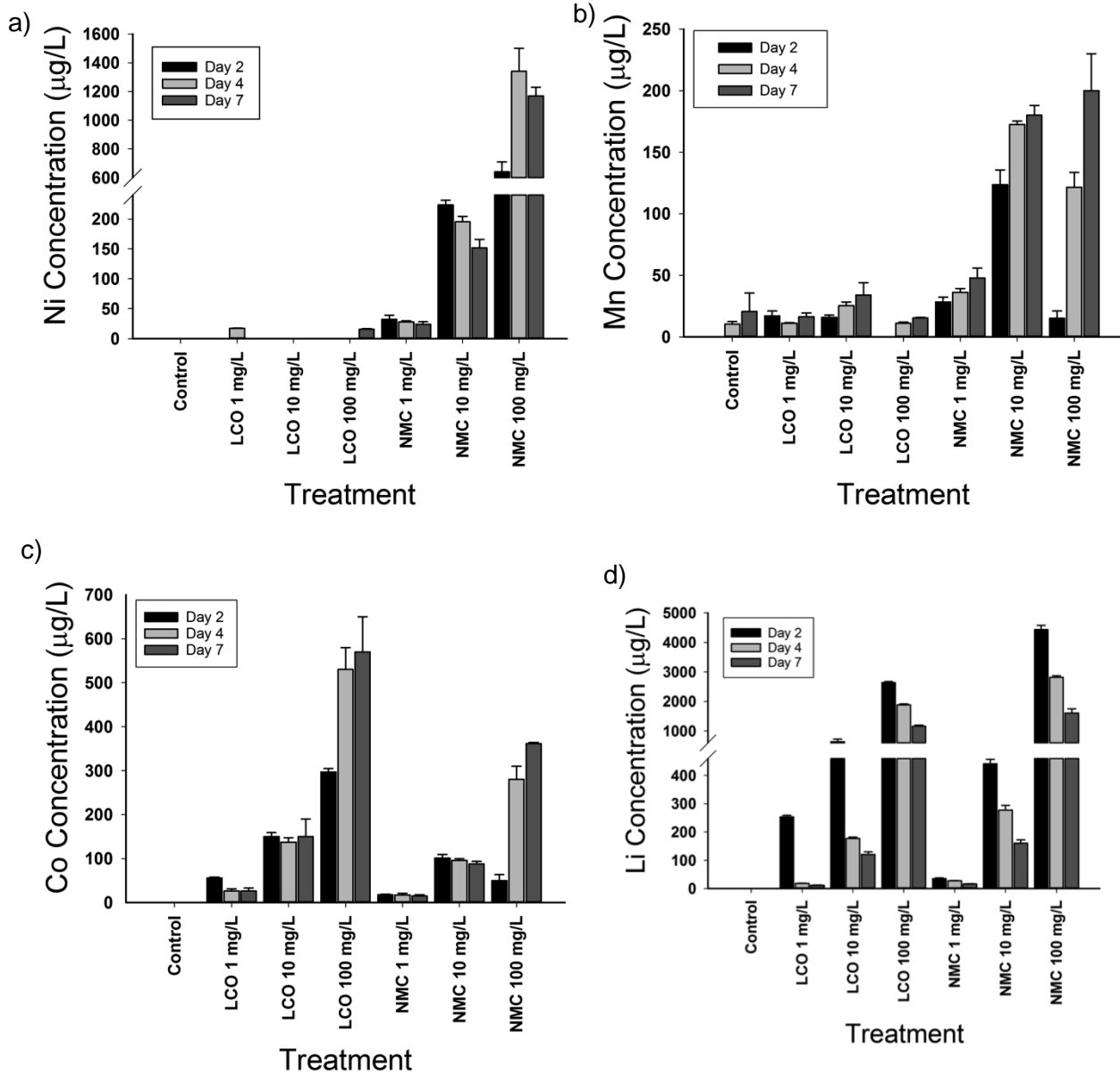


**Fig S4. ICP-MS quantification of ions released into media over 7 d.** Concentrations of dissolved ions released into media on days 2, 4, and 7 for LCO and NMC exposures. a) Nickel, b) Manganese, c) Cobalt, d) Lithium as determined by ICP-MS. Error bars represent SD.

**Figure S5. Dissolved vs settled material by metal**

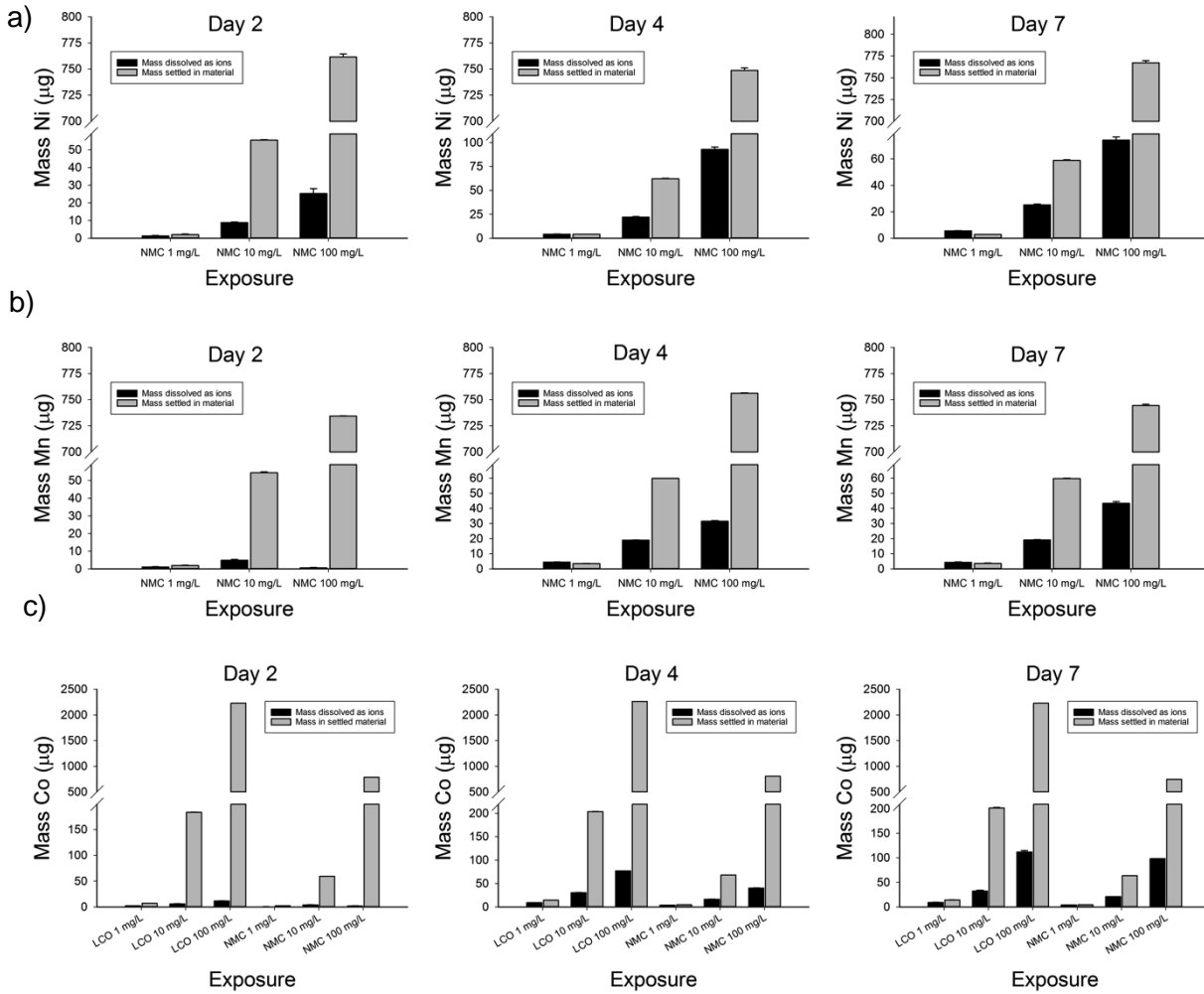


**Fig S5. Dissolved vs settled material by metal.** Mass of material dissolved (black bars) versus settled (gray bars) by metal on days 2, 4, and 7 of each exposure for a) Ni, b) Mn, c) Co.

**Figure S6. Images of control and LCO 100 mg·L<sup>-1</sup> larvae at 7d.**

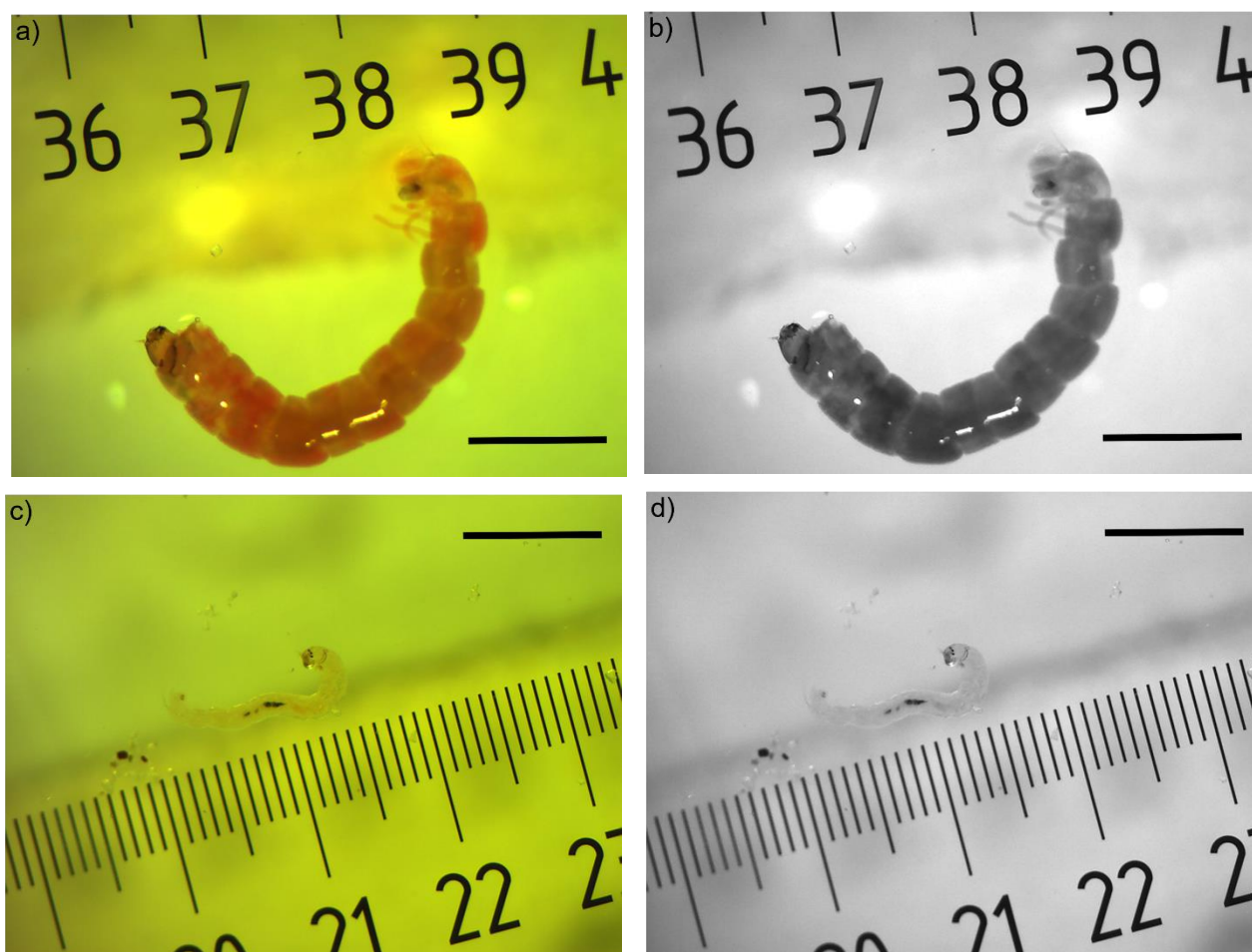


**Fig S6. Representative images of control and LCO 100 mg·L<sup>-1</sup> larvae at 7 d.** Representative a) color and b) green channel grayscale images for a control larva and c) color and d) green channel grayscale images for a larva exposed to 100 mg·L<sup>-1</sup> LCO.

**CHAPTER III:**  
**PROTEIN FE-S CENTERS AS A MOLECULAR TARGET OF TOXICITY OF A  
COMPLEX TRANSITION METAL OXIDE NANOMATERIAL WITH DOWNSTREAM  
IMPACTS ON METABOLISM AND GROWTH**

**Published in:**

American Chemical Society, *Environmental Science & Technology*

DOI: 10.1021/acs.est.0c04779

Nicholas J Niemuth<sup>1</sup>, Yonqian Zhang<sup>2</sup>, Aurash A Mohaimani<sup>1</sup>, Angela Schmoltdt<sup>1</sup>, Elizabeth D  
Laudadio<sup>2</sup>, Robert J Hamers<sup>2</sup>, Rebecca D Klaper<sup>1\*</sup>

<sup>1</sup> School of Freshwater Sciences, University of Wisconsin-Milwaukee, 600 E Greenfield Ave.,  
Milwaukee, WI 53204

<sup>2</sup> Department of Chemistry, University of Wisconsin-Madison, 1101 University Ave., Madison,  
WI 53706

\* Corresponding author: rklaper@uwm.edu

*(Received 17 July 2020, Accepted 23 October 2020)*

## Abstract

Oxidative stress is frequently identified as a mechanism of toxicity of nanomaterials. However, rarely have the specific underlying molecular targets responsible for these impacts been identified. We previously demonstrated significant negative impacts of transition metal oxide (TMO) lithium ion battery cathode nanomaterial lithium cobalt oxide (LCO) on growth, development, hemoglobin, and heme synthesis gene expression in larvae of model sediment invertebrate *Chironomus riparius*. Here, we propose that alteration of Fe-S protein function by LCO is a molecular initiating event leading to these changes. A 10 mg/L LCO exposure causes significant oxidation of the aconitase 4Fe-4S center after 7 d by electron paramagnetic resonance spectrometry of intact larvae and a significant reduction in aconitase activity of larval protein after 48 hr ( $p < 0.05$ ). Next-generation RNA sequencing identified significant changes in expression of genes involved in 4Fe-4S center binding, Fe-S center synthesis, iron ion binding, and metabolism for 10 mg/L LCO at 48 hr (FDR-adjusted  $p < 0.1$ ). We propose an adverse outcome pathway whereby oxidation of metabolic and regulatory Fe-S centers of proteins by LCO disrupts metabolic homeostasis, which negatively impacts growth and development, a mechanism which may apply for these conserved proteins across species and for other TMO nanomaterials.

## Introduction

In the past two decades substantial work has occurred toward understanding potential implications of increasing commercial use of engineered nanomaterials (ENMs) on human health and the environment, with more than 18,000 nanotoxicology articles published between the years 2000 and 2018.<sup>1-3</sup> Over this period, studies of ENM impacts grew from basic toxicity exposures to increasingly sophisticated studies aimed at understanding how ENM properties determine toxicity, mechanisms by which materials interact with biological systems, and how and what materials and their environmental transformations may be of potential concern.<sup>1,2</sup> To date nanotoxicology has focused largely on first-generation ENMs (*e.g.* Au, Ag, graphene).<sup>1,4,5</sup> When an underlying mechanism is proposed, toxicity is frequently attributed to reactive oxygen species (ROS) for a diversity of ENMs including Au, Ag, CeO, Si, and carbon nanotubes.<sup>6-9</sup> ROS such as superoxide, hydrogen peroxide, and hydroxyl radical have long been classified as damaging to DNA, RNA, proteins, and lipids.<sup>10</sup> However, research within the last decade has revealed ROS – specifically superoxide and its hydrogen peroxide product, generated in the mitochondria or by NADPH oxidases – as important signaling molecules,<sup>11,12</sup> involved in regulating fundamental biological processes through oxidation of cysteines of protein redox sensors including in metabolism (*e.g.* GAPDH, PKM2, AMPK),<sup>13</sup> proliferation (*e.g.* PTEN, PTP1b, EGFR),<sup>14</sup> autophagy (*e.g.* PTEN, AMPK, Atg4, FOXO),<sup>15</sup> and apoptosis (*e.g.* VDAC, caspases, ERO1, PDI);<sup>16</sup> and ROS are actively generated during and required for normal embryonic development across species.<sup>17</sup> Thus, ROS as a universal explanation for nanotoxicity is not explanatory or mechanistic, and its blanket assertion may be limiting advancement of our understanding of nano-bio interactions.

In recent years, increasing effort has been made to integrate the concept of the adverse outcome pathway (AOP) into nanotoxicology, defining impacts of materials on organisms from the initial molecular interaction between nanoparticles and cellular components of organisms, or molecular initiating event, through a resulting series of key events, and ultimately to a phenotypically observable adverse outcome, *e.g.* decreased reproduction or survival. Despite these efforts, identification of specific molecular initiating events for nanomaterial exposures is still rare in the literature, and studies are usually limited to identifying key events and adverse outcomes.<sup>18–20</sup> Finding specific, testable molecular initiating events is necessary for identify unifying mechanisms of nanotoxicity applicable across nanomaterials and organisms. Within this AOP framework, observed ROS, if acting as signaling molecules, may be correlative rather than causative and a key event in the AOP rather than the molecular initiating event.<sup>21</sup> Singling out ROS as the molecular initiating event in a nanotoxicity AOP requires identifying specific molecular targets of ROS that lead to key events and ultimately to adverse outcomes in exposed organisms.

Complex transition metal oxides (TMOs) are a category of next-generation ENM where two or more transition metals are incorporated with oxygen into a crystalline lattice. Lithium cobalt oxide (LCO) and related compositions are complex TMOs with large and growing commercial use as the active cathode material of lithium ion batteries (LIBs) in consumer electronics and electric vehicles.<sup>22–25</sup> Due to large manufacturing volume and a dearth of recycling facilities, LIB waste is expected to accumulate in landfills, and accidental release of LCO and related compounds from landfill leachate or manufacturing presents a potential environmental concern.<sup>26–28</sup> In 2016, 374 kilotons of LIBs were in use, and LIB waste from electric vehicles

alone is expected to reach 200 kilotons annually by 2025.<sup>26</sup> LIB waste was shown to leach 164 g Co per kg of battery, 16% of its total mass.<sup>26</sup>

LCO can aggregate and settle in aquatic systems, creating particularly high exposure concentrations for sediment-dwelling organisms.<sup>29</sup> *Chironmus riparius* is a model sediment-dwelling invertebrate used for sediment toxicity assays, including for ENMs, and is important in many freshwater systems, with larval stages that reside in the sediment where they consume detritus from silt particles, eventually emerging as adult flies.<sup>30-36</sup> We showed previously that exposure to 10 mg/L LCO for 7 d significantly reduced growth by about 25% and increased time to adult emergence by 35% for *C. riparius* larvae, as well as reducing larval hemoglobin 40% and levels of heme synthesis gene *porphobilinogen synthase* 1.4-fold.<sup>29</sup>

These results suggested a key event for LCO toxicity in which exposure disrupts normal heme synthesis in exposed larvae. Synthesis of heme and iron metabolism more broadly is regulated by the iron-responsive protein (IRP1), whose mRNA-binding activity is governed by the status of its Fe-S center. This [4Fe-4S]<sup>2+</sup> center also allows IRP1 to act as an aconitase (ACO1), converting citrate to isocitrate in the citric acid cycle.<sup>37-40</sup> Both heme synthesis and energy metabolism are thus dependent on this Fe-S center's status, which has been shown to be sensitive to ROS.<sup>41</sup> Prior studies of LCO's biological impacts showed production of ROS in trout epithelial cells,<sup>42</sup> with possible direct production of ROS due to its Co<sup>3+</sup> oxidation state.<sup>28</sup> Oxidation by ROS transforms the aconitase [4Fe-4S]<sup>2+</sup> site into an enzymatically inactive [3Fe-4S]<sup>1+</sup> visible by electron paramagnetic resonance (EPR).<sup>41</sup> Many other important metabolic enzymes including succinate dehydrogenase and NADH dehydrogenase (involved in the citrate cycle and the electron

transport chain) require Fe-S centers for their activity.<sup>38,43-46</sup> Thus, the growth and development defect adverse outcomes observed in LCO-exposed larvae, along with the key event of dysregulation of hemoglobin and heme synthesis,<sup>29</sup> suggest that *C. riparius* LCO toxicity could occur by the molecular initiating event of Fe-S center disruption in regulatory and enzymatic proteins. These proteins are ubiquitous across bacterial, animal, and plant kingdoms,<sup>46</sup> indicating impacts on Fe-S centers could be a molecular initiating event common to TMO nanomaterials across species, potentially providing a framework for understanding the impacts of these materials more broadly.

This molecular mechanism of LCO toxicity has not previously been explored, with previous studies attributing LCO impacts to generic ROS.<sup>42,47,48</sup> Here we test the hypothesis that the disruption of Fe-S centers could be the molecular initiating event causing observed adverse outcomes. We used EPR to examine the oxidation state of the Fe-S protein aconitase and examined its enzyme activity to determine the impact of LCO on this protein as one of the important Fe-S proteins that may be impacted by exposure in larvae. We also used next-generation RNA sequencing to gain an overall picture of the impacts of LCO exposure on molecular pathways in *C. riparius*.

## **Materials and methods**

### ***LCO nanosheet synthesis and characterization***

Sheet-like  $\text{Li}_x\text{CoO}_2$  nanoparticles were synthesized as described previously.<sup>49</sup> A cobalt hydroxide ( $\text{Co}(\text{OH})_2$ ) precursor was synthesized by precipitation by adding a 0.1 M solution of LiOH in 420 mL 18.2 M $\Omega$  water (ultrapure water used here and in all future steps) dropwise to a 1 M

$\text{Co}(\text{NO}_3)_2 \cdot 6\text{H}_2\text{O}$  solution in 20 mL water ( $[\text{OH}^-]$  5% stoichiometric excess for  $\text{Co}^{2+} + 2\text{OH}^- \rightarrow \text{Co}(\text{OH})_2$ ). The resulting precipitate was immediately isolated by centrifugation at 4696 g at room temperature for 3 min, redispersed in water to wash, and isolated by centrifugation again. Washing was repeated two more times. The final supernatant was then decanted and the product dried in a 30 °C vacuum oven overnight. The dried  $\text{Co}(\text{OH})_2$  product was then transformed to  $\text{LiCoO}_2$  by adding 0.20 g of the  $\text{Co}(\text{OH})_2$  particles to a molten salt flux of 6:4 molar ratio of  $\text{LiNO}_3$ : $\text{LiOH}$  (10 g total) at 200 °C in a poly(tetrafluoroethylene) container with magnetic stirring assembled in a silicone oil bath, forming  $\text{Li}_x\text{CoO}_2$ . After 30 min, the reaction was quenched with water, and  $\text{Li}_x\text{CoO}_2$  particles were isolated by centrifugation at 4969 g at room temperature for 5 min. The particle pellet was washed by redispersing in water and isolating by centrifugation three times. The final product was dried in a vacuum oven overnight at 30 °C. To verify extent of lithiation, particles were digested in aqua regia and analyzed via inductively coupled plasma – optical emission spectroscopy (ICP-OES) using a Perkin Elmer Optima 2000 ICP-OES, yielding a Li:Co ratio of 0.92:1. We refer to this composition,  $\text{Li}_{0.92}\text{CoO}_2$  as “LCO.” ICP-OES calibration data are available in Supplementary Figure S1. Surface area measured by BET was determined to be 125  $\text{m}^2/\text{g}$ . Particles were imaged edge-on using scanning electron microscopy and showed sheet-like structures consistent with previously published synthesis of this material (Supplementary Figure S2).<sup>49</sup> Size analysis from the previously published synthesis showed approximate nanosheet diameters of 25 nm and widths of 5 nm by transmission electron microscopy.<sup>49</sup> Powder X-Ray Diffraction patterns were also consistent with previously published work that can be indexed to the  $R\bar{3}m$  space group (Supplementary Figure S3).<sup>49</sup> Zeta potential for these materials in exposure media (moderately hard reconstituted water, MHRW:  $\text{NaHCO}_3$  96 mg/L,  $\text{CaSO}_4$  60 mg/L,  $\text{MgSO}_4$  60 mg/L,  $\text{KCl}$  4 mg/L,  $\text{Na}_2\text{SeO}_3$  0.004 mg/L) was measured

using a Malvern Zetasizer Nano ZS with results of  $-12.6 \pm 0.6$  mV for 1 mg/L LCO and  $-3.7 \pm 0.5$  mV for 10 mg/L LCO, similar to previous results for these materials in these conditions (Supplementary Table S1).<sup>29</sup> As shown previously, zeta potential increases toward neutral with higher LCO particle concentration, which may be related to electrostatic repulsion and higher aggregation rates for LCO particles at higher concentrations.<sup>29</sup> Quality data for zeta potential results are included as Supplementary Figure S4.

### ***RNA-Seq***

#### *Larval exposure*

*C. riparius* egg ropes were obtained from Aquatic Research Organisms (ARO; Hampton, NH). Once hatched, larvae were fed once daily 0.5 mL of supernatant from finely ground TetraMin® Tropical Flake fish food at 20 mg/mL for 2 d and the full TetraMin® suspension for another 3 d. At 5 d post-hatch, animals were transferred to 100 mL exposure beakers containing 5 g 140-270 mesh fine silica sand (AGSCO Corp) and 20 mL 2x moderately hard reconstituted water (MHRW).<sup>47</sup> Final exposures were made up by adding 20 mL of Milli-Q® ultrapure H<sub>2</sub>O to control beakers, Li and Co ions to a final concentration 660 µg/L Li as LiCl and 150 µg/L Co as CoCl<sub>2</sub>, equivalent to ions released by LCO at 10 mg/L in MHRW over 48 hr,<sup>29</sup> or LCO for final concentrations of 1 and 10 mg/L. The 10 mg/L LCO concentration was chosen as the high exposure as this was shown to have chronic impacts over 7 d in our previous study,<sup>29</sup> and the 48 hr timepoint was selected to detect early impacts that could underlie our previously observed changes in growth and hemoglobin from 10 mg/L LCO at 7 d.<sup>29</sup> Five animals were added to each of 6 replicate beakers per condition. Animals were fed 125 µL of 20 mg/mL finely ground TetraMin® suspension per beaker daily over the 48 hr exposure period. After 48 hr of exposure,

animals were carefully removed from exposure beakers, the 5 larvae from each replicate beaker pooled as a single replicate, rinsed 3x in fresh 1x MHRW, flash frozen in liquid N<sub>2</sub>, and stored at -80 °C for subsequent RNA extraction, library creation, and sequencing.

#### *RNA-extraction, library prep, and sequencing*

Replicate-pooled, flash frozen larvae were homogenized in TRIzol and RNA purified using the Direct-zol RNA MiniPrep (Zymo Research, R2051). RNA quality and yield were determined using the NanoDrop 1000 spectrophotometer, Agilent Bioanalyzer 2100, and Qubit fluorometer. RNA quality for all samples were as follows: 260/280 ratio 1.8-2.0, 260/230 ratio 2.0-2.2, and RIN > 7. 200ng of total RNA from each sample was used to prepare RNA sequencing libraries using the Illumina TruSeq Stranded mRNA kit (Illumina, RS-122-2102) and IDT for Illumina – TruSeq RNA UD Indexes (Illumina, 20022371). Libraries were sequenced on the Illumina NovaSeq6000, with paired-end reads of 150 bp.

#### *Processing of RNA-Seq data*

Total genomic yield approached 996 million paired-end reads, median per-sample yield 49.45 million fragments, population standard deviation 16.77 million fragments, data was quality-assessed using FastQC v0.11.5,<sup>50</sup> and no apparent base-calling errors were flagged for removal. Cutadapt v1.18 was used to clip Illumina TruSeq 3'-anchored primers,<sup>51</sup> and Trinity v2.8.3 used to *de novo* assemble the quality-controlled data into a draft reference transcriptome.<sup>52</sup>

In order to overcome poor annotation in available databases for *C. riparius*, the BLASTX aligner within the NCBI-BLAST+ package v2.2.28 was used to iteratively annotate the assembly against available NCBI proteins for *C. riparius*;<sup>53</sup> followed by the genome releases of well-annotated

fellow Nematocerans (Culicomorpha) *Anopheles gambiae*, *Culex quinquefasciatus*, and *Aedes aegypti*,<sup>54,55</sup> and finally against the February 2019 release of UniProt-SwissProt. Kallisto v0.45.0 was then used to pseudoalign and sample-quantify paired-end data against the annotated draft reference transcriptome.<sup>56</sup>

DESeq2 was used to perform differential expression analysis on sample pairs using R v3.5.3.<sup>57</sup> Differentially expressed genes determined by DESeq2 were then re-annotated using reference sequence metadata and joined relationally with Kallisto sample quantification counts using custom tooling.

#### *Analysis of RNA-Seq data using DAVID and KEGG*

Differentially expressed, annotated contigs present in at least 80% of samples were analyzed for function and functional enrichment using the Database for Annotation, Visualization and Integrated Discovery (DAVID).<sup>58,59</sup> DAVID statistical enrichment was determined based on a Benjamini-adjusted FDR < 0.1. The Kyoto Encyclopedia of Genes and Genomes (KEGG) was used to assign KEGG orthology (KO) terms to annotated contigs and perform pathway analysis.<sup>60-62</sup> A total of 28,101 contigs were successfully assembled and present in at least 80% of samples. Of these 10,014 could be successfully annotated using BLASTX (e-value  $\leq$  0.1). 1409 annotated contigs were differentially expressed between control and 10 mg/L LCO samples and found in at least 80% of samples (Wald FDR < 0.1). Of these 1,373 could be assigned functions in DAVID and 354 could be assigned KOs by KEGG, of which 319 could be assigned to pathways.

### ***Aconitase enzyme activity assay***

Aconitase enzyme activity assays were carried out on protein extracted from exposed larvae using the Cayman Chemical Aconitase Assay Kit (Cayman Chemical, 705502). Larvae were fed and exposed as described above: control, released ion control, 1 mg/L LCO, 10 mg/L LCO for 48 hr. At 48 hr, larvae from 10 replicate beakers per condition (50 larvae total) were pooled and homogenized in aconitase assay buffer on ice. Samples were centrifuged at 800 x g at 4 °C for 10 min and the supernatant of soluble protein harvested per kit instructions. Total protein concentration was quantified using the Pierce™ BCA Protein Assay Kit (Thermo Scientific, 23225). Samples were assayed for activity using 500 µg/mL of total protein per aconitase kit instructions. A total of 5 independent replicates per condition were assayed.

### ***EPR measurements***

For EPR analysis, *C. riparius* larvae 5 d post-hatch were exposed to control, released ion control, and 10 mg/L LCO for 7 d. One egg rope (containing hundreds of larvae) was used for each of 5 replicates per condition. A high number of larvae per condition and increased exposure time were used to ensure sufficient animal mass for the assay; and the 10 mg/L LCO dose only was selected for feasibility and due to limited or no observable impacts from 1 mg/L for other endpoints in this and our previous study.<sup>29</sup> Animals were loaded into Wilmad® quartz (CFQ) O.D. 4 mm EPR tubes (Sigma-Aldrich, Z566535) cut to 14 cm and were first frozen slowly and stored briefly in liquid N<sub>2</sub> to avoid the possibility of cracking inside the cryostat of the EPR instrument. All samples were measured using a Bruker ELEXSYS E500 X-Band CW- ESR spectrometer at a temperature of 10 K using a liquid helium ESR900 continuous flow cryostat.

To ensure data reproducibility and consistency of our measurements, we repeated each EPR measurement on 5 independent samples for each condition. We prepared fresh animals as standard materials and loaded them immediately for analysis. To validate that our signals resulted from the animals themselves, we prepared and analyzed water, MHRW, LCO ion, and LCO nanosheet-only samples without animals as control materials (Supplementary Figure S5). Spectra were analyzed using Mnova version 14.1.2 software with a beta version EPR plug-in (Mestrelab). For quantitative analysis, all spectra were converted into their first integrals and background-corrected to yield final spectra. The integrated area for peaks of interest were obtained by double integration of the EPR spectra and were normalized by their ratio to the  $\text{Mn}^{2+}$  peak at  $\sim 3250$  G ( $g \sim 2.08$ ) to account for differences in sample loading, an intrasample normalization approach.<sup>63,64</sup> Specifically, the peaks of interest are: the peak at  $\sim 3350$  G ( $g \sim 2.02$ ), characteristic of oxidized aconitase  $[\text{3Fe-4S}]^{1+}$ ; the peak at  $\sim 3470$  G ( $g \sim 1.98$ ), characteristic of Complex II  $[\text{3Fe-4S}]^{1+}$ ; and the peak at  $\sim 3560$  G ( $g \sim 1.91$ ), characteristic of Complex I and II  $[\text{2Fe-2S}]^{1+}$  and  $[\text{4Fe-4S}]^{1+}$ .<sup>41,63</sup>

### *Statistics*

Data from EPR and aconitase assays were analyzed for normality using the Shapiro-Wilk test and equality of variance using Levene's test. Statistical significance of differences between treatments was determined using a One-way ANOVA with Tukey HSD post-hoc tests for data with equal variance and a One-way Welch ANOVA with Dunnett T3 post-hoc tests for data with unequal variance. Statistical tests were performed using SPSS version 23 for Mac.

## Results and Discussion

### *Impacts of LCO on aconitase and Fe-S centers of other proteins*

Impacts of LCO on the Fe-S centers of *C. riparius* larvae were evident from whole-animal EPR spectra (Fig 1). Significant increases were observed in the level of oxidized aconitase  $[3\text{Fe-4S}]^{1+}$  in animals exposed to 10 mg/L LCO for 7 d (Fig 1b; One-way Welch ANOVA,  $df = 2$ ,  $F = 101.805$ ,  $p < 0.001$ ; Dunnett T3 post-hoc  $p < 0.05$ ). Oxidation of the aconitase  $[4\text{Fe-4S}]^{2+}$  center to the inactive but EPR-visible  $[3\text{Fe-4S}]^{1+}$  would be expected to negatively affect metabolism,<sup>41,45</sup> and metabolic defects could underlie the reduced size and delayed development observed to result from 10 mg/L LCO exposure in our previous study.<sup>29</sup> Cobalt alone has also been shown to impact function of Fe-S centers in bacteria and impact oxidative metabolism,<sup>45,65</sup> however, this is the first study to our knowledge showing impacts on Fe-S centers by EPR in a whole multicellular organism as well as the first exploration of this mechanism of toxicity for an ENM.

Impacts of LCO on the Fe-S center of aconitase was confirmed by aconitase activity assays on extracted larval protein. Aconitase activity of protein extracted from *C. riparius* larvae exposed to LCO at 10 mg/L for 48 hr was significantly reduced compared to control and ion treatment (Fig 2; One-way ANOVA,  $df = 3$ ,  $F = 5.557$ ,  $p < 0.05$ ; Tukey HSD post-hoc  $p < 0.05$ ). While transcripts for both cytosolic and mitochondrial aconitase were identified by RNA-Seq, expression did not differ significantly between LCO exposures and controls. Lack of expression change at the transcript level along with observation of increased oxidation of the aconitase Fe-S center by EPR (Fig 1b) suggest that observed reduction in activity is likely due to oxidation of the solvent-exposed aconitase  $[4\text{Fe-4S}]^{2+}$  to the inactive  $[3\text{Fe-4S}]^{1+}$  as a result of LCO exposure.

As stated earlier, reduced aconitase activity as a result of LCO exposure would be expected to cause disruptions to metabolism that could be a cause of the reduced larval size and delayed development observed in our previous study.<sup>29</sup>

We also observed significant increases in the [2Fe-2S]<sup>1+</sup> and [4Fe-4S]<sup>1+</sup> centers of complex I and II NADH dehydrogenase and succinate dehydrogenase from EPR spectra (Fig 1c; One-way Welch ANOVA, df = 2, F = 56.033, p < 0.001; Dunnett T3 post-hoc p < 0.05). The [3Fe-4S]<sup>1+</sup> center of succinate dehydrogenase also showed an increasing trend for ion and LCO-exposed animals but was not significantly different from control (Fig 1d; One-way Welch ANOVA, df = 2, F = 5.157, p < 0.05; Dunnett T3 post-hoc p > 0.05). NADH dehydrogenase comprises part of electron transport chain (ETC) complex I. Succinate dehydrogenase functions as part of the citric acid cycle and as part of complex II of the ETC. The Fe-S centers of these proteins are embedded within a protein complex where they shuttle electrons.<sup>43,44</sup> The Fe-S centers of complex II have been shown to be relatively insensitive to oxidation by ROS as compared with aconitase,<sup>66</sup> which may be due to their being buried in protein while the aconitase 4Fe-4S is solvent exposed. An increase in the levels of complex I and II Fe-S centers suggests potential compensation for LCO impacts: increased Fe-S synthesis to compensate for Fe-S oxidation, increased ETC activity to compensate for metabolic impairments, or both.

### ***Impacts of LCO on Fe-S and metabolic gene expression***

The impacts of LCO on Fe-S centers were also evidenced by gene expression changes observed by RNA-Seq. Thirteen genes with molecular functions associated with Fe-S proteins directly and many others associated with downstream functions related to Fe-S genes were differentially

expressed. Table 1 shows differentially expressed genes (Wald FDR adjusted  $p < 0.1$ ) with molecular functions related to Fe-S binding between MHRW control and 10 mg/L LCO-exposed larvae.<sup>58,59</sup> These include genes involved in assembly of 4Fe-4S centers: *NUBP1*, *NUPB2*, and *ISCA2*. *ISCS*, involved in assembly of 2Fe-2S centers, is also significantly upregulated.<sup>67</sup> In addition, genes for important Fe-S center-containing enzymes succinate dehydrogenase and NADH dehydrogenase, involved in the citrate cycle and oxidative phosphorylation, were also significantly upregulated.<sup>43,44</sup> The Fe-S centers of succinate dehydrogenase and NADH dehydrogenase were also observed to be increased in 10 mg/L LCO-exposed larvae versus controls by EPR (Fig 1c). Upregulation of Fe-S center-containing DNA repair protein genes *endonuclease III* and *RTEL1* suggest that LCO-exposed larvae could be more sensitive to DNA damage due to impacts on repair proteins that require Fe-S centers for their function. No differentially expressed genes were detected between released ion exposure equivalent to ions released by 10 mg/L LCO and MHRW control, demonstrating ENM-specific LCO impacts. Genes related to iron and iron ion binding and 4Fe-4S binding were significantly enriched among genes differentially expressed between MHRW control and 10 mg/L LCO exposures (Figure 3; Benjamini-adjusted FDR  $< 0.1$ ). This also supports the hypothesis that iron metabolism is disrupted by LCO exposure (observed in Niemuth *et al.* 2019 as reduced hemoglobin in LCO-exposed larvae)<sup>29</sup> and the specific hypothesis that impacts of LCO on Fe-S centers could underlie observed impacts on iron metabolism and metabolism more generally.

Our previous research suggested that broader metabolism may be impacted by LCO exposure,<sup>29</sup> which is supported here, as metabolic pathways are significantly enriched with 156 genes differentially regulated (Fig 3; Benjamini-adjusted FDR  $< 0.001$ ). Of the 319 KEGG orthologies

that map to pathways, 156, or nearly half, are involved in metabolic pathways. The distribution of up and downregulation of genes in these pathways suggest an upregulation of genes involved in energy production (Fig 4) and downregulation of processes that use energy (Fig 4, Supp Fig S6). For example, genes involved in glycolysis/gluconeogenesis (14 genes), the citrate cycle (7 genes), and oxidative phosphorylation (17 genes) are all upregulated (Fig 4). Decreased protein processing (Supp Fig S6), changes in amino acid metabolism toward catabolism, and downregulation of lipid metabolism all suggest increases in energy production with concomitant decreases in energy use and storage (Fig 4). In addition, changes in genes involved in PI3K-Akt and AMPK signaling suggest regulatory changes toward energy production and away from energy use in cells and tissues (Supp Fig S7). Changes in autophagy (8 genes; Supp Fig S8), glucagon signaling (11 genes), insulin signaling (6 genes), and retrograde endocannabinoid signaling (14 genes) also indicate changes toward energy production and uptake (Supp Fig S9). This result, along with significant enrichment for specific metabolic pathways including carbon metabolism, lipid metabolism, glycolysis/gluconeogenesis, and amino acid metabolism (Fig 3; Benjamini-adjusted FDR < 0.1) support the hypothesis proposed in Niemuth *et al.* 2019 that changes observed in size and development of LCO-exposed larvae may be the results of metabolic effects.

Given the conservation across species of Fe-S proteins involved in processes such as heme synthesis (*e.g.* ferredoxin, ferrochelatase), iron homeostasis (*e.g.* IRP1), energy metabolism (*e.g.* aconitase, NADH dehydrogenase, succinate dehydrogenase), and DNA repair (*e.g.* endonuclease III),<sup>46</sup> changes in these centers due to LCO exposure would be expected to have broad impacts on cellular processes, both in *C. riparius* and in other species. Observations of increased iron in

mouse lung associated with LCO exposure<sup>48</sup> and decreased expression of heme-containing *catalase* in *Daphnia magna*<sup>47</sup> suggest this mechanism may indeed apply to other organisms. This mechanism may also be indicated for other transition metal oxide nanomaterials. Specifically, components of pathways found to be significantly impacted in our results (Figs 2, 3, and 4) have been shown to be affected by exposure to TMO nanomaterials in other studies, including: decreased aconitase activity in liver of ZnO-exposed white sucker;<sup>68</sup> changes in expression of aconitase, succinate dehydrogenase, and other citrate cycle genes in *Pseudomonas aeruginosa* exposed to CuO ENMs;<sup>69</sup> increased expression of electron transport chain proteins from exposure to ZnO, TiO<sub>2</sub>, and CuO nanoparticles in mouse hepatocytes;<sup>70</sup> increased gluconeogenesis from ZnO particles in rat liver cells;<sup>71</sup> decreases in succinate and citrate (involved in the citrate cycle) and hemoglobin in ZnO-exposed rat kidney;<sup>72</sup> negative impacts of TiO<sub>2</sub> on carbon metabolism in algae;<sup>73</sup> and decreases in citrate cycle metabolites from TiO<sub>2</sub> exposure in *C. elegans*.<sup>74</sup> Although impacts of materials specifically on Fe-S centers were not explored in these studies, the impacts observed in this study and the relevance of Fe-S proteins to the observed impacts may recommend broader investigation of this mechanism in future TMO nanomaterial toxicity studies.

#### ***Additional molecular impacts identified by RNA-Seq***

One molecular function significantly enriched among differentially expressed genes between MHRW control and LCO 10 mg/L exposures (Benjamini-adjusted FDR < 0.001) not related to Fe-S proteins was chitin binding and metabolism (49 genes, Fig 3). Chitin is a biopolymer important in the formation of invertebrate exoskeletons as well as the protective peritrophic matrix of the gut.<sup>75</sup> Included among the differentially expressed genes with functions related to

chitin binding and metabolism are a number of peritrophins (*e.g. Peritrophin 1, Peritrophin 44, Obstructor b*), involved in reorganizing the peritrophic matrix that protects the gut.

Reorganization of the peritrophic matrix is a common strategy for invertebrates to cope with exogenous stressors that have been consumed and enter the digestive tract.<sup>76</sup> The changes in expression of peritrophin genes and other genes related to chitin synthesis and organization may indicate that alterations in these environment-facing structures may be an important first-line response for invertebrates encountering nanomaterials such as LCO in the environment.

Relatively few genes were identified as being differentially expressed (Wald FRD adjusted  $p < 0.1$ ) between 1 mg/L LCO exposed larvae and controls, only 34 versus the 1409 differentially expressed between 10 mg/L LCO and control. No molecular functions or pathways were identified as statistically enriched by DAVID between 1mg/L LCO and control. However, of the 29 differentially expressed genes annotated by DAVID, eight, or more than a quarter, were peptidases. This could indicate a shift toward protein catabolism even at an LCO exposure concentration that did not cause observable effects on aconitase activity in this study (Fig 2) or on growth or development in our previous study.<sup>29</sup>

### ***Implications and proposed adverse outcome pathway***

This work provides evidence for the oxidative disruption of Fe-S centers of proteins as a molecular initiating event, and subsequent metabolic disruption as a key event, of the toxicity of the complex transition metal oxide ENM LCO. A proposed AOP summarizing our findings and how they relate to previous studies of LCO is included as Figure 5. We propose that ROS generated by LCO<sup>42</sup> oxidizes the Fe-S center of aconitase (observed by EPR; Fig 1b) and likely other Fe-S enzymes with solvent-exposed Fe-S centers. This results in lower enzyme activity

(observed for aconitase; Fig 2), which results in metabolic disruption and energy starvation (observed by RNA-Seq; Figs 3 and 4) that lead to reduced growth and delayed adult emergence.<sup>29</sup> The conservation of Fe-S proteins as important enzymatic and regulatory proteins across species<sup>46</sup> suggests that this mechanism may also be broadly relevant, for LCO specifically, and potentially for other transition metal oxide ENMs.

An interesting consideration for this AOP is to what extent the toxic effects of LCO is dependent on LCO particle uptake into *C. riparius* tissues. LCO was found to be taken up into cultured rainbow trout gill epithelial cells, where nanosheets were found to induce ROS and localized within membrane-bound organelles.<sup>42</sup> Cellular uptake has been demonstrated to be predictive of tissue uptake in mice for polystyrene, TiO<sub>2</sub>, dextran sulfate, hyaluronic acid, and glycol chitosan ENMs.<sup>77</sup> A suite of transition metal oxide ENMs (*e.g.* CoO, Co<sub>3</sub>O<sub>4</sub>, Ni<sub>2</sub>O<sub>3</sub>) have been shown to impact cellular metabolism *in vitro* and induce ROS specifically in the mitochondria,<sup>78</sup> suggesting cellular uptake and a specific site of cellular impact for this class of ENMs that is consistent with our observed metabolic impacts. Uptake of ENMs has rarely been studied in detail in *C. riparius*, and in the incidence when it has been (*i.e.* for fullerenes) particles were not seen to be taken up into tissues, but remained in the lumen of the gut.<sup>34</sup> However, carbon nanofibers were observed to enter intestinal cells of related *Diamesa* chironomid larvae,<sup>84</sup> suggesting that the ability of ENMs to cross the barrier of the gut lumen and into tissues may be material-specific. In the better-studied aquatic invertebrate *Daphnia magna*, fullerenes have also not been observed to be taken up into tissues, again remaining in the gut lumen,<sup>79</sup> while Ag nanoparticles,<sup>80</sup> Au nanoparticles,<sup>81</sup> carbon nanotubes,<sup>82</sup> and GaInP nanowires<sup>83</sup> have been observed to be taken up. Thus, uptake of LCO is plausible based on the literature and our

observed impacts, but whether observed LCO impacts in this and other organisms are the result of direct interaction of LCO nanosheets with cellular components or if an indirect interaction may be occurring at the cell surface in the gut is an interesting avenue for future investigation.

### **Acknowledgement**

This work was supported by National Science Foundation under the Center for Sustainable Nanotechnology (CSN), CHE-1503408. The CSN is part of the Centers for Chemical Innovation Program. This project used the UW-Milwaukee Great Lakes Genomics Center for RNA isolation, Illumina NovaSeq RNA sequencing, and bioinformatics services. EPR analysis was carried out at the UW-Madison Department of Chemistry's Paul Bender Chemical Instrumentation Center. The authors would like to thank Dr Olaf Mueller of the Great Lakes Genomics Center for assistance in uploading RNA-seq data to NCBI.

### **Conflict of interest statement**

The authors have no conflicts to declare.

### **Supporting Information**

Supporting information includes supplementary figures and tables referenced in the text and a list of relevant genes identified as differentially expressed by RNA-Seq.

## References

- (1) Klaper, R. D. The Known and Unknown about the Environmental Safety of Nanomaterials in Commerce. *Small* **2020**, 2000690.  
<https://doi.org/10.1002/sml.202000690>.
- (2) Friedersdorf, L. E.; Bjorkland, R.; Klaper, R. D.; Sayes, C. M.; Wiesner, M. R. Fifteen Years of NanoEHS Research Advances Science and Fosters a Vibrant Community. *Nat. Nanotechnol.* **2019**, *14* (11), 996–998. <https://doi.org/10.1038/s41565-019-0574-z>.
- (3) Anlar, H. G. Worldwide Nanotoxicology Research Productivity and Contribution of Turkey. *FABAD J. Pharm. Sci.* **2019**, *44* (3), 205–214.
- (4) Halappanavar, S.; van den Brule, S.; Nymark, P.; Gaté, L.; Seidel, C.; Valentino, S.; Zhernovkov, V.; Høgh Danielsen, P.; De Vizcaya, A.; Wolff, H.; et al. Adverse Outcome Pathways as a Tool for the Design of Testing Strategies to Support the Safety Assessment of Emerging Advanced Materials at the Nanoscale. *Part. Fibre Toxicol.* **2020**, *17* (1), 16.  
<https://doi.org/10.1186/s12989-020-00344-4>.
- (5) Chen, X. Mapping the Decadal (2009–2018) Research Landscape of Nanotoxicity: Insights from a Bibliometric Study. *Nanosci. Nanotechnol. Lett.* **2019**, *11* (10), 1327–1337. <https://doi.org/10.1166/nnl.2019.3015>.
- (6) Khanna, P.; Ong, C.; Bay, B.; Baeg, G.; Khanna, P.; Ong, C.; Bay, B. H.; Baeg, G. H. Nanotoxicity: An Interplay of Oxidative Stress, Inflammation and Cell Death. *Nanomaterials* **2015**, *5* (3), 1163–1180. <https://doi.org/10.3390/nano5031163>.
- (7) Mendoza, R. P.; Brown, J. M. Engineered Nanomaterials and Oxidative Stress: Current Understanding and Future Challenges. *Curr. Opin. Toxicol.* **2018**.  
<https://doi.org/10.1016/J.COTOX.2018.09.001>.

- (8) Manickam, V.; George, L.; Tanny, A.; Lochana, R.; Velusamy, R. K.; Kumar, M. M.; Rajendran, B.; Tamizhselvi, R.; George, L.; Tanny, A.; et al. Methods and Protocols for In Vitro Animal Nanotoxicity Evaluation: A Detailed Review. In *Nanotoxicology*; CRC Press: Boca Raton : CRC Press, Taylor & Francis Group, 2018., 2018; pp 285–321.  
<https://doi.org/10.1201/b21545-12>.
- (9) Qiu, T. A.; Clement, P. L.; Haynes, C. L. Linking Nanomaterial Properties to Biological Outcomes: Analytical Chemistry Challenges in Nanotoxicology for the next Decade. *Chem. Commun.* **2018**, 54 (91), 12787–12803. <https://doi.org/10.1039/C8CC06473C>.
- (10) Mittler, R. ROS Are Good. *Trends Plant Sci.* **2017**, 22 (1), 11–19.  
<https://doi.org/10.1016/J.TPLANTS.2016.08.002>.
- (11) Reczek, C. R.; Chandel, N. S. ROS-Dependent Signal Transduction. *Curr. Opin. Cell Biol.* **2015**, 33, 8–13. <https://doi.org/10.1016/J.CEB.2014.09.010>.
- (12) Ray, P. D.; Huang, B.-W.; Tsuji, Y. Reactive Oxygen Species (ROS) Homeostasis and Redox Regulation in Cellular Signaling. *Cell. Signal.* **2012**, 24 (5), 981–990.  
<https://doi.org/10.1016/J.CELLSIG.2012.01.008>.
- (13) Wang, K.; Jiang, J.; Lei, Y.; Zhou, S.; Wei, Y.; Huang, C. Targeting Metabolic–Redox Circuits for Cancer Therapy. *Trends Biochem. Sci.* **2019**.  
<https://doi.org/10.1016/J.TIBS.2019.01.001>.
- (14) Diebold, L.; Chandel, N. S. Mitochondrial ROS Regulation of Proliferating Cells. *Free Radic. Biol. Med.* **2016**, 100, 86–93.  
<https://doi.org/10.1016/J.FREERADBIOMED.2016.04.198>.

- (15) Wen, X.; Wu, J.; Wang, F.; Liu, B.; Huang, C.; Wei, Y. Deconvoluting the Role of Reactive Oxygen Species and Autophagy in Human Diseases. *Free Radic. Biol. Med.* **2013**, *65*, 402–410. <https://doi.org/10.1016/J.FREERADBIOMED.2013.07.013>.
- (16) Redza-Dutordoir, M.; Averill-Bates, D. A. Activation of Apoptosis Signalling Pathways by Reactive Oxygen Species. *Biochim. Biophys. Acta - Mol. Cell Res.* **2016**, *1863* (12), 2977–2992. <https://doi.org/10.1016/J.BBAMCR.2016.09.012>.
- (17) Rampon, C.; Volovitch, M.; Joliot, A.; Vriza, S.; Rampon, C.; Volovitch, M.; Joliot, A.; Vriza, S. Hydrogen Peroxide and Redox Regulation of Developments. *Antioxidants* **2018**, *7* (11), 159. <https://doi.org/10.3390/antiox7110159>.
- (18) Boyes, W. K.; Thornton, B. L. M.; Al-Abed, S. R.; Andersen, C. P.; Bouchard, D. C.; Burgess, R. M.; Hubal, E. A. C.; Ho, K. T.; Hughes, M. F.; Kitchin, K.; et al. A Comprehensive Framework for Evaluating the Environmental Health and Safety Implications of Engineered Nanomaterials. *Crit. Rev. Toxicol.* **2017**, *47* (9), 771–814. <https://doi.org/10.1080/10408444.2017.1328400>.
- (19) Gerloff, K.; Landesmann, B.; Worth, A.; Munn, S.; Palosaari, T.; Whelan, M. The Adverse Outcome Pathway Approach in Nanotoxicology. *Comput. Toxicol.* **2017**, *1*, 3–11. <https://doi.org/10.1016/J.COMTOX.2016.07.001>.
- (20) Halappanavar, S.; Ede, J. D.; Shatkin, J. A.; Krug, H. F. A Systematic Process for Identifying Key Events for Advancing the Development of Nanomaterial Relevant Adverse Outcome Pathways. *NanoImpact* **2019**, *15*, 100178. <https://doi.org/10.1016/J.IMPACT.2019.100178>.

- (21) Allen, T. E. H.; Goodman, J. M.; Gutsell, S.; Russell, P. J. Defining Molecular Initiating Events in the Adverse Outcome Pathway Framework for Risk Assessment. *Chem. Res. Toxicol.* **2014**, *27* (12), 2100–2112. <https://doi.org/10.1021/tx500345j>.
- (22) Brodd, R. J. *Batteries for Sustainability : Selected Entries from the Encyclopedia of Sustainability Science and Technology*; Springer, 2012.
- (23) Grey, C. P.; Ceder, G.; Kang, K.; Meng, Y. S.; Bre, J. Electrodes with High Power and High Capacity for Rechargeable Lithium Batteries. *Science* (80-. ). **2005**, *311* (December), 1–5. <https://doi.org/10.1126/science.1122152>.
- (24) Pollet, B. G.; Staffell, I.; Shang, J. L. Current Status of Hybrid, Battery and Fuel Cell Electric Vehicles: From Electrochemistry to Market Prospects. *Electrochim. Acta* **2012**, *84*, 235–249. <https://doi.org/10.1016/j.electacta.2012.03.172>.
- (25) Wang, Y.; Yu, Y.; Huang, K.; Chen, B.; Deng, W.; Yao, Y. Quantifying the Environmental Impact of a Li-Rich High-Capacity Cathode Material in Electric Vehicles via Life Cycle Assessment. *Environ. Sci. Pollut. Res.* **2017**, *24* (2), 1251–1260. <https://doi.org/10.1007/s11356-016-7849-9>.
- (26) Winslow, K. M.; Laux, S. J.; Townsend, T. G. A Review on the Growing Concern and Potential Management Strategies of Waste Lithium-Ion Batteries. *Resources, Conservation and Recycling*. Elsevier 2018, pp 263–277. <https://doi.org/10.1016/j.resconrec.2017.11.001>.
- (27) Hamers, R. J. Nanomaterials and Global Sustainability. *Acc. Chem. Res.* **2017**, *50* (3), 633–637. <https://doi.org/10.1021/acs.accounts.6b00634>.
- (28) Hamers, R. J. Energy Storage Materials as Emerging Nano-Contaminants. *Chem. Res. Toxicol.* **2020**, *acs.chemrestox.0c00080*. <https://doi.org/10.1021/acs.chemrestox.0c00080>.

- (29) Niemuth, N. J.; Curtis, B. J.; Hang, M. N.; Gallagher, M. J.; Fairbrother, D. H.; Hamers, R. J.; Klaper, R. D. Next-Generation Complex Metal Oxide Nanomaterials Negatively Impact Growth and Development in the Benthic Invertebrate *Chironomus Riparius* upon Settling. *Environ. Sci. Technol.* **2019**, *53* (7), 3860–3870.  
<https://doi.org/10.1021/acs.est.8b06804>.
- (30) Armitage, P. D.; Cranston, P. S.; Pinder, L. C. V. *The Chironomidae : Biology and Ecology of Non-Biting Midges*, 1st ed.; Chapman & Hall, 1995.
- (31) Besten, P. J. den.; Munawar, M. *Ecotoxicological Testing of Marine and Freshwater Ecosystems : Emerging Techniques, Trends, and Strategies*; Taylor & Francis, 2005.
- (32) Park, S.-Y.; Chung, J.; Colman, B. P.; Matson, C. W.; Kim, Y.; Lee, B.-C.; Kim, P.-J.; Choi, K.; Choi, J. Ecotoxicity of Bare and Coated Silver Nanoparticles in the Aquatic Midge, *Chironomus Riparius*. *Environ. Toxicol. Chem.* **2015**, *34* (9), 2023–2032.  
<https://doi.org/10.1002/etc.3019>.
- (33) Gopalakrishnan Nair, P. M.; Chung, I. M. Alteration in the Expression of Antioxidant and Detoxification Genes in *Chironomus Riparius* Exposed to Zinc Oxide Nanoparticles. *Comp. Biochem. Physiol. Part B Biochem. Mol. Biol.* **2015**, *190*, 1–7.  
<https://doi.org/10.1016/j.cbpb.2015.08.004>.
- (34) Waissi-Leinonen, G. C.; Petersen, E. J.; Pakarinen, K.; Akkanen, J.; Leppänen, M. T.; Kukkonen, J. V. K. Toxicity of Fullerene (C60) to Sediment-Dwelling Invertebrate *Chironomus Riparius* Larvae. *Environ. Toxicol. Chem.* **2012**, *31* (9), 2108–2116.  
<https://doi.org/10.1002/etc.1926>.
- (35) Nair, P. M. G.; Park, S. Y.; Lee, S.-W.; Choi, J. Differential Expression of Ribosomal Protein Gene, Gonadotrophin Releasing Hormone Gene and Balbiani Ring Protein Gene

- in Silver Nanoparticles Exposed *Chironomus Riparius*. *Aquat. Toxicol.* **2011**, *101* (1), 31–37. <https://doi.org/10.1016/j.aquatox.2010.08.013>.
- (36) Lee, S.-W.; Kim, S.-M.; Choi, J. Genotoxicity and Ecotoxicity Assays Using the Freshwater Crustacean *Daphnia Magna* and the Larva of the Aquatic Midge *Chironomus Riparius* to Screen the Ecological Risks of Nanoparticle Exposure. *Environ. Toxicol. Pharmacol.* **2009**, *28* (1), 86–91. <https://doi.org/10.1016/j.etap.2009.03.001>.
- (37) Beinert, H. Iron-Sulfur Proteins: Ancient Structures, Still Full of Surprises. *Journal of Biological Inorganic Chemistry*. Springer-Verlag February 2000, pp 2–15. <https://doi.org/10.1007/s007750050002>.
- (38) Castello, A.; Hentze, M. W.; Preiss, T. Metabolic Enzymes Enjoying New Partnerships as RNA-Binding Proteins. *Trends Endocrinol. Metab.* **2015**, *26* (12), 746–757. <https://doi.org/10.1016/j.tem.2015.09.012>.
- (39) Resch, V.; Hanefeld, U. The Selective Addition of Water. *Catal. Sci. Technol.* **2015**, *5* (3), 1385–1399. <https://doi.org/10.1039/C4CY00692E>.
- (40) Tong, J.; Feinberg, B. A. Direct Square-Wave Voltammetry of Superoxidized [4Fe-4S]<sup>3+</sup> Aconitase and Associated 3Fe/4Fe Cluster Interconversions. *J. Biol. Chem.* **1994**, *269* (40), 24920–24927.
- (41) Kalyanaraman, B.; Cheng, G.; Zielonka, J.; Bennett, B. Low-Temperature EPR Spectroscopy as a Probe-Free Technique for Monitoring Oxidants Formed in Tumor Cells and Tissues: Implications in Drug Resistance and OXPHOS-Targeted Therapies. *Cell Biochem. Biophys.* **2019**, *77* (1), 89–98. <https://doi.org/10.1007/s12013-018-0858-1>.
- (42) Melby, E. S.; Cui, Y.; Borgatta, J.; Mensch, A. C.; Hang, M. N.; Chrisler, W. B.; Dohnalkova, A.; Van Gilder, J. M.; Alvarez, C. M.; Smith, J. N.; et al. Impact of

- Lithiated Cobalt Oxide and Phosphate Nanoparticles on Rainbow Trout Gill Epithelial Cells. *Nanotoxicology* **2018**, *12* (10), 1166–1181.  
<https://doi.org/10.1080/17435390.2018.1508785>.
- (43) Sazanov, L. A. A Giant Molecular Proton Pump: Structure and Mechanism of Respiratory Complex I. *Nat. Rev. Mol. Cell Biol.* **2015**, *16* (6), 375–388.  
<https://doi.org/10.1038/nrm3997>.
- (44) Van Vranken, J. G.; Na, U.; Winge, D. R.; Rutter, J. Protein-Mediated Assembly of Succinate Dehydrogenase and Its Cofactors. *Crit. Rev. Biochem. Mol. Biol.* **2015**, *50* (2), 168–180. <https://doi.org/10.3109/10409238.2014.990556>.
- (45) Barras, F.; Fontecave, M. Cobalt Stress in Escherichia Coli and Salmonella Enterica: Molecular Bases for Toxicity and Resistance. *Metallomics* **2011**, *3* (11), 1130–1134.  
<https://doi.org/10.1039/c1mt00099c>.
- (46) Lill, R.; Mühlhoff, U. Iron–Sulfur-Protein Biogenesis in Eukaryotes. *Trends Biochem. Sci.* **2005**, *30* (3), 133–141. <https://doi.org/10.1016/j.tibs.2005.01.006>.
- (47) Bozich, J.; Hang, M.; Hamers, R.; Klaper, R. Core Chemistry Influences the Toxicity of Multicomponent Metal Oxide Nanomaterials, Lithium Nickel Manganese Cobalt Oxide, and Lithium Cobalt Oxide to Daphnia Magna. *Environ. Toxicol. Chem.* **2017**, *36* (9), 2493–2502. <https://doi.org/10.1002/etc.3791>.
- (48) Sironval, V.; Reylandt, L.; Chaurand, P.; Ibouaadaten, S.; Palmai-Pallag, M.; Yakoub, Y.; Ucakar, B.; Rose, J.; Poleunis, C.; Vanbever, R.; et al. Respiratory Hazard of Li-Ion Battery Components: Elective Toxicity of Lithium Cobalt Oxide (LiCoO<sub>2</sub>) Particles in a Mouse Bioassay. *Arch. Toxicol.* **2018**, *92* (5), 1673–1684.  
<https://doi.org/10.1007/s00204-018-2188-x>.

- (49) Laudadio, E. D.; Bennett, J. W.; Green, C. M.; Mason, S. E.; Hamers, R. J. Impact of Phosphate Adsorption on Complex Cobalt Oxide Nanoparticle Dispersibility in Aqueous Media. *Environ. Sci. Technol.* **2018**, *52* (17), 10186–10195.  
<https://doi.org/10.1021/acs.est.8b02324>.
- (50) Andrews, S.; Krueger, F.; Seconda-Pichon, A.; Biggins, F.; Wingett, S. FastQC: A Quality Control Tool for High Throughput Sequence Data. Babraham Bioinformatics, Babraham Institute, Cambridge, United Kingdom 2010.
- (51) Martin, M. Cutadapt Removes Adapter Sequences from High-Throughput Sequencing Reads. *EMBnet.journal* **2011**, *17* (1), 10. <https://doi.org/10.14806/ej.17.1.200>.
- (52) Grabherr, M. G.; Haas, B. J.; Yassour, M.; Levin, J. Z.; Thompson, D. A.; Amit, I.; Adiconis, X.; Fan, L.; Raychowdhury, R.; Zeng, Q.; et al. Full-Length Transcriptome Assembly from RNA-Seq Data without a Reference Genome. *Nat. Biotechnol.* **2011**, *29* (7), 644–652. <https://doi.org/10.1038/nbt.1883>.
- (53) Camacho, C.; Coulouris, G.; Avagyan, V.; Ma, N.; Papadopoulos, J.; Bealer, K.; Madden, T. L. BLAST+: Architecture and Applications. *BMC Bioinformatics* **2009**, *10* (1), 421. <https://doi.org/10.1186/1471-2105-10-421>.
- (54) Marinković, M.; de Leeuw, W. C.; de Jong, M.; Kraak, M. H. S.; Admiraal, W.; Breit, T. M.; Jonker, M. J. Combining Next-Generation Sequencing and Microarray Technology into a Transcriptomics Approach for the Non-Model Organism *Chironomus Riparius*. *PLoS One* **2012**, *7* (10), e48096. <https://doi.org/10.1371/journal.pone.0048096>.
- (55) Nair, P. M. G.; Park, S. Y.; Choi, J. Analyses of Expressed Sequence Tags from *Chironomus Riparius* Using Pyrosequencing : Molecular Ecotoxicology Perspective.

- Environ. Health Toxicol.* **2011**, *26*, e2011010.  
<https://doi.org/10.5620/eht.2011.26.e2011010>.
- (56) Bray, N. L.; Pimentel, H.; Melsted, P.; Pachter, L. Near-Optimal Probabilistic RNA-Seq Quantification. *Nat. Biotechnol.* **2016**, *34* (5), 525–527. <https://doi.org/10.1038/nbt.3519>.
- (57) Love, M. I.; Huber, W.; Anders, S. Moderated Estimation of Fold Change and Dispersion for RNA-Seq Data with DESeq2. *Genome Biol.* **2014**, *15* (12), 550.  
<https://doi.org/10.1186/s13059-014-0550-8>.
- (58) Huang, D. W.; Sherman, B. T.; Lempicki, R. A. Systematic and Integrative Analysis of Large Gene Lists Using DAVID Bioinformatics Resources. *Nat. Protoc.* **2009**, *4* (1), 44–57. <https://doi.org/10.1038/nprot.2008.211>.
- (59) Huang, D. W.; Sherman, B. T.; Lempicki, R. A. Bioinformatics Enrichment Tools: Paths toward the Comprehensive Functional Analysis of Large Gene Lists. *Nucleic Acids Res.* **2009**, *37* (1), 1–13. <https://doi.org/10.1093/nar/gkn923>.
- (60) Kanehisa, M.; Goto, S. KEGG: Kyoto Encyclopedia of Genes and Genomes. *Nucleic Acids Res.* **2000**, *28* (1), 27–30. <https://doi.org/10.1093/nar/28.1.27>.
- (61) Kanehisa, M.; Sato, Y.; Furumichi, M.; Morishima, K.; Tanabe, M. New Approach for Understanding Genome Variations in KEGG. *Nucleic Acids Res.* **2019**, *47* (D1), D590–D595. <https://doi.org/10.1093/nar/gky962>.
- (62) Kanehisa, M. Toward Understanding the Origin and Evolution of Cellular Organisms. *Protein Sci.* **2019**, *28* (11), 1947–1951. <https://doi.org/10.1002/pro.3715>.
- (63) Haddy, A.; Smith, G. Transition Metal and Organic Radical Components of Carp Liver Tissue Observed by Electron Paramagnetic Resonance Spectroscopy. *Comp. Biochem.*

- Physiol. Part B Biochem. Mol. Biol.* **1999**, *123* (4), 407–415.  
[https://doi.org/10.1016/S0305-0491\(99\)00087-5](https://doi.org/10.1016/S0305-0491(99)00087-5).
- (64) Borzone, G.; Zhao, B.; Merola, A. J.; Berliner, L.; Clanton, T. L. Detection of Free Radicals by Electron Spin Resonance in Rat Diaphragm after Resistive Loading. *J. Appl. Physiol.* **1994**, *77* (2), 812–818. <https://doi.org/10.1152/jappl.1994.77.2.812>.
- (65) Ranquet, C.; Ollagnier-de-Choudens, S.; Loiseau, L.; Barras, F.; Fontecave, M. Cobalt Stress in Escherichia Coli. The Effect on the Iron-Sulfur Proteins. *J. Biol. Chem.* **2007**, *282* (42), 30442–30451. <https://doi.org/10.1074/jbc.M702519200>.
- (66) Pearce, L. L.; Martinez-Bosch, S.; Manzano, E. L.; Winnica, D. E.; Epperly, M. W.; Peterson, J. The Resistance of Electron-Transport Chain Fe–S Clusters to Oxidative Damage during the Reaction of Peroxynitrite with Mitochondrial Complex II and Rat-Heart Pericardium. *Nitric Oxide* **2009**, *20* (3), 135–142.  
<https://doi.org/10.1016/j.niox.2008.12.001>.
- (67) Rouault, T. A.; Tong, W. H. Iron–Sulfur Cluster Biogenesis and Human Disease. *Trends Genet.* **2008**, *24* (8), 398–407. <https://doi.org/10.1016/j.tig.2008.05.008>.
- (68) Dieni, C. A.; Callaghan, N. I.; Gormley, P. T.; Butler, K. M. A.; MacCormack, T. J. Physiological Hepatic Response to Zinc Oxide Nanoparticle Exposure in the White Sucker, *Catostomus Commersonii*. *Comp. Biochem. Physiol. Part C Toxicol. Pharmacol.* **2014**, *162*, 51–61. <https://doi.org/10.1016/j.cbpc.2014.03.009>.
- (69) Guo, J.; Gao, S.-H.; Lu, J.; Bond, P. L.; Verstraete, W.; Yuan, Z. Copper Oxide Nanoparticles Induce Lysogenic Bacteriophage and Metal-Resistance Genes in *Pseudomonas Aeruginosa* PAO1. *ACS Appl. Mater. Interfaces* **2017**, *9* (27), 22298–22307. <https://doi.org/10.1021/acsami.7b06433>.

- (70) Tedesco, S.; Bayat, N.; Danielsson, G.; Buque, X.; Aspichueta, P.; Fresnedo, O.; Cristobal, S. Proteomic and Lipidomic Analysis of Primary Mouse Hepatocytes Exposed to Metal and Metal Oxide Nanoparticles. *J. Integr. OMICS* **2015**, *5* (1).  
<https://doi.org/10.5584/jiomics.v5i1.184>.
- (71) Filippi, C.; Pryde, A.; Cowan, P.; Lee, T.; Hayes, P.; Donaldson, K.; Plevris, J.; Stone, V. Toxicology of ZnO and TiO<sub>2</sub> Nanoparticles on Hepatocytes: Impact on Metabolism and Bioenergetics. *Nanotoxicology* **2015**, *9* (1), 126–134.  
<https://doi.org/10.3109/17435390.2014.895437>.
- (72) Yan, G.; Huang, Y.; Bu, Q.; Lv, L.; Deng, P.; Zhou, J.; Wang, Y.; Yang, Y.; Liu, Q.; Cen, X.; et al. Zinc Oxide Nanoparticles Cause Nephrotoxicity and Kidney Metabolism Alterations in Rats. *J. Environ. Sci. Heal. Part A* **2012**, *47* (4), 577–588.  
<https://doi.org/10.1080/10934529.2012.650576>.
- (73) Cardinale, B. J.; Bier, R.; Kwan, C. Effects of TiO<sub>2</sub> Nanoparticles on the Growth and Metabolism of Three Species of Freshwater Algae. *J. Nanoparticle Res.* **2012**, *14* (8), 913. <https://doi.org/10.1007/s11051-012-0913-6>.
- (74) Ratnasekhar, C.; Sonane, M.; Satish, A.; Mudiam, M. K. R. Metabolomics Reveals the Perturbations in the Metabolome of *Caenorhabditis Elegans* Exposed to Titanium Dioxide Nanoparticles. *Nanotoxicology* **2015**, *9* (8), 994–1004.  
<https://doi.org/10.3109/17435390.2014.993345>.
- (75) Merzendorfer, H. Chitin Metabolism in Insects: Structure, Function and Regulation of Chitin Synthases and Chitinases. *J. Exp. Biol.* **2003**, *206* (24), 4393–4412.  
<https://doi.org/10.1242/jeb.00709>.

- (76) Lehane, M. J. PERITROPHIC MATRIX STRUCTURE AND FUNCTION. *Annu. Rev. Entomol.* **1997**, *42* (1), 525–550. <https://doi.org/10.1146/annurev.ento.42.1.525>.
- (77) Chang, H.; Yhee, J. Y.; Jang, G. H.; You, D. G.; Ryu, J. H.; Choi, Y.; Na, J. H.; Park, J. H.; Lee, K. H.; Choi, K.; et al. Predicting the in Vivo Accumulation of Nanoparticles in Tumor Based on in Vitro Macrophage Uptake and Circulation in Zebrafish. *J. Control. Release* **2016**, *244*, 205–213. <https://doi.org/10.1016/j.jconrel.2016.07.025>.
- (78) Zhang, H.; Ji, Z.; Xia, T.; Meng, H.; Low-Kam, C.; Liu, R.; Pokhrel, S.; Lin, S.; Wang, X.; Liao, Y.-P.; et al. Use of Metal Oxide Nanoparticle Band Gap To Develop a Predictive Paradigm for Oxidative Stress and Acute Pulmonary Inflammation. *ACS Nano* **2012**, *6* (5), 4349–4368. <https://doi.org/10.1021/nm3010087>.
- (79) Tervonen, K.; Waissi, G.; Petersen, E. J.; Akkanen, J.; Kukkonen, J. V. K. Analysis of Fullerene-C 60 and Kinetic Measurements for Its Accumulation and Depuration in Daphnia Magna. *Environ. Toxicol. Chem.* **2010**, n/a-n/a. <https://doi.org/10.1002/etc.124>.
- (80) Audinot, J.-N.; Georgantzopoulou, A.; Piret, J.-P.; Gutleb, A. C.; Dowsett, D.; Migeon, H. N.; Hoffmann, L. Identification and Localization of Nanoparticles in Tissues by Mass Spectrometry. *Surf. Interface Anal.* **2013**, *45* (1), 230–233. <https://doi.org/10.1002/sia.5099>.
- (81) Lovern, S. B.; Owen, H. A.; Klaper, R. Electron Microscopy of Gold Nanoparticle Intake in the Gut of Daphnia Magna. *Nanotoxicology* **2008**, *2* (1), 43–48. <https://doi.org/10.1080/17435390801935960>.
- (82) Bacchetta, R.; Santo, N.; Valenti, I.; Maggioni, D.; Longhi, M.; Tremolada, P. Comparative Toxicity of Three Differently Shaped Carbon Nanomaterials on Daphnia

Magna : Does a Shape Effect Exist? *Nanotoxicology* **2018**, *12* (3), 201–223.

<https://doi.org/10.1080/17435390.2018.1430258>.

- (83) Mattsson, K.; Adolfsson, K.; Ekvall, M. T.; Borgström, M. T.; Linse, S.; Hansson, L.-A.; Cedervall, T.; Prinz, C. N. Translocation of 40 Nm Diameter Nanowires through the Intestinal Epithelium of *Daphnia Magna*. *Nanotoxicology* **2016**, *10* (8), 1160–1167.  
<https://doi.org/10.1080/17435390.2016.1189615>.
- (84) Chaika, V.; Pikula, K.; Vshivkova, T.; Zakharenko, A.; Reva, G.; Drozdov, K.; Vardavas, A. I.; Stivaktakis, P. D.; Nikolouzakis, T. K.; Stratidakis, A. K.; et al. The Toxic Influence and Biodegradation of Carbon Nanofibers in Freshwater Invertebrates of the Families Gammaridae, Ephemerellidae, and Chironomidae. *Toxicol. Reports* **2020**, *7*, 947–954. <https://doi.org/10.1016/j.toxrep.2020.07.011>.

## Tables

**Table 1. Differentially expressed Fe-S protein genes by function.**

Function	Gene name	Pathway	Fold Change
4Fe-4S binding			
	<i>NUBP2; nucleotide binding protein 2</i>	Iron-sulfur cluster assembly	+1.5
	<i>NUBP1; nucleotide binding protein 1</i>	Iron-sulfur cluster assembly	+1.4
	<i>ISCA2; iron-sulfur cluster assembly 2</i>	Iron-sulfur cluster assembly	+1.4
	<i>SDHB; succinate dehydrogenase (ubiquinone) iron-sulfur subunit</i>	Citrate cycle (TCA cycle), Oxidative phosphorylation	+1.5
	<i>NDUFS7; NADH dehydrogenase (ubiquinone) Fe-S protein 7</i>	Oxidative phosphorylation	+1.2
	<i>NDUFV1; NADH dehydrogenase (ubiquinone) flavoprotein 1</i>	Oxidative phosphorylation	+1.3
	<i>NDUFS8; NADH dehydrogenase (ubiquinone) Fe-S protein 8</i>	Oxidative phosphorylation	+1.2
	<i>LIPA; lipoyl synthase</i>	Lipoic acid metabolism	+1.4
	<i>NTH; endonuclease III</i>	Base excision repair	+1.7
	<i>RTEL1; regulator of telomere elongation helicase 1</i>	Telomere maintenance, DNA replication, DNA repair	+1.2
Fe-S biogenesis			
	<i>ISCS; cysteine desulfurase</i>	[2Fe-2S] cluster assembly	+1.2
Fe-S binding			
	<i>Amidophosphoribosyl transferase</i>	Purine metabolism	-1.7
	<i>XDH; xanthine dehydrogenase/oxidase</i>	Purine metabolism	-1.7

## Figures

**Figure 1. Electron paramagnetic resonance spectroscopy of intact larvae shows changes in Fe-S centers from LCO exposure.**

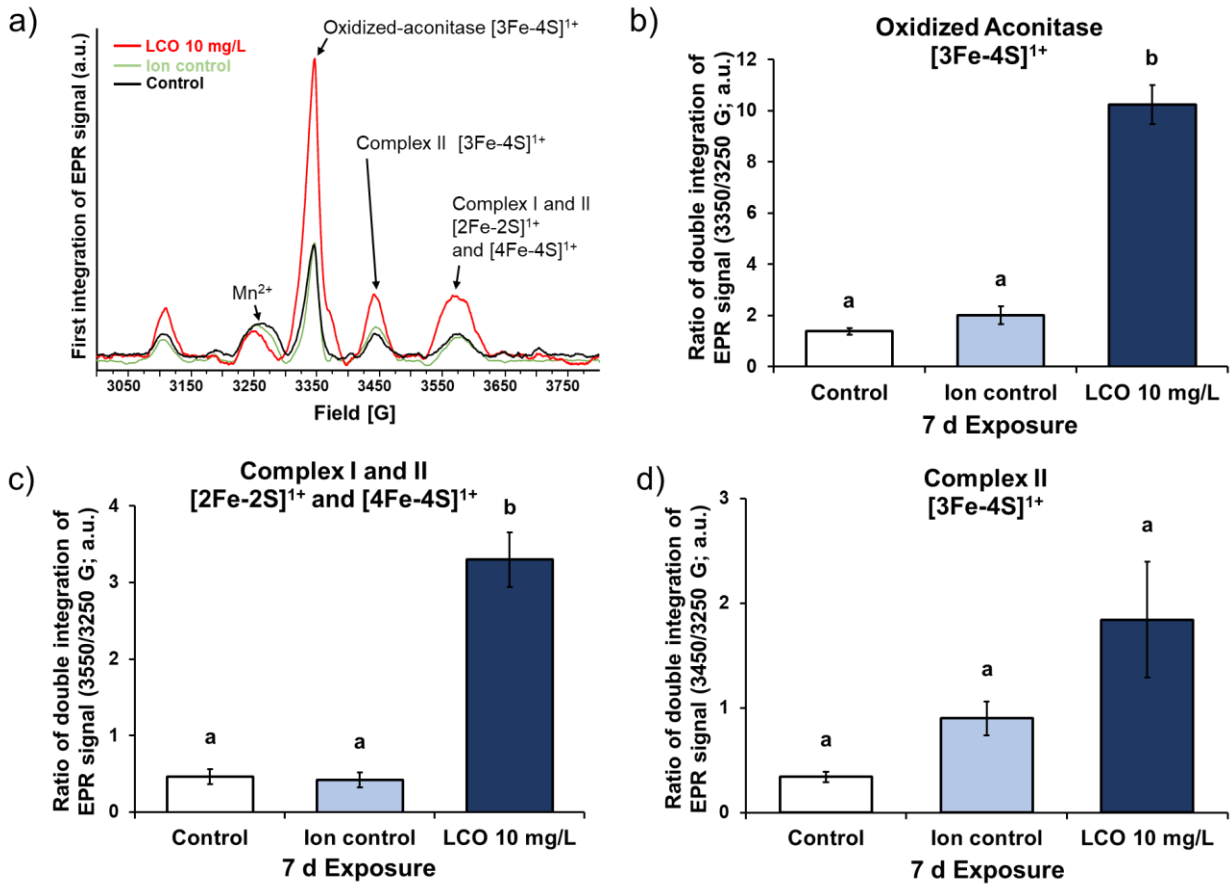


**Figure 1. Electron paramagnetic resonance spectroscopy of intact larvae shows changes in Fe-S centers from LCO exposure.** Representative electron paramagnetic resonance spectra (a) for *C. riparius* larvae exposed to control, released Li and Co ion control, and 10 mg/L LCO for 7 days; and quantification of peak area for (b) oxidized aconitase [3Fe-4S]<sup>1+</sup>, (c) [2Fe-2S]<sup>1+</sup> and [4Fe-4S]<sup>1+</sup> from complex I and II of the electron transport chain (ETC), and (d) [3Fe-4S]<sup>1+</sup> from complex I of the ETC relative to the peak area for Mn<sup>2+</sup>, which was invariant across samples. Letters (panels b-d) indicate significant differences by one-way Welch ANOVA with Dunnett T3 post-hoc,  $p < 0.05$ . Average of 5 replicate samples; error bars indicate standard error of the mean.

Increased oxidation of the aconitase Fe-S center in LCO-exposed larvae identifies these sites as a target of LCO-induced oxidative stress.

**Figure 2. Aconitase activity of larval protein is negatively impacted by LCO.**

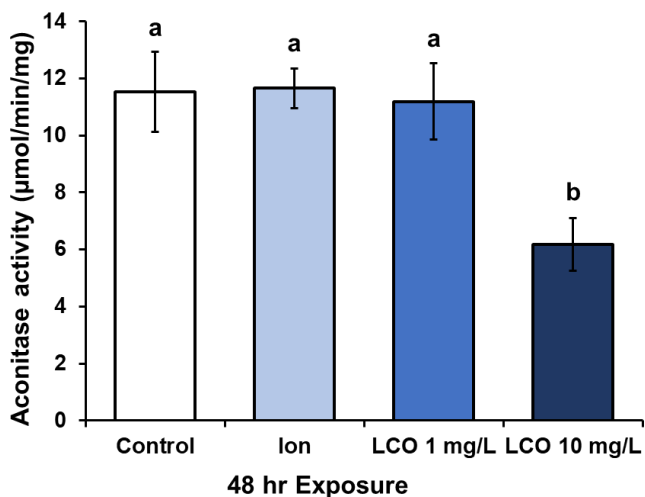


**Figure 2. Aconitase activity of larval protein is negatively impacted by LCO.** Aconitase activity of protein extracted from *C. riparius* larvae exposed to control, released Li and Co ion control, 1 mg/L LCO, and 10 mg/L LCO for 48 hr. Letters indicate significant differences by One-way ANOVA with Tukey HSD post-hoc,  $p < 0.05$ . Average of 5 replicate samples; error bars indicate standard error of the mean. The significant reduction in aconitase activity in 10 mg/L LCO-exposed larvae supports disruption of the Fe-S center of this enzyme as a potential mechanism of LCO impact.

**Figure 3. Significantly enriched molecular functions and pathways show importance of metabolism and Fe-S centers in LCO impacts.**

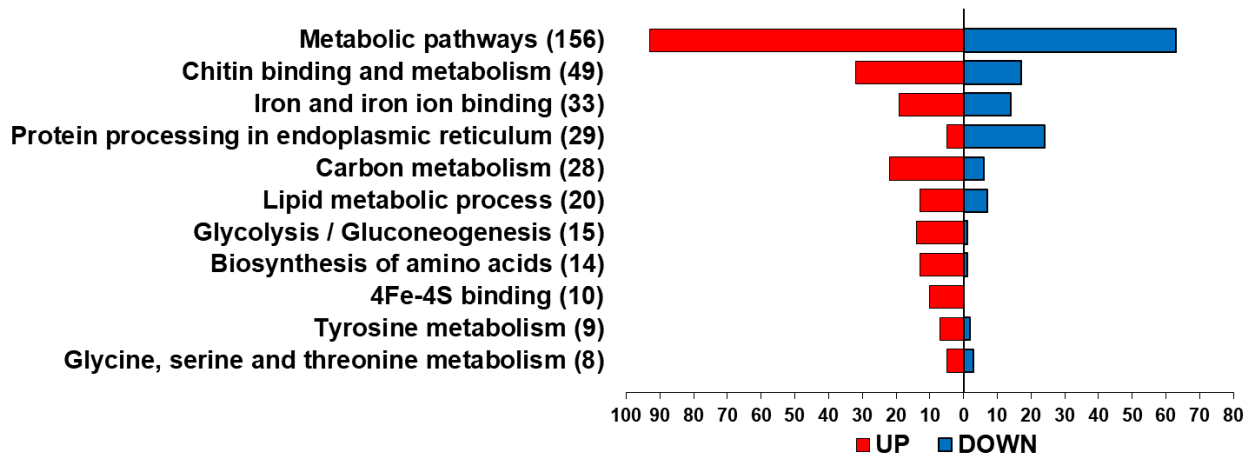


**Figure 3. Significantly enriched molecular functions and pathways show importance of metabolism and Fe-S centers in LCO impacts.** Molecular functions and pathways identified as significantly enriched (Benjamini-adjusted FDR < 0.1) in genes differentially expressed (Wald FDR < 0.1) between MHRW control and 10 mg/L LCO-exposed *C. riarius* larvae at 48 hr by the Database for Annotation, Visualization and Integrated Discovery (DAVID) v6.8. Metabolic pathways are significantly enriched (156 genes), which includes Carbon metabolism (28 genes), Lipid metabolic processes (20 genes), Glycolysis/Gluconeogenesis (15 genes), Biosynthesis of amino acids (14 genes), Tyrosine metabolism (9 genes), and Glycine, serine and threonine metabolism (8 genes) all being significantly enriched. Molecular functions significantly enriched include Chitin binding and metabolism (49 genes), Iron and iron ion binding (33 genes), and 4Fe-4S binding (10 genes). Changes in Fe-S centers could potentially induce observed differences in metabolism and iron ion binding because of their role in enzymatic and regulatory proteins involved in these processes.

**Figure 4. Differentially expressed metabolic gene pathways indicate shift toward energy production in LCO-exposed larvae.**

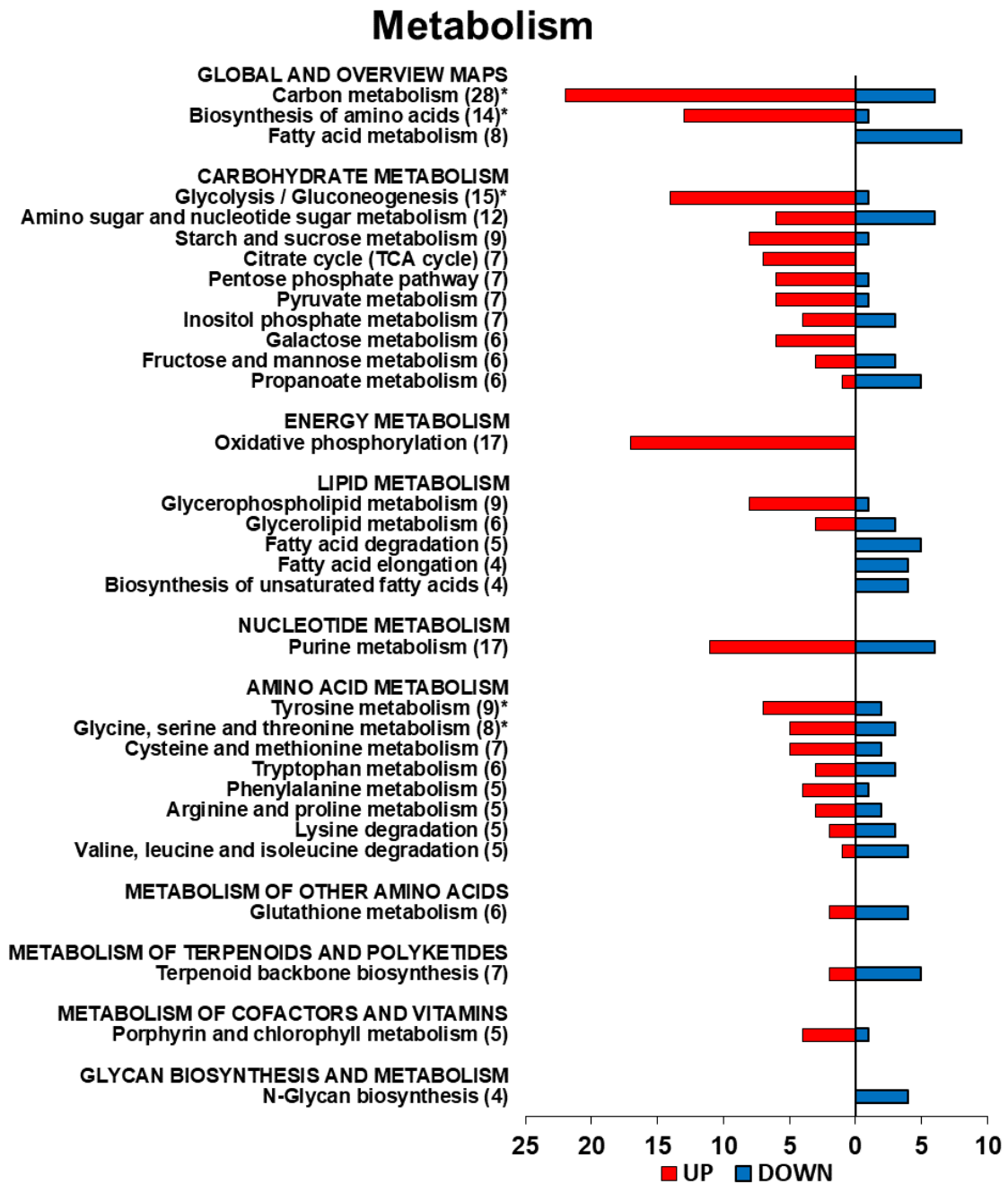


**Figure 4. Differentially expressed metabolic gene pathways indicate shift toward energy production in LCO-exposed larvae.** Breakdown of Kyoto Encyclopedia of Genes and Genomes (KEGG) pathways containing genes identified as differentially expressed (Wald FDR < 0.1) between MHRW control and 10 mg/L LCO-exposed *C. riparius* larvae at 48 hr. \*

Indicates specific pathways identified as significantly enriched by DAVID (Benjamini-adjusted FDR < 0.1; Fig 3). Overall metabolic changes, specifically changes in Carbon metabolism (28 genes), including Glycolysis/gluconeogenesis (15 genes), the Citrate cycle (7 genes), and Oxidative phosphorylation (17 genes), indicate a shift toward energy production in exposed larvae. The critical role of Fe-S proteins in the Citrate cycle and Oxidative phosphorylation and their disruption by LCO exposure could potentially explain observed changes.

**Figure 5. Proposed adverse outcome pathway showing observed LCO impacts from molecular initiating event through adverse outcomes.**

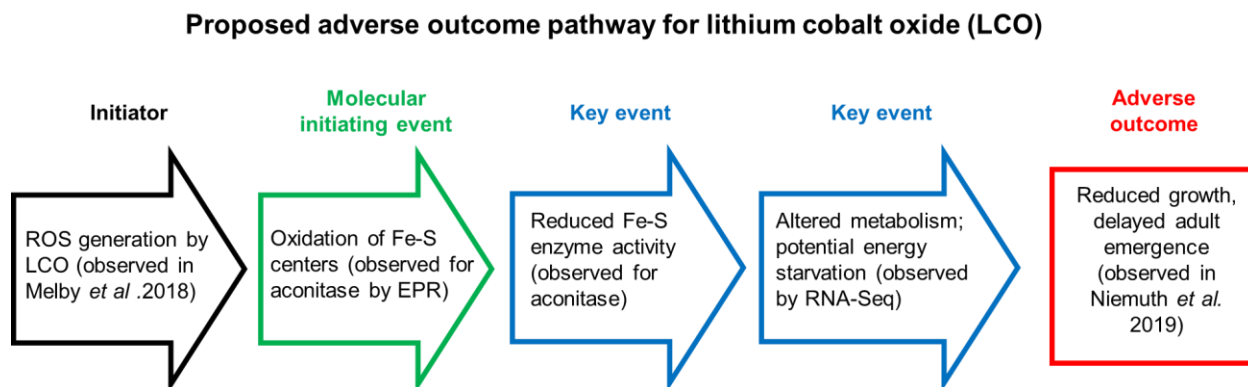


**Figure 5. Proposed adverse outcome pathway showing observed LCO impacts from molecular initiating event through adverse outcomes.** In the proposed adverse outcome

pathway (AOP), reactive oxygen species (ROS) generated by LCO (observed in Melby *et al.* 2018)<sup>42</sup> oxidize the of Fe-S centers in regulatory and metabolic proteins (observed for aconitase in this study by electron paramagnetic resonance), reducing Fe-S enzyme activity (observed for aconitase in this study) and changing regulatory activity. This disrupts metabolism, particularly energy generation (observed in this study by RNA-Seq), ultimately causing reductions in growth of larvae and delaying their development into adult flies (observe in Niemuth *et al.* 2019).<sup>29</sup>

## SUPPORTING INFORMATION

### **Supporting information for:**

Protein Fe-S centers as a molecular target of toxicity of a complex transition metal oxide nanomaterial with downstream impacts on metabolism and growth

Nicholas J Niemuth, Yongqian Zhang, Aurash A Mohaimani, Angela Schmoldt, Elizabeth D Laudadio, Robert J Hamers, Rebecca D Klaper\*

**Pages:** 56

**Tables:** 2

**Figures:** 9

## Supporting tables

**Supplementary Table S1. LCO zeta potential in MHRW exposure media.**

ENM (conc)	$\zeta$ -potential (mV)*	Electrophoretic mobility ( $\mu\text{m}\cdot\text{cm}\cdot\text{Vs}^{-1}$ )
LCO (1 mg·L <sup>-1</sup> )	-12.6 ± 0.6	-0.99 ± 0.05
LCO (10 mg·L <sup>-1</sup> )	-3.7 ± 0.5	-0.28 ± 0.04

\* Calculated using Smoluchowski method.

**Supplementary Table S2. Differentially expressed genes between MHRW control and LCO**

**10 mg/L 48 hr exposure.**

Protein ID	Annotation Source	KEGG Orthology	Fold change	Adjusted P-value
XP_307890	NCBI	K00021	-1.672188425	0.022757515
XP_003436731	NCBI	K00029	1.65213697	0.022757515
XP_751388	NCBI	K00045	-2.196867891	1.45761E-06
XP_321329	NCBI	K00069	1.635337399	0.068284394
XP_316291	NCBI	K00106	1.717436485	0.014995264
XP_310333	NCBI	K00108	-11.05148459	0.051485036
XP_003436808	NCBI	K00111	1.691483065	0.028280899
XP_318655	NCBI	K00134	1.528417702	0.004774834
XP_312441	NCBI	K00140	1.409184628	0.051003096
XP_318026	NCBI	K00161	1.437248707	0.050431881
XP_311527	NCBI	K00162	1.399883725	0.070614214
XP_320718	NCBI	K00232	-1.316126082	0.097896273
XP_311518	NCBI	K00234	1.280433635	0.084822104
XP_308512	NCBI	K00235	1.467850092	0.003075894
XP_311387	NCBI	K00236	1.282276718	0.0964316
XP_315115	NCBI	K00286	-1.501113355	0.02651537
XP_312663	NCBI	K00286	1.480286031	0.002956368
XP_312083	NCBI	K00288	3.002911542	1.70327E-10
XP_318638	NCBI	K00451	2.171024011	0.013087606
XP_312204	NCBI	K00453	1.707237332	0.001140227
XP_318007	NCBI	K00457	2.619820639	0.021791581
XP_315450	NCBI	K00474	2.105394647	9.77159E-05

XP_315983	NCBI	K00486	4.050804038	5.90381E-07
XP_001688715	NCBI	K00500	2.88470618	0.000444175
XP_312474	NCBI	K00522	1.493846812	0.000643819
XP_316898	NCBI	K00547	-5.477637729	0.005593703
NP_012607	NCBI	K00551	1.887162588	0.01560531
XP_640104	NCBI	K00551	1.883812383	0.046147444
XP_565619	NCBI	K00552	-8.892790241	0.022211057
XP_313697	NCBI	K00586	-1.290635659	0.076014187
XP_314502	NCBI	K00591	1.81332105	8.34185E-10
XP_314504	NCBI	K00591	1.748267862	6.23434E-05
XP_321828	NCBI	K00626	-1.272184134	0.044989945
XP_317493	NCBI	K00627	1.442657116	0.051456515
XP_312882	NCBI	K00643	2.390699326	0.011888166
XP_317541	NCBI	K00688	1.438903342	0.025288123
XP_311519	NCBI	K00700	-2.034253671	0.051715264
XP_308833	NCBI	K00710	-1.820779236	0.000949232
XP_314708	NCBI	K00710	-1.306133416	0.093186707
XP_315359	NCBI	K00726	-1.245696643	0.047783196
XP_318249	NCBI	K00747	-1.170790766	0.097507151
XP_318827	NCBI	K00784	1.456623383	0.000783264
XP_308653	NCBI	K00787	1.687335648	0.001327994
XP_307863	NCBI	K00789	1.44008212	0.00436022
XP_310975	NCBI	K00799	1.611425481	0.007539016
XP_311299	NCBI	K00799	1.349161777	0.01478489
XP_315341	NCBI	K00802	-1.305424486	0.083175648
XP_308860	NCBI	K00804	1.312750761	0.008095403
XP_310789	NCBI	K00815	2.074042568	0.012136323
XP_309676	NCBI	K00830	1.479065766	0.02425688
XP_564589	NCBI	K00850	1.379448141	0.049910292
XP_319291	NCBI	K00856	1.439135791	0.003142549
XP_321549	NCBI	K00864	-1.456975172	0.011821358
XP_315228	NCBI	K00873	1.436668016	0.024877519
XP_310885	NCBI	K00884	-1.778298273	0.023463589
XP_319468	NCBI	K00898	1.491231102	0.022836951
XP_319464	NCBI	K00914	-1.391337825	0.040343066
XP_320429	NCBI	K00915	1.44861534	0.008233907
XP_308155	NCBI	K00939	-1.354191354	0.047369419
XP_318704	NCBI	K00944	-1.323471285	0.011821358
XP_001688552	NCBI	K00948	1.562354011	0.010123266
XP_003435790	NCBI	K00963	1.732682708	0.000643819
XP_319628	NCBI	K00993	-2.257098365	0.059676775

XP_552478	NCBI	K00993	-1.197694522	0.030740997
XP_317328	NCBI	K01001	-1.238925041	0.051333314
XP_313654	NCBI	K01017	-1.788412065	0.005962876
XP_318096	NCBI	K01047	1.625497069	0.056240353
XP_321444	NCBI	K01052	4.187045563	1.54192E-07
XP_309657	NCBI	K01052	11.10234057	0.003118065
XP_309839	NCBI	K01057	-1.329974747	0.09138875
XP_001237723	NCBI	K01063	-7.161509207	0.016327919
XP_320295	NCBI	K01079	-6.583159145	0.00203368
XP_321503	NCBI	K01081	1.475029305	0.073488464
XP_001866718	NCBI	K01084	2.1217504	0.004743871
XP_311485	NCBI	K01092	1.392218038	0.000217804
XP_316595	NCBI	K01092	1.167506754	0.047607955
XP_316448	NCBI	K01183	1.997319651	0.008856666
XP_001862401	NCBI	K01183	1.622913097	0.00166271
XP_308446	NCBI	K01185	1.927935004	0.001281836
XP_308448	NCBI	K01185	1.97357308	9.92392E-08
XP_320158	NCBI	K01187	2.148933564	0.00059404
XP_320471	NCBI	K01194	1.384421561	0.088708052
XP_317823	NCBI	K01197	-2.629526503	0.05071954
XP_318652	NCBI	K01204	-2.229099915	0.020669336
XP_320760	NCBI	K01205	-2.593653801	0.030050774
XP_310876	NCBI	K01227	1.4499905	0.06768958
XP_311257	NCBI	K01251	1.91864942	5.62689E-06
XP_560264	NCBI	K01262	-1.572788319	0.026568322
XP_552611	NCBI	K01273	-2.904311004	7.47843E-06
XP_308012	NCBI	K01360	1.464522395	0.070579963
NP_999094	NCBI	K01366	1.546021982	0.010678097
XP_001844355	NCBI	K01373	1.640592187	0.005697826
XP_316360	NCBI	K01446	8.074117146	0.024664488
XP_310208	NCBI	K01489	2.448563979	3.82157E-08
XP_003436355	NCBI	K01528	1.858642057	9.14035E-05
XP_312283	NCBI	K01530	1.562164059	0.097281467
XP_556439	NCBI	K01551	-1.415016064	0.008768406
XP_315893	NCBI	K01555	1.656840894	0.065389255
XP_320233	NCBI	K01581	12.88042228	2.00863E-16
XP_320707	NCBI	K01581	8.665126143	8.57737E-22
XP_319840	NCBI	K01593	-127.4590984	9.77372E-10
XP_320631	NCBI	K01599	1.337240401	0.031006675
XP_315872	NCBI	K01641	-2.142540895	0.012206038
XP_321179	NCBI	K01679	1.393482291	0.022757515

XP_317672	NCBI	K01689	1.508570388	0.016202421
XP_310977	NCBI	K01697	1.776961253	0.000342852
XP_308963	NCBI	K01711	-2.388112786	0.021791581
XP_317395	NCBI	K01719	-1.531650583	0.002633057
XP_308239	NCBI	K01768	1.566346125	0.02710083
XP_321074	NCBI	K01769	1.652248349	0.0472589
XP_003436289	NCBI	K01800	1.502361723	0.010066685
XP_321467	NCBI	K01803	1.271595644	0.086349197
XP_320366	NCBI	K01810	1.264556061	0.074239631
XP_321710	NCBI	K01834	1.383356304	0.042753069
XP_315885	NCBI	K01835	1.471018805	0.021612578
XP_308570	NCBI	K01836	-1.56645505	0.019629668
XP_308773	NCBI	K01872	-1.432973325	0.025288123
XP_317207	NCBI	K01875	-7.643047518	0.013882443
XP_312366	NCBI	K01885	1.481561391	1.80592E-06
XP_318119	NCBI	K01887	-1.299517573	0.079596979
XP_003437081	NCBI	K01892	-1.326932149	0.019402374
XP_321651	NCBI	K01908	-1.696266506	0.08756042
XP_308920	NCBI	K01934	1.550034735	0.028358684
XP_319294	NCBI	K01951	-1.181783033	0.075887564
XP_001237894	NCBI	K01988	-11.62707879	0.004615328
XP_321341	NCBI	K02259	1.824046259	1.59473E-06
XP_314839	NCBI	K02263	1.214362657	0.077128158
XP_556301	NCBI	K02296	2.188173479	0.02534977
XP_003435770	NCBI	K02350	1.637354584	0.001128233
XP_317364	NCBI	K02377	-1.370983822	0.035520282
XP_316586	NCBI	K02437	1.551233683	0.000129005
XP_319800	NCBI	K02516	-1.397112445	0.080602697
XP_321212	NCBI	K02633	1.807850738	0.057243373
XP_320252	NCBI	K02882	2.233820865	0.032687974
XP_001237272	NCBI	K02890	-1.384946212	0.08563945
XP_316083	NCBI	K02893	1.554756859	0.076003699
XP_321578	NCBI	K02896	3.622341902	3.58027E-06
XP_001865476	NCBI	K02900	2.184294072	0.001459816
XP_315433	NCBI	K02903	2.025195691	0.058612045
XP_316641	NCBI	K02905	1.677820254	0.043070523
XP_316827	NCBI	K02906	-1.280109993	0.084502223
XP_001864160	NCBI	K02943	-6.436071858	0.018889571
XP_315982	NCBI	K02953	1.97404644	0.095403898
XP_310152	NCBI	K03002	-1.513109463	0.030240088
XP_320161	NCBI	K03016	1.337859555	0.051456515

XP_317312	NCBI	K03021	1.40718508	0.007004831
XP_320558	NCBI	K03025	1.286045025	0.09298872
XP_319831	NCBI	K03033	-1.347515646	0.074927908
XP_320986	NCBI	K03037	-1.404784645	0.070026619
XP_310465	NCBI	K03065	-1.318015766	0.089496919
XP_320076	NCBI	K03098	3.097462857	1.71784E-07
XP_315212	NCBI	K03106	-1.345360516	0.02338583
XP_308003	NCBI	K03107	-1.324707658	0.042308107
XP_003436707	NCBI	K03163	-1.326217648	0.066317974
XP_558148	NCBI	K03232	1.31640165	0.003992512
XP_316859	NCBI	K03233	1.250706183	0.05315321
XP_309455	NCBI	K03237	-1.272031213	0.058108761
XP_317984	NCBI	K03243	-1.537960718	0.0125909
XP_319981	NCBI	K03247	-1.294880761	0.089898772
XP_312631	NCBI	K03251	-1.308647412	0.07905947
XP_318103	NCBI	K03252	-1.375319509	0.05315321
XP_320387	NCBI	K03253	-1.269183894	0.067327798
XP_320668	NCBI	K03255	-1.418490695	0.027222931
XP_001237267	NCBI	K03258	-1.367641834	0.009874035
XP_312438	NCBI	K03260	-1.429318596	0.070026619
XP_319502	NCBI	K03265	-1.432279005	0.049077726
XP_320105	NCBI	K03267	-1.521912109	0.007539016
XP_315042	NCBI	K03283	1.403877518	0.073577253
XP_308813	NCBI	K03372	-1.471188385	0.001327994
XP_321732	NCBI	K03377	1.477364803	3.82269E-05
XP_316220	NCBI	K03424	-1.501242904	0.001827292
XP_308209	NCBI	K03495	-1.294115873	0.0964316
XP_321547	NCBI	K03514	-1.277029194	0.047607955
XP_314540	NCBI	K03644	1.425059798	0.001427115
XP_308583	NCBI	K03671	1.532682881	0.000512601
XP_314995	NCBI	K03781	1.431265915	0.004893931
XP_316316	NCBI	K03833	1.411833993	0.068620117
XP_319937	NCBI	K03841	1.48389933	0.007872225
NP_008069	NCBI	K03879	3.558889671	0.024778791
NP_008078	NCBI	K03882	2.333528796	0.013892787
XP_310968	NCBI	K03940	1.220673974	0.053350904
XP_321378	NCBI	K03941	1.202371261	0.075550457
XP_319184	NCBI	K03942	1.251871031	0.014716807
XP_315631	NCBI	K03949	1.278925881	0.008736113
XP_314225	NCBI	K03950	1.932360592	0.073862379
XP_308839	NCBI	K03952	1.36113275	0.076193141

XP_318516	NCBI	K03953	1.242187914	0.049591801
XP_309517	NCBI	K03954	1.185691504	0.096741214
XP_308577	NCBI	K03956	1.275334462	0.035347754
XP_318629	NCBI	K03962	1.230572345	0.047518487
XP_318461	NCBI	K04077	-1.426530106	0.071911302
XP_308800	NCBI	K04079	-16.52342046	0.005609873
XP_310647	NCBI	K04266	1.547833424	0.003905507
XP_313800	NCBI	K04354	-1.147756347	0.0964316
XP_003436788	NCBI	K04437	-2.022349611	0.041359774
XP_319845	NCBI	K04487	1.167798192	0.064329213
XP_311134	NCBI	K04515	1.575907269	0.056212645
XP_320124	NCBI	K04539	1.408922014	0.006260372
XP_001687859	NCBI	K04560	-1.384968467	0.025268825
XP_314490	NCBI	K04564	1.415587058	0.003322335
XP_001843582	NCBI	K04571	-1.601690926	0.004918993
XP_316287	NCBI	K04599	2.361597734	0.007812622
XP_003437124	NCBI	K04699	1.31652939	0.017306108
XP_308109	NCBI	K04794	-1.45539403	0.079244359
XP_312473	NCBI	K04919	1.770187996	0.000613376
XP_308462	NCBI	K05036	1.448106551	0.046443766
XP_309846	NCBI	K05038	3.133411595	0.000263492
XP_311164	NCBI	K05048	1.609593937	0.06371429
XP_314941	NCBI	K05096	1.170294135	0.07905947
XP_003436317	NCBI	K05291	-1.344913133	0.033263222
XP_313756	NCBI	K05304	-13.29782759	0.001628855
XP_316832	NCBI	K05546	-1.33530682	0.05386078
Q5NRB3	UniProt- SwissProt	K05601	-1.550961568	0.088148954
XP_315540	NCBI	K05610	-1.338303291	0.05243897
XP_555667	NCBI	K05637	1.239747492	0.06474883
XP_320377	NCBI	K05643	1.464832755	0.04167812
XP_552044	NCBI	K05643	1.711493408	0.047782387
XP_001688853	NCBI	K05662	1.831366885	0.032942813
XP_554876	NCBI	K05768	1.555854895	0.028782186
XP_001852645	NCBI	K05770	1.306098699	0.048182038
XP_319865	NCBI	K05858	-1.184020577	0.065389255
XP_312640	NCBI	K05940	-1.381932741	0.072697249
XP_313721	NCBI	K06062	1.515346015	0.003012905
XP_320293	NCBI	K06184	-1.322812152	0.066967408
XP_321114	NCBI	K06229	1.9342352	3.2948E-05
XP_001688514	NCBI	K06265	-1.215818808	0.074422778

XP_316311	NCBI	K06515	1.320811085	0.030705137
XP_308420	NCBI	K06700	1.51371967	2.56678E-07
XP_309467	NCBI	K06709	1.43352497	0.015542239
XP_562161	NCBI	K06874	-1.386009348	0.058618016
XP_001237680	NCBI	K06890	1.262625976	0.039765904
XP_311697	NCBI	K07050	1.318742245	0.051494552
XP_320408	NCBI	K07178	-1.351434524	0.095141605
XP_003435861	NCBI	K07189	1.610240412	0.05243897
XP_308381	NCBI	K07192	1.184063207	0.040796836
XP_311735	NCBI	K07206	1.383221496	0.014366859
XP_001846718	NCBI	K07342	-1.582274272	0.001190859
NP_462790	NCBI	K07391	6.366595441	0.042233131
XP_321709	NCBI	K07466	1.4430514	2.38422E-05
XP_317731	NCBI	K07515	-1.312550207	0.075033858
XP_311060	NCBI	K07750	2.294343157	0.046513652
XP_316514	NCBI	K07868	1.586562754	0.088969534
XP_313029	NCBI	K07874	-1.265853484	0.024778791
XP_320516	NCBI	K07937	-1.308558489	0.03770879
XP_308884	NCBI	K07976	1.351012993	0.054195966
XP_313116	NCBI	K08057	-1.466040329	0.01001656
XP_316428	NCBI	K08074	-1.535349201	0.059095313
XP_001848294	NCBI	K08131	1.716946018	0.059676775
XP_003437178	NCBI	K08145	-1.752525755	0.002258674
XP_317786	NCBI	K08193	-4.294773259	0.073500398
XP_318686	NCBI	K08193	1.38147098	0.005964426
XP_309233	NCBI	K08267	1.31997099	0.08574975
XP_312238	NCBI	K08341	1.715913353	9.63535E-06
XP_552919	NCBI	K08371	-1.816647981	0.015451781
XP_322035	NCBI	K08471	-4.479219464	0.000107776
XP_001238322	NCBI	K08585	1.57118991	0.003427361
XP_317037	NCBI	K08601	1.386010976	8.27594E-05
XP_321277	NCBI	K08635	-2.444017516	0.003489325
XP_312790	NCBI	K08635	1.836109827	0.02746314
XP_312826	NCBI	K08656	-1.513133249	0.074546519
XP_313190	NCBI	K08678	1.841346101	0.02743854
XP_320316	NCBI	K08701	-2.847461353	0.07439324
XP_315680	NCBI	K08705	-5.93715588	0.036064356
XP_319335	NCBI	K08765	-1.610817913	0.096667053
XP_552786	NCBI	K08766	-1.336083384	0.051705349
XP_562694	NCBI	K08852	1.507670645	0.00454276
XP_563710	NCBI	K08853	-6.111321341	0.00017901

XP_320250	NCBI	K08869	-1.727325793	0.011988071
XP_311995	NCBI	K08869	1.461915728	4.22973E-07
XP_319133	NCBI	K08872	1.835809805	1.66243E-07
XP_003437215	NCBI	K08876	-1.18217124	0.08705342
XP_001688970	NCBI	K09067	-1.751350182	0.099671018
XP_319121	NCBI	K09084	1.46731408	0.083616695
XP_320880	NCBI	K09180	-1.46410732	0.057645184
XP_001652959	NCBI	K09273	-8.4131399	0.038449324
XP_310195	NCBI	K09364	-1.300424432	0.088952814
XP_003435730	NCBI	K09365	-1.603277697	0.050486185
XP_001689344	NCBI	K09382	-2.060840258	0.00094082
XP_321536	NCBI	K09408	-1.513800808	0.03887855
XP_313616	NCBI	K09441	1.426238087	0.032535684
XP_310201	NCBI	K09443	2.298660415	0.007993969
XP_317795	NCBI	K09481	-1.756610495	0.000433617
XP_321706	NCBI	K09487	-1.483652994	0.000117419
XP_313085	NCBI	K09490	-1.516615932	0.053935483
XP_313154	NCBI	K09493	-1.321537121	0.098279104
XP_312164	NCBI	K09495	-1.353469702	0.073842666
XP_317219	NCBI	K09497	-1.355174429	0.017255242
XP_312160	NCBI	K09499	-1.313861511	0.051485036
XP_314553	NCBI	K09500	-1.292357145	0.096667053
XP_316024	NCBI	K09502	-1.373828633	0.052355691
XP_317136	NCBI	K09517	-1.221320842	0.084265337
XP_321247	NCBI	K09518	1.270880748	0.021791581
XP_310857	NCBI	K09521	-1.319253413	0.044559544
XP_308338	NCBI	K09522	-1.443247151	0.010703928
XP_319734	NCBI	K09527	1.35028497	0.071911302
XP_308470	NCBI	K09540	-1.402861849	0.055132405
XP_310523	NCBI	K09552	1.281090523	0.089432607
XP_314956	NCBI	K09577	-1.602704481	0.009052644
XP_319582	NCBI	K09595	-1.68636559	0.000338826
XP_312914	NCBI	K09598	-1.355089129	0.089008699
XP_317861	NCBI	K09646	-1.656018632	0.00070611
XP_312303	NCBI	K09650	1.398134141	0.000434062
XP_310535	NCBI	K09699	-1.181315179	0.074546519
XP_307730	NCBI	K09856	-1.451303457	0.051485036
XP_315851	NCBI	K09881	-1.210824838	0.098777336
XP_319585	NCBI	K09884	1.537789906	1.62694E-05
XP_309553	NCBI	K10052	-196.5655049	1.05043E-05
XP_315413	NCBI	K10080	-1.601736619	0.001207417

XP_314865	NCBI	K10086	-1.166577516	0.082652843
XP_320349	NCBI	K10105	-3.10740165	2.35551E-05
XP_316389	NCBI	K10106	1.532639396	0.086909479
XP_001237830	NCBI	K10203	-1.507684372	0.001723565
XP_311410	NCBI	K10249	-3.409264817	0.052520353
XP_320603	NCBI	K10275	1.343776829	0.098474767
XP_319486	NCBI	K10280	-1.651791242	0.020098847
XP_308962	NCBI	K10295	1.467783446	0.006681269
XP_319376	NCBI	K10343	-1.362602131	0.095097897
XP_003435947	NCBI	K10373	2.080620653	0.047518487
XP_001688553	NCBI	K10436	-1.471757284	0.015125576
XP_318675	NCBI	K10454	-1.371801827	0.090242567
XP_307933	NCBI	K10575	-1.353572711	0.05958496
XP_310376	NCBI	K10703	-1.355888074	0.004753913
XP_321857	NCBI	K10754	3.261027864	0.047370443
XP_312566	NCBI	K10773	1.719334353	0.049574577
XP_312938	NCBI	K10798	1.259572538	0.010264697
XP_314244	NCBI	K10838	1.657007123	0.000691154
XP_319742	NCBI	K10842	1.414871522	0.026127305
XP_320364	NCBI	K10843	1.609839727	0.008395923
XP_319031	NCBI	K10885	1.450990897	0.0001149
XP_320741	NCBI	K10891	1.377562815	0.012158969
XP_001848863	NCBI	K10901	2.310271201	0.003918226
XP_319412	NCBI	K10949	-1.391875401	0.007573092
XP_319948	NCBI	K10956	-1.837693084	0.000327817
XP_312415	NCBI	K10994	1.302080466	0.091077001
XP_318082	NCBI	K11131	-1.484903629	0.022500474
XP_311162	NCBI	K11136	1.180055586	0.082210261
XP_001662888	NCBI	K11140	-2.049625593	0.03820956
XP_001842717	NCBI	K11140	-1.992254181	0.000253318
XP_313478	NCBI	K11140	-1.61488191	0.002929058
XP_310427	NCBI	K11142	-1.177355458	0.074164759
XP_317656	NCBI	K11155	1.261107274	0.018304737
XP_001853961	NCBI	K11251	-3.735992797	0.077128158
XP_318363	NCBI	K11251	-3.368488646	0.093052114
XP_307083	NCBI	K11251	-1.259746992	0.074913598
XP_311486	NCBI	K11275	-2.107829398	0.083683469
XP_001237521	NCBI	K11278	-1.523743111	0.045028264
XP_321135	NCBI	K11279	-1.318366545	0.021131171
XP_319707	NCBI	K11426	1.360307132	0.011720236
XP_313350	NCBI	K11436	-1.33853334	0.096562905

XP_314784	NCBI	K11652	-1.60211759	0.007539016
XP_320324	NCBI	K11703	-1.565445545	0.076193141
XP_317045	NCBI	K11713	1.406847702	0.054686763
XP_313307	NCBI	K11718	-1.288356117	0.060589493
XP_318881	NCBI	K11787	-3.852815526	2.02081E-05
XP_001237068	NCBI	K11855	-1.249918795	0.083319156
XP_001688392	NCBI	K12046	1.840012517	0.041392364
XP_317705	NCBI	K12114	-2.609427156	0.012516315
XP_317357	NCBI	K12165	-1.609980315	0.007539016
XP_316550	NCBI	K12197	1.315341276	0.007671872
XP_314840	NCBI	K12236	1.367915533	0.014408766
XP_001850565	NCBI	K12260	1.983445521	0.00010327
XP_316726	NCBI	K12272	-1.625087326	0.00054993
XP_318883	NCBI	K12275	-1.639849712	9.63535E-06
XP_314790	NCBI	K12323	1.910660837	0.07200667
XP_309165	NCBI	K12349	-2.362126394	0.074546519
XP_320591	NCBI	K12350	-6.863504905	0.000905009
XP_307483	NCBI	K12373	-15.99320503	0.008564991
XP_003436771	NCBI	K12394	-1.257902444	0.090208221
XP_320438	NCBI	K12486	-1.340669405	0.077128158
XP_565746	NCBI	K12504	-1.746258455	0.000166713
XP_001688773	NCBI	K12505	-8.912388935	0.00037864
XP_552338	NCBI	K12587	1.385740961	0.015125576
XP_319893	NCBI	K12614	-1.685146901	0.007912559
XP_308231	NCBI	K12667	-1.284173299	0.028280899
XP_311375	NCBI	K12811	-1.206068987	0.048212358
XP_310958	NCBI	K12828	1.186520884	0.076748991
XP_306246	NCBI	K12835	1.294646293	0.005130181
XP_315991	NCBI	K12841	1.160091708	0.08756042
XP_314488	NCBI	K12868	1.295370842	0.02372264
XP_321188	NCBI	K12869	-1.244376604	0.086349197
XP_003436593	NCBI	K12897	-6.726736267	0.009632055
XP_309550	NCBI	K13051	-4.832596634	6.66326E-07
XP_312940	NCBI	K13096	-1.199036343	0.086217812
XP_309558	NCBI	K13126	-1.281989614	0.039765904
XP_556004	NCBI	K13171	-1.230212064	0.048221152
XP_314700	NCBI	K13179	-1.445857713	0.059524408
XP_321364	NCBI	K13249	-1.696324693	0.000633271
XP_312634	NCBI	K13254	1.180164174	0.084595516
XP_312558	NCBI	K13278	1.582800281	0.024832608
XP_312755	NCBI	K13280	-1.364921393	0.024676513

XP_003436833	NCBI	K13295	1.41937245	0.002765213
XP_001689352	NCBI	K13348	2.002802176	9.72513E-05
XP_315515	NCBI	K13356	-1.504219437	0.015542239
XP_320774	NCBI	K13356	-6.161360922	0.000338711
XP_313370	NCBI	K13356	1.310217484	0.049923536
XP_001687783	NCBI	K13403	-1.357913045	0.003933345
XP_320203	NCBI	K13443	-1.691106012	0.067654721
XP_309203	NCBI	K13499	-1.477680729	0.099352299
XP_003436023	NCBI	K13506	1.354768394	0.005925747
XP_321034	NCBI	K13509	1.412293631	9.5041E-05
XP_003435788	NCBI	K13811	-1.667741255	0.069305664
XP_318819	NCBI	K13861	1.480363554	0.009219356
XP_321324	NCBI	K14006	-1.379795466	0.043135665
XP_001850746	NCBI	K14007	-1.494829862	0.007430185
XP_314530	NCBI	K14009	1.679685199	0.000327817
XP_311560	NCBI	K14010	-1.558286526	0.015807682
XP_003435791	NCBI	K14014	1.251948038	0.070614214
XP_308198	NCBI	K14073	-11.23476108	0.00037864
XP_317515	NCBI	K14156	1.437240002	0.007902533
XP_317242	NCBI	K14165	1.714888958	0.022500474
YP_498670	NCBI	K14196	-4.445632988	0.051165424
XP_316954	NCBI	K14209	1.245213722	0.097650273
XP_001689011	NCBI	K14319	-1.340730675	0.066977687
XP_563485	NCBI	K14343	1.67113355	0.000231061
XP_312333	NCBI	K14416	1.632476862	0.002956368
XP_318743	NCBI	K14455	1.346461467	0.025428187
XP_001848007	NCBI	K14464	-6.492018011	0.011333705
XP_313813	NCBI	K14538	-1.390360126	0.034850895
XP_554389	NCBI	K14544	-1.322104051	0.074546519
XP_316150	NCBI	K14548	-1.421408061	0.051800072
XP_311407	NCBI	K14558	-1.447604443	0.071945574
XP_319629	NCBI	K14559	-1.32009353	0.076003699
XP_320984	NCBI	K14564	-1.354482517	0.083319156
XP_308017	NCBI	K14565	-1.40030662	0.051837426
XP_313396	NCBI	K14567	-1.552189488	0.02540691
XP_315898	NCBI	K14569	-1.4282521	0.055819205
XP_003436333	NCBI	K14610	-6.434949974	1.38435E-16
XP_316371	NCBI	K14610	-1.507186218	0.001202874
XP_310954	NCBI	K14620	1.817431503	0.000410378
XP_310627	NCBI	K14676	1.381517922	0.026817573
XP_003436878	NCBI	K14708	3.371183793	1.10822E-20

XP_320239	NCBI	K14708	1.509127027	0.000335359
XP_311937	NCBI	K14767	-1.404281062	0.0884664
XP_308548	NCBI	K14775	-1.612419994	0.005901357
XP_001230842	NCBI	K14776	-1.412319883	0.049329527
XP_317303	NCBI	K14788	-1.259684257	0.098879513
XP_311936	NCBI	K14794	-1.42429652	0.076743881
XP_307850	NCBI	K14799	-1.328259927	0.082955849
XP_308815	NCBI	K14807	-1.311502359	0.071829356
XP_308366	NCBI	K14808	-1.308122856	0.099628843
XP_313490	NCBI	K14821	-1.478121286	0.073561472
XP_308400	NCBI	K14826	-1.696400671	0.004145167
XP_310613	NCBI	K14829	-1.269115607	0.071124383
XP_314636	NCBI	K14834	-1.306052566	0.0884664
XP_314123	NCBI	K14835	-1.301186984	0.084237421
XP_001237501	NCBI	K14837	-1.446845112	0.012310101
XP_316147	NCBI	K14838	-1.344966491	0.04167812
XP_310849	NCBI	K14840	-1.350019589	0.054686763
XP_313594	NCBI	K14844	-1.416105063	0.057690806
XP_001847938	NCBI	K14861	-1.397987117	0.076014187
XP_317372	NCBI	K14950	-1.313019894	0.066977687
XP_316569	NCBI	K14998	1.741819802	5.25896E-08
XP_312054	NCBI	K14999	-1.664733627	0.083516159
XP_312050	NCBI	K14999	2.539178745	0.016327919
XP_317257	NCBI	K14999	2.925585281	0.033337638
XP_001865807	NCBI	K14999	-3.316177811	9.63535E-06
XP_307987	NCBI	K15001	-3.356817465	0.039011255
XP_001238280	NCBI	K15003	2.78275999	0.0107212
XP_558354	NCBI	K15005	-3.035160457	0.000289797
XP_308120	NCBI	K15014	-1.439076783	0.035408325
XP_312412	NCBI	K15026	1.234347878	0.079244359
XP_320254	NCBI	K15030	-1.447080441	0.02196688
XP_317020	NCBI	K15033	-1.362348778	0.057690806
XP_315411	NCBI	K15042	-1.187790275	0.046969894
NP_596201	NCBI	K15073	16.19784971	1.27812E-13
XP_552102	NCBI	K15104	1.579179841	0.012087641
XP_316164	NCBI	K15109	-1.310306174	0.036228599
XP_320467	NCBI	K15178	-1.181323301	0.093795603
XP_320439	NCBI	K15190	-1.302142636	0.017306108
XP_310411	NCBI	K15210	-1.628847926	0.00393581
XP_314130	NCBI	K15235	1.428957596	0.072966344
NP_650949	NCBI	K15275	2.388793583	0.000203763

XP_321679	NCBI	K15275	-1.443011204	0.017306108
NP_068697	NCBI	K15310	1.944738641	0.075841427
XP_314926	NCBI	K15369	1.444582255	0.003235529
XP_308991	NCBI	K15424	-1.246470412	0.081413288
XP_321237	NCBI	K15433	1.367950422	0.0272767
XP_314551	NCBI	K15437	-1.423162087	0.030240088
XP_315372	NCBI	K15683	-1.350047442	0.0101065
XP_317334	NCBI	K15734	-3.73979267	7.61743E-05
XP_317161	NCBI	K15779	1.833645277	1.27173E-05
XP_319835	NCBI	K16340	1.81123126	0.051003096
XP_317997	NCBI	K16343	1.447749645	0.007749392
XP_320491	NCBI	K16482	-1.507357363	0.090930829
XP_001237917	NCBI	K16674	-2.547867099	0.047244653
XP_319363	NCBI	K16680	-1.746083494	0.083762357
XP_310433	NCBI	K16681	-1.47702615	0.039616984
XP_001237548	NCBI	K16682	1.203018684	0.093691693
XP_313496	NCBI	K16743	-1.424465507	0.066553181
XP_315868	NCBI	K16830	-1.220850401	0.092399546
XP_313330	NCBI	K17198	-14.58332135	0.002929058
XP_318581	NCBI	K17254	1.452995641	0.015542239
XP_311025	NCBI	K17262	-1.282199852	0.083683469
XP_316887	NCBI	K17264	-1.228641655	0.075745945
XP_316655	NCBI	K17268	-1.352176826	0.068019085
XP_309978	NCBI	K17285	1.475566667	0.004158647
XP_309330	NCBI	K17307	1.863546765	0.062922699
XP_001689072	NCBI	K17383	-1.308430503	0.057926266
XP_322027	NCBI	K17409	-1.290386156	0.061341717
XP_310856	NCBI	K17479	-1.848129404	0.002474383
XP_309361	NCBI	K17583	-1.323755155	0.057690806
XP_311414	NCBI	K17586	1.276094763	0.071421652
XP_321014	NCBI	K17603	1.243161936	0.053452043
XP_316299	NCBI	K17617	-1.42740197	0.021250647
XP_308574	NCBI	K17654	-1.381736483	0.066659134
XP_318858	NCBI	K17659	-1.259750298	0.04023767
XP_314233	NCBI	K17725	1.626350322	8.68459E-05
XP_318431	NCBI	K17776	1.872241829	1.06003E-07
XP_311964	NCBI	K17782	1.290920117	0.018063991
XP_557147	NCBI	K17783	1.780832664	1.77141E-06
XP_319394	NCBI	K17794	1.430640769	0.002956368
XP_308794	NCBI	K17885	-1.217662019	0.047783196
XP_001688881	NCBI	K17914	-41.66686167	5.07127E-09

XP_318377	NCBI	K17916	1.312185552	0.000539824
XP_318964	NCBI	K17969	1.635373355	1.01051E-07
XP_003435899	NCBI	K18080	1.43619089	0.006681269
XP_318935	NCBI	K18086	-1.283038746	0.081327301
XP_316811	NCBI	K18159	1.412529599	0.018630936
XP_308878	NCBI	K18170	1.354331869	0.055356265
XP_001689044	NCBI	K18171	1.328029798	0.005939358
XP_317162	NCBI	K18283	-2.436845013	0.032687974
XP_310291	NCBI	K18400	1.224611548	0.08224856
XP_311436	NCBI	K18415	1.517103216	0.048496386
NP_011291	NCBI	K18551	-2.573085514	0.087354965
XP_308441	NCBI	K18588	1.526312973	0.048182038
XP_319430	NCBI	K18592	-4.068474254	0.049100414
XP_319663	NCBI	K18592	1.245767801	0.051456515
XP_315358	NCBI	K18733	-4.079855225	1.79974E-05
XP_319357	NCBI	K18734	1.61221821	0.000249762
NP_564239	NCBI	K18749	2.02406722	0.006104726
XP_001689211	NCBI	K19363	1.367221951	0.071829356
XP_321117	NCBI	K19366	2.23743438	4.6888E-13
XP_308621	NCBI	K19370	-5.818641434	0.092190309
XP_316797	NCBI	K19371	-1.509331684	0.009866536
XP_311448	NCBI	K19511	1.897096696	0.007746511
XP_311106	NCBI	K19511	-45.44579286	3.55679E-05
XP_307904	NCBI	K19539	2.299169586	7.7742E-06
XP_309067	NCBI	K19572	2.366575274	0.00164371
XP_320677	NCBI	K19584	1.415855303	0.082113521
XP_559033	NCBI	K19671	1.597906327	0.039765904
XP_311215	NCBI	K19672	1.506043956	0.095218666
XP_310880	NCBI	K19684	-1.627753918	0.013729481
XP_003435948	NCBI	K19904	1.438184231	0.072553834
XP_003436759	NCBI	K19948	-1.764862433	0.007056232
XP_310704	NCBI	K20011	1.334808645	0.000387642
XP_313427	NCBI	K20095	-1.429370096	0.041392364
XP_310378	NCBI	K20102	-1.388818042	0.073287613
XP_317575	NCBI	K20168	1.429476654	0.072697249
XP_313909	NCBI	K20173	1.652337562	0.074164759
XP_308814	NCBI	K20221	-1.445043681	0.016096417
XP_308523	NCBI	K20223	-1.3299802	0.079796814
XP_556725	NCBI	K20351	-1.455458044	0.040838534
XP_318301	NCBI	K20352	-1.360284996	0.047879005
XP_001688188	NCBI	K20353	-1.361241312	0.06157595

XP_315186	NCBI	K20364	-1.305860428	0.003202739
XP_318287	NCBI	K20369	-1.659874655	1.73906E-05
XP_308391	NCBI	K20474	-1.285600758	0.025288123
XP_001237372	NCBI	K20478	-1.234765298	0.047769119
XP_318759	NCBI	K20656	1.338202918	0.075745945
XP_317538	NCBI	K20721	-1.28249133	0.003489325
XP_321572	NCBI	K20777	1.194930059	0.077285491
XP_307895	NCBI	K20792	-1.443867287	0.016327919
XP_309015	NCBI	K20804	1.27091759	0.047518487
XP_311884	NCBI	K20840	1.515856897	0.061498728
XP_001238509	NCBI	K21406	1.429540026	0.074913598
XP_553771	NCBI	K21890	2.092416547	4.40278E-06
XP_321635	NCBI	K22037	-1.56860566	0.072762493
XP_001230875	NCBI	K22069	1.267677522	0.02540691
XP_319229	NCBI	K22072	1.415631772	0.046513652
XP_320070	NCBI	K22128	1.776287161	1.55361E-08
XP_314997	NCBI	K22139	1.329790111	0.0561599
XP_312784	NCBI	K22203	2.402066844	0.000803117
XP_311061	NCBI	K22282	1.492677584	0.051003096
XP_308521	NCBI	K22329	-1.45490198	0.08672936
XP_001865645	NCBI	K22378	3.63937535	0.012206038
XP_308151	NCBI	K22381	-1.245477992	0.029300763
XP_312834	NCBI	K22470	2.588215681	2.0297E-21
XP_315584	NCBI	K22503	1.228899828	0.07746276
XP_320719	NCBI	K22524	1.682775346	0.000821628
XP_316105	NCBI	K22544	1.837998796	3.58027E-06
XP_311862	NCBI	K22556	-1.530539178	0.00085375
XP_001868606	NCBI	K22758	1.822640117	0.035935467
XP_309588	NCBI	K22791	2.058698978	0.004854569
XP_311902	NCBI	K22804	1.537784156	0.000539824
XP_309508	NCBI	K22816	-1.223839813	0.08864863
XP_315017	NCBI	K22873	1.225668884	0.075379366
XP_313823	NCBI	K23112	1.394111999	0.016658907
XP_310667	NCBI	K23168	1.584472886	0.000434062
XP_317090	NCBI	K23490	1.472925595	0.004774834
XP_320337	NCBI	K23498	-1.470543393	0.040838534
XP_001687843	NCBI	K23499	1.290102202	0.007142484
XP_320572	NCBI	K23541	1.573994341	1.402E-06
XP_003437151	NCBI	K23542	1.212620802	0.077629419
XP_003437121	NCBI	K23551	-1.426807449	0.075875826
XP_317623	NCBI	K23552	-1.336497977	0.074546449

XP_562511	NCBI	K23562	-1.423150188	0.021969666
XP_317608	NCBI	K23564	1.582657737	9.81708E-07
XP_309304	NCBI	K23570	1.22612725	0.086349197
XP_318870	NCBI	K23605	1.261593104	0.000821628
XP_314666	NCBI	K23617	-1.904584494	0.045028264
XP_003436589	NCBI	K23625	-1.27225759	0.052355691
XP_559490	NCBI		1.353375665	0.04394437
XP_556818	NCBI		1.269681816	0.072381328
XP_564580	NCBI		1.534141766	0.084295263
XP_312629	NCBI		1.560832194	9.28237E-05
XP_311323	NCBI		9.662197604	4.40278E-06
XP_316926	NCBI		3.625785227	0.044787596
XP_310822	NCBI		-15.17243787	0.000107776
XP_307652	NCBI		-1.617445657	0.033460223
XP_312182	NCBI		-3.625882351	0.049524356
XP_308033	NCBI		1.56082209	0.089432607
XP_308255	NCBI		-3.311321768	0.000763666
XP_315695	NCBI		2.050761505	0.000628027
XP_315931	NCBI		1.628654891	0.000901025
XP_001842340	NCBI		1.594660157	0.044962533
XP_001842908	NCBI		1.569250649	0.050197011
XP_552135	NCBI		6.455301475	3.74205E-05
XP_310332	NCBI		-9.802866894	0.002156887
XP_313829	NCBI		-1.668173072	0.087861321
XP_551513	NCBI		-1.748833083	0.03916109
XP_311713	NCBI		-2.061917323	0.001887373
XP_309925	NCBI		-1.298672221	0.051456515
XP_313467	NCBI		-6.207645816	0.00041033
XP_309398	NCBI		-1.318766879	0.088853449
XP_321764	NCBI		-716.1049744	8.35862E-07
XP_314157	NCBI		1.383358127	0.004626311
XP_308845	NCBI		1.536034357	0.051456515
XP_001238538	NCBI		1.357286641	0.089496919
XP_312891	NCBI		2.112134697	0.017434676
XP_321762	NCBI		1.583011146	0.070030549
XP_317380	NCBI		1.654933773	0.025586033
XP_003436278	NCBI		-2.047250466	0.002171364
XP_321623	NCBI		-3.531792246	5.52623E-05
XP_312953	NCBI		1.574020052	0.003610602
XP_321464	NCBI		-1.640135264	0.096864441
XP_314136	NCBI		-2.290311437	0.02746314

XP_321072	NCBI	1.81675641	0.047607955
XP_551285	NCBI	1.369675458	0.057917446
XP_310464	NCBI	-2.824111984	0.004882767
XP_312123	NCBI	1.988141404	8.70371E-06
XP_309111	NCBI	-2.443964914	0.003109638
XP_319049	NCBI	2.079893166	0.000635568
XP_311022	NCBI	-19.85325792	0.002076072
XP_562185	NCBI	1.802107939	0.079244359
XP_309061	NCBI	-6.576543545	0.009105809
XP_001868128	NCBI	2.029127614	0.007872225
XP_317948	NCBI	4.258564369	0.053242192
XP_003436420	NCBI	-1.319376166	0.086960611
XP_003436386	NCBI	1.57464328	0.040838534
XP_001660233	NCBI	1.615467074	0.086307258
XP_001866792	NCBI	2.687063386	0.00193815
XP_312344	NCBI	2.304818069	0.00412347
XP_563568	NCBI	4.890394754	8.40751E-18
XP_001688720	NCBI	1.318218717	0.011090443
XP_001237266	NCBI	-1.429460469	0.021250647
XP_001851254	NCBI	-2.295061618	0.036393719
XP_318986	NCBI	-1936.573225	5.08172E-07
XP_001238069	NCBI	-150.6335282	3.42591E-05
XP_308891	NCBI	-6.12203465	0.077872463
XP_308915	NCBI	-28.39689807	0.001335026
XP_311111	NCBI	-8.032951372	0.006060946
XP_311430	NCBI	-3.869872998	0.000634941
XP_316036	NCBI	-23.66502615	0.002605951
XP_316348	NCBI	-72.81288156	6.66488E-05
XP_316784	NCBI	-11.46902859	0.075458665
XP_318996	NCBI	-22.41276432	0.012764272
XP_001850720	NCBI	1.993902862	0.099628843
XP_001862829	NCBI	2.359564833	0.015542239
XP_309807	NCBI	1.853580848	0.025268825
XP_315459	NCBI	2.311825379	0.040838534
XP_316040	NCBI	2.372568469	0.029131734
XP_556672	NCBI	1.703625562	0.011128895
XP_312844	NCBI	-1.341021157	0.006124122
XP_003436286	NCBI	1.504075704	0.050432683
XP_308187	NCBI	1.298486308	0.09021606
XP_001688756	NCBI	1.53115462	0.050869021
XP_313611	NCBI	-2.476701074	0.000454726

XP_321691	NCBI	-1.473324278	0.024022198
NP_001263884	NCBI	-8.661696952	0.016361223
XP_320372	NCBI	-1.815961137	0.048322299
XP_308038	NCBI	-1.210356092	0.026040601
XP_313732	NCBI	-1.401228011	0.089139737
XP_312202	NCBI	1.528495663	0.073842666
XP_311553	NCBI	-15.47866292	3.493E-06
XP_310922	NCBI	-2.110981921	0.024186965
XP_321319	NCBI	1.564218547	0.085655627
XP_001848045	NCBI	-5.584380331	0.029487839
XP_313740	NCBI	1.528458819	0.029585642
XP_317476	NCBI	-159.2677862	6.90571E-14
XP_310814	NCBI	-12.42242403	0.000231061
XP_001845802	NCBI	5.493670965	0.000464421
XP_313980	NCBI	2.131499152	0.003157849
XP_318018	NCBI	2.348800999	6.23434E-05
XP_312372	NCBI	1.636426363	0.010887158
XP_317502	NCBI	-1.236689251	0.086217812
XP_318850	NCBI	1.802365582	0.000209308
XP_320173	NCBI	-2.522104644	0.080383565
XP_318851	NCBI	1.393854574	0.08546531
XP_311849	NCBI	1.702202657	0.056870625
XP_306771	NCBI	1.416280724	0.02540691
XP_003436643	NCBI	-1.392911157	0.024445657
XP_310437	NCBI	1.259624925	0.041854929
XP_001689184	NCBI	-111.2542979	2.17444E-11
XP_314131	NCBI	2.95651196	7.36625E-08
XP_309085	NCBI	3.141185481	6.93201E-10
XP_309831	NCBI	1.510735646	3.34103E-05
XP_320535	NCBI	1.386792073	0.017882927
XP_311764	NCBI	1.568857189	0.001134674
XP_001688826	NCBI	-1.561603465	0.018889571
XP_317082	NCBI	-1.84045624	0.001307348
XP_001688825	NCBI	-5.132515229	1.38844E-06
XP_001689001	NCBI	-2.091099861	1.14555E-09
XP_003437177	NCBI	-1.304656018	0.093447776
XP_554784	NCBI	-2.137052426	1.69268E-08
XP_316275	NCBI	1.574593771	0.084502223
XP_317868	NCBI	2.004789179	0.001140227
XP_311292	NCBI	-15.53068704	0.000500035
XP_314288	NCBI	1.269547847	0.02710083

XP_003436932	NCBI	-1.727872373	0.046969894
XP_310956	NCBI	-2.701807231	0.051333314
XP_315979	NCBI	2.168078859	0.005985456
XP_308842	NCBI	-51.91880639	2.38554E-05
XP_317269	NCBI	-24.41749968	9.75963E-05
XP_318855	NCBI	1.586112343	0.009059865
XP_320619	NCBI	-1.315408711	0.07762983
XP_001651919	NCBI	-1.949719207	6.16537E-05
XP_001230545	NCBI	-1.611980413	0.010294355
XP_307609	NCBI	-1.400089047	0.067710288
XP_308753	NCBI	4.13623806	1.20179E-20
XP_307887	NCBI	1.582745702	0.085750366
XP_001865659	NCBI	2.583869587	0.017948223
XP_313383	NCBI	-1.837449074	0.030685979
XP_312208	NCBI	-1.520419734	0.049328883
XP_557683	NCBI	-1.430469974	0.019966084
XP_560023	NCBI	-1.369636663	0.091722622
XP_003436490	NCBI	1.398325042	0.008072906
XP_316885	NCBI	2.078244157	0.020548704
XP_557684	NCBI	-2.761128904	1.21911E-08
XP_318513	NCBI	-1.510831078	0.039220822
XP_316144	NCBI	-1.49451097	0.070026619
XP_319152	NCBI	1.424991648	0.010648483
XP_309303	NCBI	-11.19259971	0.056882599
XP_001238440	NCBI	-2.849521053	1.99839E-11
XP_309808	NCBI	1.543258401	0.08036787
XP_313985	NCBI	-1.511547257	0.011955055
XP_320248	NCBI	1.427455142	0.000134316
XP_309581	NCBI	1.322976709	0.083546007
XP_308598	NCBI	-1.214766646	0.085075506
XP_308471	NCBI	-9.778179246	7.82616E-05
XP_309983	NCBI	-6.651711028	0.034476243
XP_310039	NCBI	-14.12101843	0.008093525
XP_312380	NCBI	-1.733454416	0.044787596
XP_318027	NCBI	2.581647321	0.000536496
XP_309359	NCBI	1.524940903	0.009213911
XP_310776	NCBI	1.297002805	0.029973669
XP_318298	NCBI	1.478072561	0.045154542
XP_315272	NCBI	-4.958515696	0.040838534
XP_001688865	NCBI	2.057324558	0.00319924
XP_307851	NCBI	1.310997141	0.008295077

XP_001688810	NCBI	-22.48709708	0.000643819
XP_316236	NCBI	-1.755818191	0.020016335
XP_001687834	NCBI	-2.566982235	0.089040766
XP_001847232	NCBI	-4.124097508	0.001327994
XP_307929	NCBI	1.313826981	0.051003096
XP_308422	NCBI	-2.49403436	0.074422778
XP_315621	NCBI	-1.340708718	0.049574577
XP_643993	NCBI	-11.93765994	0.053724874
XP_001237659	NCBI	1.889924524	0.006338916
XP_319318	NCBI	-1.708380848	0.002050606
XP_309220	NCBI	1.946691212	0.09238602
XP_309979	NCBI	-1.434742195	0.087036444
XP_307865	NCBI	4.925387227	0.017948223
XP_307655	NCBI	1.972652398	0.050779729
XP_001688641	NCBI	2.047494866	0.049235658
XP_316142	NCBI	2.158508209	0.014014768
XP_314312	NCBI	1.924555217	1.4654E-06
XP_314306	NCBI	1.572979045	0.029046025
XP_308320	NCBI	-2.797467649	0.085783002
XP_558477	NCBI	-1.377640753	0.03954604
XP_001688495	NCBI	3.105047549	3.00145E-10
XP_001688497	NCBI	1.369119692	0.072450881
XP_001870896	NCBI	-3.814954024	0.092031471
XP_312135	NCBI	-3.500707807	0.066566904
XP_317365	NCBI	-1.726431806	0.02732187
XP_001689275	NCBI	1.8147357	0.009884339
XP_001688885	NCBI	-1.662089368	0.019615097
XP_316714	NCBI	-21.96960073	4.82524E-07
XP_001843408	NCBI	1.938161624	0.069728008
XP_319658	NCBI	1.736166656	0.092799071
XP_319102	NCBI	-2.085117062	0.00205549
XP_001867890	NCBI	-1.665696326	0.015316918
XP_001843395	NCBI	-1.822230794	0.034850895
XP_001845720	NCBI	-14.41409853	6.66488E-05
XP_001845723	NCBI	-9.687625342	0.004255075
XP_319744	NCBI	-14.89276021	1.73906E-05
XP_552892	NCBI	-10.18991665	0.029131734
XP_001847489	NCBI	-2.838763929	0.026526827
XP_308888	NCBI	-2.411866649	0.061377376
XP_313869	NCBI	-21.13518408	8.2673E-06
XP_001689276	NCBI	1.711312201	0.077629419

XP_308550	NCBI	1.400290222	0.025984817
XP_315686	NCBI	1.740485441	9.70644E-05
XP_315688	NCBI	1.4559204	0.053242192
XP_317829	NCBI	1.464388543	0.000747904
XP_321960	NCBI	1.577292588	0.005876809
XP_311382	NCBI	-2.564842666	0.008520166
XP_314667	NCBI	2.572940878	0.019026762
XP_319997	NCBI	2.823292835	0.000709306
XP_308802	NCBI	-99.99701765	0.000117419
XP_003436670	NCBI	2.364339527	0.003489325
XP_308721	NCBI	1.467087432	0.021751427
XP_320722	NCBI	2.91376489	0.00033384
XP_320729	NCBI	2.594088184	0.016327919
XP_321961	NCBI	1.283425093	0.049909178
XP_307757	NCBI	1.995916923	0.006191732
XP_321698	NCBI	-3.815428782	0.024778791
XP_310507	NCBI	2.667896015	0.008126052
XP_318957	NCBI	1.647621391	0.025282021
XP_552698	NCBI	1.621737752	0.046172759
XP_320721	NCBI	2.866137301	0.004025211
XP_001653095	NCBI	-1.459580227	0.087799295
XP_316522	NCBI	-2.025805095	0.001164222
XP_316523	NCBI	-1.799610573	0.01107697
XP_310953	NCBI	1.536059015	0.001761547
YP_009143402	NCBI	-5.211146086	0.042332901
XP_311871	NCBI	-1.343787388	0.0659317
XP_316061	NCBI	1.935201496	0.052355735
XP_309601	NCBI	-2.025354103	0.043161359
XP_317349	NCBI	2.071477178	0.002929058
XP_316453	NCBI	2.446511191	7.37483E-06
XP_310755	NCBI	2.02425111	2.01432E-06
XP_316454	NCBI	2.13297204	1.24149E-06
XP_001237058	NCBI	1.394990743	0.016327919
XP_001688077	NCBI	-1.678516419	0.099352299
XP_003436181	NCBI	-26.96301742	4.24688E-05
XP_308425	NCBI	2.047837878	0.00094082
XP_001237815	NCBI	-21.9294078	2.06358E-08
XP_315346	NCBI	-20.37148928	0.009632055
XP_319374	NCBI	-8.853269451	0.002090528
XP_001866371	NCBI	-1.832442576	0.08911698
XP_001688966	NCBI	2.098023428	0.081857948

XP_001688472	NCBI	1.575186041	0.061401882
XP_001237095	NCBI	-4.008363421	0.050007266
XP_309521	NCBI	-1.331230667	0.051456515
XP_316058	NCBI	1.453811477	0.082955849
XP_003436619	NCBI	1.56694814	0.025962875
XP_003436665	NCBI	-6.614494146	0.064329213
XP_318553	NCBI	1.707729118	0.002956368
XP_311326	NCBI	-6.09250715	0.051003096
XP_309038	NCBI	-5.960256895	0.042233131
XP_311329	NCBI	-74.76601006	0.000477818
XP_312919	NCBI	-9.873082034	1.38744E-11
XP_311867	NCBI	-9.524139856	0.038488339
XP_312656	NCBI	-7.375164234	0.081776201
XP_001237468	NCBI	1.565688578	0.000204705
XP_313899	NCBI	-1.309633312	0.053242192
XP_003435853	NCBI	1.52014878	0.039438807
XP_318490	NCBI	-1.945367668	0.079596979
XP_315149	NCBI	-3.067530226	0.097707224
XP_320813	NCBI	2.706194465	2.87354E-10
XP_320812	NCBI	-5.117308641	0.040254918
XP_308200	NCBI	-1.225033016	0.097855899
XP_558461	NCBI	-1.37373442	0.029708677
XP_317652	NCBI	-2.585681976	0.033930423
XP_001231034	NCBI	2.201113078	0.023503839
XP_317759	NCBI	3.086924685	0.062950156
XP_321630	NCBI	1.639035111	3.34044E-05
XP_312396	NCBI	1.688776048	0.023920918
XP_314696	NCBI	2.195325915	0.000553694
XP_317834	NCBI	3.072619784	8.40751E-18
XP_314362	NCBI	-1.318234628	0.0884664
XP_320129	NCBI	1.274427652	0.062061525
NP_036739	NCBI	-5.581087708	0.049329527
XP_317752	NCBI	1.417994907	0.088602867
XP_318047	NCBI	-1.358288672	0.072208515
XP_308133	NCBI	-1.531727399	0.088952814
XP_317661	NCBI	-1.35508453	0.076743881
XP_321371	NCBI	1.175810538	0.091707328
XP_558416	NCBI	-75.14783993	0.000434062
XP_003435743	NCBI	1.8857734	5.08962E-11
XP_003436010	NCBI	-1.462673849	0.084774219
XP_550942	NCBI	-1.292986186	0.008342125

XP_001845601	NCBI	7.209999042	0.000230626
XP_001869781	NCBI	1.198401228	0.060589493
XP_001843932	NCBI	1.504971107	0.002771187
XP_313161	NCBI	-1.510093593	0.084265337
XP_559104	NCBI	-1.401164124	0.042472041
A0A0R4IBK5	UniProt- SwissProt	1.902725134	0.085527146
XP_321060	NCBI	-1.606271825	0.054746891
XP_557438	NCBI	1.327082909	0.018764338
XP_319307	NCBI	1.472583236	0.045154542
XP_553643	NCBI	7.978290795	1.44738E-12
XP_001237649	NCBI	-1.498662651	0.035172372
XP_001237650	NCBI	-1.561148904	0.065372754
XP_001870180	NCBI	1.36649106	0.043293787
XP_310951	NCBI	1.897973455	0.007127033
XP_320780	NCBI	1.774756366	0.074120462
XP_313322	NCBI	3.709440312	0.0125909
XP_001861871	NCBI	-1.608746278	0.0884664
XP_003436570	NCBI	-2.113049786	0.022757515
XP_003436571	NCBI	-2.411187986	0.011577215
XP_562562	NCBI	-1.933212432	0.029973669
XP_003436573	NCBI	2.438798744	1.54186E-06
XP_311017	NCBI	1.496296603	0.061929292
XP_001662885	NCBI	-2.395942733	0.073446171
XP_314331	NCBI	-1.894532854	0.070848175
XP_313708	NCBI	-1.563968279	0.009059865
XP_003437193	NCBI	1.360031025	0.099439711
XP_315309	NCBI	1.950732925	0.034169767
XP_309025	NCBI	2.454330063	0.019802815
XP_001850100	NCBI	-1.685262295	0.026477415
XP_312564	NCBI	-2.582465782	2.66642E-05
XP_317277	NCBI	1.282035389	0.037600355
XP_321363	NCBI	2.122559529	5.90381E-07
XP_322067	NCBI	-4.829812013	0.088148954
XP_316295	NCBI	1.748483296	0.02743854
XP_312232	NCBI	1.597999145	0.001327994
XP_316247	NCBI	-15.59282303	0.001956018
XP_315158	NCBI	1.952612488	0.007497027
XP_320457	NCBI	2.534839857	0.05344504
XP_311555	NCBI	-2.705561072	0.000204824
XP_003436798	NCBI	-2.038022547	0.064662302

XP_313656	NCBI	-3.069435317	0.019903089
XP_001237679	NCBI	-1.99128807	0.061377376
XP_313655	NCBI	-1.640111373	0.034850895
XP_564957	NCBI	-2.21138556	0.070042804
XP_320705	NCBI	1.623899769	0.083516159
XP_001231136	NCBI	-2.741877031	0.057659901
XP_310397	NCBI	-1.918519418	0.095141605
XP_318922	NCBI	1.419673334	0.063077816
XP_313053	NCBI	-5.173851532	0.021969666
XP_001850044	NCBI	-6.822722312	0.000657832
XP_315733	NCBI	-1.7912704	0.002194454
XP_315741	NCBI	1.573829123	0.068310563
XP_319288	NCBI	1.399387893	0.023614961
XP_317336	NCBI	-8.882231244	0.000446938
XP_320596	NCBI	-7.895990319	0.061929292
XP_316120	NCBI	-4.300220032	0.007902573
XP_559757	NCBI	1.328353932	0.065567947
XP_003436736	NCBI	-1.651913429	0.051003096
XP_314059	NCBI	-1.333349423	0.009059865
XP_001687884	NCBI	1.68172075	2.51354E-06
XP_312497	NCBI	-9.329986232	0.000512601
XP_317477	NCBI	1.838601442	0.022422714
XP_315766	NCBI	3.518089747	0.000527485
XP_311711	NCBI	-2.06390303	0.006640608
XP_317936	NCBI	-1.537263785	0.003566408
XP_307644	NCBI	-1.308655478	0.053910468
XP_001866722	NCBI	-4.637076998	0.038100282
XP_311364	NCBI	-1.828447819	0.026420375
XP_315453	NCBI	-10.60260776	0.000139787
XP_001842298	NCBI	1.888430987	0.016947462
XP_310753	NCBI	-6.181754687	0.081902634
XP_313282	NCBI	2.149678299	3.87257E-10
XP_311695	NCBI	1.804137657	0.003602536
XP_001237817	NCBI	2.700918315	0.029973669
XP_001230737	NCBI	-6.933539694	0.001092107
XP_001689110	NCBI	-20.55385491	0.001293225
XP_003435888	NCBI	-118.8161478	4.03571E-09
XP_003436306	NCBI	-13.60845058	0.000612251
XP_310217	NCBI	-5.917961174	0.088708052
XP_313650	NCBI	-83.47437899	6.105E-05
XP_555580	NCBI	-22.91345468	7.36625E-08

XP_001230800	NCBI	2.606809057	1.10095E-05
XP_001238397	NCBI	1.639422388	0.095141605
XP_001849542	NCBI	2.054568699	0.094511587
XP_309884	NCBI	3.080444446	0.001998227
XP_320394	NCBI	1.655050443	0.003930219
XP_308259	NCBI	-38.12773228	3.74205E-05
XP_308951	NCBI	-1.89947096	8.68459E-05
XP_315598	NCBI	-6.182303676	0.08864863
XP_316471	NCBI	-7.187349838	0.062950156
XP_321953	NCBI	-33.43938471	0.006214773
XP_001655681	NCBI	1.729718772	0.000737278
XP_001655687	NCBI	1.821662267	0.000158027
XP_001689299	NCBI	2.407347045	0.010887158
XP_001689300	NCBI	1.821667482	0.00852981
XP_001842246	NCBI	3.37586083	0.000356291
XP_001845643	NCBI	2.917219541	0.012560682
XP_001845648	NCBI	1.645693188	0.086349197
XP_001846755	NCBI	1.648709788	0.001337627
XP_001846758	NCBI	1.59172213	0.041630315
XP_001848925	NCBI	1.778040884	0.080894707
XP_001861005	NCBI	1.568212482	0.050869021
XP_001864216	NCBI	1.868373501	0.000566668
XP_003437166	NCBI	1.793809838	0.01560531
XP_003437168	NCBI	1.420514686	0.084950458
XP_011493626	NCBI	2.349891058	0.000107776
XP_318942	NCBI	1.616413359	0.01500606
XP_320892	NCBI	2.044942667	0.057243373
XP_552066	NCBI	1.989564954	1.4875E-07
XP_554263	NCBI	1.597708938	0.066625287
XP_558971	NCBI	1.903530437	0.000242328
XP_001850411	NCBI	3.150246439	0.004223668
XP_310573	NCBI	1.420749665	0.098279104
XP_308211	NCBI	-14.29247621	0.00043764
XP_321637	NCBI	-8.949024897	0.005338482
XP_562083	NCBI	-1.350150044	0.021131171
XP_319624	NCBI	2.081395751	0.064662302
NP_110212	NCBI	5.021207931	0.072915157
XP_313264	NCBI	1.533615284	0.014432719
XP_001866934	NCBI	1.776557203	0.020158685
XP_312778	NCBI	-1.671306859	0.017271007
XP_312067	NCBI	-1.430479231	0.00454276

XP_312539	NCBI	-1.354895745	0.08672936
XP_313294	NCBI	-2.714127212	0.018319748
XP_553659	NCBI	1.477163919	0.075887564
XP_319635	NCBI	1.516887774	0.026509772
XP_319698	NCBI	1.54151135	0.060197805
XP_310916	NCBI	-1.438552159	0.057917446
XP_314755	NCBI	1.426920237	0.043076964
XP_317143	NCBI	1.597208821	0.070030549
XP_321956	NCBI	1.656925325	0.014881299
XP_554133	NCBI	-1.89390288	0.033893536
XP_553184	NCBI	1.502439643	0.087359618
XP_319752	NCBI	-1.63656156	0.051934996
XP_314829	NCBI	1.958653059	3.03616E-05
XP_308163	NCBI	2.366360298	5.24592E-09
XP_316604	NCBI	1.579851593	0.003918226
XP_314885	NCBI	1.545752137	0.02177579
XP_003437005	NCBI	1.582893884	0.046443208
XP_312594	NCBI	-1.444080524	0.083546007
XP_310012	NCBI	1.781756986	0.007484745
XP_310012	NCBI	2.04425967	2.47108E-14
XP_003437030	NCBI	1.517280707	0.001895277
XP_003435872	NCBI	-1.757169049	0.001875619
XP_003435874	NCBI	-1.764032377	0.083319156
XP_310299	NCBI	-1.473255125	0.092662342
XP_003436594	NCBI	1.968864761	1.42292E-05
XP_317528	NCBI	1.845137861	0.041630315
XP_559533	NCBI	1.973459413	0.064014639
XP_310546	NCBI	-27.92873975	0.011609982
XP_001687778	NCBI	-413.5638574	6.0938E-07
XP_001848719	NCBI	-2731.431806	1.22331E-07
XP_003435930	NCBI	-1.255113041	0.012310101
XP_312022	NCBI	1.29869255	0.070793435
XP_321387	NCBI	-4.483546195	1.94079E-05
XP_321236	NCBI	4.959256126	8.16683E-14
XP_001868035	NCBI	2.37925784	0.049329527
XP_321663	NCBI	1.537364494	0.07439324
XP_314882	NCBI	1.409100855	0.036210426
XP_321497	NCBI	-1.364454147	0.04591571
XP_003435923	NCBI	1.59870022	0.016327919
XP_313849	NCBI	1.368924152	0.086349197
XP_003436649	NCBI	1.752396475	0.054195966

XP_313250	NCBI	-6.944941552	0.000612251
XP_317401	NCBI	-2.546853439	0.021969666
XP_317405	NCBI	-1.587808971	0.06474883
XP_317407	NCBI	-1.491056317	0.060477944
XP_312273	NCBI	-1.302016673	0.035640563
XP_312971	NCBI	-1.364207758	0.002901456
XP_311973	NCBI	-1.250289604	0.045181953
XP_311228	NCBI	1.398123866	4.96072E-05
XP_316107	NCBI	-10.2515746	0.000795377
XP_001687880	NCBI	3.631528877	0.000193857
XP_321716	NCBI	1.241279808	0.065389255
XP_320776	NCBI	-1.517004653	0.00852981
XP_317713	NCBI	1.68496218	0.030240088
XP_001656768	NCBI	5.17788683	0.003696965
XP_313569	NCBI	-1.420302216	0.053605171
XP_313877	NCBI	-4.600156306	0.002200648
XP_311819	NCBI	2.378480022	0.000800666
XP_314482	NCBI	-1.487756534	0.038493511
XP_311267	NCBI	1.52210879	0.09745044
XP_319528	NCBI	-1.726187571	0.000201743
XP_320175	NCBI	-1.802034175	0.000238804
XP_321745	NCBI	-1.575655057	0.003937399
XP_319712	NCBI	1.796874734	0.097132654
XP_553055	NCBI	1.342830578	0.056212645
XP_317131	NCBI	1.315465347	0.015508557
XP_308279	NCBI	1.569044518	0.019448223
XP_564945	NCBI	-15.58057167	0.001269446
XP_001687968	NCBI	2.082821782	0.044989945
XP_001230506	NCBI	2.284256012	0.060978367
XP_556168	NCBI	9.036507892	0.000290124
XP_314275	NCBI	1.237079412	0.011720236
XP_001849814	NCBI	1.385011914	0.076193141
XP_321331	NCBI	-1.261955966	0.064557914
XP_312750	NCBI	-1.30826887	0.080269648
XP_001689309	NCBI	-2.036745071	0.000761123
XP_001238321	NCBI	1.54694421	0.055235596
XP_001238089	NCBI	1.504169435	0.003951005
XP_309080	NCBI	-1.475884023	0.057690806
XP_318631	NCBI	1.309973344	0.073715623
XP_316431	NCBI	1.514800876	0.000230626
XP_001231158	NCBI	-8.518779511	0.001859988

XP_001688413	NCBI	-30.06637081	5.25896E-08
XP_311915	NCBI	-14.34588668	0.000949067
XP_311916	NCBI	-6.239775536	0.026509772
XP_319496	NCBI	-72.87361315	0.004389553
XP_563132	NCBI	-10.99902464	0.000846726
XP_311756	NCBI	-74.74736635	3.08193E-06
XP_001688192	NCBI	-1.44273981	0.00037864
XP_001688731	NCBI	1.773757118	0.051494552
XP_310200	NCBI	-1.701627385	0.017220595
XP_312810	NCBI	1.498236742	0.046895408
XP_001237434	NCBI	-2.840110045	0.003408571
XP_003436238	NCBI	1.449991948	0.083516159
XP_309133	NCBI	1.992739188	0.056212645
XP_308599	NCBI	-1.78883732	0.005901357
XP_318058	NCBI	-1.358957949	0.049077726
XP_308997	NCBI	1.723054738	0.000905389
XP_310010	NCBI	1.447548953	0.065876075
XP_558523	NCBI	2.443104247	0.000230006
XP_314929	NCBI	-1.364680094	0.033672223
XP_315985	NCBI	1.390109981	0.047325385
XP_321688	NCBI	-1.312121323	0.074160817
XP_314623	NCBI	-1.459840029	0.056278108
XP_003436900	NCBI	-1.444334798	0.051456515
XP_001847847	NCBI	1.512440164	0.072915157
XP_001867651	NCBI	1.726764214	4.96072E-05
XP_310602	NCBI	1.361755799	0.005797592
XP_311428	NCBI	1.309908092	0.051003096
XP_315965	NCBI	-1.316954706	0.041072605
XP_317375	NCBI	1.459021861	0.082622231
XP_001663904	NCBI	3.096439957	0.088218062
XP_318399	NCBI	1.366253445	0.053605171
XP_312603	NCBI	1.446803434	0.0964316
XP_003436471	NCBI	-1.464551667	0.015634137
XP_558852	NCBI	-1.342331565	0.015807682
XP_319250	NCBI	2.343219395	0.007539016
XP_001861990	NCBI	-41.18655787	0.000230006
XP_310826	NCBI	1.4600282	0.017449678
XP_321475	NCBI	1.212431152	0.081809046
XP_001689359	NCBI	1.285577329	0.068415673
XP_318917	NCBI	-1.253900293	0.093447776
XP_313374	NCBI	-2.029557942	6.77043E-07

XP_309527	NCBI	-1.627734759	0.063460569
XP_320073	NCBI	-1.661336439	0.095433712
XP_001868268	NCBI	-1.744918104	0.031913911
XP_001689125	NCBI	-2.060489885	4.43718E-09
XP_556532	NCBI	-1.554224501	0.008889703
XP_001688096	NCBI	1.453932232	0.011821358
XP_001238271	NCBI	-1.427869501	0.011720236
XP_001238451	NCBI	-1.64189901	0.011201597
XP_315791	NCBI	1.720534105	0.003633807
XP_308614	NCBI	2.323475301	8.40751E-18
XP_317011	NCBI	-1.769012626	0.015542239
XP_308253	NCBI	2.239211424	9.94804E-18
XP_001689030	NCBI	1.723430421	1.95023E-07
XP_314041	NCBI	-2.607383015	0.000370891
XP_321148	NCBI	1.261801236	0.085655627
XP_003436189	NCBI	3.469744102	6.29606E-05
XP_003436193	NCBI	5.778005024	3.12096E-08
XP_003435990	NCBI	1.317652327	0.05543576
XP_001653028	NCBI	1.270431655	0.056212645
XP_001864316	NCBI	1.306102534	0.044986637
XP_317285	NCBI	2.722647766	0.016947462
XP_321077	NCBI	-12.57072787	0.016327919
XP_321079	NCBI	-16.52154974	0.001478048
XP_003435988	NCBI	2.577894576	0.026127305
XP_321793	NCBI	1.771474261	0.00140675
XP_551486	NCBI	3.803863232	0.001207417
XP_321574	NCBI	-1.5111305	0.001547679
XP_313838	NCBI	1.800751605	0.000520458
XP_308822	NCBI	-1.270535321	0.01954613
XP_312904	NCBI	1.371258214	0.040930738
XP_321231	NCBI	1.58348548	0.0964316
XP_001664257	NCBI	5.276306652	0.019056667
XP_321172	NCBI	1.520013054	0.089898772
XP_319473	NCBI	2.126711884	0.005962876
XP_313014	NCBI	-9.122414916	0.008343485
XP_001849398	NCBI	-2.884333985	0.000117419
XP_001870332	NCBI	-1.836046018	0.06474883
XP_311120	NCBI	-1.217842625	0.093691693
XP_313631	NCBI	-4.038531869	0.001485591
XP_317877	NCBI	-2.065427805	0.00035264
XP_320291	NCBI	-1.736261952	0.010454955

XP_003436882	NCBI	3.271333049	0.005901365
XP_315403	NCBI	1.751005542	0.026526827
XP_321808	NCBI	3.089925405	0.014383104
XP_562148	NCBI	1.63240928	0.001370609
XP_555163	NCBI	1.707829727	0.000387537
XP_314285	NCBI	1.265978133	0.035907224
XP_001688299	NCBI	-1.327740268	0.079244359
XP_309766	NCBI	1.872869085	0.049079296
XP_317062	NCBI	-1.280044356	0.035283093
XP_557337	NCBI	2.010538291	0.000311876
XP_308437	NCBI	1.377140635	0.003415733
XP_001688504	NCBI	1.425843339	0.087966833
XP_001230863	NCBI	-1047.336703	1.2575E-08
XP_311753	NCBI	-2250.346569	5.69972E-21
XP_311757	NCBI	-5.092023766	0.001841993
XP_311759	NCBI	-17.61531047	0.005489317
XP_313002	NCBI	-47.79210144	1.4883E-05
XP_313007	NCBI	-28.75078142	0.024778791
XP_313009	NCBI	-3.337035302	0.028196395
XP_313010	NCBI	-2.634754696	0.07439324
XP_553285	NCBI	-1.435389417	0.04347241
XP_310358	NCBI	-1.570370069	0.039616984
XP_314349	NCBI	1.528168634	0.000447794
XP_319151	NCBI	-1.320694606	0.014985889
XP_318025	NCBI	1.457878823	0.032535684
XP_559779	NCBI	1.780578552	0.083516159
XP_315882	NCBI	-1.334185088	0.005609873
XP_316427	NCBI	1.263605211	0.050197011
XP_309616	NCBI	-1.374599709	0.053994039
XP_003436369	NCBI	-6.84393115	0.004909552
XP_316877	NCBI	-6.801032876	8.82232E-14
XP_312390	NCBI	-1.415250638	0.0001149
XP_320402	NCBI	1.445910516	0.088969534
XP_320383	NCBI	1.457890941	0.000774743
XP_314074	NCBI	-2.438456671	0.043388093
XP_309396	NCBI	1.32425267	0.031844066
XP_309961	NCBI	-1.462427048	0.097507151
XP_320746	NCBI	1.230688763	0.010841874
XP_314877	NCBI	-1.400706049	0.008093525
XP_308021	NCBI	1.175488842	0.081857948
XP_001844764	NCBI	1.331409604	0.084774219

XP_318929	NCBI	-1.501454209	0.023920918
NP_056517	NCBI	1.560301776	1.95101E-07
XP_312998	NCBI	-1.238982866	0.057243373
XP_316194	NCBI	-1.156280073	0.057645184
XP_315043	NCBI	-1.609400882	0.020158685
XP_318559	NCBI	1.418727243	0.089139737
XP_317782	NCBI	-3.823079497	7.33106E-07
XP_314086	NCBI	1.534878512	0.001020062
XP_312092	NCBI	-5.553131389	0.019802815
XP_001230655	NCBI	-14.4197038	0.027173338
XP_001687771	NCBI	1.914606075	0.004715754
XP_319457	NCBI	1.595419411	0.074422778
XP_321926	NCBI	1.315989178	0.05048431
XP_311147	NCBI	2.082869556	0.026381139
XP_006507138	NCBI	-1.710993771	0.082596934
XP_562817	NCBI	2.017838591	0.017882927
XP_320623	NCBI	1.732869815	0.061340786
XP_320633	NCBI	2.533079247	0.000229163
XP_321472	NCBI	-3.137108356	0.051800072
XP_560368	NCBI	-1.342197954	0.0964316
XP_315389	NCBI	-2.390649471	0.051837426
XP_313371	NCBI	-1.482834578	0.013435573
XP_308002	NCBI	1.375980761	0.086960611
XP_635619	NCBI	-2.709618956	0.025445515
XP_308700	NCBI	-1.806885808	0.000109519
XP_311831	NCBI	-1.523923528	0.054686763
XP_313277	NCBI	-1.363610596	0.010558752
XP_001689313	NCBI	-11.38173391	0.003489282
XP_001689180	NCBI	-1.298060125	0.016327919
XP_001845559	NCBI	-1.552098628	0.056212645
XP_001868653	NCBI	-1.290666409	0.089892521
XP_310285	NCBI	-3.708292988	0.002673766
XP_310994	NCBI	-1.471103014	0.052214879
XP_551305	NCBI	-1.405493788	0.087966833
XP_552123	NCBI	-1.88575539	0.050869021
XP_001654988	NCBI	1.304705463	0.022401707
XP_001850960	NCBI	1.969451213	0.022185086
XP_001851132	NCBI	1.469158261	0.031039172
XP_003436592	NCBI	1.467513372	0.056870625
XP_311358	NCBI	1.801551342	0.02743854
XP_553061	NCBI	1.375340495	0.061061061

XP_001688030	NCBI	-5.187732289	0.010027669
XP_003437040	NCBI	-6.339455061	0.002929058
XP_320317	NCBI	1.356676915	0.024487699
XP_001688385	NCBI	-9.900402202	0.003136905
XP_001688687	NCBI	-15.70239609	5.88886E-05
XP_001688688	NCBI	-17.55588498	0.000743715
XP_001844731	NCBI	1.774068959	6.68938E-07
XP_001861893	NCBI	1.347156609	0.014811198
XP_003435877	NCBI	1.806490975	0.000793668
XP_003436242	NCBI	1.299579332	0.088602867
NP_001262647	NCBI	1.332300111	0.073715623
XP_003436142	NCBI	-157.3483211	4.94908E-08
XP_308309	NCBI	-11.34123442	0.047369419
XP_310080	NCBI	-1.366816211	0.016310149
XP_310878	NCBI	-4.370309499	5.41503E-05
XP_314146	NCBI	-1.567611241	0.040291463
XP_001238452	NCBI	1.727708282	0.003992512
XP_001688078	NCBI	1.356519509	0.076014187
XP_001688895	NCBI	1.308200709	0.018101243
XP_001843464	NCBI	1.723775855	0.05818618
XP_001863938	NCBI	3.862082184	2.1271E-06
XP_001869031	NCBI	2.002788041	0.001723565
XP_310268	NCBI	1.669211949	0.046875112
XP_311056	NCBI	2.38033403	5.82969E-14
XP_311473	NCBI	1.270238047	0.050432683
XP_319669	NCBI	1.651716805	0.048027477
NP_498735	NCBI	1.908525031	0.007164135
XP_001238206	NCBI	-1.404472558	0.078630073
XP_001238350	NCBI	-1.293907218	0.041958502
XP_001238575	NCBI	-2.256122932	0.022534682
XP_001687820	NCBI	-3.935738571	0.048212358
XP_001688366	NCBI	-61.56316318	1.05693E-05
XP_001688505	NCBI	-16.43200245	0.017901526
XP_001689060	NCBI	-13.3450656	5.17549E-07
XP_001842012	NCBI	-2.970877068	0.089432607
XP_001851516	NCBI	-3.200558981	0.051003096
XP_001864349	NCBI	-1.686455196	0.08126684
XP_001867255	NCBI	-7.792528534	0.099628843
XP_001869508	NCBI	-10.10054752	0.010887158
XP_001869723	NCBI	-5.121547661	0.024085275
XP_003435768	NCBI	-8.259168055	0.00085375

XP_003436140	NCBI	-18.38501924	0.008093525
XP_003436349	NCBI	-12.46748321	0.077128158
XP_003436694	NCBI	-1.393058111	0.04378296
XP_003436984	NCBI	-3.365328797	0.022500339
XP_308478	NCBI	-2.323195871	0.046969894
XP_313994	NCBI	-1.34982659	0.019830175
XP_314946	NCBI	-9.371868182	0.003616568
XP_317093	NCBI	-2.74558788	0.01118491
XP_317614	NCBI	-12.50149348	0.023514002
XP_319794	NCBI	-7.278682948	0.026956532
XP_321767	NCBI	-2.276662351	0.016616882
XP_552911	NCBI	-40.96311655	0.000228193
XP_557166	NCBI	-7.714721613	0.065389255
XP_559110	NCBI	-11.8401359	9.50108E-05
XP_564581	NCBI	-8.576352725	0.000664134
XP_001688170	NCBI	1.402505902	0.007539016
XP_001688259	NCBI	5.41168808	0.006429929
XP_001688353	NCBI	1.443581148	0.070354408
XP_001688843	NCBI	1.738528426	0.023184412
XP_001688861	NCBI	2.055503244	0.086995682
XP_001689191	NCBI	1.464920907	0.044378505
XP_001842180	NCBI	1.292348183	0.043328684
XP_001842443	NCBI	1.433108708	0.061061061
XP_001842689	NCBI	1.465877619	0.031304995
XP_001846593	NCBI	2.126450718	0.007903712
XP_001849599	NCBI	2.509093217	0.061340786
XP_001850386	NCBI	1.454535771	0.071138351
XP_001863281	NCBI	1.439455321	0.095351065
XP_001867493	NCBI	1.5651734	0.025962875
XP_001870310	NCBI	1.328655534	0.054555606
XP_001870682	NCBI	2.130463715	0.07439324
XP_001870995	NCBI	1.473360634	0.017371051
XP_003436007	NCBI	1.531445807	0.043894979
XP_003436108	NCBI	1.613831484	0.016327919
XP_307906	NCBI	1.447676063	0.086217812
XP_308552	NCBI	2.996112078	0.012136323
XP_308615	NCBI	1.250437127	0.096272169
XP_309217	NCBI	1.531989903	0.05324836
XP_309463	NCBI	1.552361951	0.0561599
XP_316506	NCBI	2.311409248	0.021791581
XP_320354	NCBI	1.335477596	0.092031471

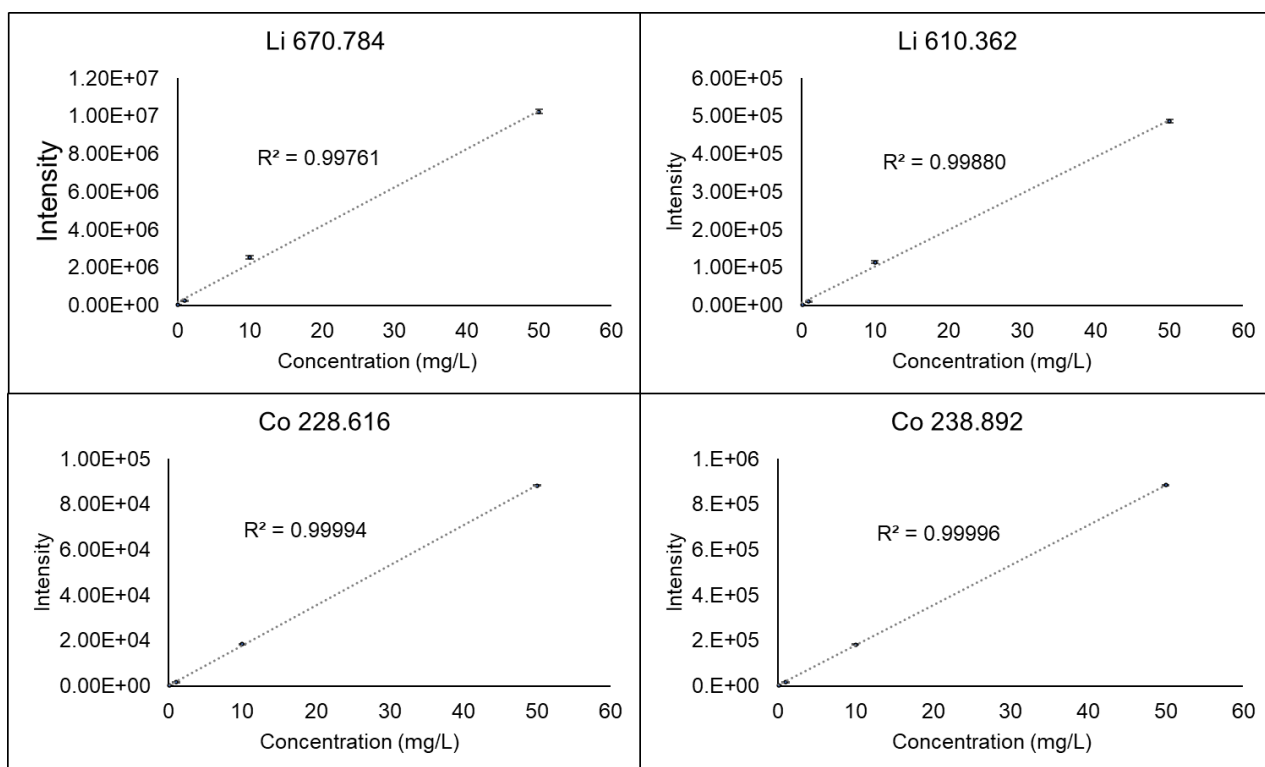
XP_321755	NCBI	1.351283569	0.093691693
XP_550879	NCBI	1.477119408	0.000327817
XP_552179	NCBI	1.507850043	0.082955849
XP_554885	NCBI	1.628983055	0.000355763
XP_564541	NCBI	2.213753732	0.000223688
XP_001238157	NCBI	-18.11720149	0.000737278
XP_001687837	NCBI	-22.09032876	0.0002013
XP_001688201	NCBI	-6.683208057	8.34931E-06
XP_001688348	NCBI	-25.62627488	0.000460975
XP_001688852	NCBI	-21.74166977	0.001303975
XP_001688883	NCBI	-28.54130961	0.024405069
XP_001689037	NCBI	-29.82271452	6.87341E-06
XP_001844992	NCBI	-11.31033862	7.15694E-05
XP_001845937	NCBI	-9.157612505	0.002982381
XP_001862431	NCBI	-2.840878074	0.027538773
XP_001864692	NCBI	-4.804345881	0.000103801
XP_003436232	NCBI	-30.3350755	0.00098566
XP_003436379	NCBI	-4.837972235	0.062950156
XP_003436564	NCBI	-10.82399533	0.000542515
XP_003436575	NCBI	-7.221896254	0.088708052
XP_003436721	NCBI	-35.41213264	0.000217599
XP_003436977	NCBI	-220.851936	6.63964E-07
XP_003437063	NCBI	-4.226211526	0.059172154
XP_003437064	NCBI	-9.048635398	0.000231061
XP_309701	NCBI	-5.532437459	0.04990427
XP_312851	NCBI	-3.26147261	0.009872401
XP_315327	NCBI	-5.645660672	0.003079669
XP_315378	NCBI	-5.305061857	0.023058054
XP_317216	NCBI	-34.98441609	0.000101784
XP_317626	NCBI	-3.55832936	2.57816E-05
XP_318844	NCBI	-10.99476271	0.03637894
XP_550737	NCBI	-3.967917114	0.025672358
XP_559373	NCBI	-1.637185196	0.038488339
XP_563533	NCBI	-606.307352	5.30504E-05
XP_001230950	NCBI	1.624236889	0.015477335
XP_001237131	NCBI	3.451820941	0.002241056
XP_001237263	NCBI	1.817803353	0.015874606
XP_001663089	NCBI	1.881952709	0.032687974
XP_001689036	NCBI	3.523598293	0.01152112
XP_001845505	NCBI	3.33477369	0.057243373
XP_001862079	NCBI	2.012202933	0.048690642

XP_003436839	NCBI	1.324490289	0.06990918
XP_307724	NCBI	1.339212988	0.000497784
XP_001230905	NCBI	2.266332847	7.05498E-11
XP_021697095	NCBI	2.048625162	0.049524356
XP_021701596	NCBI	1.683014673	0.029877223
XP_021703344	NCBI	4.306538633	2.41863E-12
XP_021704203	NCBI	1.883673936	0.041630315
XP_021704648	NCBI	1.449230894	0.041714857
XP_021707247	NCBI	4.031646927	0.071925283
XP_021707795	NCBI	1.614402432	0.077128158
XP_021709279	NCBI	4.801639426	1.17664E-11
XP_021711059	NCBI	2.247274413	2.3487E-05
B5KL40	UniProt-SwissProt	-2.80312724	0.041753076
P02226	UniProt-SwissProt	-4.882781764	1.45212E-09
P0C5P9	UniProt-SwissProt	-8.388197045	0.055473271
P15609	UniProt-SwissProt	-6.119782957	0.075498751
P38507	UniProt-SwissProt	-2.795180438	0.063132016
P45386	UniProt-SwissProt	-2.458540389	0.049235658
Q23762	UniProt-SwissProt	-2.997149115	0.071829356
P02221	UniProt-SwissProt	2.615425322	0.001238312
P02851	UniProt-SwissProt	2.186075584	0.0884664
P24243	UniProt-SwissProt	7.06497701	3.91672E-41
P83404	UniProt-SwissProt	3.783039943	4.58036E-05
P86242	UniProt-SwissProt	2.0689712	0.016005081
AHV85224	NCBI	-3.515258969	0.015718879
AHV85228	NCBI	-11.12810585	0.00037864
AHV85229	NCBI	-9.374544952	0.01989564
AHV85230	NCBI	-15.26944965	6.58852E-07
AHV85232	NCBI	-4.060345371	0.052811803
AHV85225	NCBI	1.420835451	0.074422778
AHV85233	NCBI	1.894132469	0.014464593
XP_021699291	NCBI	-4.032994068	0.074335114
XP_021702052	NCBI	-3.309319041	0.081472924
XP_021702201	NCBI	-1.76359746	0.069305664

XP_021709311	NCBI	-1.421411067	0.020158685
XP_024667099	NCBI	-10.04361858	0.006976815

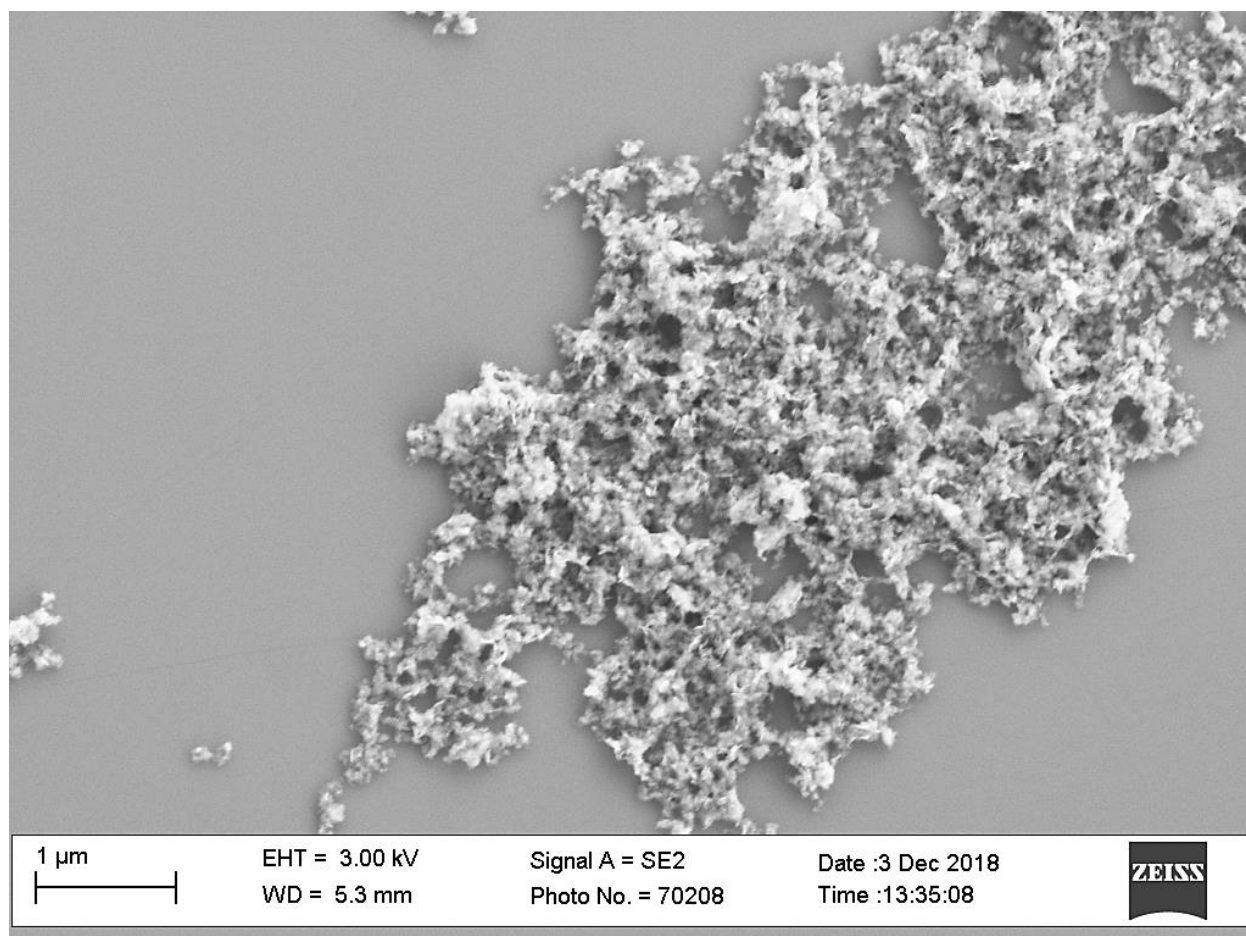
## Supporting Figures

### Supplementary Figure S1. Calibration data for ICP-OES.



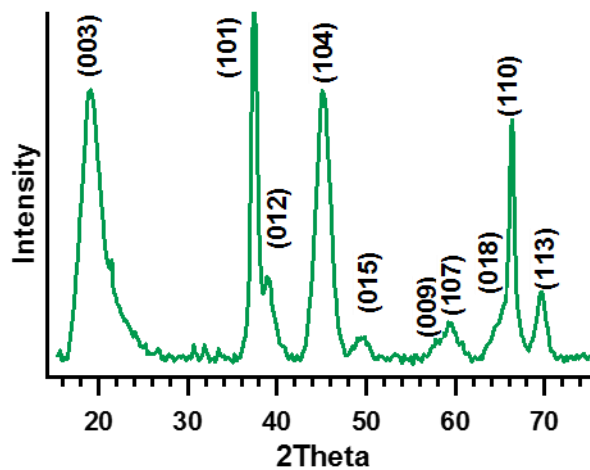
**Supplementary Figure S1. Calibration data for ICP-OES.** Calibration data for inductively coupled plasma - optical emission spectroscopy used to calculate LCO lithiation.

**Supplementary Figure S2. SEM of LCO nanosheets.**



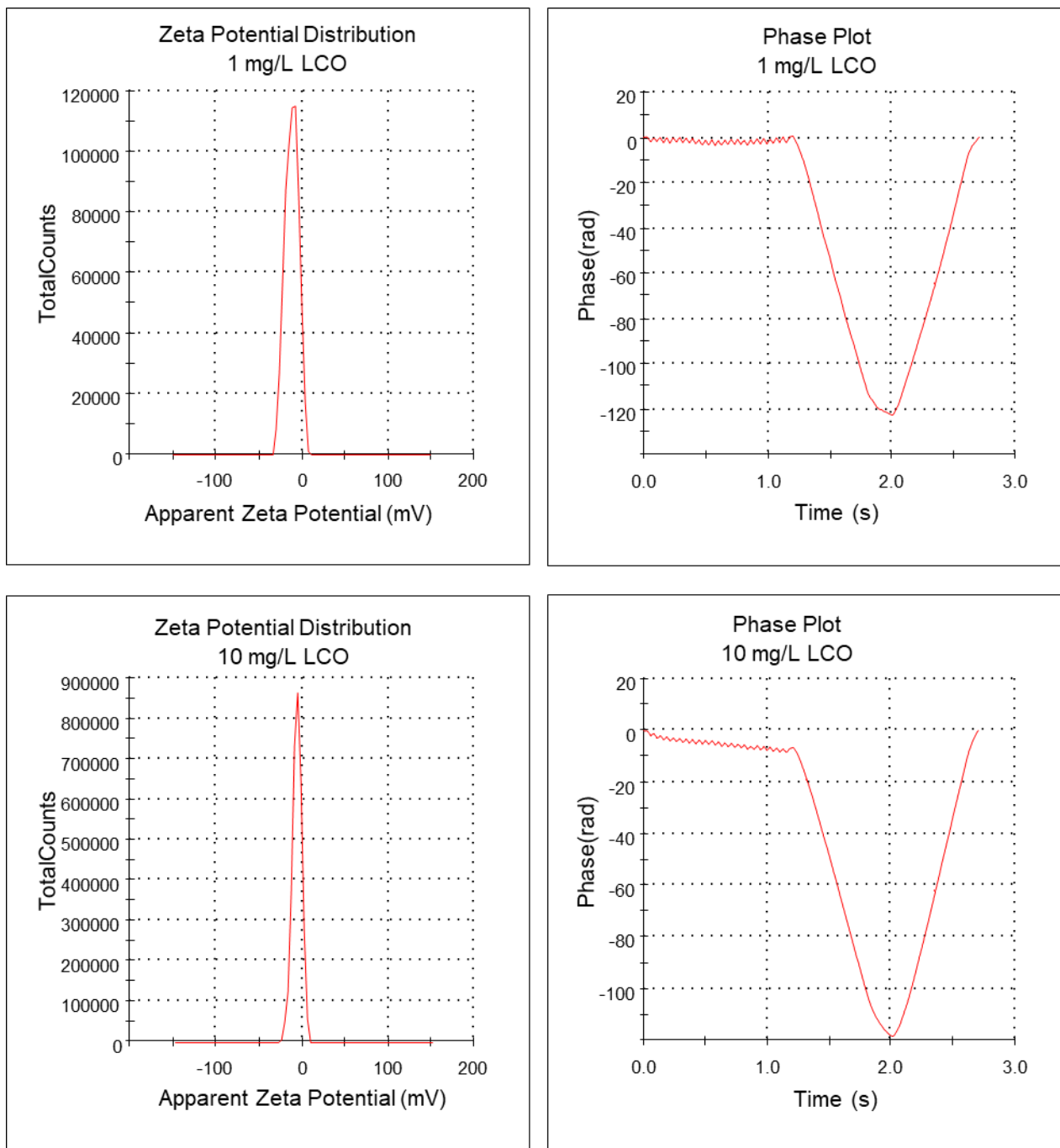
**Supplementary Figure S2. SEM of LCO nanosheets.** Scanning electron micrograph of LCO nanosheets.

**Supplementary Figure S3. XRD of LCO nanosheets.**



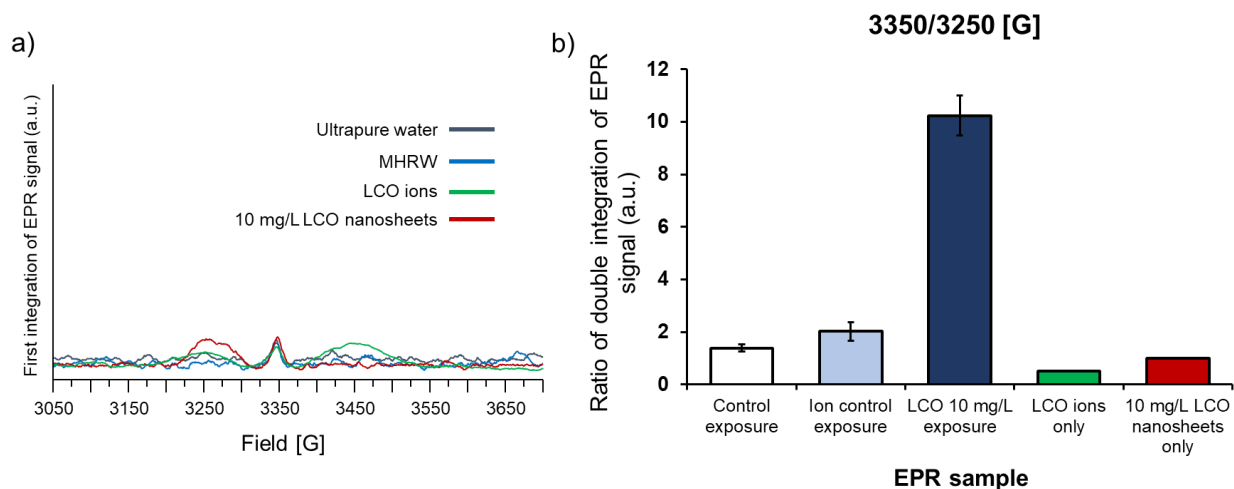
**Supplementary Figure S3. XRD of LCO nanosheets.** Powder X-Ray Diffraction spectra of LCO nanosheets. Peak indices are indicated above each reflection.

**Supplementary Figure S4. Zeta potential quality data.**



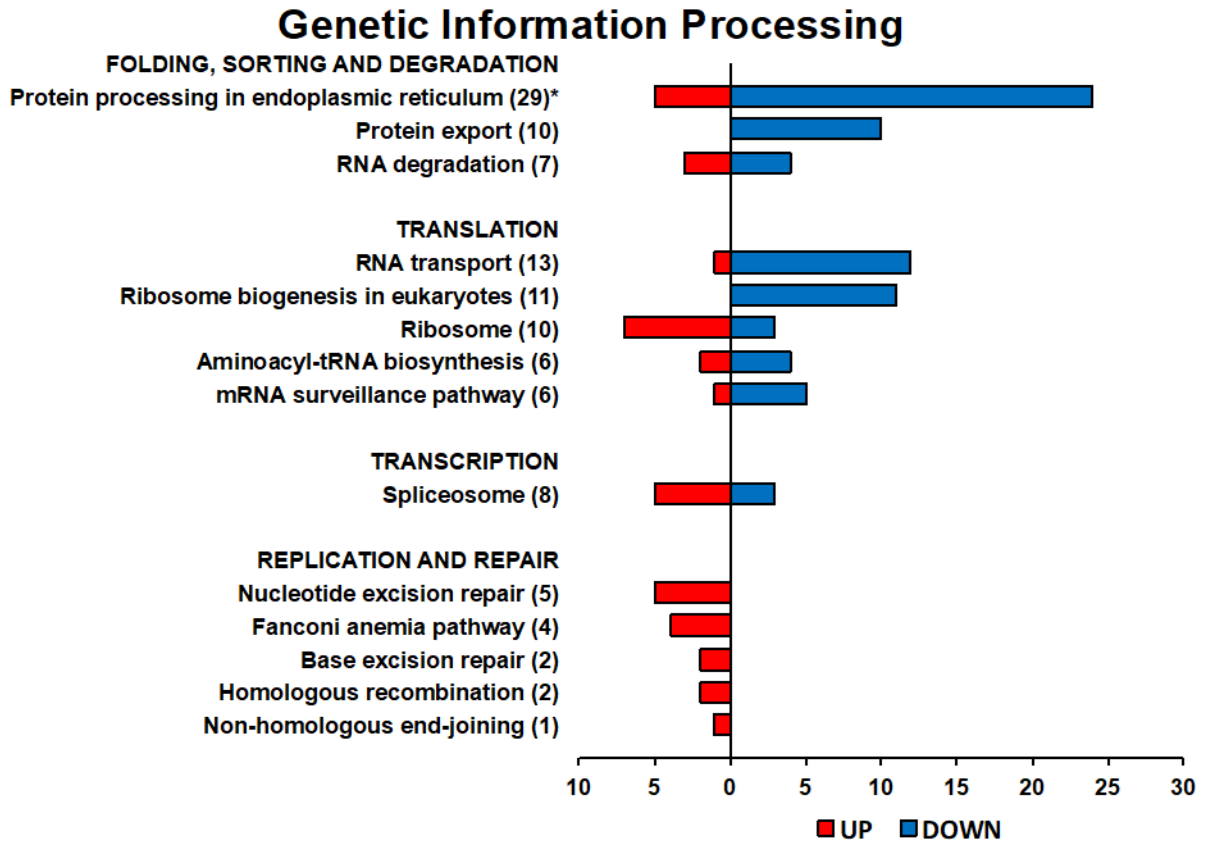
**Supplementary Figure S4. Zeta potential quality data.** Count and phase data for zeta potential data from instrument quality report.

**Supplementary Figure S5. EPR validation data.**



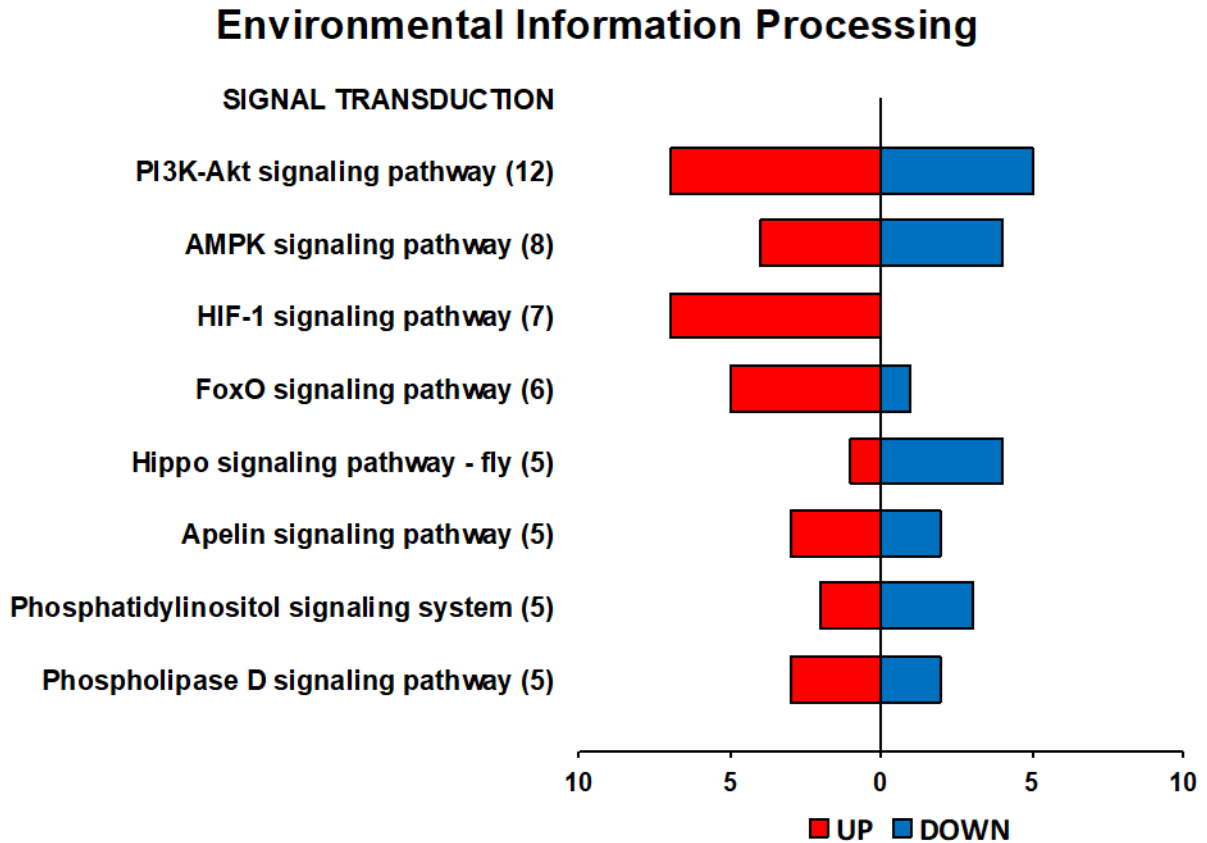
**Supplementary Figure S5. EPR validation data.** (a) EPR spectra for no-animal control samples: ultrapure water, MHRW exposure media, LCO ions equivalent to Li and Co released by 10 mg/L LCO nanosheets in MHRW, and 10 mg/L LCO nanosheets in MHRW. Compare to Figure 1a. (b) Ratio of peak integrations for animal samples and no-animal ion and LCO nanosheet controls. Compare to Figure 1b.

**Supplementary Figure S6. Differentially expressed genes in pathways related to genetic information processing for LCO-exposed larvae.**



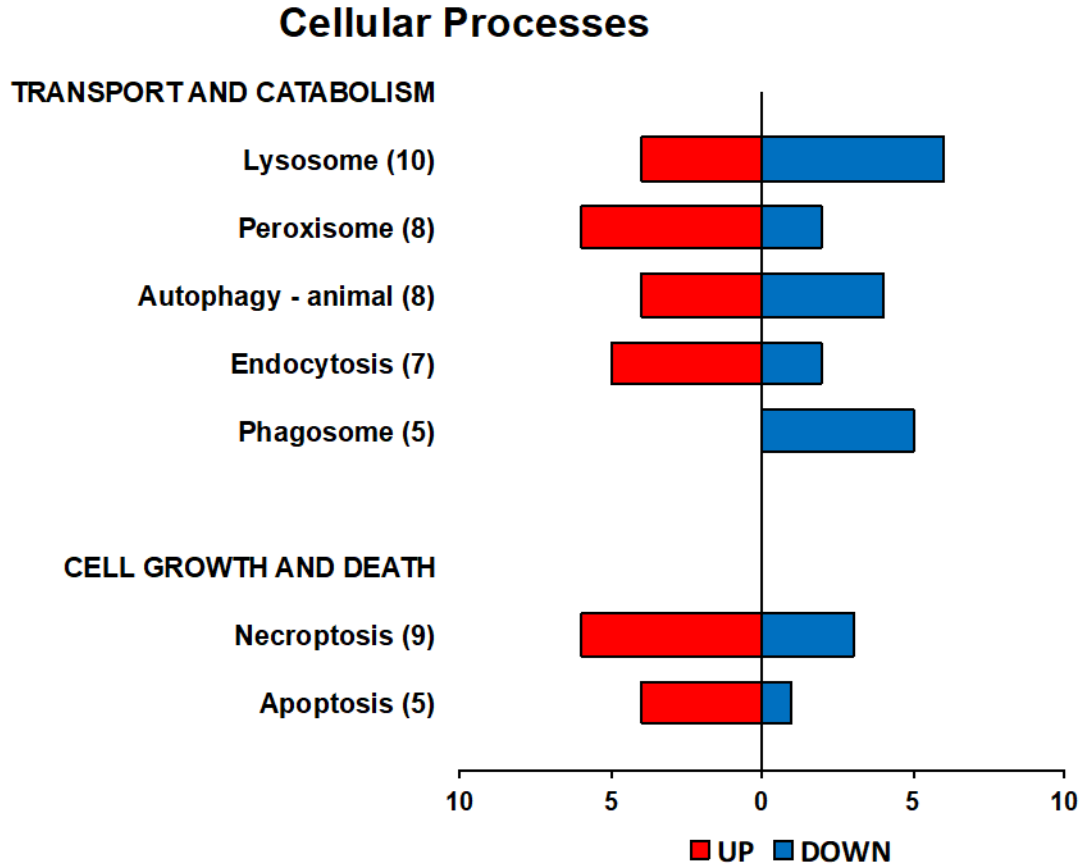
**Supplementary Figure S6. Differentially expressed genes in pathways related to genetic information processing for LCO-exposed larvae.** Kyoto Encyclopedia of Genes and Genomes (KEGG) pathways containing genes identified as differentially expressed (Wald FDR < 0.1) between control and 10 mg/L LCO-exposed *C. riparius* larvae at 48 hr. \* Indicates pathway identified as significantly enriched by DAVID (Benjamini-adjusted FDR < 0.1; Fig 3).

Supplementary Figure S7. Differentially expressed genes in pathways related to environmental information processing for LCO-exposed larvae.



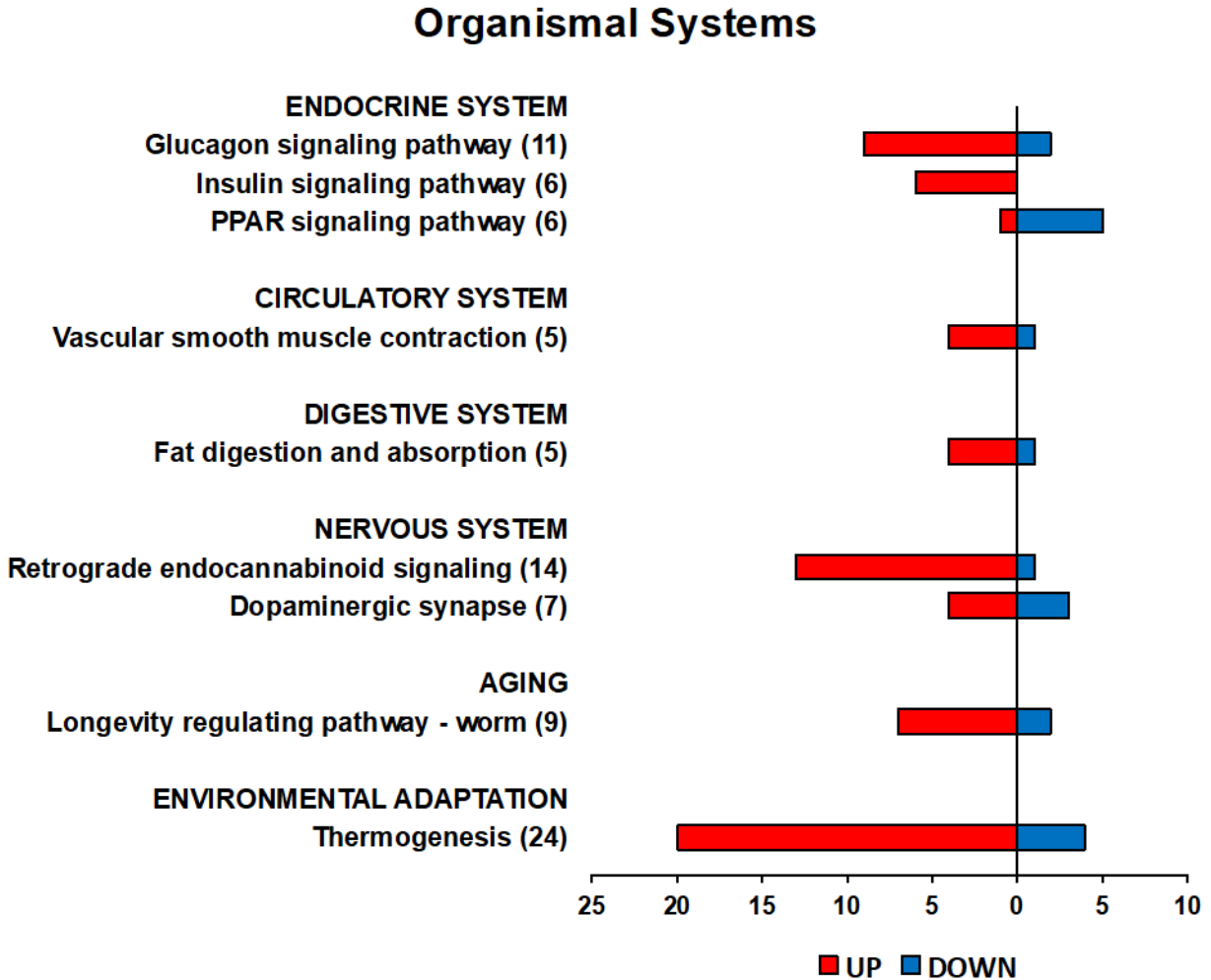
Supplementary Figure S7. Differentially expressed genes in pathways related to environmental information processing for LCO-exposed larvae. Kyoto Encyclopedia of Genes and Genomes (KEGG) pathways containing genes identified as differentially expressed (Wald FDR < 0.1) between control and 10 mg/L LCO-exposed *C. riparius* larvae at 48 hr.

Supplementary Figure S8. Differentially expressed genes in pathways related to cellular processes for LCO-exposed larvae.



Supplementary Figure S8. Differentially expressed genes in pathways related to cellular processes for LCO-exposed larvae. Kyoto Encyclopedia of Genes and Genomes (KEGG) pathways containing genes identified as differentially expressed (Wald FDR < 0.1) between control and 10 mg/L LCO-exposed *C. riparius* larvae at 48 hr.

**Supplementary Figure S9. Differentially expressed genes in pathways related to organismal systems for LCO-exposed larvae.**



**Supplementary Figure S9. Differentially expressed genes in pathways related to organismal systems for LCO-exposed larvae.** Kyoto Encyclopedia of Genes and Genomes (KEGG) pathways containing genes identified as differentially expressed (Wald FDR < 0.1) between control and 10 mg/L LCO-exposed *C. riparius* larvae at 48 hr.

**CHAPTER IV:**  
**ENERGY STARVATION IN *DAPHNIA MAGNA* FROM EXPOSURE TO A LITHIUM  
COBALT OXIDE NANOMATERIAL**

Nicholas Niemuth<sup>1</sup>, Becky Curtis<sup>1</sup>, Liz Laudadio<sup>2</sup>, Jelena Sostare<sup>3</sup>, Evan Bennet<sup>1</sup>, Nicklaus Neureuther<sup>1</sup>, Aurash Mohaimani<sup>1</sup>, Angela Schmoldt<sup>1</sup>, Eric Ostovich<sup>1</sup>, Mark Viant<sup>3</sup>, Robert Hamers<sup>2</sup>, Rebecca Klaper<sup>1\*</sup>

<sup>1</sup> School of Freshwater Sciences, University of Wisconsin-Milwaukee, 600 E Greenfield Ave., Milwaukee, WI 53204

<sup>2</sup> Department of Chemistry, University of Wisconsin-Madison, 1101 University Ave., Madison, WI 53706

<sup>3</sup> School of Biosciences, University of Birmingham, Edgbaston, Birmingham, B15 2TT, UK

\* Corresponding author: rklaper@uwm.edu

## Abstract

Growing evidence across organisms points to altered energy metabolism as an adverse outcome of metal oxide nanomaterial toxicity, with a mechanism of toxicity potentially related to the redox chemistry of processes involved in energy production. Despite this evidence, the significance of this mechanism has gone unrecognized in nanotoxicology due to the field's focus on oxidative stress as a universal—but non-specific—nanotoxicity mechanism. Our previous research demonstrated that energy metabolism is significantly impacted in sediment-dwelling invertebrate *Chironomus riparius* upon exposure to metal oxide nanomaterial lithium cobalt oxide (LCO), an impact that is not replicated by ion controls. To further explore metabolic impacts, we determined LCO's effects on these pathways in the model organism *Daphnia magna* through RNA-Seq global gene expression analysis and non-targeted metabolomics. Our results show a sublethal 1 mg/L 48 hr LCO exposure causes significant impacts on *D. magna* metabolic pathways. Specifically, transcriptomic analysis indicated disruption (FDR-adjusted  $p < 0.1$ ) in pathways involved in the cellular response to starvation, mitochondrial function, ATP-binding, oxidative phosphorylation, NADH dehydrogenase activity, and protein biosynthesis. Metabolomic analysis indicated alteration of amino acid metabolism and starch, sucrose, and galactose metabolism. Overlap of significantly impacted pathways by RNA-seq and metabolomics suggests amino acid breakdown and increased sugar import for energy production. Results indicate that LCO-exposed *Daphnia* are responding to energy starvation by altering metabolic pathways, both at the gene expression and metabolite level. Results support altered energy production as a sensitive nanotoxicity adverse outcome for LCO and suggest avenues for future study in other biological systems and with other metal oxide nanomaterials.

## **Introduction**

In the field of nanotoxicology, the search for mechanisms of action has focused to a large extent on oxidative stress, with more than 7000 papers attributing toxicity of a diversity of engineered nanomaterials (ENMs) to this cause.<sup>1,2</sup> However, lost in the focus on reactive oxygen species (ROS) is research showing that ROS can be involved in numerous processes as signaling molecules,<sup>3</sup> as well as the importance of redox processes in cells for functions as universal as energy metabolism.<sup>4</sup> Importantly, for metal oxide ENMs, it has been demonstrated that overlap of the conduction band of these materials with the redox potential of biological reactions is predictive of toxicity.<sup>5</sup> In this way, redox active ENMs could interact with and impact critical biological processes that rely on redox chemistry, including metabolic pathways. However, the focus on ROS has prevented more sophisticated nanotoxicity mechanisms from being proposed, with oxidative stress suggested as the general cause of metal oxide ENM toxicity, in spite of clear metabolic impacts of these ENMs.<sup>5</sup>

Oxidative phosphorylation (i.e. the electron transport chain; ETC) is a metabolic process of energy production that is highly-conserved across eukaryotes as the primary means to produce sufficient levels of adenosine triphosphate (ATP) to meet the energy demands of the cell.<sup>7</sup> Both the tricarboxylic acid (TCA) cycle, which produces reducing equivalents for the ETC, and the ETC itself rely on redox processes to transfer electrons from sugars, fats, and amino acids to molecular oxygen to produce the mitochondrial proton gradient that allows production of large amounts of ATP.<sup>4,7,8</sup> The centrality of redox processes in these widely conserved mechanisms required for energy metabolism,<sup>4</sup> and the potential for metal oxide ENMs to interact with these

processes,<sup>5</sup> indicate that these pathways could be an important target of metal oxide ENM toxicity, particularly at sublethal concentrations.

In fact, numerous studies have demonstrated metabolic impacts of metal oxide ENM exposures across cell and animal models. These include: increased gluconeogenesis in rat liver cells exposed to ZnO ENMs;<sup>9</sup> negative impacts on carbon metabolism in algae exposed to TiO<sub>2</sub>;<sup>10</sup> a decline in activity of tricarboxylic acid (TCA) cycle enzyme aconitase in ZnO ENM-exposed white sucker liver;<sup>11</sup> changes in expression of TCA cycle genes in CuO ENM-exposed *Pseudomonas aeruginosa* bacteria;<sup>12</sup> decreases in TCA cycle metabolites in kidney of ZnO-exposed rat kidneys<sup>13</sup> and TiO<sub>2</sub>-exposed *C. elegans*;<sup>14</sup> changes in expression of electron transport chain (ETC) genes in human lung cells exposed to TiO<sub>2</sub> ENMs;<sup>15</sup> increased expression of ETC proteins in mouse liver cells exposed to ZnO, TiO<sub>2</sub>, and CuO ENMs;<sup>16</sup> and declines in NADH dehydrogenase activity and ATP production in mammalian cells exposed to Co<sub>3</sub>O<sub>4</sub>, Cr<sub>2</sub>O<sub>3</sub>, Ni<sub>2</sub>O<sub>3</sub>, CuO, Mn<sub>2</sub>O<sub>3</sub>, CoO, ZnO ENMs.<sup>5</sup> In spite of this evidence, the broad implication of the impact of a range of metal oxide ENMs on as universally-conserved of processes as energy metabolism has not been recognized. However, available evidence makes clear that the metabolic impacts of metal oxide ENMs should be concretely explored as a mechanism of nanotoxicity.

One class of transition metal oxide ENM that is relatively understudied in the nanotoxicology literature are the lithium intercalating cathode materials used in lithium ion batteries (LIBs): lithium cobalt oxide (LCO) and the alternative lithium nickel manganese cobalt oxide. The use of LIBs in electronic devices and increasingly in electric vehicles means an estimated 200,000

tons of these cathode materials were produced in 2020, and this is anticipated to rise to 380,000 tons annually by 2025, comparable to or exceeding production quantities of better-studied ENMs such as Ag and TiO<sub>2</sub>.<sup>17-21</sup> Less than 5% of these materials are currently recycled, with disposed material accumulating in landfills, where it may pose an environmental concern,<sup>17,22,23</sup> as some 16% of LIB cathode waste is leached from disposed material.<sup>22</sup> The 60,000 tons or more of LIB leachate annually that this represents puts it on par with TiO<sub>2</sub>, a mass of material that could be of environmental concern.<sup>24</sup>

We have previously demonstrated that LCO is capable of negatively impacting survival and reproduction of the model aquatic invertebrate *Daphnia magna* at concentrations as low as 0.25 mg/L over 21 days.<sup>25</sup> *Daphnia magna* is a well-established and sensitive model for aquatic toxicology specifically, but with application as an important screening model for the toxicity of materials and compounds across species.<sup>26</sup> Previously, we showed that LCO causes negative impacts on growth, development, hemoglobin levels, expression of genes related to metabolism, and activity and oxidation state of the Fe-S TCA cycle enzyme aconitase in larvae of the sediment-dwelling midge *Chironomus riparius* at exposure concentrations as low as 10 mg/L.<sup>24,27</sup> In order to determine if metabolic impacts of LCO are a mechanism conserved across species, and to gain further insight into potential metabolic changes resulting from LCO exposure, we employed RNA-seq and metabolomics to examine global changes in gene expression and metabolite levels in response to a sublethal 1 mg/L LCO exposure in *D. magna* at 48 hr.

## Materials and Methods

### *LCO nanosheet synthesis and characterization*

The  $\text{Li}_x\text{CoO}_2$  nanosheets used in this study were synthesized and characterized as previously described in Niemuth *et al.* 2020.<sup>27</sup> Cobalt hydroxide ( $\text{Co}(\text{OH})_2$ ) precursor was synthesized by adding a 0.1 M LiOH solution in 420 mL of 18.2 M $\Omega$  water (ultrapure water used here and in all future steps) dropwise to a 1 M  $\text{Co}(\text{NO}_3)_2 \cdot 6\text{H}_2\text{O}$  solution in 20 mL of water ([OH] at 5% stoichiometric excess for  $\text{Co}^{2+} + 2\text{OH}^- \rightarrow \text{Co}(\text{OH})_2$ ). This created a precipitate that we immediately isolated by centrifugation (4696 g, room temperature, 3 min), redispersed in water to wash, and then re-isolated by centrifugation. This wash step was repeated twice, for a total of 3 washes. We then decanted the final supernatant and dried the product in a 30 °C vacuum oven overnight. The dried  $\text{Co}(\text{OH})_2$  was transformed into  $\text{Li}_x\text{CoO}_2$  by adding 0.20 g of  $\text{Co}(\text{OH})_2$  particles to a 10 g  $\text{LiNO}_3$ :LiOH (6:4 molar ratio) molten salt flux at 200 °C in a poly(tetrafluoroethylene) container with magnetic stirring in a silicone oil bath. The reaction was quenched with water after 30 min and isolated the  $\text{Li}_x\text{CoO}_2$  nanosheets by centrifugation (4969 g, room temperature, 5 min). The pellet was redispersing in water and isolated by centrifugation. The final product was dried in a vacuum oven overnight at 30 °C. Lithiation was verified by digesting a portion of the nanosheets in aqua regia and analyzing the metal content of the digestate via inductively coupled plasma – optical emission spectroscopy (ICP-OES) with a Perkin Elmer Optima 2000 ICP-OES. This analysis suggested a Li:Co ratio of 0.92:1 which indicated a resulting LCO stoichiometric composition of  $\text{Li}_{0.92}\text{CoO}_2$ . ICP-OES calibration data are included as Supplementary Figure S1. Nanosheet surface area was determined by BET and found to be 125 m<sup>2</sup>/g. Nanosheets were imaged edge-on using scanning electron microscopy and sheet-like structures were found to be consistent with previously published syntheses

(Supplementary Figure S2).<sup>28</sup> Previously published transmission electron microscopy showed approximate nanosheet diameters of 25 nm and widths of 5 nm.<sup>28</sup> Powder X-Ray Diffraction patterns can be indexed to the  $R\bar{3}m$  space group (Supplementary Figure S3), consistent with previously published work.<sup>28</sup> Nanosheet zeta potential was measured in moderately hard reconstituted water (MHRW) exposure media (NaHCO<sub>3</sub> 96 mg/L, CaSO<sub>4</sub> 60 mg/L, MgSO<sub>4</sub> 60 mg/L, KCl 4 mg/L, Na<sub>2</sub>SeO<sub>3</sub> 0.004 mg/L) with results of  $-12.6 \pm 0.6$  mV for 1 mg/L LCO (Zetasizer Nano ZS, Malvern), similar to previous results (Supplementary Table S1).<sup>29</sup> Supplementary Figure S4 shows quality data for zeta potential measurements.

### ***RNA-seq***

#### *Animal culture maintenance*

*Daphnia magna* were obtained from Aquatic Research Organisms (Hampton, NH) and cultured following US EPA guidelines in moderately hard reconstituted water (MHRW; NaHCO<sub>3</sub> 96 mg/L, CaSO<sub>4</sub> 60 mg/L, MgSO<sub>4</sub> 60 mg/L, KCl 4 mg/L, Na<sub>2</sub>SeO<sub>3</sub> 0.004 mg/L in 18 M $\Omega$  ultrapure water).<sup>25</sup> Cultures were maintained at 20° C with a 16 h:8 h light:dark photoperiod, 20 adult daphnids per liter. Cultures were fed 3 times weekly with 25 mL *Raphidocelis subcapitata* (~500,000 algal cells/mL) and 10 mL alfalfa solution (8 g *Medicago sativa* in 1 L of 18 M $\Omega$  ultrapure water). Media was changed 100% and neonates removed 3 times per week. Cultures were maintained using only third or fourth brood neonates less than 24 hr old.

#### *Exposure*

Six replicates were prepared for each treatment: MHRW control, 1 mg/L LCO, and ion control (660  $\mu$ g/L Li as LiCl and 150  $\mu$ g/L Co as CoCl<sub>2</sub>; 10 $\times$  the ions released by 1 mg/L LCO in 48

hr).<sup>29</sup> LCO exposure at 1 mg/L was chosen for this study as a concentration at which no negative impacts were apparent in daphnids at 48 hr in our previous study, but which is known to cause impacts by 14 d.<sup>25</sup> This concentration also acts as a point of comparison to *C. riparius* larvae, which are unaffected by LCO at a 1 mg/L concentration.<sup>27,29</sup> Each replicate consisted of ten 5-day-old daphnids, which were then exposed for 48 hr. Animals were fed alfalfa solution immediately after exposure setup and again after 24 hr. After 48 hr, animals were collected, pooled by replicate (i.e. 6 replicates per condition, each replicate containing 10 pooled daphnia), and flash frozen in liquid nitrogen. Flash frozen animals were then stored at -80°C for subsequent RNA extraction, cDNA library creation, and next-generation RNA-sequencing.

#### *RNA-extraction, library preparation, and sequencing*

Pooled flash frozen daphnids were homogenized by replicate in TRIzol (Thermo Fisher Scientific), and RNA was purified using the Direct-zol RNA MiniPrep kit (Zymo Research). RNA quality, determined using a NanoDrop 1000 spectrophotometer (Thermo Fisher Scientific), Bioanalyzer 2100 (Agilent), and Qubit fluorometer (Thermo Fisher Scientific), were: 260/280 ratio 1.8-2.0, 260/230 ratio 2.0-2.2, and RIN > 7. RNA sequencing libraries were prepared from 200ng of total RNA from each sample using the Illumina TruSeq Stranded mRNA kit (Illumina, RS-122-2102) and IDT for Illumina – TruSeq RNA UD Indexes (Illumina, 20022371). Prepared libraries were then sequenced using an Illumina NovaSeq6000, with paired-end reads of 150 bp.

#### *Processing of RNA-Seq data*

Raw sequence data from the Illumina NovaSeq 6000 instrument gave a total genomic yield surpassing 919 million paired-end reads, a median per-sample yield of 41.85 million fragments,

and a population standard deviation of 9.811 million fragments. FastQC v0.11.5 was used to quality assess the sequence data,<sup>30</sup> and no apparent base-calling errors needed to be removed. Illumina TruSeq 3'-anchored primers were clipped using Cutadapt v1.18,<sup>31</sup> and the resulting quality-controlled data was pseudoaligned and sample-quantified against the daphmag2.4 Ensembl release of the *Daphnia magna* reference transcriptome using Kallisto v0.45.0.<sup>32</sup> Differential expression analysis of sample pairs was performed using the DESeq2 package<sup>33</sup> within R v3.5.3, and the resulting tables of differentially expressed transcripts were re-annotated with Ensembl reference information and relationally joined with Kallisto sample quantification counts using custom tooling. As limited annotation data exists for *D. magna* genes, assembled contigs were annotated against the Refseq protein database for the well-annotated model invertebrate *Drosophila melanogaster* (e-value  $\leq 0.1$ ) using the BLASTX tool in the NCBI-BLAST+ package v2.2.28.<sup>34</sup> High-throughput parallelization of Kallisto was achieved using a compute cluster leveraging the Slurm job scheduler,<sup>35</sup> while all other steps were completed using a high-performance local workstation employing GNU Parallel.<sup>36</sup>

#### *RNA-Seq data analysis using DAVID and KEGG*

A total of 17,604 contigs were successfully assembled and present in at least 80% of samples. Of these, 15,223 were successfully annotated against *D. melanogaster* using BLASTX. 3,280 contigs were differentially expressed between MHRW control and 1 mg/L LCO samples (Wald FDR < 0.1) and found in at least 80% of samples. Of these, 2,988 could be annotated against *D. melanogaster*. These differentially expressed, annotated contigs were analyzed for functional enrichment using the Database for Annotation, Visualization and Integrated Discovery (DAVID) using a Benjamini-adjusted FDR < 0.1.<sup>37,38</sup> Pathway analysis was performed using the Kyoto

Encyclopedia of Genes and Genomes (KEGG) mapper based on assigned KEGG orthology (KO) terms.<sup>39–41</sup> Of annotated, differentially expressed contigs between MHRW control and 1 mg/L LCO samples, 2,446 could be assigned functions in DAVID and 1,071 could be assigned KOs by KEGG.

## ***Metabolomics***

### *Daphnid cultures*

*D. magna* were cultured as indicated above: density of 20 animals per liter MHRW, 16 h:8 h light:dark photoperiod, and a temperature of 20 °C. For metabolomics, cultures were fed daily on suspensions of unicellular green alga, *Chlorella vulgaris* ( $7.84 \times 10^7$  cells/ml) at 2 ml/L. Algae was supplemented daily by 50 µl/L of dried bakers yeast (1mg/ml stock, Sigma–Aldrich). Cultures were maintained using third or fourth brood neonates less than 24 hr old.

### *Exposure Details and Procedures*

Ten replicates were prepared for each treatment: MHRW control, 1 mg/L LCO, and ion control (66 µg/L Li as LiCl and 15 µg/L Co as CoCl<sub>2</sub>; equivalent to ions released by 1 mg/L LCO over 48 hr).<sup>25,29</sup> Twenty neonates per replicate (< 9 hr old) were transferred to 100 ml beakers 48 hours prior to exposure and fed proportionate amounts of food for 48 hours. At the end of the 48-hour feeding period, daphnids were transferred to 200 ml control or exposure beakers. Exposures were carried out for 48 h without food per standard OECD guidelines for *D. magna*.

At the end of the exposure daphnids were collected and transferred (20 pooled animals per replicate) into labeled Precellys tubes using a fine sable brush and flash frozen in liquid nitrogen.

Samples were stored at -80 °C and shipped to the Viant lab at the University of Birmingham, UK on dry ice.

#### *Daphnia Tissue Extraction*

For the extraction, all solvents were chilled to 4 °C. A mixture of 320µl of HPLC grade MeOH and 128 µl of HPLC grade H<sub>2</sub>O were added to each sample tube and kept on ice. Tubes were then placed in a Precellys 24 homogeniser for 2 × 10s bursts at 6400 rpm. The homogenised mixture was then transferred into a clean 1.8ml glass vial (Fisher TUL 520 006 J) using a Pasteur pipette. 320 µl (32 µl/mg) CHCl<sub>3</sub> (HPLC grade) and 160 µl (16 µl/mg) dH<sub>2</sub>O (HPLC grade) were then added to each vial. These vials were vortexed on full power for 15 s each to thoroughly mix polar and nonpolar solvents. Vials were then left on ice for 10 min to allow initial phase separation. Vials were then centrifuged at 4000 rpm at 4 °C for 10 min to ensure complete phase separation. Centrifuged vials were allowed to come to room temperature by setting them on the lab bench for 5 min.

Samples were then visibly biphasic, with protein debris separating the upper (polar) and lower (non-polar) layers. A 500 uL Hamilton syringe was then used to remove the polar phase (~ 2 × 150 µl aliquots) into 2 clean 1.5 mL Eppendorf tubes (one for positive, one for negative ion analysis). Polar samples were then dried using a Speed Vac concentrator and stored at -80 °C until analysis.

### *Sample Preparation and FT-ICR MS*

For positive ion analysis 30  $\mu$ l of 4 °C 80:20 methanol:water plus 0.25% formic acid was added to each of the frozen, dried extract samples, and each sample vortexed for 30s. For negative ion analysis 30  $\mu$ l of 4 °C 80:20 methanol:water plus 20 mM ammonium acetate was added to each of the frozen, dried extract samples, and each sample vortexed for 30s. Samples were then centrifuged at 4000 g at 4°C for 10 mins. For both positive and negative ion plates, samples were randomized and 5  $\mu$ l of sample supernatant was pipetted into a pre-washed 96 well sample plate in quadruplicate. Three quality control (QC) samples (a mixture with equal volume from all samples) and a blank were also included on each plate. Loaded plates were covered with a foil seal using heat sealer and loaded into a TriVersa Nano-Mate® electro-spray ionizer (Advion) with the cooler set at 10 °C. Non-targeted analysis was carried out on polar fractions by direct-injection mass spectrometry (DIMS) using an LTQ Orbitrap Velos (Thermo Fisher Scientific). 21 overlapping selected ion monitoring (SIM) windows were collected covering m/z values from 50 to 620.

### *Data analysis*

#### Galaxy

The Galaxy pipeline at the University of Birmingham<sup>42</sup> was used to process raw data collected. SIM windows were assembled into single spectra for each sample (SIM-Stitching).

#### Filtering

A signal to noise ratio (SNR) of 10 was selected to filter out background noise from the data. A replicate filter was applied to retain only peaks found in at least 3 out of 4 technical replicates,

and samples aligned across biological samples. A blank filter was applied to only retain peaks if they are a specified % larger than blank values. Finally a sample filter was applied to keep only those peaks found in greater than 80% of biological samples.

#### Missing-value imputation, normalization, and quality assessment

A probabilistic quotient normalization (PQN) was applied to data to normalize all spectra to QCs to account for differences in dilution between samples. A K-nearest neighbor (KNN) algorithm was then applied to fill in missing values. A G-log transformation was then applied to normalize small and large peaks so that all changes would be on the same scale. To assess data quality, the average relative standard deviation (RSD) was measured across technical replicates and a desired RSD cutoff value was specified.

#### Data analysis

Univariate ANOVAs were carried out on metabolite data with a false discovery rate (FDR) correction to account for the large number of possible comparisons. Peaks were annotated using the Functional Analysis tool for MS peaks on the MetaboAnalyst 5.0 online web server.<sup>43</sup> Peak list files were uploaded containing m/z values and FDR corrected p-values obtained by the processing above, and analyzed in the respective (positive or negative) ion mode with a 5.0 ppm mass tolerance. For enrichment analysis, the Mummichog algorithm was applied with a p-value cutoff of  $p < 0.1$  and analyzed against the KEGG database for *Homo sapiens* and *Drosophila melanogaster*.

## Results and discussion

### *RNA-seq supports metabolic response to LCO exposure*

DAVID enrichment analysis shows significant enrichment (Benjamini-adjusted  $p < 0.1$ ) for a series of gene ontology (GO) terms, UniProt keywords, and KEGG pathways associated with energy metabolism for genes identified by RNA-Seq as differentially expressed (Wald FDR-adjusted  $p < 0.01$ ) between MHRW control and 1 mg/L LCO-exposed *D. magna* at 48 hr (Table 1). Specifically, 8 different categories related to components and functioning of the electron transport chain (ETC) are significantly enriched: Mitochondrial respiratory chain complex I, 17 genes,  $p = 0.0002$ ; Ubiquinone, 16 genes,  $p = 0.0004$ ; Oxidoreductase, 80 genes,  $p = 0.0006$ ; Mitochondrion, 70 genes,  $p = 0.004$ ; Oxidative phosphorylation, 53 genes,  $p = 0.01$ ; NADH dehydrogenase activity, 12 genes,  $p = 0.05$ ; NADH dehydrogenase (ubiquinone) activity, 13 genes,  $p = 0.05$ ; and Mitochondrial electron transport, NADH to ubiquinone, 12 genes,  $p = 0.06$ . The cellular response to energy starvation was also specifically identified as enriched by DAVID (25 genes,  $p = 0.002$ ), as well as ATP binding (70 genes,  $p = 0.006$ ) and one-carbon metabolism (5 genes,  $p = 0.07$ ).

The electron transport chain is the primary energy source for all multicellular eukaryotes, utilizing reducing equivalents such as NADH derived from the breakdown of sugars, amino acids, and fatty acids in the tricarboxylic acid (TCA) cycle to produce adenosine triphosphate (ATP), the so-called “energy currency of the cell,” essential for life due to its use as the energy source for numerous biochemical processes.<sup>7,8</sup> Figure 1 demonstrates the specific genes in the ETC differentially expressed (Wald FDR-adjusted  $p < 0.01$ ) in *D. magna* exposed to LCO at 1 mg/L for 48 hr versus control animals. As can be seen (Fig 1, Supplementary Table S2), 34

different ETC genes are upregulated in response to LCO exposure, including 20 components of Complex I (NADH dehydrogenase Fe-S proteins *NDUFS2*, 3, 4, 6, and 8; NADH dehydrogenase flavoprotein 1 *NDUFV1*; NADH dehydrogenase 1 alpha subcomplex subunits *NDUFA2*, 4, 5, 6, 7, 10, 12, and 13; and NADH dehydrogenase 1 beta subunits *NDUFB2*, 3, 4, 9, 10, and 11; note that NADH dehydrogenase activity and NADH dehydrogenase ubiquinone activity were identified as significantly enriched by DAVID, Table 1), one subunit of Complex II (succinate dehydrogenase flavoprotein subunit *SDHA*), two components of Complex III (ubiquinol-cytochrome c reductase subunits *QCR7* and *QCR8*), five components of Complex IV (cytochrome c oxidase subunits *COX 1*, 4, 5B, 6A, and 6B), and six components of Complex V (F-type H<sup>+</sup>-transporting ATPase subunits *ATPeF0B*, *D*, *F*, *F6*, and *O*, and F-type H<sup>+</sup>-transporting ATPase subunit epsilon *ATPeF1E*).

Complex I, also known as NADH dehydrogenase, is the critical first complex of the ETC and allows the transfer of electrons from NADH into the ETC, transferring electrons via an FMN cofactor, through a series of Fe-S centers, and ultimately to ubiquinone, pumping protons into the mitochondrial intermembrane space in the process.<sup>44</sup> We previously showed that expression of Complex I subunit genes as well as levels of Complex I Fe-S centers are upregulated in response to LCO exposure in larvae of sediment-dwelling invertebrate *Chironomus riparius*.<sup>27</sup> NADH dehydrogenase activity has also been shown to be negatively impacted by metal oxide ENM exposure in mammalian cells.<sup>5</sup> Thus, changes in Complex I may be a sensitive indicator of metal oxide ENM toxicity across species and particle types.

Complex II, Succinate dehydrogenase, is also an Fe-S enzyme complex, and uses an FAD cofactor to transfer electrons from succinate through a series of Fe-S centers to ubiquinone. Like Complex I, succinate dehydrogenase genes and Fe-S centers are also increased in response to LCO exposure in *C. riparius*.<sup>27</sup> Complexes III and IV, Cytochrome c reductase and Cytochrome c oxidase, are involved in transferring electrons to Cytochrome c from ubiquinol and from cytochrome c to oxygen, respectively.<sup>7</sup> Cytochrome c itself was shown to be oxidized by metal oxide ENMs (including CoO and Co<sub>2</sub>O<sub>3</sub>) *in vitro*,<sup>5</sup> which may indicate that metal oxide ENMs are capable of interacting directly with redox-active cellular components, including in the ETC. Complex V, ATP synthase, utilizes the proton gradient created by electron transfer in Complexes I, III, and IV, to couple P<sub>i</sub> and ADP, creating ATP.<sup>7</sup> ATP production was shown to be negatively impacted in mammalian cells exposed to metal oxide ENMs,<sup>5</sup> indicating that the ultimate endpoint of oxidative metabolism can indeed be negatively impacted by metal oxide ENM exposure.

In this study, the upregulation of these ETC components (Fig 1), along with enrichment of genes associated with energy starvation (Table 1), clearly demonstrate the negative impacts of LCO on metabolism, and also provide evidence that may explain the impacts of LCO and other complex metal oxide ENMs on the growth and reproduction of *D. magna* after exposure to these materials in the literature,<sup>25</sup> as well as growth and development impacts observed for the sediment-dwelling invertebrate *Chironomus riparius*.<sup>24</sup> These results also accord well with previous demonstrations of metabolic impacts of LCO in other models by RNA-seq, both in *C. riparius* larvae and in gill cell culture from trout species *Oncorhynchus mykiss*, where metabolism was identified as significantly enriched.<sup>27,45</sup> Impacts of other metal oxides on expression of genes in

the ETC have also been demonstrated for TiO<sub>2</sub> nanoparticles,<sup>15</sup> and exposure to numerous metal oxide nanoparticles (i.e. Co<sub>3</sub>O<sub>4</sub>, Cr<sub>2</sub>O<sub>3</sub>, Ni<sub>2</sub>O<sub>3</sub>, CuO, Mn<sub>2</sub>O<sub>3</sub>, CoO, ZnO) have been demonstrated to negatively impact metabolism of cells *in vitro*, specifically by reducing NADH dehydrogenase activity as measured by MTS assay as well as ATP production at sub-cytotoxic concentrations.<sup>5</sup> Thus, metabolism may be a sensitive endpoint for metal oxide ENM exposure, showing impacts at sub-lethal exposure concentrations in daphnia in this study, as well as for chironomids,<sup>27</sup> trout gill cells,<sup>45</sup> and mammalian cell culture.<sup>5,15</sup>

Also supporting impacts related to the ETC, and specifically to ATP, is the identification by DAVID of enrichment for Plasma membrane proton-transporting V-type ATPase complex (13 genes; Benjamini-adjusted p = 0.002) and ATP hydrolysis coupled proton transport (18 genes; Benjamini-adjusted p = 0.06). As shown in Fig 1, 13 subunits of the vacuole-localized V-type H<sup>+</sup>-transporting ATPase (*ATPeV0A, 0B, 0C, 0D, 0E, 1A, 1B, 1C, 1D, 1E, 1F, 1G, and 1H*) are all downregulated. This transporter uses ATP to pump protons into vacuoles,<sup>46</sup> and its downregulation suggests conservation of ATP as a result of energy starvation.

Downregulated components of the ETC include Complex IV genes heme a synthase (*COX15*) and cytochrome c oxidase assembly subunit 17 (*COX17*), both potentially related to metal homeostasis (Fig 1). *COX15* is involved in synthesizing the heme a cofactor for Complex IV.<sup>47</sup> Heme synthesis was also seen as being downregulated by LCO exposure in *C. riparius* larvae,<sup>24</sup> and heme-containing catalase was downregulated in *D. magna* as a result of LCO exposure by qPCR.<sup>25</sup> We proposed that the heme impacts of LCO exposure were the result of deregulation of iron homeostasis as a result of oxidation of the Fe-S center of the iron-responsive protein, which

we showed to be oxidized using both activity assay and electron paramagnetic resonance in *C. riparius* larvae.<sup>27</sup> *COX17* is involved in the transfer of copper during the assembly of Complex IV.<sup>48</sup> It's downregulation could indicate a broader disruption of metal homeostasis as a result of LCO exposure. Disruption of iron homeostasis was indicated by RNA-Seq in *C. riparius* larvae exposed to LCO.<sup>27</sup>

Also identified as enriched by DAVID (Benjamini-adjusted  $p < 0.1$ ) were a series of terms related to protein synthesis, degradation, and amino acids (Table 1). Specifically enriched were: Ribosome biogenesis, 21 genes,  $p = 0.0009$ ; Protein biosynthesis, 40 genes,  $p = 0.003$ ; Aminoacyl-tRNA synthetase, 20 genes,  $p = 0.003$ ; Ribosome biogenesis in eukaryotes, 38 genes,  $p = 0.01$ ; Protein export, 17 genes,  $p = 0.01$ ; Protease, 86 genes,  $p = 0.02$ ; Aminoacyl-tRNA biosynthesis, 25 genes,  $p = 0.08$ ; and rRNA processing, 13 genes,  $p = 0.08$ . Supplementary Table 1 shows that genes in KEGG pathways for Ribosome biogenesis (37 genes), Ribosome (30 genes), Protein export (16 genes), and Aminoacyl-tRNA biosynthesis (26 genes) are all downregulated. These processes are all necessary for protein synthesis, and their coordinated downregulation suggests a metabolic shift away from anabolic processes like protein synthesis and, as will be discussed in the context of metabolomics data below, toward catabolism, specifically the breakdown of proteins for energy. The enrichment for protease genes (Table 1), necessary for the breakdown of proteins into amino acids, also supports this conclusion.

### ***Metabolomics and RNA-Seq support metabolic switch to energy production***

Table 2 shows enriched KEGG pathways as identified by MetaboAnalyst (gamma-adjusted  $p < 0.1$ ) for metabolites significantly different (FDR-adjusted  $p < 0.1$ ) between MHRW control and 1

mg/L LCO exposed daphnids at 48 hr. As can be seen, amino acid metabolism is the most common pathway type identified as significantly enriched among identified likely metabolites, with 10 enriched pathways: Histidine metabolism, 3 metabolites,  $p = 0.02$ ; beta-Alanine metabolism, 4 metabolites,  $p = 0.03$ ; Valine leucine and isoleucine biosynthesis, 3 metabolites,  $p = 0.03$ ; Aminoacyl-tRNA biosynthesis, 5 metabolites,  $p = 0.04$ ; D-Arginine and D-ornithine metabolism, 2 metabolites,  $p = 0.05$ ; Tryptophan metabolism, 3 metabolites,  $p = 0.05$ ; Valine leucine and isoleucine degradation, 3 metabolites,  $p = 0.07$ ; Glycine serine and threonine metabolism, 3 metabolites,  $p = 0.08$ ; Lysine degradation, 2 metabolites,  $p = 0.08$ ; and Arginine and proline metabolism, 3 metabolites,  $p = 0.09$ .

The combination of metabolomics results with RNA-seq data for differentially expressed genes demonstrates important overlap between significantly changed amino acid metabolites, their breakdown metabolite intermediates, and expression changes for genes of enzymes involved in amino acid metabolism and degradation between MHRW control and 1 mg/L LCO-exposed daphnids (Supplementary Table S2). Particularly striking are the lower levels of the amino acids L-Leucine (Leu), L-Valine (Val), and L-Isoleucine (Ile), the increased levels of their breakdown intermediates Isoveryl-CoA and (S)-2-Methylbutanoyl-CoA, and the increase in expression of 14 genes for enzymes involved in the breakdown of these amino acids (Fig 2). These changes support the breakdown of these amino acids to produce Acetyl-CoA, the critical entry metabolite for production of reducing equivalents in the TCA cycle (and ultimately ATP in the ETC).<sup>8</sup> Other changes observed in combined metabolomics and RNA-seq data supporting this conclusion are changes in Tryptophan metabolism, specifically the increase in levels of 7 breakdown intermediates for Tryptophan (L-Kynurenine, 5-Hydroxy-L-tryptophan, 3-Hydroxy-

L-kynurenine, Formyl-5-hydroxykynurenamine, 5-Hydroxy-N-formylkynurenine, 5-Hydroxykynurenine, N-Methyltryptamine) and increased expression for 6 enzyme genes involved in Tryptophan degradation (glutaryl-CoA dehydrogenase, tryptophan 5-monooxygenase, dihydrolipoamide succinyltransferase, arylalkylamine N-acetyltransferase, L-tryptophan decarboxylase, and enoyl-CoA hydratase; Supplementary table S2). As was noted above, 26 genes involved in Aminoacyl-tRNA biosynthesis, that is loading of amino acids onto tRNAs for subsequent protein synthesis, are all downregulated (Supplementary Table S2). The amino acids to be loaded in this process that are lower in LCO-exposed animals are: L-Arginine, L-Leucine, L-Histidine, L-Valine, and L-Isoleucine (Supplementary Table S2). Taken together, decreases in protein synthesis genes, enrichment for protease genes, decreases in levels of amino acids, increases in amino acid breakdown intermediates, and increases in expression of enzyme genes involved in breakdown of amino acids support a shift in LCO-exposed animals toward protein catabolism, likely in response to energy starvation (seen as enriched by DAVID, Table 1).

Also found to be enriched by MetaboAnalyst are Starch and sucrose metabolism (4 metabolites, gamma-adjusted  $p = 0.03$ ) and Galactose metabolism (6 metabolites, gamma-adjusted  $p = 0.04$ ; Table 2). Unlike amino acids, similarities in mass between sugar isomers and other transformation products makes positive identification of specific sugars difficult by DIMS. However, as seen in Table 3, ions corresponding to 7 sugars are all increased in LCO-exposed daphnids. Corresponding changes in expression of Starch and sucrose metabolism and Galactose metabolism can also be seen by RNA-Seq (Supplementary Table S2). Increases in expression of glucose transporters was previously seen in trout gill cells exposed to LCO.<sup>45</sup> The increase in

sugars in LCO-exposed daphnids, like the breakdown of amino acids, supports a response in exposed animals to energy starvation.

Taken together, changes observed by both RNA-seq and metabolomics support metabolic changes in daphnia in response to LCO exposure toward increasing energy production, likely as a response to energy starvation. These include: enrichment of gene expression changes related to the Cellular response to energy starvation and to Oxidative phosphorylation (Table 1), the upregulation of ETC components and downregulation of ATP using complexes (Fig 1), the enrichment for and downregulation of genes involved in protein synthesis (Table 1; Supplementary Table S2), decreases in levels of amino acids and increases in their breakdown products and expression of amino acid degradation enzyme genes (Table 2, Fig 2, Supplementary Table S2), and increases in levels of sugars (Table 3) and changes in sugar metabolism enzyme genes (Supplementary Table S2). These results accord with metabolic impacts seen from LCO and other metal oxides in the literature including changes in metabolic gene expression in *C. riparius* larvae and trout gill cells exposed to LCO,<sup>27,45</sup> changes in expression of oxidative phosphorylation genes in human lung cells following TiO<sub>2</sub> exposure,<sup>15</sup> reduced in NADH dehydrogenase activity and ATP production in mammalian cells exposed to a range of metal oxide ENMs,<sup>5</sup> and metabolic changes observed in components of the TCA cycle and ETC from exposure to numerous metal oxide ENMS in different biological systems.<sup>11–14,16</sup> Thus, evidence both provided by this study as well as that available in the literature suggest that metabolic impacts of metal oxide ENMs may be a mechanism of nanotoxicity applicable across species and particle type.

### *Nano-specificity of RNA-seq and metabolomic changes*

Released ion control showed no significant impact on metabolites versus MHRW control at concentrations equivalent to that released by 1 mg/L LCO at 48 hr (66 µg/L Li and 15 µg/L Co). RNA-seq showed gene-expression changes for ion exposure only at a concentration equivalent to 10× the ions released from 1 mg/L LCO in 48 hr (660 µg/L Li and 150 µg/L Co).<sup>29</sup> In this case, DAVID functional enrichment terms shared with particles included the Ribosome KEGG pathway (Benjamini-adjusted  $p = 0.000002$ ) but did not include enrichment for oxidative phosphorylation or other ETC components, demonstrating the nano-specificity of metabolic impacts of LCO.

### *Potential mechanism and implications of metabolic impacts*

The mechanism by which LCO and other metal oxide ENMs may be able to impact metabolism has been suggested in the literature, but only from the standpoint of ROS generation and oxidative stress, ultimately missing what may be a far more nuanced process with broad implications: the ability of metal oxide ENMs to participate in redox chemistry.<sup>5,17</sup> Zhang *et al.* 2012 demonstrate that the overlap of the conduction band of metal oxide ENMs with the biological redox potential is predictive of toxicity, including reduced NADH dehydrogenase activity and ATP production.<sup>5</sup> In the case of LCO, its bandgap energy is similar to that of  $\text{Co}_3\text{O}_4$  nanoparticles shown to negatively impact metabolism in Zhang *et al.* 2012 (2.7 versus 2.53 eV respectively),<sup>5,49,50</sup> supporting the possibility that LCO's bandgap may explain its metabolic impacts in this and other studies.<sup>27,45</sup> Zhang *et al.* 2012 also show oxidation of cytochrome c by these metal oxide ENMs, but ultimately attribute impacts to general oxidative stress.<sup>5</sup> Hamers 2020 proposes that the toxicity of LCO may be due to reduction of  $\text{Co}^{3+}$  to  $\text{Co}^{2+}$  during metal

release into aqueous solution, with concomitant oxidation of other species to produce ROS.<sup>17</sup> LCO has been shown to oxidize the non-specific ROS-sensitive fluorescent dye CM-H<sub>2</sub>DCFDA in trout gill cells<sup>51</sup> and oxidize the Fe-S center of aconitase in *C. riparius* larvae,<sup>27</sup> indicating that it can participate directly or indirectly in redox processes. An important point in this context is that energy metabolism is reliant on redox processes<sup>4</sup> and may thus represent a sensitive endpoint to redox-active materials, potentially as a result of redox chemistry occurring at the particle surface or via an ROS intermediate. This could be the result of the overlap of the redox potential of these metabolic processes with the ENM conduction band, of oxidative metal release, or of the combination of these or other redox processes. The conservation of these redox-dependent processes for energy metabolism across eukaryotes,<sup>4,7</sup> and the conservation of energy metabolism across species more broadly,<sup>6</sup> in combination with the observation of changes in energy metabolism in response to metal oxide ENM exposure across metal types and biological systems,<sup>5,9-16,27,45</sup> suggest that this may be a fruitful avenue of future nanotoxicity research, both from the standpoint of chemistry and biology.

### **Acknowledgement**

This work was supported by National Science Foundation under the Center for Sustainable Nanotechnology (CSN), CHE-1503408. The CSN is part of the Centers for Chemical Innovation Program. This project used the UW-Milwaukee Great Lakes Genomics Center for RNA isolation, Illumina NovaSeq RNA sequencing, and bioinformatics services. Metabolomics experiments were carried out in the Environmental Metabolomics Research Laboratory at the University of Birmingham.

**Conflict of interest statement**

The authors have no conflicts to declare.

**Supporting Information**

Supporting information includes supplementary figures and tables referenced in the text.

## References

- (1) Murphy, C. J.; Vartanian, A. M.; Geiger, F. M.; Hamers, R. J.; Pedersen, J.; Cui, Q.; Haynes, C. L.; Carlson, E. E.; Hernandez, R.; Klaper, R. D.; et al. Biological Responses to Engineered Nanomaterials: Needs for the Next Decade. *ACS Cent. Sci.* **2015**, *1* (3), 117–123. <https://doi.org/10.1021/acscentsci.5b00182>.
- (2) Chen, X. Mapping the Decadal (2009–2018) Research Landscape of Nanotoxicity: Insights from a Bibliometric Study. *Nanosci. Nanotechnol. Lett.* **2019**, *11* (10), 1327–1337. <https://doi.org/10.1166/nnl.2019.3015>.
- (3) Ray, P. D.; Huang, B.-W.; Tsuji, Y. Reactive Oxygen Species (ROS) Homeostasis and Redox Regulation in Cellular Signaling. *Cell. Signal.* **2012**, *24* (5), 981–990. <https://doi.org/10.1016/J.CELLSIG.2012.01.008>.
- (4) Griffiths, H. R.; Gao, D.; Pararasa, C. Redox Regulation in Metabolic Programming and Inflammation. *Redox Biol.* **2017**, *12*, 50–57. <https://doi.org/10.1016/j.redox.2017.01.023>.
- (5) Zhang, H.; Ji, Z.; Xia, T.; Meng, H.; Low-Kam, C.; Liu, R.; Pokhrel, S.; Lin, S.; Wang, X.; Liao, Y.-P.; et al. Use of Metal Oxide Nanoparticle Band Gap To Develop a Predictive Paradigm for Oxidative Stress and Acute Pulmonary Inflammation. *ACS Nano* **2012**, *6* (5), 4349–4368. <https://doi.org/10.1021/nn3010087>.
- (6) Peregrín-Alvarez, J. M.; Sanford, C.; Parkinson, J. The Conservation and Evolutionary Modularity of Metabolism. *Genome Biol.* **2009**, *10* (6), R63. <https://doi.org/10.1186/gb-2009-10-6-r63>.
- (7) Chaban, Y.; Boekema, E. J.; Dudkina, N. V. Structures of Mitochondrial Oxidative Phosphorylation Supercomplexes and Mechanisms for Their Stabilisation. *Biochim. Biophys. Acta - Bioenerg.* **2014**, *1837* (4), 418–426.

- <https://doi.org/10.1016/j.bbabbio.2013.10.004>.
- (8) Polyzos, A. A.; McMurray, C. T. The Chicken or the Egg: Mitochondrial Dysfunction as a Cause or Consequence of Toxicity in Huntington's Disease. *Mech. Ageing Dev.* **2017**, *161*, 181–197. <https://doi.org/10.1016/j.mad.2016.09.003>.
- (9) Filippi, C.; Pryde, A.; Cowan, P.; Lee, T.; Hayes, P.; Donaldson, K.; Plevris, J.; Stone, V. Toxicology of ZnO and TiO<sub>2</sub> Nanoparticles on Hepatocytes: Impact on Metabolism and Bioenergetics. *Nanotoxicology* **2015**, *9* (1), 126–134. <https://doi.org/10.3109/17435390.2014.895437>.
- (10) Cardinale, B. J.; Bier, R.; Kwan, C. Effects of TiO<sub>2</sub> Nanoparticles on the Growth and Metabolism of Three Species of Freshwater Algae. *J. Nanoparticle Res.* **2012**, *14* (8), 913. <https://doi.org/10.1007/s11051-012-0913-6>.
- (11) Dieni, C. A.; Callaghan, N. I.; Gormley, P. T.; Butler, K. M. A.; MacCormack, T. J. Physiological Hepatic Response to Zinc Oxide Nanoparticle Exposure in the White Sucker, *Catostomus Commersonii*. *Comp. Biochem. Physiol. Part C Toxicol. Pharmacol.* **2014**, *162*, 51–61. <https://doi.org/10.1016/j.cbpc.2014.03.009>.
- (12) Guo, J.; Gao, S.-H.; Lu, J.; Bond, P. L.; Verstraete, W.; Yuan, Z. Copper Oxide Nanoparticles Induce Lysogenic Bacteriophage and Metal-Resistance Genes in *Pseudomonas Aeruginosa* PAO1. *ACS Appl. Mater. Interfaces* **2017**, *9* (27), 22298–22307. <https://doi.org/10.1021/acsami.7b06433>.
- (13) Yan, G.; Huang, Y.; Bu, Q.; Lv, L.; Deng, P.; Zhou, J.; Wang, Y.; Yang, Y.; Liu, Q.; Cen, X.; et al. Zinc Oxide Nanoparticles Cause Nephrotoxicity and Kidney Metabolism Alterations in Rats. *J. Environ. Sci. Heal. Part A* **2012**, *47* (4), 577–588. <https://doi.org/10.1080/10934529.2012.650576>.

- (14) Ratnasekhar, C.; Sonane, M.; Satish, A.; Mudiam, M. K. R. Metabolomics Reveals the Perturbations in the Metabolome of *Caenorhabditis Elegans* Exposed to Titanium Dioxide Nanoparticles. *Nanotoxicology* **2015**, *9* (8), 994–1004.  
<https://doi.org/10.3109/17435390.2014.993345>.
- (15) Jayaram, D. T.; Kumar, A.; Kippner, L. E.; Ho, P.-Y.; Kemp, M. L.; Fan, Y.; Payne, C. K. TiO<sub>2</sub> Nanoparticles Generate Superoxide and Alter Gene Expression in Human Lung Cells. *RSC Adv.* **2019**, *9* (43), 25039–25047. <https://doi.org/10.1039/C9RA04037D>.
- (16) Tedesco, S.; Bayat, N.; Danielsson, G.; Buque, X.; Aspichueta, P.; Fresnedo, O.; Cristobal, S. Proteomic and Lipidomic Analysis of Primary Mouse Hepatocytes Exposed to Metal and Metal Oxide Nanoparticles. *J. Integr. OMICS* **2015**, *5* (1).  
<https://doi.org/10.5584/jiomics.v5i1.184>.
- (17) Hamers, R. J. Energy Storage Materials as Emerging Nano-Contaminants. *Chem. Res. Toxicol.* **2020**, *acs.chemrestox.0c00080*. <https://doi.org/10.1021/acs.chemrestox.0c00080>.
- (18) Brodd, R. J. *Batteries for Sustainability : Selected Entries from the Encyclopedia of Sustainability Science and Technology*; Springer, 2012.
- (19) Grey, C. P.; Ceder, G.; Kang, K.; Meng, Y. S.; Bre, J. Electrodes with High Power and High Capacity for Rechargeable Lithium Batteries. *Science (80-. )*. **2005**, *311* (December), 1–5. <https://doi.org/10.1126/science.1122152>.
- (20) Pollet, B. G.; Staffell, I.; Shang, J. L. Current Status of Hybrid, Battery and Fuel Cell Electric Vehicles: From Electrochemistry to Market Prospects. *Electrochim. Acta* **2012**, *84*, 235–249. <https://doi.org/10.1016/j.electacta.2012.03.172>.
- (21) Wang, Y.; Yu, Y.; Huang, K.; Chen, B.; Deng, W.; Yao, Y. Quantifying the Environmental Impact of a Li-Rich High-Capacity Cathode Material in Electric Vehicles

- via Life Cycle Assessment. *Environ. Sci. Pollut. Res.* **2017**, *24* (2), 1251–1260.  
<https://doi.org/10.1007/s11356-016-7849-9>.
- (22) Winslow, K. M.; Laux, S. J.; Townsend, T. G. A Review on the Growing Concern and Potential Management Strategies of Waste Lithium-Ion Batteries. *Resources, Conservation and Recycling*. Elsevier 2018, pp 263–277.  
<https://doi.org/10.1016/j.resconrec.2017.11.001>.
- (23) Hamers, R. J. Nanomaterials and Global Sustainability. *Acc. Chem. Res.* **2017**, *50* (3), 633–637. <https://doi.org/10.1021/acs.accounts.6b00634>.
- (24) Niemuth, N. J.; Curtis, B. J.; Hang, M. N.; Gallagher, M. J.; Fairbrother, D. H.; Hamers, R. J.; Klaper, R. D. Next-Generation Complex Metal Oxide Nanomaterials Negatively Impact Growth and Development in the Benthic Invertebrate *Chironomus Riparius* upon Settling. *Environ. Sci. Technol.* **2019**, *53* (7). <https://doi.org/10.1021/acs.est.8b06804>.
- (25) Bozich, J.; Hang, M.; Hamers, R.; Klaper, R. Core Chemistry Influences the Toxicity of Multicomponent Metal Oxide Nanomaterials, Lithium Nickel Manganese Cobalt Oxide, and Lithium Cobalt Oxide to *Daphnia Magna*. *Environ. Toxicol. Chem.* **2017**, *36* (9), 2493–2502. <https://doi.org/10.1002/etc.3791>.
- (26) Martins, J.; Oliva Teles, L.; Vasconcelos, V. Assays with *Daphnia Magna* and *Danio Rerio* as Alert Systems in Aquatic Toxicology. *Environ. Int.* **2007**, *33* (3), 414–425.  
<https://doi.org/10.1016/j.envint.2006.12.006>.
- (27) Niemuth, N. J.; Zhang, Y.; Mohaimani, A. A.; Schmoldt, A.; Laudadio, E. D.; Hamers, R. J.; Klaper, R. D. Protein Fe–S Centers as a Molecular Target of Toxicity of a Complex Transition Metal Oxide Nanomaterial with Downstream Impacts on Metabolism and Growth. *Environ. Sci. Technol.* **2020**, *54* (23), 15257–15266.

- <https://doi.org/10.1021/acs.est.0c04779>.
- (28) Laudadio, E. D.; Bennett, J. W.; Green, C. M.; Mason, S. E.; Hamers, R. J. Impact of Phosphate Adsorption on Complex Cobalt Oxide Nanoparticle Dispersibility in Aqueous Media. *Environ. Sci. Technol.* **2018**, *52* (17), 10186–10195.  
<https://doi.org/10.1021/acs.est.8b02324>.
- (29) Niemuth, N. J.; Curtis, B. J.; Hang, M. N.; Gallagher, M. J.; Fairbrother, D. H.; Hamers, R. J.; Klaper, R. D. Next-Generation Complex Metal Oxide Nanomaterials Negatively Impact Growth and Development in the Benthic Invertebrate *Chironomus Riparius* upon Settling. *Environ. Sci. Technol.* **2019**, *53* (7), 3860–3870.  
<https://doi.org/10.1021/acs.est.8b06804>.
- (30) Andrews, S.; Krueger, F.; Secongs-Pichon, A.; Biggins, F.; Wingett, S. FastQC: A Quality Control Tool for High Throughput Sequence Data. Babraham Bioinformatics, Babraham Institute, Cambridge, United Kingdom 2010.
- (31) Martin, M. Cutadapt Removes Adapter Sequences from High-Throughput Sequencing Reads. *EMBnet.journal* **2011**, *17* (1), 10. <https://doi.org/10.14806/ej.17.1.200>.
- (32) Bray, N. L.; Pimentel, H.; Melsted, P.; Pachter, L. Near-Optimal Probabilistic RNA-Seq Quantification. *Nat. Biotechnol.* **2016**, *34* (5), 525–527. <https://doi.org/10.1038/nbt.3519>.
- (33) Love, M. I.; Huber, W.; Anders, S. Moderated Estimation of Fold Change and Dispersion for RNA-Seq Data with DESeq2. *Genome Biol.* **2014**, *15* (12), 550.  
<https://doi.org/10.1186/s13059-014-0550-8>.
- (34) Camacho, C.; Coulouris, G.; Avagyan, V.; Ma, N.; Papadopoulos, J.; Bealer, K.; Madden, T. L. BLAST+: Architecture and Applications. *BMC Bioinformatics* **2009**, *10* (1), 421.  
<https://doi.org/10.1186/1471-2105-10-421>.

- (35) Yoo, A. B.; Jette, M. A.; Grondona, M. SLURM: Simple Linux Utility for Resource Management; 2003; pp 44–60. [https://doi.org/10.1007/10968987\\_3](https://doi.org/10.1007/10968987_3).
- (36) Tange, O. Gnu Parallel-the Command-Line Power Tool. *USENIX Mag.* **2011**, *36* (1), 42–47.
- (37) Huang, D. W.; Sherman, B. T.; Lempicki, R. A. Systematic and Integrative Analysis of Large Gene Lists Using DAVID Bioinformatics Resources. *Nat. Protoc.* **2009**, *4* (1), 44–57. <https://doi.org/10.1038/nprot.2008.211>.
- (38) Huang, D. W.; Sherman, B. T.; Lempicki, R. A. Bioinformatics Enrichment Tools: Paths toward the Comprehensive Functional Analysis of Large Gene Lists. *Nucleic Acids Res.* **2009**, *37* (1), 1–13. <https://doi.org/10.1093/nar/gkn923>.
- (39) Kanehisa, M.; Goto, S. KEGG: Kyoto Encyclopedia of Genes and Genomes. *Nucleic Acids Res.* **2000**, *28* (1), 27–30. <https://doi.org/10.1093/nar/28.1.27>.
- (40) Kanehisa, M.; Sato, Y.; Furumichi, M.; Morishima, K.; Tanabe, M. New Approach for Understanding Genome Variations in KEGG. *Nucleic Acids Res.* **2019**, *47* (D1), D590–D595. <https://doi.org/10.1093/nar/gky962>.
- (41) Kanehisa, M. Toward Understanding the Origin and Evolution of Cellular Organisms. *Protein Sci.* **2019**, *28* (11), 1947–1951. <https://doi.org/10.1002/pro.3715>.
- (42) Davidson, R. L.; Weber, R. J. M.; Liu, H.; Sharma-Oates, A.; Viant, M. R. Galaxy-M: A Galaxy Workflow for Processing and Analyzing Direct Infusion and Liquid Chromatography Mass Spectrometry-Based Metabolomics Data. *Gigascience* **2016**, *5* (1), 10. <https://doi.org/10.1186/s13742-016-0115-8>.
- (43) Xia, J.; Psychogios, N.; Young, N.; Wishart, D. S. MetaboAnalyst: A Web Server for Metabolomic Data Analysis and Interpretation. *Nucleic Acids Res.* **2009**, *37* (Web Server),

- W652–W660. <https://doi.org/10.1093/nar/gkp356>.
- (44) Efremov, R. G.; Baradaran, R.; Sazanov, L. A. The Architecture of Respiratory Complex I. *Nature* **2010**, *465* (7297), 441–445. <https://doi.org/10.1038/nature09066>.
- (45) Mensch, A. C.; Mitchell, H. D.; Markillie, L. M.; Laudadio, E. D.; Hedlund Orbeck, J. K.; Dohnalkova, A.; Schwartz, M. P.; Hamers, R. J.; Orr, G. Subtoxic Dose of Lithium Cobalt Oxide Nanosheets Impacts Critical Molecular Pathways in Trout Gill Epithelial Cells. *Environ. Sci. Nano* **2020**, *7* (11), 3419–3430. <https://doi.org/10.1039/D0EN00844C>.
- (46) Futai, M.; Sun-Wada, G.-H.; Wada, Y.; Matsumoto, N.; Nakanishi-Matsui, M. Vacuolar-Type ATPase: A Proton Pump to Lysosomal Trafficking. *Proc. Japan Acad. Ser. B* **2019**, *95* (6), 261–277. <https://doi.org/10.2183/pjab.95.018>.
- (47) Bareth, B.; Dennerlein, S.; Mick, D. U.; Nikolov, M.; Urlaub, H.; Rehling, P. The Heme a Synthase Cox15 Associates with Cytochrome c Oxidase Assembly Intermediates during Cox1 Maturation. *Mol. Cell. Biol.* **2013**, *33* (20), 4128–4137. <https://doi.org/10.1128/MCB.00747-13>.
- (48) Banci, L.; Bertini, I.; Ciofi-Baffoni, S.; Hadjiloi, T.; Martinelli, M.; Palumaa, P. Mitochondrial Copper(I) Transfer from Cox17 to Sco1 Is Coupled to Electron Transfer. *Proc. Natl. Acad. Sci.* **2008**, *105* (19), 6803–6808. <https://doi.org/10.1073/pnas.0800019105>.
- (49) Wang, K.; Wan, J.; Xiang, Y.; Zhu, J.; Leng, Q.; Wang, M.; Xu, L.; Yang, Y. Recent Advances and Historical Developments of High Voltage Lithium Cobalt Oxide Materials for Rechargeable Li-Ion Batteries. *J. Power Sources* **2020**, *460*, 228062. <https://doi.org/10.1016/j.jpowsour.2020.228062>.
- (50) Hitkari, G.; Sandhya, S.; Gajanan, P.; Shrivash, M. K.; Kumar, D. Synthesis of Chromium

Doped Cobalt Oxide (Cr:Co<sub>3</sub>O<sub>4</sub>) Nanoparticles by Co-Precipitation Method and Enhanced Photocatalytic Properties in the Visible Region. *J. Mater. Sci. Eng.* **2018**, *07* (01). <https://doi.org/10.4172/2169-0022.1000419>.

- (51) Melby, E. S.; Cui, Y.; Borgatta, J.; Mensch, A. C.; Hang, M. N.; Chrisler, W. B.; Dohnalkova, A.; Van Gilder, J. M.; Alvarez, C. M.; Smith, J. N.; et al. Impact of Lithiated Cobalt Oxide and Phosphate Nanoparticles on Rainbow Trout Gill Epithelial Cells. *Nanotoxicology* **2018**, *12* (10), 1166–1181. <https://doi.org/10.1080/17435390.2018.1508785>.

## Tables

**Table 1.** Selected DAVID enrichment terms for differentially expressed genes between LCO 1 mg/L and control.

Category	Term	Gene count	Benjamini -adjusted p-value
<u>Energy metabolism</u>			
GO: Cellular component	Mitochondrial respiratory chain complex I	17	0.0002
UniProt keyword	Ubiquinone	16	0.0004
UniProt keyword	Oxidoreductase	80	0.0006
GO: Cellular component	Plasma membrane proton-transporting V-type ATPase complex	13	0.002
GO: Biological process	Cellular response to starvation	25	0.002
GO: Cellular component	Mitochondrion	70	0.004
UniProt keyword	ATP-binding	70	0.006
KEGG pathway	Oxidative phosphorylation	53	0.01
GO: Molecular function	NADH dehydrogenase activity	12	0.05
GO: Molecular function	NADH dehydrogenase (ubiquinone) activity	13	0.05
GO: Biological process	ATP hydrolysis coupled proton transport	18	0.06
GO: Biological process	Mitochondrial electron transport, NADH to ubiquinone	12	0.06
UniProt keyword	One-carbon metabolism	5	0.07
<u>Proteins and amino acids</u>			
UniProt keyword	Ribosome biogenesis	21	0.0009
UniProt keyword	Protein biosynthesis	40	0.003
UniProt keyword	Aminoacyl-tRNA synthetase	20	0.003
KEGG pathway	Ribosome biogenesis in eukaryotes	38	0.01
KEGG pathway	Protein export	17	0.01
UniProt keyword	Protease	86	0.02
KEGG pathway	Aminoacyl-tRNA biosynthesis	25	0.08
GO: Biological process	rRNA processing	13	0.08

**Table 2.** MetaboAnalyst enriched KEGG pathways for differential metabolites between LCO 1 mg/L and control.

KEGG pathway	Gamma-adjusted p-value	KEGG ID	Compound names
Histidine metabolism	0.02	C00386, C00135, C01262	Carnosine; L-Histidine; beta-Alanyl-N(pi)-methyl-L-histidine
beta-Alanine metabolism	0.03	C01013, C00429, C00386, C00135	3-Hydroxypropanoate; 5,6-Dihydrouracil; Carnosine; L-Histidine
Starch and sucrose metabolism	0.03	C00089, C01083, C00208, C00721	Sucrose; alpha,alpha-Trehalose; Maltose; Dextrin
Valine leucine and isoleucine biosynthesis	0.03	C00123, C00407, C00183	L-Leucine; L-Isoleucine; L-Valine
Glycerophospholipid metabolism	0.04	C00588, C00114, C01996, C01233	Choline phosphate; Choline; Acetylcholine; sn-Glycero-3-phosphoethanolamine
Insect hormone biosynthesis	0.04	C00448, C03461	trans,trans-Farnesyl diphosphate; 2-trans,6-trans-Farnesal
Galactose metabolism	0.04	C05404, C00089, C00492, C05402, C05400, C01235, C00243	D-Gal alpha; Sucrose; Raffinose; Melibiose; Epimelibiose; alpha-D-Galactosyl-(1->3)-1D-myo-inositol; Lactose
Aminoacyl-tRNA biosynthesis	0.04	C00135, C00183, C00407, C00123, C00148, C01110	L-Histidine; L-Valine; L-Isoleucine; L-Leucine; L-Proline; 5-Amino-2-oxopentanoic acid
D-Arginine and D-ornithine metabolism	0.05	C01110, C03771	5-Amino-2-oxopentanoic acid; 5-Guanidino-2-oxopentanoate
Tryptophan metabolism	0.05	C00643, C05648, C05639, C01252, C05637, C05635, C00448	5-Hydroxy-L-tryptophan; 5-Hydroxy-N-formylkynurenine; 4,6-Dihydroxyquinoline; 4-(2-Aminophenyl)-2,4-dioxobutanoate; 4,8-Dihydroxyquinoline; 5-Hydroxyindoleacetate; trans,trans-Farnesyl diphosphate
Terpenoid backbone biosynthesis	0.06	C00448, C03461	trans,trans-Farnesyl diphosphate; 2-trans,6-trans-Farnesal
Valine leucine and isoleucine degradation	0.07	C00183, C00407, C00123	L-Valine; L-Isoleucine; L-Leucine

Glycine serine and threonine metabolism	0.08	C00114, C00719, C00430	Choline; Betaine; 5-Aminolevulinate
Lysine degradation	0.08	C01181, C00449	4-Trimethylammoniobutanoate; N6-(L-1,3-Dicarboxypropyl)-L-lysine
Pantothenate and CoA biosynthesis	0.09	C00429, C00183	5,6-Dihydrouracil; L-Valine
Arginine and proline metabolism	0.09	C00763, C00148, C03440, C01165, C05945, C00884, C01157	D-Proline; L-Proline; cis-4-Hydroxy-D-proline; L-Glutamate 5-semialdehyde; L-Arginine phosphate; Homocarnosine; Hydroxyproline

**Table 3.** Differential sugars in Starch, Sucrose, and Galactose metabolism identified by Metaboanalyst between LCO 1 mg/L and control.

m/z	Matched Form	KEGG Compound	Compound Name	Fold change	FDR-adjusted p-value
342.112020020871	M(C13)-H[-]	C00089, C00185, C00208, C00243, C00252, C01083, C01235, C05400, C05402	Sucrose, Cellobiose, Maltose, Lactose, Isomaltose, Trehalose, Galactinol, Epimelibiose, Melibiose	1.5	0.08
377.085576703436	M+Cl[-]	C00089, C00185, C00208, C00243, C00252, C01083, C01235, C05400, C05402	Sucrose, Cellobiose, Maltose, Lactose, Isomaltose , Trehalose, Galactinol, Epimelibiose, Melibiose	2.3	0.024
379.082582371242	M+Cl37[-]	C00089, C00185, C00208, C00243, C00252, C01083, C01235, C05400, C05402	Sucrose, Cellobiose, Maltose, Lactose, Isomaltose, Trehalose, Galctinol, Epimelibiose, Melibiose	2.2	0.03
503.161996000661	M-H[-]	C00492, C00721, C05404	Raffinose, Dextrin, Manninotriose	1.03	0.008
527.1595751	M+Na[1+]	C00492, C00721, C05404	Raffinose, Dextrin, Manninotriose	2.2	0.01
539.13874187578	M+Cl[-]	C00492, C00721, C05404	Raffinose, Dextrin, Manninotriose	1.03	0.009
563.18264508	M+CH3COO[-]	C00492, C00721, C05404	Raffinose, Dextrin, Manninotriose	1.03	0.004

## Figures

**Figure 1. Diagram of oxidative phosphorylation showing genes differentially expressed between LCO 1 mg/L and control.**

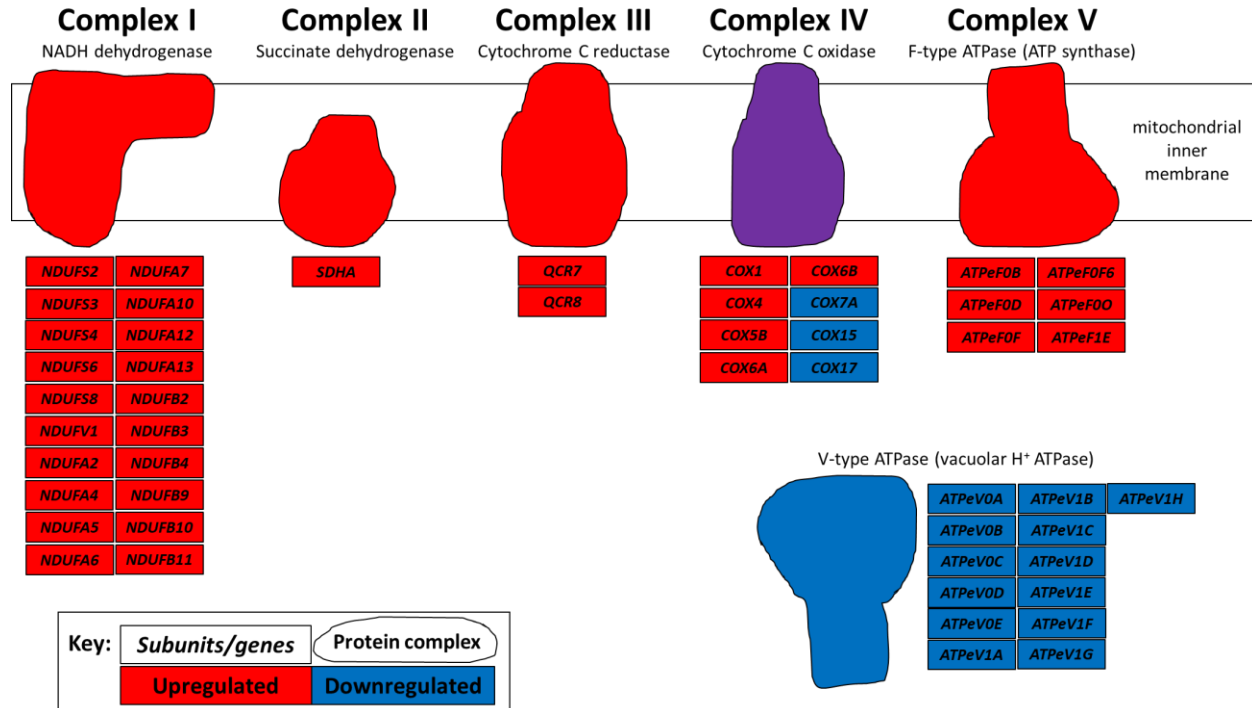


**Figure 1. Diagram of oxidative phosphorylation showing genes differentially expressed between LCO 1 mg/L and control.** Diagram of oxidative phosphorylation, based on KEGG map 00190, showing genes differentially expressed (FDR-adjusted  $p < 0.1$ ) between LCO 1 mg/L exposed and control daphnids at 48 hrs. Upregulated genes include: Complex I genes NADH dehydrogenase Fe-S proteins (*NDUFS*) 2, 3, 4, 6, and 8, NADH dehydrogenase flavoprotein 1 (*NDUFVI*), NADH dehydrogenase 1 alpha subcomplex (*NDUFA*) subunits 2, 4, 5, 6, 7, 10, 12, and 13, and NADH dehydrogenase 1 beta (*NDUFB*) subunits 2, 3, 4, 9, 10, and 11; Complex II gene succinate dehydrogenase flavoprotein subunit (*SDHA*); Complex III genes ubiquinol-cytochrome c reductase (*QCR*) subunits 7 and 8; Complex IV genes cytochrome c oxidase (*COX*) subunits 1, 4, 5B, 6A, and 6B; and Complex V genes F-type H<sup>+</sup>-transporting

ATPase (*ATPeF0*) subunits *B*, *D*, *F*, *F6*, and *O*, and F-type H<sup>+</sup>-transporting ATPase subunit epsilon (*ATPeF1E*). This coordinated upregulation supports compensation for energy starvation. Downregulated genes include: Complex IV genes heme a synthase (*COX15*), involved synthesis of heme a, cytochrome c oxidase assembly protein subunit 17 (*COX17*), involved in transfer of copper, and cytochrome c oxidase subunit 7a (*COX7A*). Downregulation of *COX15* and *COX17* support disruption of heme synthesis and metal homeostasis by LCO exposure. Also downregulated are subunits of the V-type H<sup>+</sup>-transporting ATPase (*ATPeV*) localized to the vacuole, which uses ATP to pump protons into the vacuole: *0A*, *0B*, *0C*, *0D*, *0E*, *1A*, *1B*, *1C*, *1D*, *1E*, *1F*, *1G*, and *1H*. Downregulation of this ATP-using complex suggests downregulation of ATP-using processes for energy conservation.

**Figure 2. Pathway for valine, leucine, and isoleucine degradation showing differential compounds and genes between LCO 1 mg/L and control.**

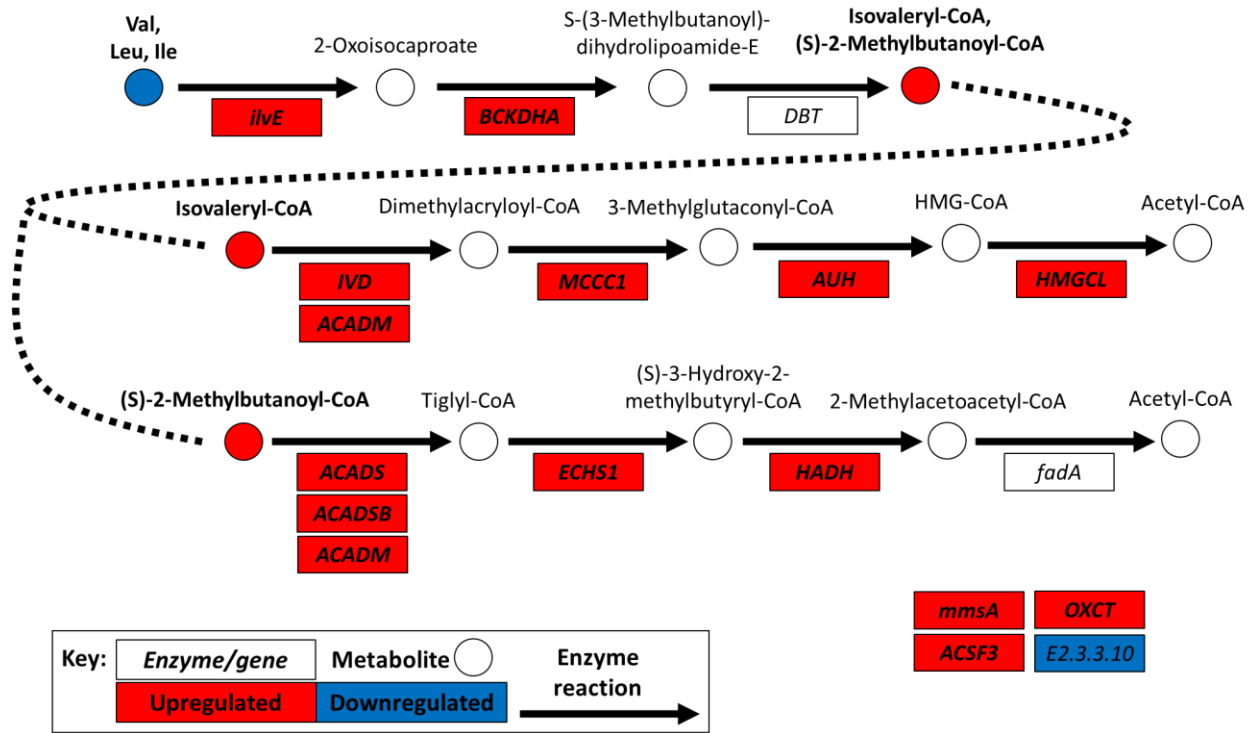


**Figure 2. Pathway for Valine, leucine, and isoleucine degradation showing differential compounds and genes between LCO 1 mg/L and control.** Diagram of valine, leucine, and isoleucine degradation based on KEGG map 00280, showing metabolites and genes significantly different (FDR-adjusted  $p < 0.1$ ) between LCO 1 mg/L exposed and control daphnids at 48 hrs. Amino acids valine (Val), leucine (Leu), and isoleucine (Ile) are significantly lower in 1 mg/L exposed daphnids than in controls, while the intermediate metabolites of Leu and Ile breakdown, isovaleryl-CoA and (S)-2-Methylbutanoyl-CoA are both significantly increased, pointing to breakdown on these amino acids. Upregulated genes involved in Val, Leu, and Ile breakdown are, in order of appearance in the highlighted pathway: branched-chain amino acid aminotransferase (*ilvE*), 2-oxoisovalerate dehydrogenase E1 component alpha subunit (*BCKDHA*), isovaleryl-CoA dehydrogenase (*IVD*), acyl-CoA dehydrogenase (*ACADM*), 3-

methylcrotonyl-CoA carboxylase alpha subunit (*MCCCI*), methylglutaconyl-CoA hydratase (*AUH*), hydroxymethylglutaryl-CoA lyase (*HMGCL*), butyryl-CoA dehydrogenase (*ACADS*), short-chain 2-methylacyl-CoA dehydrogenase (*ACADSB*), enoyl-CoA hydratase (*ECHS1*), and 3-hydroxyacyl-CoA dehydrogenase (*HADH*). Not significantly changed genes in the highlighted pathway are: dihydrolipoyl transacylase (*DBT*) and acetyl-CoA acyltransferase (*fadA*). Ancillary genes included in KEGG map 00280 that were upregulated are: methylmalonate-semialdehyde dehydrogenase (*mmsA*), 3-oxoacid CoA-transferase (*OXCT*), and malonyl-CoA/methylmalonyl-CoA synthetase (*ACSF3*). Ancillary gene hydroxymethylglutaryl-CoA synthase (*E2.3.3.10*) was downregulated. Taken together, metabolite and gene expression changes support amino acid breakdown as a means to compensate for energy starvation, by increasing production of Acetyl-CoA for the citric acid cycle.

## **SUPPORTING INFORMATION**

### **Supporting information for:**

**Energy starvation in *Daphnia magna* from exposure to a lithium cobalt oxide nanomaterial**

**Authors:** Nicholas Niemuth, Becky Curtis, Liz Laudadio, Jelena Sostare, Evan Bennet, Nicklaus Neureuther, Aurash Mohaimani, Angela Schmoltdt, Eric Ostovich, Mark Viant, Robert Hamers, Rebecca Klaper\*

**Pages:** 12

**Tables:** 2

**Figures:** 4

## Supporting Tables

**Supplementary Table S1.** LCO zeta potential in MHRW exposure media.

ENM (conc)	$\zeta$ -potential (mV)*	Electrophoretic mobility ( $\mu\text{m}\cdot\text{cm}\cdot\text{Vs}^{-1}$ )
LCO (1 mg·L <sup>-1</sup> )	-12.6 ± 0.6	-0.99 ± 0.05

\* Calculated using Smoluchowski method.

Reprinted (adapted) with permission from (Niemuth, N. J.; Zhang, Y.; Mohaimani, A. A.; Schmoldt, A.; Laudadio, E. D.; Hamers, R. J.; Klaper, R. D. Protein Fe–S Centers as a Molecular Target of Toxicity of a Complex Transition Metal Oxide Nanomaterial with Downstream Impacts on Metabolism and Growth. *Environ. Sci. Technol.* **2020**, *54* (23), 15257–15266). Copyright (2020) American Chemical Society.

**Supplementary Table S2. KEGG genes and compounds**

KEGG ID	Gene or compound symbol	Gene or compound name	Fold change	FDR-adj p-value
<u>Oxidative phosphorylation</u>				
K00234	SDHA	succinate dehydrogenase (ubiquinone) flavoprotein subunit	1.43	0.001
K00417	QCR7	ubiquinol-cytochrome c reductase subunit 7	1.29	2E-05
K00418	QCR8	ubiquinol-cytochrome c reductase subunit 8	1.28	4.2E-05
K02127	ATPeF0B	F-type H <sup>+</sup> -transporting ATPase subunit b	1.20	0.009
K02130	ATPeF0F	F-type H <sup>+</sup> -transporting ATPase subunit f	1.14	0.09
K02131	ATPeF0F6	F-type H <sup>+</sup> -transporting ATPase subunit 6	1.17	0.03
K02135	ATPeF1E	F-type H <sup>+</sup> -transporting ATPase subunit epsilon	1.22	0.009
K02137	ATPeF0O	F-type H <sup>+</sup> -transporting ATPase subunit O	1.16	0.04
K02138	ATPeF0D	F-type H <sup>+</sup> -transporting ATPase subunit d	1.20	0.004
K02144	ATPeV1H	V-type H <sup>+</sup> -transporting ATPase subunit H	-1.39	0.001
K02145	ATPeV1A	V-type H <sup>+</sup> -transporting ATPase subunit A	-1.67	3.7E-06
K02146	ATPeV0D	V-type H <sup>+</sup> -transporting ATPase subunit d	-1.47	3.5E-05
K02147	ATPeV1B	V-type H <sup>+</sup> -transporting ATPase subunit B	-1.56	1.6E-05
K02148	ATPeV1C	V-type H <sup>+</sup> -transporting ATPase subunit C	-1.27	0.02
K02149	ATPeV1D	V-type H <sup>+</sup> -transporting ATPase subunit D	-1.69	0.0004
K02150	ATPeV1E	V-type H <sup>+</sup> -transporting ATPase subunit E	-1.55	9.7E-05
K02151	ATPeV1F	V-type H <sup>+</sup> -transporting ATPase subunit F	-1.22	0.07
K02152	ATPeV1G	V-type H <sup>+</sup> -transporting ATPase subunit G	-1.54	8.1E-05
K02153	ATPeV0E	V-type H <sup>+</sup> -transporting ATPase subunit e	-1.47	2.1E-06
K02154	ATPeV0A	V-type H <sup>+</sup> -transporting ATPase subunit a	-1.32	0.001
K02155	ATPeV0C	V-type H <sup>+</sup> -transporting ATPase 16kDa proteolipid subunit	-1.78	5.2E-10
K02256	COX1	cytochrome c oxidase subunit 1	1.79	0.001
K02259	COX15	heme a synthase	-1.16	0.09
K02260	COX17	cytochrome c oxidase assembly protein subunit 17	-1.27	0.003
K02263	COX4	cytochrome c oxidase subunit 4	1.19	0.05
K02265	COX5B	cytochrome c oxidase subunit 5b	1.18	0.03
K02266	COX6A	cytochrome c oxidase subunit 6a	1.14	0.097
K02267	COX6B	cytochrome c oxidase subunit 6b	1.25	0.001
K02270	COX7A	cytochrome c oxidase subunit 7a	-1.40	0.05
K03661	ATPeV0B	V-type H <sup>+</sup> -transporting ATPase 21kDa proteolipid subunit	-1.34	0.0002
K03935	NDUFS2	NADH dehydrogenase (ubiquinone) Fe-S protein 2	1.32	0.0002
K03936	NDUFS3	NADH dehydrogenase (ubiquinone) Fe-S protein 3	1.20	0.02
K03937	NDUFS4	NADH dehydrogenase (ubiquinone) Fe-S protein 4	1.37	6.1E-06
K03939	NDUFS6	NADH dehydrogenase (ubiquinone) Fe-S protein 6	1.22	0.009
K03941	NDUFS8	NADH dehydrogenase (ubiquinone) Fe-S protein 8	1.22	0.02
K03942	NDUFV1	NADH dehydrogenase (ubiquinone) flavoprotein 1	1.32	1.8E-05

K03946	NDUFA2	NADH dehydrogenase (ubiquinone) 1 alpha subcomplex subunit 2	1.11	0.04
K03948	NDUFA4	NADH dehydrogenase (ubiquinone) 1 alpha subcomplex subunit 4	1.16	0.09
K03949	NDUFA5	NADH dehydrogenase (ubiquinone) 1 alpha subcomplex subunit 5	1.30	1.5E-05
K03950	NDUFA6	NADH dehydrogenase (ubiquinone) 1 alpha subcomplex subunit 6	1.18	0.07
K03951	NDUFA7	NADH dehydrogenase (ubiquinone) 1 alpha subcomplex subunit 7	1.23	0.002
K03954	NDUFA10	NADH dehydrogenase (ubiquinone) 1 alpha subcomplex subunit 10	1.26	0.003
K03958	NDUFB2	NADH dehydrogenase (ubiquinone) 1 beta subcomplex subunit 2	1.21	0.01
K03959	NDUFB3	NADH dehydrogenase (ubiquinone) 1 beta subcomplex subunit 3	1.30	6E-09
K03960	NDUFB4	NADH dehydrogenase (ubiquinone) 1 beta subcomplex subunit 4	1.18	0.009
K03965	NDUFB9	NADH dehydrogenase (ubiquinone) 1 beta subcomplex subunit 9	1.23	0.0001
K03966	NDUFB10	NADH dehydrogenase (ubiquinone) 1 beta subcomplex subunit 10	1.15	0.02
K11351	NDUFB11	NADH dehydrogenase (ubiquinone) 1 beta subcomplex subunit 11	1.28	7.4E-05
K11352	NDUFA12	NADH dehydrogenase (ubiquinone) 1 alpha subcomplex subunit 12	1.30	0.0002
K11353	NDUFA13	NADH dehydrogenase (ubiquinone) 1 alpha subcomplex subunit 13	1.20	0.002
K11726	NURF38	nucleosome-remodeling factor 38 kDa subunit	-1.55	2.7E-05

Valine, leucine and isoleucine degradation

C00123	Leu	L-Leucine	-2.22	0.009
C00183	Val	L-Valine	-2.94	0.002
C00407	Ile	L-Isoleucine	-2.22	0.009
C02939	Isovaleryl-CoA	3-Methylbutanoyl-CoA	1.87	0.05
C15980		(S)-2-Methylbutanoyl-CoA	1.87	0.05
K00140	mmsA	malonate-semialdehyde dehydrogenase (acetylating) / methylmalonate-semialdehyde dehydrogenase	1.26	0.09
K00166	BCKDHA	2-oxoisovalerate dehydrogenase E1 component alpha subunit	1.27	0.006
K00248	ACADS	butyryl-CoA dehydrogenase	1.35	0.0003
K00249	ACADM	acyl-CoA dehydrogenase	1.32	0.05
K00253	IVD	isovaleryl-CoA dehydrogenase	1.47	4.9E-05
K00826	ilvE	branched-chain amino acid aminotransferase	1.43	7.6E-06

K01027	OXCT	3-oxoacid CoA-transferase	1.38	3.3E-05
K01640	HMGCL	hydroxymethylglutaryl-CoA lyase	1.16	0.04
K01641	E2.3.3.10	hydroxymethylglutaryl-CoA synthase	-1.26	0.096
K01968	MCCC1	3-methylcrotonyl-CoA carboxylase alpha subunit	1.33	0.003
K05607	AUH	methylglutaconyl-CoA hydratase	1.38	7.4E-05
K07511	ECHS1	enoyl-CoA hydratase	1.24	0.03
K08683	HADH	3-hydroxyacyl-CoA dehydrogenase / 3-hydroxy-2-methylbutyryl-CoA dehydrogenase	1.14	0.002
K09478	ACADSB	short-chain 2-methylacyl-CoA dehydrogenase	1.37	0.004
K18660	ACSF3	malonyl-CoA/methylmalonyl-CoA synthetase	1.25	0.04

#### Ribosome biogenesis in eukaryotes

K03264	EIF6	translation initiation factor 6	-1.26	0.006
K03537	POP5	ribonuclease P/MRP protein subunit POP5	-1.42	0.02
K07178	RIOK1	RIO kinase 1	-1.29	0.01
K07179	RIOK2	RIO kinase 2	-1.31	0.05
K07562	NMD3	nonsense-mediated mRNA decay protein 3	-1.25	0.05
K07936	RAN	GTP-binding nuclear protein Ran	-1.49	0.0009
K11108	RCL1	RNA 3'-terminal phosphate cyclase-like protein	-1.39	0.08
K11128	GAR1	H/ACA ribonucleoprotein complex subunit 1	-1.70	0.004
K11129	NHP2	H/ACA ribonucleoprotein complex subunit 2	-1.62	0.02
K11131	DKC1	H/ACA ribonucleoprotein complex subunit 4	-1.55	0.03
K11883	NOB1	RNA-binding protein NOB1	-1.41	0.03
K12619	XRN2	5'-3' exoribonuclease 2	1.20	0.02
K12845	SNU13	U4/U6 small nuclear ribonucleoprotein SNU13	-1.72	0.01
K14290	XPO1	exportin-1	-1.34	0.005
K14521	NAT10	N-acetyltransferase 10	-1.47	0.02
K14538	NUG1	nuclear GTP-binding protein	-1.34	0.07
K14539	LSG1	large subunit GTPase 1	-1.24	0.08
K14544	UTP22	U3 small nucleolar RNA-associated protein 22	-1.55	0.002
K14545	RRP7	ribosomal RNA-processing protein 7	-1.45	0.002
K14546	UTP5	U3 small nucleolar RNA-associated protein 5	-1.42	0.04
K14548	UTP4	U3 small nucleolar RNA-associated protein 4	-1.49	0.03
K14549	UTP15	U3 small nucleolar RNA-associated protein 15	-1.33	0.07
K14553	UTP18	U3 small nucleolar RNA-associated protein 18	-1.43	0.05
K14557	UTP6	U3 small nucleolar RNA-associated protein 6	-1.34	0.08
K14559	MPP10	U3 small nucleolar RNA-associated protein MPP10	-1.24	0.08
K14560	IMP3	U3 small nucleolar ribonucleoprotein protein IMP3	-1.41	0.06
K14563	NOP1	rRNA 2'-O-methyltransferase fibrillar	-1.59	0.01
K14564	NOP56	nucleolar protein 56	-1.36	0.08
K14565	NOP58	nucleolar protein 58	-1.45	0.06
K14566	UTP24	U3 small nucleolar RNA-associated protein 24	-1.52	0.02

K14567	UTP14	U3 small nucleolar RNA-associated protein 14	-1.68	0.05
K14568	EMG1	rRNA small subunit pseudouridine methyltransferase Nep1	-1.41	0.06
K14569	BMS1	ribosome biogenesis protein BMS1	-1.39	0.03
K14570	REX1	RNA exonuclease 1	-1.67	0.01
K14571	RIX7	ribosome biogenesis ATPase	-1.19	0.02
K14573	NOP4	nucleolar protein 4	-1.40	0.05
K14575	AFG2	AAA family ATPase	-1.41	0.03

#### Ribosome

K02868	RP-L11e	large subunit ribosomal protein L11e	-1.23	0.04
K02870	RP-L12e	large subunit ribosomal protein L12e	-1.30	0.01
K02876	RP-L15	large subunit ribosomal protein L15	-1.23	0.02
K02878	RP-L16	large subunit ribosomal protein L16	-1.19	0.05
K02891	RP-L22e	large subunit ribosomal protein L22e	-1.24	0.05
K02896	RP-L24e	large subunit ribosomal protein L24e	-1.17	0.08
K02902	RP-L28	large subunit ribosomal protein L28	-1.17	0.03
K02905	RP-L29e	large subunit ribosomal protein L29e	-1.22	0.01
K02908	RP-L30e	large subunit ribosomal protein L30e	-1.23	0.02
K02911	RP-L32	large subunit ribosomal protein L32	-1.26	0.03
K02914	RP-L34	large subunit ribosomal protein L34	-1.64	3.9E-05
K02916	RP-L35	large subunit ribosomal protein L35	-1.22	0.03
K02922	RP-L37e	large subunit ribosomal protein L37e	-1.39	0.003
K02923	RP-L38e	large subunit ribosomal protein L38e	-1.17	0.08
K02924	RP-L39e	large subunit ribosomal protein L39e	-1.30	0.003
K02925	RP-L3e	large subunit ribosomal protein L3e	-1.28	0.02
K02935	RP-L7	large subunit ribosomal protein L7/L12	-1.25	0.04
K02941	RP-LP0	large subunit ribosomal protein LP0	-1.31	0.009
K02948	RP-S11	small subunit ribosomal protein S11	1.17	0.01
K02949	RP-S11e	small subunit ribosomal protein S11e	-1.16	0.006
K02951	RP-S12e	small subunit ribosomal protein S12e	-1.26	0.04
K02957	RP-S15Ae	small subunit ribosomal protein S15Ae	-1.21	0.03
K02958	RP-S15e	small subunit ribosomal protein S15e	-1.18	0.09
K02963	RP-S18	small subunit ribosomal protein S18	-1.31	0.01
K02964	RP-S18e	small subunit ribosomal protein S18e	-1.22	0.02
K02969	RP-S20e	small subunit ribosomal protein S20e	-1.29	0.04
K02980	RP-S29e	small subunit ribosomal protein S29e	-1.22	0.007
K02981	RP-S2e	small subunit ribosomal protein S2e	-1.20	0.09
K02996	RP-S9	small subunit ribosomal protein S9	-1.20	0.03
K02997	RP-S9e	small subunit ribosomal protein S9e	-1.29	0.03
K02998	RP-SAe	small subunit ribosomal protein SAe	-1.22	0.06

### Protein export

K03104	SRP14	signal recognition particle subunit SRP14	-1.15	0.095
K03105	SRP19	signal recognition particle subunit SRP19	-1.13	0.05
K03106	SRP54	signal recognition particle subunit SRP54	-1.20	0.05
K03107	SRP68	signal recognition particle subunit SRP68	-1.19	0.02
K03109	SRP9	signal recognition particle subunit SRP9	-1.46	0.0002
K07342	SEC61G	protein transport protein SEC61 subunit gamma and related proteins	-1.47	6.3E-07
K09481	SEC61B	protein transport protein SEC61 subunit beta	-1.79	1.8E-07
K09490	HSPA5	endoplasmic reticulum chaperone BiP	-1.68	0.03
K09540	SEC63	translocation protein SEC63	-1.43	9.9E-07
K09648	IMP2	mitochondrial inner membrane protease subunit 2	1.18	0.01
K10956	SEC61A	protein transport protein SEC61 subunit alpha	-2.17	2.7E-08
K12272	SRPRB	signal recognition particle receptor subunit beta	-1.49	1.3E-09
K12946	SPCS1	signal peptidase complex subunit 1	-1.36	0.0005
K12947	SPCS2	signal peptidase complex subunit 2	-1.57	4.9E-05
K12948	SPCS3	signal peptidase complex subunit 3	-1.75	1.7E-05
K13280	SEC11	signal peptidase I	-1.43	0.002
K13431	SRPR	signal recognition particle receptor subunit alpha	-1.39	0.0004

### Aminoacyl-tRNA biosynthesis

C00062	Arg	L-Arginine	-1.43	0.04
C00123	Leu	L-Leucine	-2.22	0.009
C00135	His	L-Histidine	-1.57	0.007
C00183	Val	L-Valine	-2.94	0.002
C00407	Ile	L-Isoleucine	-2.22	0.009
K01866	YARS	tyrosyl-tRNA synthetase	-1.18	0.03
K01867	WARS	tryptophanyl-tRNA synthetase	-1.56	0.001
K01868	TARS	threonyl-tRNA synthetase	-1.58	1.8E-10
K01869	LARS	leucyl-tRNA synthetase	-1.46	0.002
K01870	IARS	isoleucyl-tRNA synthetase	-1.53	9.5E-05
K01872	AARS	alanyl-tRNA synthetase	-1.59	8.4E-06
K01873	VARS	valyl-tRNA synthetase	-1.83	0.02
K01874	MARS	methionyl-tRNA synthetase	-1.42	0.001
K01875	SARS	seryl-tRNA synthetase	-1.49	0.004
K01880	GARS	glycyl-tRNA synthetase	-1.64	1.1E-06
K01883	CARS	cysteinyl-tRNA synthetase	-1.31	0.0002
K01886	QARS	glutamyl-tRNA synthetase	-1.41	0.002
K01887	RARS	arginyl-tRNA synthetase	-1.35	0.007
K01889	FARSA	phenylalanyl-tRNA synthetase alpha chain	-1.47	2.1E-06
K01890	FARSB	phenylalanyl-tRNA synthetase beta chain	-1.30	0.002
K01892	HARS	histidyl-tRNA synthetase	-1.65	0.0006

K01893	NARS	asparaginyl-tRNA synthetase	-1.83	0.0004
K02435	gatC	aspartyl-tRNA(Asn)/glutamyl-tRNA(Gln) amidotransferase subunit C	-1.37	0.04
K04567	KARS	lysyl-tRNA synthetase, class II	-1.71	5.6E-06
K10837	PSTK	O-phosphoserine-tRNA(Sec) kinase	-1.33	0.03
K14163	EPRS	bifunctional glutamyl/prolyl-tRNA synthetase	-1.48	8.4E-07

#### Tryptophan metabolism

C00328		L-Kynurenine	1.27	0.06
C00643		5-Hydroxy-L-tryptophan	2.16	3.3E-06
C03227		3-Hydroxy-L-kynurenine	2.97	0.007
C05647		Formyl-5-hydroxykynurenamine	1.27	0.06
C05648		5-Hydroxy-N-formylkynurenine	3.29	2.1E-06
C05651		5-Hydroxykynurenine	2.97	0.007
C06213		N-Methyltryptamine	19.32	3.6E-05
K00252	GCDH	glutaryl-CoA dehydrogenase	1.45	5.7E-08
K00502	TPH1_2	tryptophan 5-monooxygenase	2.94	9.4E-05
K00658	DLST	2-oxoglutarate dehydrogenase E2 component (dihydrolipoamide succinyltransferase)	1.26	0.05
K00669	AANAT	arylalkylamine N-acetyltransferase	1.21	0.05
K01593	DDC	aromatic-L-amino-acid/L-tryptophan decarboxylase	2.67	1.7E-09
K07511	ECHS1	enoyl-CoA hydratase	1.24	0.03

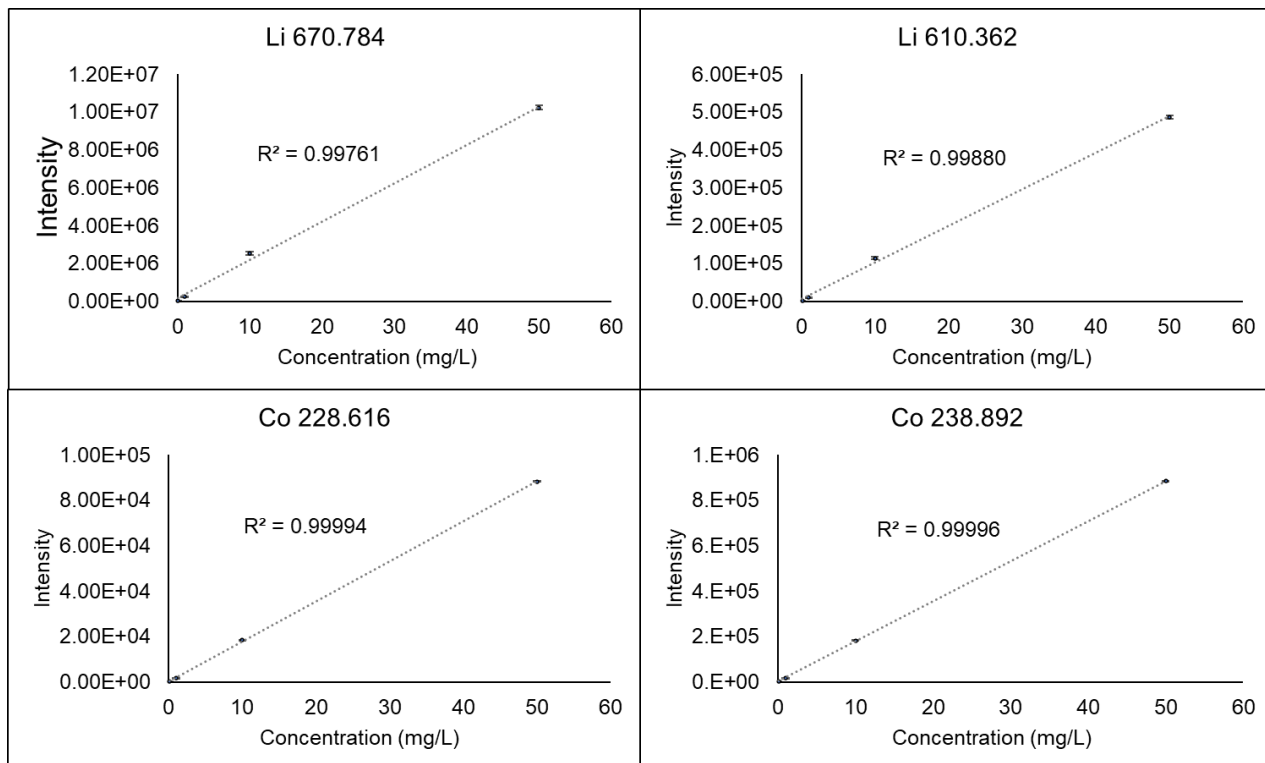
#### Starch and sucrose metabolism

C00089		Sucrose	1.51	0.08
C00185		Cellobiose	1.51	0.08
C00208		Maltose	1.51	0.08
C00252		Isomaltose	1.51	0.08
C00721		Dextrin	1.03	0.008
C01083		Trehalose	1.51	0.08
K00700	GBE1	1,4-alpha-glucan branching enzyme	-1.38	0.03
K01084	G6PC	glucose-6-phosphatase	-2.40	0.0005
K01176	AMY	alpha-amylase	3.70	7.4E-07
K01187	malZ	alpha-glucosidase	1.59	0.009
K01194	TREH	alpha,alpha-trehalase	1.95	0.001
K01810	GPI	glucose-6-phosphate isomerase	-1.54	0.003
K01835	pgm	phosphoglucomutase	-1.28	0.07
K16055	TPS	trehalose 6-phosphate synthase/phosphatase	1.34	0.09

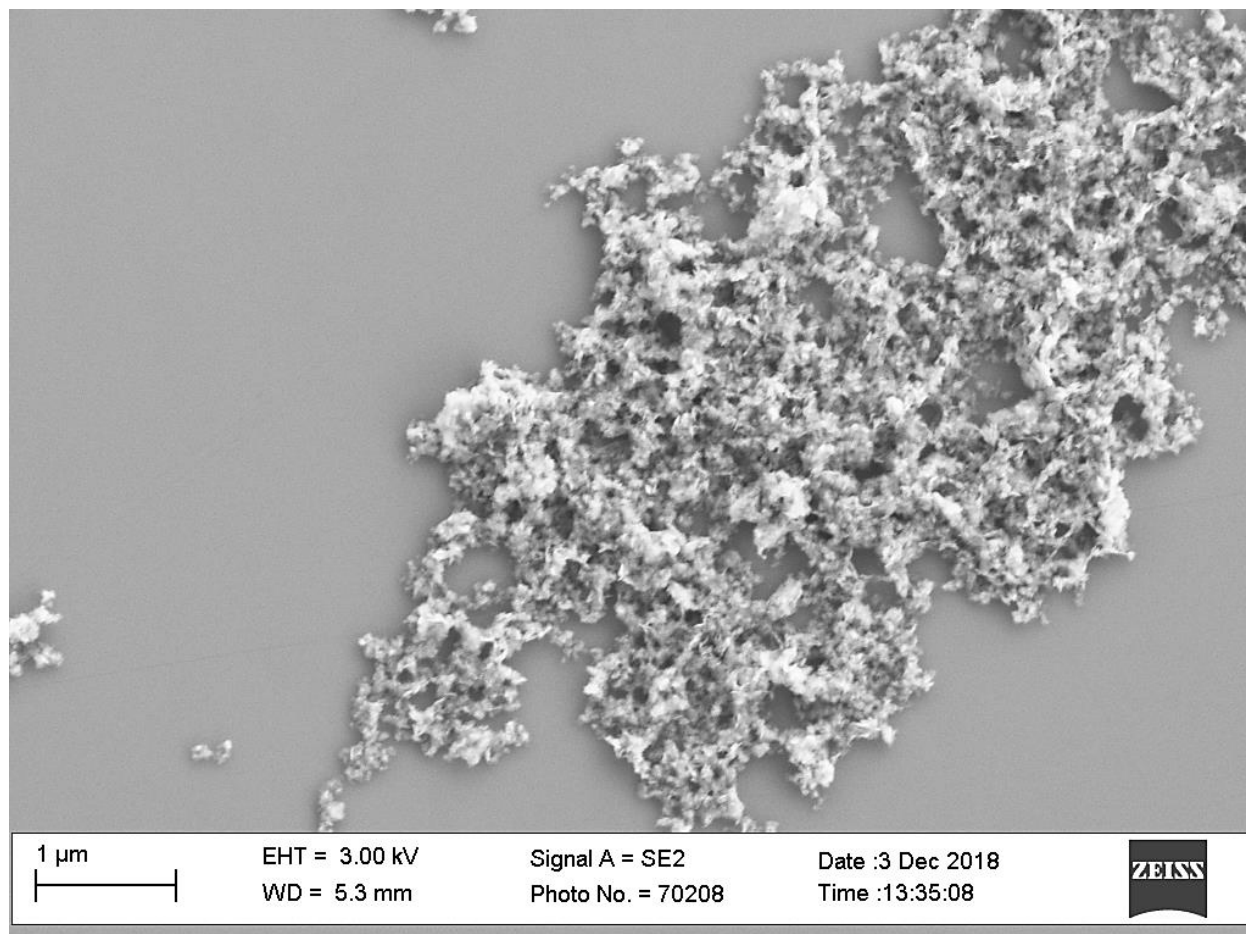
#### Galactose metabolism

C00089		Sucrose	1.51	0.08
C00243		Lactose	1.51	0.08
C00492		Raffinose	1.03	0.01
C01235		Galactinol	1.51	0.08
C05400		Epimelibiose	1.51	0.08
C05402		Melibiose	1.51	0.08
C05404		Manninotriose	1.03	0.01
K00011	AKR1B	aldehyde reductase	-1.30	0.02
K00850	pfkA	6-phosphofructokinase 1	2.50	0.0001
K01084	G6PC	glucose-6-phosphatase	-2.40	0.001
K01187	malZ	alpha-glucosidase	1.59	0.01
K01785	galM	aldose 1-epimerase	2.56	5.2E-10
K01835	pgm	phosphoglucomutase	-1.28	0.07

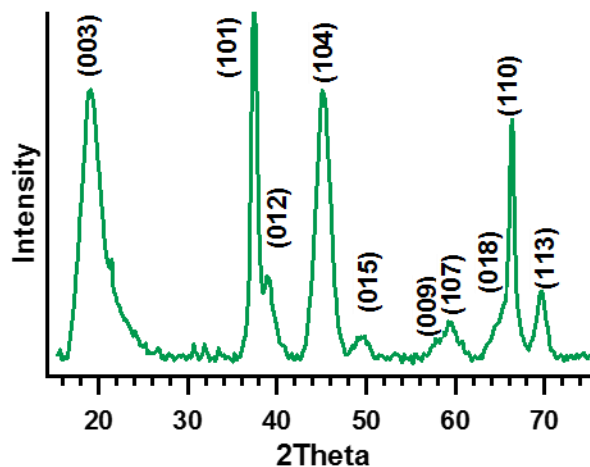
## Supporting Figures



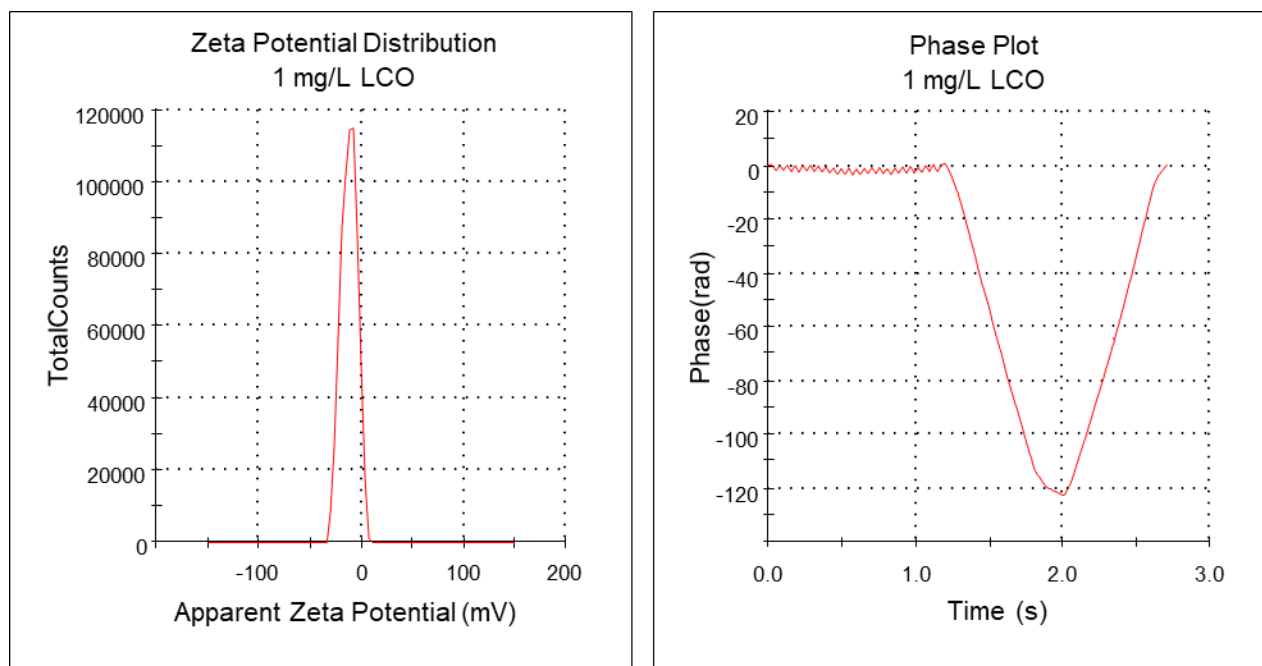
**Supplementary Figure S1. Calibration data for ICP-OES.** Calibration data for inductively coupled plasma - optical emission spectroscopy used to calculate LCO lithiation. Reprinted with permission from (Niemuth, N. J.; Zhang, Y.; Mohaimani, A. A.; Schmoldt, A.; Laudadio, E. D.; Hamers, R. J.; Klaper, R. D. Protein Fe–S Centers as a Molecular Target of Toxicity of a Complex Transition Metal Oxide Nanomaterial with Downstream Impacts on Metabolism and Growth. *Environ. Sci. Technol.* **2020**, *54* (23), 15257–15266). Copyright (2020) American Chemical Society.



**Supplementary Figure S2. SEM of LCO nanosheets.** Scanning electron micrograph of LCO nanosheets. Reprinted with permission from (Niemuth, N. J.; Zhang, Y.; Mohaimani, A. A.; Schmoldt, A.; Laudadio, E. D.; Hamers, R. J.; Klaper, R. D. Protein Fe–S Centers as a Molecular Target of Toxicity of a Complex Transition Metal Oxide Nanomaterial with Downstream Impacts on Metabolism and Growth. *Environ. Sci. Technol.* **2020**, *54* (23), 15257–15266). Copyright (2020) American Chemical Society.



**Supplementary Figure S3. XRD of LCO nanosheets.** Powder X-Ray Diffraction spectra of LCO nanosheets. Peak indices are indicated above each reflection. Reprinted with permission from (Niemuth, N. J.; Zhang, Y.; Mohaimani, A. A.; Schmoldt, A.; Laudadio, E. D.; Hamers, R. J.; Klaper, R. D. Protein Fe–S Centers as a Molecular Target of Toxicity of a Complex Transition Metal Oxide Nanomaterial with Downstream Impacts on Metabolism and Growth. *Environ. Sci. Technol.* **2020**, *54* (23), 15257–15266). Copyright (2020) American Chemical Society.



**Supplementary Figure S4. Zeta potential quality data.** Count and phase data for zeta potential data from instrument quality report. Reprinted (adapted) with permission from (Niemuth, N. J.; Zhang, Y.; Mohaimani, A. A.; Schmoltdt, A.; Laudadio, E. D.; Hamers, R. J.; Klaper, R. D. Protein Fe–S Centers as a Molecular Target of Toxicity of a Complex Transition Metal Oxide Nanomaterial with Downstream Impacts on Metabolism and Growth. *Environ. Sci. Technol.* **2020**, *54* (23), 15257–15266). Copyright (2020) American Chemical Society.

## CHAPTER V: DISCUSSION AND CONCLUSION

The goals of this thesis were to advance the field of nanotoxicology by exploring mechanisms of nanotoxicity at the molecular level beyond the simplistic paradigm of oxidative stress, to expand the scope of engineered nanomaterials (ENMs) investigated by studying impacts of the next-generation lithium-ion battery (LIB) cathode material lithium cobalt oxide (LCO), and to include impacts of ENMs on a sediment-dwelling model organism. To accomplish this, three aims were set out: Aim 1, test the hypothesis that settled LCO negatively impacts sediment-dwelling organism *Chironomus riparius* (Chapter II); Aim 2, test the hypothesis that LCO disrupts *C. riparius* Fe-S centers, causing negative impacts on metabolism (Chapter III); and Aim 3, test the hypothesis that metabolic impacts of LCO are conserved across species and observable by metabolomics (Chapter IV). In addressing these hypotheses, these three chapters developed a body of evidence that can be used to establish mechanisms of LCO toxicity within the adverse outcome pathway (AOP) framework: observing adverse outcomes (AOs) of LCO toxicity, establishing a series of key events (KEs) underlying these observations, and uncovering a molecular initiating event (MIE) related to observed KEs. By establishing this framework of understanding of LCO toxicity, this work demonstrates the possibility of providing a molecular-level understanding of ENM toxicity and provides evidence for a mechanism likely conserved across species and metal oxide ENMs.

## **Evidence of LCO nanotoxicity and development of an AOP**

Chapter II established that LCO and alternative LIB cathode material NMC cause significant, 30% reductions in *C. riparius* larval size at 10 mg/L and 60% declines in size at 100 mg/L exposure after 7 d (Fig II-1 panels a, c, and e; p. 58). Time to emergence as adult flies was also significantly delayed by LCO and NMC exposure, by 7 d for LCO 10 mg/L and NMC 100 mg/L exposures, with LCO 100 mg/L exposed animals failing to reach adult stage after 25 d (Fig II-2 panel a; p. 59). These impacts were specific to the nano forms of LCO and NMC, as impacts on size and adult development were not recapitulated by released ion controls (Fig II-1 panels b, d, f; Fig II-2 panel b; pp. 58-59), and metal doping of sediments in the literature at concentrations equivalent to the metal contained in these particles did not cause impacts on chironomids comparable to LCO and NMC exposures.<sup>1,2</sup> Within the AOP framework, these impacts on growth and development are considered AOs, the ultimate end result of molecular changes stemming from the initial ENM impact.<sup>3</sup>

Chapter II also established that LCO and NMC significantly, negatively impact levels of hemoglobin (Hb) in larvae at 10 and 100 mg/L exposure concentrations after 7 d (Fig II-1 panel g; p. 58). It was also observed that a 100 mg/L exposure of LCO or NMC negatively impacted expression of the heme synthesis gene *porphobilinogen synthase* (*PBGS*; Fig II-3 panel f; p. 60). Heme is an iron-containing porphyrin cofactor required for the function of numerous enzymes,<sup>4</sup> including electron transfer by electron transport chain (ETC) protein cytochrome c as well as for binding of O<sub>2</sub> by Hb, which allows Hb to transport O<sub>2</sub> to metabolically active cells where O<sub>2</sub> acts as the terminal electron acceptor of the ETC.<sup>5-8</sup> Impacts on heme would be expected to negatively impact function of the ETC, and thus energy metabolism across all species that rely

on oxidative phosphorylation for adenosine triphosphate (ATP) production, due to heme's critical role in Hb and cytochrome c.<sup>9</sup> Indeed, exposure of chironomids to heme inhibitor carbon monoxide was shown to negatively impact chironomid energy metabolism.<sup>10</sup> In the AOP framework, observed changes in Hb levels and *PBGS* expression would be identified as KEs.

Reduction of *PBGS* gene expression suggested that reduced Hb levels in *C. riparius* larvae could be the result of impacts of LCO and NMC on heme synthesis at the level of regulation of gene expression. The conserved mechanism for regulation of heme synthesis and iron homeostasis more broadly across species is through the iron-responsive protein (IRP1), whose regulatory Fe-S center determines its mRNA binding status and thus levels of expression of genes involved in the uptake and utilization of Fe.<sup>11-14</sup> Degradation of this Fe-S center signals that Fe levels are depleted, turning off expression of pathways that utilize Fe, such as heme synthesis, and increasing expression of iron uptake genes.<sup>11-14</sup> The Fe-S center of IRP1 also allows it to act as an aconitase (ACO1), converting citrate to isocitrate in the tricarboxylic acid (TCA) cycle, making IRP1/ACO1 a key enzyme for energy metabolism.<sup>15</sup> The [4Fe-4S]<sup>2+</sup> center of IRP1/ACO1 is also sensitive to oxidation, being converted to an inactive [3Fe-4S]<sup>1+</sup> center.<sup>16</sup> Thus, if impacts on IRP1/ACO1 were indeed responsible for observed impacts of LCO and NMC on Hb levels and *PBGS* expression, this likely would be the result of oxidation of its Fe-S center.

Oxidation of this Fe-S center would represent an MIE in the AOP framework. Moreover, these impacts would be expected to cause downstream changes in KEs related to energy metabolism because of the central role of IRP1/ACO1 in regulating both the levels of heme necessary for

activity of Hb and cytochrome c—critical to functioning of the ETC—and its possessing aconitase enzymatic activity required for functioning of the TCA cycle.<sup>11–15</sup> This understanding led to the hypothesis that LCO would cause negative impacts on the aconitase Fe-S center that would be observable in exposed larvae, and that energy metabolism would be impacted by LCO exposure, explored in Chapter III.

Chapter III demonstrated negative impacts of LCO exposure on the functioning and oxidation status of the aconitase Fe-S center of *C. riparius* larvae. Aconitase activity of larvae exposed to LCO at 10 mg/L for 48 hr was significantly lower than MHRW controls (Fig III-2; p. 114). Moreover, as the oxidized aconitase  $[3\text{Fe-4S}]^{1+}$  center is visible by electron paramagnetic resonance (EPR),<sup>16</sup> it was demonstrated that LCO exposure causes significant oxidation of the aconitase Fe-S center in *C. riparius* larvae at 10 mg/L after 7 d (Fig III-1 panel b; p. 113). These results support oxidation of the aconitase Fe-S center as an MIE for LCO toxicity.

Examination of global gene expression by RNA-seq in LCO-exposed *C. riparius* larvae confirms downstream changes in expression of genes related to metabolism (156 genes), Fe and Fe ion binding (33 genes), and 4Fe-4S binding (10 genes; Fig III-3; p. 115) after 48 hr at 10 mg/L. Upregulated genes related to energy metabolism included components of the ETC (17 genes; Fig III-4; p. 116) and TCA cycle (7 genes; Fig III-4; p. 116), including 12 subunits of NADH dehydrogenase (ETC Complex I) and 3 components of succinate dehydrogenase (TCA cycle and ETC Complex II). ETC Complexes I and II are also Fe-S enzymes, and the levels of the Fe-S centers of these upregulated complexes were significantly increased by LCO exposure, as seen by EPR (Fig III-1 panel c; p. 113). These results indicate an increase in levels of components of

the ETC in response to LCO exposure, perhaps as compensation for negative impacts of LCO on energy production resulting from aconitase inhibition. Gene expression analysis also showed significant changes in genes related to carbohydrate metabolism (37 genes), downregulation of genes related to lipid metabolism (9 genes), changes in synthesis and degradation of amino acids (43 genes), and downregulation of protein synthesis genes (106 genes; Fig III-4, Supplementary Fig III-S6; pp. 116 & 159) that suggest a reorganization of metabolism to reduce energy utilization and storage processes such as protein, amino acid, and lipid syntheses and increase energy generating processes including breaking down amino acids and sugars. Overall, gene expression changes indicate a response to energy starvation as a KE in LCO nanotoxicity, increasing energy generating processes of carbohydrate metabolism, amino acid degradation, the TCA cycle and the ETC, while decreasing energy utilizing processes of lipid and protein syntheses.

Thus, Chapter III establishes oxidation of the aconitase Fe-S center as an MIE for LCO exposure in *C. riparius* by EPR and enzyme activity assay. It also uses global gene expression data to provide evidence for KEs from LCO exposure related to changes in metabolism suggestive of a response to energy starvation. Within an AOP framework, this MIE and these resulting KEs can explain the AOs of reduced growth and development observed in Chapter II. An AOP summarizing these results is laid out in Figure III-5 (p. 117).

Chapter IV builds upon these results to establish if these KEs are conserved for LCO across species and if evidence for these impacts exist at the metabolite level by using RNA-seq and metabolomics to examine LCO impacts in *Daphnia magna*. Global gene expression results for

*D. magna* exposed to LCO at 1 mg/L for 48 hr confirms a response similar to that seen in *C. riparius* larvae, with significant changes in genes related to the cellular response to starvation, mitochondrial function, ATP-binding, oxidative phosphorylation, NADH dehydrogenase activity, and protein biosynthesis (Table IV-1; p. 195). Changes in expression were observed for 53 genes in the ETC, including upregulation of 20 components of Complex I (NADH dehydrogenase) as well as components of other ETC complexes (Fig IV-1; p. 199). These results accord with changes in ETC gene expression observed in *C. riparius* larvae in response to LCO exposure (Chapter III; Fig III-4; p. 116), demonstrating the conservation of these KEs across species. Chapter IV, however, goes further by integrating RNA-seq results with results from non-targeted metabolomics. Metabolomics reveals that breakdown of amino acids and changes in sugar metabolism are important for the response of *D. magna* to LCO exposure (Table IV-2; p. 196), changes also evident in expression of genes related to amino acid and carbon metabolism by RNA-seq (Table IV-1; p. 195). By combining RNA-seq and metabolomics results in *D. magna*, changes in pathways can be seen at both the level of specific metabolites such as amino acids and their breakdown products and at the level of expression of genes involved in these pathways. This is illustrated for the valine, leucine, and isoleucine degradation pathway in Figure IV-2 (p. 201), showing reductions in concentrations of the amino acid metabolites, increases in levels of their breakdown metabolites, and increases in expression of enzymes that degrade these metabolites. Such impacts are also evident at the gene expression and metabolite levels for breakdown of other amino acids such as tryptophan (Supplementary Table IV-S2; p. 205). Thus, combined RNA-seq and metabolomics provides evidence that amino acid degradation pathways are indeed active at this 48 hr time point in response to 1 mg/L LCO exposure in *D. magna*, breaking down amino acids to produce acetyl-CoA to feed into the TCA cycle. In this way, the

KE of reduced protein synthesis and increased amino acid degradation suggested by RNA-seq results in *C. riparius* larvae in Chapter III (Fig III-4 and Supplementary Fig S6; pp. 116 & 159) is confirmed concretely in *D. magna*.

Taken together, these results support an AOP for LCO in which the MIE of oxidation of the aconitase Fe-S center by LCO results in KEs of negative impacts on heme synthesis and TCA cycle activity, with subsequent KEs of disrupted energy metabolism, and ultimate AOs of reduced growth and development. By establishing an AOP for LCO nanotoxicity through this series of molecular-level investigations, this work provides a paradigm for the field of nanotoxicology to move it in the direction of a mechanistic understanding of ENM-biological interactions beyond oxidative stress. However, while this evidence is sufficient to provide a complete AOP for LCO, it does not in itself address the specific mechanism by which LCO can oxidize the aconitase Fe-S center. Addressing the specifics of this mechanism with evidence from the literature makes clear that this proposed AOP has implications across species for many metal oxide ENMs.

### **Proposed mechanism and implications for AOP across metal oxide ENMs**

The evidence from this thesis demonstrates the impact of LCO on energy metabolism—specifically Complex I (NADH dehydrogenase) upregulation, ETC component upregulation, protein synthesis downregulation, and amino acid breakdown—in both *C. riparius* and *D. magna*. In the literature, impacts on NADH dehydrogenase activity and ATP production have been demonstrated for a suite of metal oxide ENMs in mammalian cells,<sup>17</sup> suggesting that impacts on energy metabolism may apply broadly to metal oxide ENMs. This study of cellular

impacts of metal oxide ENMs also demonstrated that metal oxide ENM toxicity could be predicted based upon the overlap of conduction band of the ENM with the physiological redox potential of biological systems.<sup>17</sup> While this study attributes these impacts to generic oxidative stress,<sup>17</sup> the implication of this finding is that metal oxide ENM toxicity could be the result of these materials coupling with and disrupting physiological redox processes. Redox processes in this range are involved in the TCA cycle and ETC, including for aconitase activity and for transfer of electrons to and from ETC complexes.<sup>15,18–20</sup> Thus, redox chemistry of metal oxide ENMs could indicate more than just generation of damaging ROS, but specific impacts on biological redox processes, either directly at the ENM surface or through an ROS intermediate.

A specific AOP for LCO and other metal oxide ENMs can be proposed based on the literature and results from this thesis. In this AOP, the mechanism behind the initial MIE is redox chemistry by metal oxide ENMs—due to overlap between their conduction band and the physiological redox potential, either by allowing redox chemistry at the ENM surface<sup>17</sup> or by the creation of ROS<sup>21,22</sup>—that oxidize redox-sensitive components in the TCA cycle and ETC, observed for the aconitase Fe-S center of *C. riparius* from LCO in this thesis (Figure III-1) and for cytochrome c from a suite of metal oxide ENMs *in vitro*.<sup>17</sup> Oxidation of these components then leads to KEs of reduced metabolic enzyme activity, observed as reduced activity of aconitase in *C. riparius* from LCO (Figure III-2) and in fish liver tissue from ZnO<sup>23</sup> as well as reduced NADH dehydrogenase activity in cells exposed to a number of metal oxide ENMs (Co<sub>3</sub>O<sub>4</sub>, Cr<sub>2</sub>O<sub>3</sub>, Ni<sub>2</sub>O<sub>3</sub>, CuO, Mn<sub>2</sub>O<sub>3</sub>, CoO, ZnO, TiO<sub>2</sub>).<sup>17,21</sup> Oxidation of the aconitase Fe-S center also leads to the KE of dysregulation of heme and iron homeostasis, seen for LCO exposure in *C. riparius* (Figure II-3; Figure III-3). These changes in enzyme and regulatory

activity lead to KEs of alterations in metabolism: seen as lower hemoglobin levels from LCO in *C. riparius* (Figure II-1); lower levels of amino acids and increased sugars from LCO exposure in *D. magna* (Tables IV-2 and IV-3); decreased TCA cycle metabolites from ZnO exposure in rat kidneys<sup>25</sup> and TiO<sub>2</sub> exposure in *C. elegans*;<sup>26</sup> increased TCA cycle and ETC gene expression from LCO exposure in *C. riparius* (Figures III-3 and III-4), *D. magna* (Figure IV-2, Table IV-1), and trout gill cells;<sup>28</sup> enrichment for ETC genes from TiO<sub>2</sub> exposure in human lung cells;<sup>21</sup> increased expression of ETC proteins from ZnO, TiO<sub>2</sub>, and CuO exposure in mouse liver cells;<sup>29</sup> and reduced ATP production in mammalian cells exposed to Co<sub>3</sub>O<sub>4</sub>, Cr<sub>2</sub>O<sub>3</sub>, Ni<sub>2</sub>O<sub>3</sub>, CuO, Mn<sub>2</sub>O<sub>3</sub>, CoO, and ZnO ENMs.<sup>17</sup> These KEs lead to AOs of reduced growth and development observed for *C. riparius* (Figures II-1 and II-2) and reduced growth and reproduction for *D. magna* exposed to LCO and NMC.<sup>30</sup>

Thus, oxidation of redox-sensitive biological components as a result of metal oxide ENM redox chemistry (the MIE) leads to disruptions of heme and energy metabolism (KEs), which negatively impact growth, development, and reproduction (the AOs). The conservation of the impacted components of heme and energy metabolism across species<sup>18–20,31</sup> and the impacts on these processes observed for multiple metal oxide ENMs in varied biological systems from cells to vertebrates<sup>17,21,23–30</sup> indicates that this AOP is likely applicable for many metal oxide ENMs across species.

### **Environmental implications of proposed AOP**

From the standpoint of sustainability of ENMs and their environmental impacts, understanding the molecular mechanisms of ENM toxicity, and thus the fundamental relationship between

ENM properties and toxicity, allows a correct assessment of the potential impacts of ENM waste. From this environmental standpoint, the potential for impacts on the entire web of life resulting from the proposed AOP for metal oxide ENMs—since species from bacteria to invertebrates, plants, and vertebrate animals all rely on oxidative phosphorylation and redox processes for energy—are evident.<sup>18–20,31</sup> An important environmental consideration is that the conservation of this AOP for metal oxide ENMs, including for metal oxide ENMs produced in high volumes—and with correspondingly high volumes of waste—such as TiO<sub>2</sub>, ZnO, and LCO, means that the environmental impact of metal oxide ENMs could be additive across metal oxide ENMs. The tens of thousands of tons of metal oxide ENM waste reaching the environment annually<sup>32</sup> could thus be anticipated to collectively impact energy metabolism throughout the ecosystem.

In the aquatic environment, this impact may be particularly magnified for sediments of lake systems, as 98% or more of input ENMs are expected to be retained in sediments due to settling.<sup>33</sup> Even small inputs, detectable in the range of tens of ng/L in surface waters, can be anticipated to accumulate in surface sediments at concentrations in the range on tens of μg/cm<sup>2</sup>.<sup>24</sup> Such concentrations correspond to the settled portion of the 10 mg/L LCO exposures observed to impact the aconitase Fe-S center, metabolism, Hb levels, and growth and development of *C. riparius* in this thesis (Chapters II and III).<sup>24</sup> Another metal oxide ENM produced in high volumes and observed to impact oxidative phosphorylation in cells, TiO<sub>2</sub>,<sup>21</sup> was observed in the surface water of a European lake at 1.4 μg/L.<sup>34</sup> Thus, metal oxide ENM waste represents a clear environmental concern.

## Future directions

The details and universal applicability of the proposed AOP for metal oxide ENMs should be further investigated in a number of ways. A first step would be to investigate the impacts of LCO and other metal oxide ENMs on heme and energy metabolism specifically across species, including vertebrate organisms (*e.g.*, fish and mice). An interesting comparison would be to determine if species capable of anaerobic metabolism (*e.g.*, yeast and bacteria) have mechanisms to cope with metal oxide ENMs that multicellular eukaryotes do not, as anaerobes can survive without using oxidative phosphorylation to generate ATP (although electron transfer is still required for energy generation by anaerobic processes).<sup>35-37</sup>

It would also be useful to validate that other metal oxide ENMs can impact Fe-S centers and that these impacts hold across species for this highly conserved class of electron transferring cofactors. This could be accomplished by activity assays and EPR in whole, small organisms (*e.g.*, bacteria, yeast, invertebrates) or in tissues isolated from larger animals (*e.g.*, fish or mammals).<sup>16,38</sup>

It would be informative as to the extent to which redox-active components of energy metabolism are sensitive to oxidation by LCO and other metal oxide ENMs to test their impacts on isolated, redox-sensitive components of the TCA cycle and ETC. Examples of isolated components that could be tested for redox interactions with metal oxide ENMs include: purified Fe-S proteins or synthetic Fe-S clusters;<sup>39-42</sup> small molecules that shuttle electrons between the TCA cycle and the ETC (*i.e.*, NADH and succinate);<sup>43,44</sup> small molecules in Complexes I and II that facilitate electron transfer from NADH and succinate to Complex I and II (FMN and FAD,

respectively);<sup>45,46</sup> cofactors that shuttle electrons between Complexes I and II and Complexes III and IV (ubiquinone and cytochrome c);<sup>17,47</sup> and isolated whole ETC complexes (Complexes I, II, III, and IV).<sup>48</sup> It would also be informative to test impacts on isolated mitochondria, by monitoring ATP production, for example.<sup>49,50</sup>

From a chemistry perspective, an interesting aspect of this interaction to explore is if the overlap of the conduction band of metal oxide ENMs with the biological redox potential is the only property that facilitates redox interactions with biological components or if other processes, such as redox mediated metal release,<sup>51</sup> also contribute to these redox interactions or even dominate for specific metal oxide ENMs.<sup>17</sup> It also remains to be determined if observed oxidation of components such as cytochrome c or the aconitase Fe-S by metal oxide ENMs is the result of ROS intermediates or if redox chemistry can occur directly at the particle surface. ROS have been detected in cells following metal oxide ENM exposure using redox sensitive dyes, including from LCO and TiO<sub>2</sub>.<sup>21,22</sup> Interestingly, increased superoxide levels observed in cells exposed to Co<sub>3</sub>O<sub>4</sub>, Cr<sub>2</sub>O<sub>4</sub>, Ni<sub>2</sub>O<sub>3</sub>, CuO, Mn<sub>2</sub>O<sub>3</sub>, CoO, and ZnO ENMs were localized to the mitochondria,<sup>17</sup> suggesting that interaction of metal oxide ENMs to generate ROS in cells involves specific substrates localized to the mitochondria, where the TCA cycle, ETC, and their associated redox components are located.<sup>20</sup> If this is true, this suggests direct interaction between metal oxide ENMs and redox-active components in the mitochondria to transfer electrons from reducing molecules to O<sub>2</sub> to generate superoxide.

Thus, numerous avenues of investigation exist to determine more concretely the applicability and mechanistic details of redox-mediated impacts of metal oxide ENMs on conserved components

of energy metabolism. Further insights into the mechanisms of metal oxide ENM toxicity will provide necessary understanding of the biological impacts of this commercially and environmentally important class of ENMs.

## **Conclusion**

By using molecular tools to investigate the toxicity of LIB cathode material LCO, this thesis has demonstrated the possibility of investigating mechanisms of nanotoxicity for ENMs at a mechanistic level, beyond simple oxidative stress, and informing an AOP from molecular initiating event, through key events, to adverse outcomes. This molecular approach to nanotoxicology, with the AOP framework as a guide, is broadly applicable to all ENMs and model systems. This approach should be applied in further studies to explore new mechanisms of nanotoxicology at the molecular level for first-generation and next-generation ENMs across model systems of human and environmental health. In this way, the tools, strategies, and concepts employed in this thesis can provide a paradigm to inform the future of nanotoxicology.

## References

- (1) Milani, D.; Reynoldson, T. B.; Borgmann, U.; Kolasa, J. The Relative Sensitivity of Four Benthic Invertebrates to Metals in Spiked-Sediment Exposures and Application to Contaminated Field Sediment. In *Environmental Toxicology and Chemistry*; John Wiley & Sons, Ltd, 2003; Vol. 22, pp 845–854. [https://doi.org/10.1897/1551-5028\(2003\)022<0845:TRSOFB>2.0.CO;2](https://doi.org/10.1897/1551-5028(2003)022<0845:TRSOFB>2.0.CO;2).
- (2) Besser, J. M.; Brumbaugh, W. G.; Ingersoll, C. G.; Ivey, C. D.; Kunz, J. L.; Kemble, N. E.; Schlekot, C. E.; Garman, E. R. Chronic Toxicity of Nickel-Spiked Freshwater Sediments: Variation in Toxicity among Eight Invertebrate Taxa and Eight Sediments. *Environ. Toxicol. Chem.* **2013**, *32* (11), n/a-n/a. <https://doi.org/10.1002/etc.2271>.
- (3) Gerloff, K.; Landesmann, B.; Worth, A.; Munn, S.; Palosaari, T.; Whelan, M. The Adverse Outcome Pathway Approach in Nanotoxicology. *Comput. Toxicol.* **2017**, *1*, 3–11. <https://doi.org/10.1016/J.COMTOX.2016.07.001>.
- (4) A. Shelnut, J.; Song, X.-Z.; Ma, J.-G.; Jia, S.-L.; Jentzen, W.; J. Medforth, C.; J. Medforth, C. Nonplanar Porphyrins and Their Significance in Proteins. *Chem. Soc. Rev.* **1998**, *27* (1), 31. <https://doi.org/10.1039/a827031z>.
- (5) Bareth, B.; Dennerlein, S.; Mick, D. U.; Nikolov, M.; Urlaub, H.; Rehling, P. The Heme a Synthase Cox15 Associates with Cytochrome c Oxidase Assembly Intermediates during Cox1 Maturation. *Mol. Cell. Biol.* **2013**, *33* (20), 4128–4137. <https://doi.org/10.1128/MCB.00747-13>.
- (6) Osmulski, P.; Leyko, W. Structure, Function and Physiological Role of Chironomus Haemoglobin. *Comp. Biochem. Physiol. Part B Comp. Biochem.* **1986**, *85* (4), 701–722. [https://doi.org/10.1016/0305-0491\(86\)90166-5](https://doi.org/10.1016/0305-0491(86)90166-5).

- (7) Mangum, C. P. Oxygen Transport in Invertebrates. *Am. J. Physiol. Integr. Comp. Physiol.* **1985**, 248 (5), R505–R514. <https://doi.org/10.1152/ajpregu.1985.248.5.R505>.
- (8) Dunn, J.-O.; Mythen, M.; Grocott, M. Physiology of Oxygen Transport. *BJA Educ.* **2016**, 16 (10), 341–348. <https://doi.org/10.1093/bjaed/mkw012>.
- (9) Queiroga, C. S. F.; Almeida, A. S.; Vieira, H. L. A. Carbon Monoxide Targeting Mitochondria. *Biochem. Res. Int.* **2012**, 2012, 1–9. <https://doi.org/10.1155/2012/749845>.
- (10) Walshe, B. Y. B. M. The Function of Haemoglobin in Tanytarsus (Chironomidae). *J. Exp. Biol.* **1947**, 24 (3–4), 343–351.
- (11) Beinert, H. Iron-Sulfur Proteins: Ancient Structures, Still Full of Surprises. *Journal of Biological Inorganic Chemistry*. Springer-Verlag February 2000, pp 2–15. <https://doi.org/10.1007/s007750050002>.
- (12) Castello, A.; Hentze, M. W.; Preiss, T. Metabolic Enzymes Enjoying New Partnerships as RNA-Binding Proteins. *Trends Endocrinol. Metab.* **2015**, 26 (12), 746–757. <https://doi.org/10.1016/j.tem.2015.09.012>.
- (13) Resch, V.; Hanefeld, U. The Selective Addition of Water. *Catal. Sci. Technol.* **2015**, 5 (3), 1385–1399. <https://doi.org/10.1039/C4CY00692E>.
- (14) Tong, J.; Feinberg, B. A. Direct Square-Wave Voltammetry of Superoxidized [4Fe-4S]<sup>3+</sup> Aconitase and Associated 3Fe/4Fe Cluster Interconversions. *J. Biol. Chem.* **1994**, 269 (40), 24920–24927.
- (15) Armstrong, J. S.; Whiteman, M.; Yang, H.; Jones, D. P. The Redox Regulation of Intermediary Metabolism by a Superoxide-Aconitase Rheostat. *BioEssays* **2004**, 26 (8), 894–900. <https://doi.org/10.1002/bies.20071>.
- (16) Kalyanaraman, B.; Cheng, G.; Zielonka, J.; Bennett, B. Low-Temperature EPR

- Spectroscopy as a Probe-Free Technique for Monitoring Oxidants Formed in Tumor Cells and Tissues: Implications in Drug Resistance and OXPHOS-Targeted Therapies. *Cell Biochem. Biophys.* **2019**, *77* (1), 89–98. <https://doi.org/10.1007/s12013-018-0858-1>.
- (17) Zhang, H.; Ji, Z.; Xia, T.; Meng, H.; Low-Kam, C.; Liu, R.; Pokhrel, S.; Lin, S.; Wang, X.; Liao, Y.-P.; et al. Use of Metal Oxide Nanoparticle Band Gap To Develop a Predictive Paradigm for Oxidative Stress and Acute Pulmonary Inflammation. *ACS Nano* **2012**, *6* (5), 4349–4368. <https://doi.org/10.1021/nn3010087>.
- (18) Griffiths, H. R.; Gao, D.; Pararasa, C. Redox Regulation in Metabolic Programming and Inflammation. *Redox Biol.* **2017**, *12*, 50–57. <https://doi.org/10.1016/j.redox.2017.01.023>.
- (19) Chaban, Y.; Boekema, E. J.; Dudkina, N. V. Structures of Mitochondrial Oxidative Phosphorylation Supercomplexes and Mechanisms for Their Stabilisation. *Biochim. Biophys. Acta - Bioenerg.* **2014**, *1837* (4), 418–426. <https://doi.org/10.1016/j.bbabi.2013.10.004>.
- (20) Polyzos, A. A.; McMurray, C. T. The Chicken or the Egg: Mitochondrial Dysfunction as a Cause or Consequence of Toxicity in Huntington’s Disease. *Mech. Ageing Dev.* **2017**, *161*, 181–197. <https://doi.org/10.1016/j.mad.2016.09.003>.
- (21) Jayaram, D. T.; Kumar, A.; Kippner, L. E.; Ho, P.-Y.; Kemp, M. L.; Fan, Y.; Payne, C. K. TiO<sub>2</sub> Nanoparticles Generate Superoxide and Alter Gene Expression in Human Lung Cells. *RSC Adv.* **2019**, *9* (43), 25039–25047. <https://doi.org/10.1039/C9RA04037D>.
- (22) Melby, E. S.; Cui, Y.; Borgatta, J.; Mensch, A. C.; Hang, M. N.; Chrisler, W. B.; Dohnalkova, A.; Van Gilder, J. M.; Alvarez, C. M.; Smith, J. N.; et al. Impact of Lithiated Cobalt Oxide and Phosphate Nanoparticles on Rainbow Trout Gill Epithelial Cells. *Nanotoxicology* **2018**, *12* (10), 1166–1181.

- <https://doi.org/10.1080/17435390.2018.1508785>.
- (23) Dieni, C. A.; Callaghan, N. I.; Gormley, P. T.; Butler, K. M. A.; MacCormack, T. J. Physiological Hepatic Response to Zinc Oxide Nanoparticle Exposure in the White Sucker, *Catostomus Commersonii*. *Comp. Biochem. Physiol. Part C Toxicol. Pharmacol.* **2014**, *162*, 51–61. <https://doi.org/10.1016/j.cbpc.2014.03.009>.
- (24) Niemuth, N. J.; Curtis, B. J.; Hang, M. N.; Gallagher, M. J.; Fairbrother, D. H.; Hamers, R. J.; Klaper, R. D. Next-Generation Complex Metal Oxide Nanomaterials Negatively Impact Growth and Development in the Benthic Invertebrate *Chironomus Riparius* upon Settling. *Environ. Sci. Technol.* **2019**, *53* (7), 3860–3870. <https://doi.org/10.1021/acs.est.8b06804>.
- (25) Yan, G.; Huang, Y.; Bu, Q.; Lv, L.; Deng, P.; Zhou, J.; Wang, Y.; Yang, Y.; Liu, Q.; Cen, X.; et al. Zinc Oxide Nanoparticles Cause Nephrotoxicity and Kidney Metabolism Alterations in Rats. *J. Environ. Sci. Heal. Part A* **2012**, *47* (4), 577–588. <https://doi.org/10.1080/10934529.2012.650576>.
- (26) Ratnasekhar, C.; Sonane, M.; Satish, A.; Mudiam, M. K. R. Metabolomics Reveals the Perturbations in the Metabolome of *Caenorhabditis Elegans* Exposed to Titanium Dioxide Nanoparticles. *Nanotoxicology* **2015**, *9* (8), 994–1004. <https://doi.org/10.3109/17435390.2014.993345>.
- (27) Niemuth, N. J.; Zhang, Y.; Mohaimani, A. A.; Schmoldt, A.; Laudadio, E. D.; Hamers, R. J.; Klaper, R. D. Protein Fe–S Centers as a Molecular Target of Toxicity of a Complex Transition Metal Oxide Nanomaterial with Downstream Impacts on Metabolism and Growth. *Environ. Sci. Technol.* **2020**, *54* (23), 15257–15266. <https://doi.org/10.1021/acs.est.0c04779>.

- (28) Mensch, A. C.; Mitchell, H. D.; Markillie, L. M.; Laudadio, E. D.; Hedlund Orbeck, J. K.; Dohnalkova, A.; Schwartz, M. P.; Hamers, R. J.; Orr, G. Subtoxic Dose of Lithium Cobalt Oxide Nanosheets Impacts Critical Molecular Pathways in Trout Gill Epithelial Cells. *Environ. Sci. Nano* **2020**, *7* (11), 3419–3430. <https://doi.org/10.1039/D0EN00844C>.
- (29) Tedesco, S.; Bayat, N.; Danielsson, G.; Buque, X.; Aspichueta, P.; Fresnedo, O.; Cristobal, S. Proteomic and Lipidomic Analysis of Primary Mouse Hepatocytes Exposed to Metal and Metal Oxide Nanoparticles. *J. Integr. OMICS* **2015**, *5* (1). <https://doi.org/10.5584/jiomics.v5i1.184>.
- (30) Bozich, J.; Hang, M.; Hamers, R.; Klaper, R. Core Chemistry Influences the Toxicity of Multicomponent Metal Oxide Nanomaterials, Lithium Nickel Manganese Cobalt Oxide, and Lithium Cobalt Oxide to *Daphnia Magna*. *Environ. Toxicol. Chem.* **2017**, *36* (9), 2493–2502. <https://doi.org/10.1002/etc.3791>.
- (31) Peregrín-Alvarez, J. M.; Sanford, C.; Parkinson, J. The Conservation and Evolutionary Modularity of Metabolism. *Genome Biol.* **2009**, *10* (6), R63. <https://doi.org/10.1186/gb-2009-10-6-r63>.
- (32) Keller, A. A.; Lazareva, A. Predicted Releases of Engineered Nanomaterials: From Global to Regional to Local. *Environ. Sci. Technol. Lett.* **2014**, *1* (1), 65–70. <https://doi.org/10.1021/ez400106t>.
- (33) Koelmans, A. A.; Quik, J. T. K.; Velzeboer, I. Lake Retention of Manufactured Nanoparticles. *Environ. Pollut.* **2015**, *196*, 171–175. <https://doi.org/10.1016/j.envpol.2014.09.025>.
- (34) Gondikas, A. P.; Kammer, F. von der; Reed, R. B.; Wagner, S.; Ranville, J. F.; Hofmann, T. Release of TiO<sub>2</sub> Nanoparticles from Sunscreens into Surface Waters: A One-Year

- Survey at the Old Danube Recreational Lake. *Environ. Sci. Technol.* **2014**, *48* (10), 5415–5422. <https://doi.org/10.1021/es405596y>.
- (35) Podolsky, I. A.; Seppälä, S.; Lankiewicz, T. S.; Brown, J. L.; Swift, C. L.; O'Malley, M. A. Harnessing Nature's Anaerobes for Biotechnology and Bioprocessing. *Annu. Rev. Chem. Biomol. Eng.* **2019**, *10* (1), 105–128. <https://doi.org/10.1146/annurev-chembioeng-060718-030340>.
- (36) Ajay, C. M.; Mohan, S.; Dinesha, P.; Rosen, M. A. Review of Impact of Nanoparticle Additives on Anaerobic Digestion and Methane Generation. *Fuel* **2020**, *277*, 118234. <https://doi.org/10.1016/j.fuel.2020.118234>.
- (37) Leng, L.; Yang, P.; Singh, S.; Zhuang, H.; Xu, L.; Chen, W.-H.; Dolfing, J.; Li, D.; Zhang, Y.; Zeng, H.; et al. A Review on the Bioenergetics of Anaerobic Microbial Metabolism Close to the Thermodynamic Limits and Its Implications for Digestion Applications. *Bioresour. Technol.* **2018**, *247*, 1095–1106. <https://doi.org/10.1016/j.biortech.2017.09.103>.
- (38) Quirós, P. M. Determination of Aconitase Activity: A Substrate of the Mitochondrial Lon Protease; 2018; pp 49–56. [https://doi.org/10.1007/978-1-4939-7595-2\\_5](https://doi.org/10.1007/978-1-4939-7595-2_5).
- (39) Kennedy, M. C.; Antholine, W. E.; Beinert, H. An EPR Investigation of the Products of the Reaction of Cytosolic and Mitochondrial Aconitases with Nitric Oxide. *J. Biol. Chem.* **1997**, *272* (33), 20340–20347. <https://doi.org/10.1074/jbc.272.33.20340>.
- (40) Weigel, J. A.; Srivastava, K. K. P.; Day, E. P.; Munck, E.; Holm, R. H. Isonitrile Binding to a Site-Differentiated Synthetic Analog of Biological [4Fe-4S] Clusters: Equilibria, Magnetic Interactions, and the Spin-Isolated [3Fe-4S] Cluster Fragment, and the Structure of a Low-Spin Iron(II) Subsite. *J. Am. Chem. Soc.* **1990**, *112* (22), 8015–8023.

- <https://doi.org/10.1021/ja00178a026>.
- (41) Saouma, C. T.; Morris, W. D.; Darcy, J. W.; Mayer, J. M. Protonation and Proton-Coupled Electron Transfer at S-Ligated [4Fe-4S] Clusters. *Chem. - A Eur. J.* **2015**, *21* (25), 9256–9260. <https://doi.org/10.1002/chem.201500152>.
- (42) Henderson, R. A. Mechanistic Studies on Synthetic Fe–S-Based Clusters and Their Relevance to the Action of Nitrogenases. *Chem. Rev.* **2005**, *105* (6), 2365–2438. <https://doi.org/10.1021/cr030706m>.
- (43) Mayevsky, A.; Chance, B. Oxidation–Reduction States of NADH in Vivo: From Animals to Clinical Use. *Mitochondrion* **2007**, *7* (5), 330–339. <https://doi.org/10.1016/j.mito.2007.05.001>.
- (44) Khan, A.; Schofield, C. J.; Claridge, T. D. W. Reducing Agent-Mediated Nonenzymatic Conversion of 2-Oxoglutarate to Succinate: Implications for Oxygenase Assays. *ChemBioChem* **2020**, *21* (20), 2898–2902. <https://doi.org/10.1002/cbic.202000185>.
- (45) Miura, R. Versatility and Specificity in Flavoenzymes: Control Mechanisms of Flavin Reactivity. *Chem. Rec.* **2001**, *1* (3), 183–194. <https://doi.org/10.1002/tcr.1007>.
- (46) Li, H.; Das, A.; Sibhatu, H.; Jamal, J.; Sligar, S. G.; Poulos, T. L. Exploring the Electron Transfer Properties of Neuronal Nitric-Oxide Synthase by Reversal of the FMN Redox Potential. *J. Biol. Chem.* **2008**, *283* (50), 34762–34772. <https://doi.org/10.1074/jbc.M806949200>.
- (47) Yamamoto, Y.; Yamashita, S. Plasma Ratio of Ubiquinol and Ubiquinone as a Marker of Oxidative Stress. *Mol. Aspects Med.* **1997**, *18*, 79–84. [https://doi.org/10.1016/S0098-2997\(97\)00007-1](https://doi.org/10.1016/S0098-2997(97)00007-1).
- (48) Frazier, A. E.; Thorburn, D. R. Biochemical Analyses of the Electron Transport Chain

- Complexes by Spectrophotometry; 2012; pp 49–62. [https://doi.org/10.1007/978-1-61779-504-6\\_4](https://doi.org/10.1007/978-1-61779-504-6_4).
- (49) Drew, B.; Leeuwenburgh, C. Method for Measuring ATP Production in Isolated Mitochondria: ATP Production in Brain and Liver Mitochondria of Fischer-344 Rats with Age and Caloric Restriction. *Am. J. Physiol. Integr. Comp. Physiol.* **2003**, *285* (5), R1259–R1267. <https://doi.org/10.1152/ajpregu.00264.2003>.
- (50) Wibom, R.; Hagenfeldt, L.; von Döbeln, U. Measurement of ATP Production and Respiratory Chain Enzyme Activities in Mitochondria Isolated from Small Muscle Biopsy Samples. *Anal. Biochem.* **2002**, *311* (2), 139–151. [https://doi.org/10.1016/S0003-2697\(02\)00424-4](https://doi.org/10.1016/S0003-2697(02)00424-4).
- (51) Hamers, R. J. Energy Storage Materials as Emerging Nano-Contaminants. *Chem. Res. Toxicol.* **2020**, *acs.chemrestox.0c00080*. <https://doi.org/10.1021/acs.chemrestox.0c00080>.

**CHAPTER VI:**  
**CURRICULUM VITAE**  
**Nicholas Joseph Niemuth**

**Education** \_\_\_\_\_

*University of Wisconsin - Milwaukee*      Milwaukee, WI      Sept 2016 – Present

Doctoral candidate in Freshwater Sciences

Research Focus: Molecular mechanisms of nanotoxicity

Dissertation title: Investigating mechanisms of nanotoxicity of a next-generation lithium cobalt oxide nanomaterial

Anticipated graduation: Spring 2021

Cumulative GPA: 3.959

*University of Michigan*      Ann Arbor, MI      June 2009 – Dec 2011

Master of Science in Cellular and Molecular Biology

Research Focus: Regulation of aging

Graduation Date: December 2011

Cumulative GPA: 7.409 (3.809 equivalent)

*University of Wisconsin*      Madison, WI      Sept 2004 – May 2009

Bachelor of Science in Natural Sciences

Major: Biochemistry

Graduation Date: May 2009

Cumulative GPA: 3.622; Dean's list (all semesters)

## Research Experience

---

*UWM School of Freshwater Sciences*

Milwaukee, WI

Sept 2016 – Present

Graduate Researcher

- Investigating mechanisms of nanomaterial (NM) impacts on *C. elegans*, *D. magna*, and *C. riparius*
- *C. elegans*, *D. magna*, and *C. riparius* culture and exposure
- Confocal fluorescence microscopy to localize fluorescent NMs *in vivo*
- Determination of gene expression impacts by qPCR, RNA-Seq, and FISH
- Enzyme assays and electron paramagnetic resonance to probe mechanism of metal NM toxicity
- Metabolomic analysis of *D. magna*

*UWM School of Freshwater Sciences*

Milwaukee, WI

Nov 2012 – Aug 2016

Research Specialist and Lab Manager

- Investigation of effects of emerging contaminants on fathead minnow (*P. promelas*)
- *P. promelas* culture, exposure, dissection, and histology
- RNA extraction and determination of gene expression by qPCR
- ELISA determination of plasma analytes
- Coordination of lab safety and purchasing
- Supervision of graduate student research projects

***UM Dept of Cell and Mol Biology***

Ann Arbor, MI

Jun 2009 - Dec 2011

Graduate Researcher

- Mouse primary epithelial cell culture
- OxICAT differential thiol-trapping and protein mass spectrometric analysis in mice
- Determination of chemical effects on *C. elegans* lifespan
- Cloning and microinjection for expression of fluorescent redox sensors in *C. elegans*
- Generation of transgenic *C. elegans* lines
- Fluorescence imaging and quantitation of tissue-specific redox status in *C. elegans*

***UW Dept of Ophthalmology***

Madison, WI

Aug 2007- May 2009

Undergraduate Researcher

- Maintenance of mammalian cell-lines for experimental use
- Design of drugs for *in vitro* and *in vivo* experimentation
- Use of HPLC and pharmacokinetic assays to determine drug properties and function

### **Honors & Awards**

---

- Graduate Student Excellence Fellowship - 2018
- NSF Graduate Research Fellowship, Honorable Mention - 2017
- Distinguished Graduate Student Fellowship - 2016
- Biology of Aging Training Grant - 2011
- Rackham Graduate Student Research Grant - 2010
- Rackham Conference Travel Grant - 2010
- Cellular and Molecular Biology Training Grant - 2010

- Rackham Merit Fellowship - 2009
- Richard & Joan Hartl Family Foundation Scholarship - 2004, 2005, 2007, 2008
- William F. Vilas Grant - 2007, 2008

## **Publications**

---

- **Niemuth NJ**, Zhang Y, Mohaimani AA, Schmoldt S, Laudadio ED, Hamers RJ, Klaper RD. Protein Fe–S centers as a molecular target of toxicity of a complex transition metal oxide nanomaterial with downstream impacts on metabolism and growth. *Environ. Sci. Technol.*, (2020): <https://doi.org/10.1021/acs.est.0c04779>
- Jones ZR, **Niemuth NJ**, Robinson ME, Shenderova OA, Klaper RD, Hamers RJ. Selective imaging of diamond nanoparticles within complex matrices using magnetically induced fluorescence contrast. *Environ. Sci. Nano*, 7 (2020): 525-534.
- **Niemuth NJ**, Curtis BJ, Hang MN, Gallagher MJ, Fairbrother DH, Hamers RJ, Klaper RD. Next-generation complex metal oxide nanomaterials negatively impact growth and development in the benthic invertebrate *Chironomus riparius* upon settling. *Environ. Sci. Technol.*, 53 (2019): 3860-3870.
- **Niemuth NJ** and Klaper RD. Low-dose metformin exposure causes changes in expression of endocrine disruption-associated genes. *Aquatic Toxicology*, 195 (2018): 33-40.

- **Niemuth NJ**, Thompson AF, Crowe ME, Lieven CJ, Levin LA. Intracellular disulfide reduction by phosphine-borane complexes: Mechanism of action for neuroprotection. *Neurochem. Int.*, 99 (2016): 24-32.
- Klaper RD and **Niemuth NJ**. On the unexpected reproductive impacts of metformin: A need for support and new directions for the evaluation of the impacts of pharmaceuticals in the environment. *Chemosphere*, 165 (2016): 570-574.
- **Niemuth NJ** and Klaper RD. Emerging contaminant metformin causes intersex and reduced fecundity in fish. *Chemosphere*, 135 (2015): 38-45.
- **Niemuth NJ**, Jordan R, Crago J, Blanksma C, Johnson R, Klaper RD. Metformin exposure at environmentally relevant concentrations causes potential endocrine disruption in adult male fish. *Environ. Toxicol. Chem.*, 34 (2015): 291-296.
- Qiu TA, Bozich JS, Lohse SE, Vartanian AM, Jakob LM, Meyer BM, Gunsolus IL, **Niemuth NJ**, Murphy CJ, Haynes CL, Klaper RD. Gene expression as an indicator of the molecular response and toxicity in the bacterium *Shewanella oneidensis* and the water flea *Daphnia magna* exposed to functionalized gold nanoparticles. *Environ. Sci. Nano*, 6 (2015): 615-629.
- Knoefler D, Thamsen M, Koniczek M, **Niemuth NJ**, Diederich A, Jakob U. Quantitative In Vivo Redox Sensors Uncover Oxidative Stress as an Early Event in Life. *Molecular Cell*, 47 (2012): 767-776.

## Conference presentations

---

- **Niemuth NJ**, Zhang Y, Mohaimani AA, Schmoldt S, Laudadio ED, Hamers RJ, Klaper RD. Molecular-level insight into Adverse Outcome Pathway for complex metal oxide nanomaterial exposure using *Chironomus riparius*. Research Talk. 2020 Sustainable Nanotechnology Organization Conference. Online.
- **Niemuth NJ**, Zhang K, Curtis BJ, Laudadio L, Mohaimani A, Hamers RJ, Klaper RD. Aqueous instability of a complex metal oxide nanomaterial and adverse outcome pathway for its interaction with benthic organism *Chironomus riparius*. Poster. 2019 SETAC North America Meeting. Toronto, ON.
- **Niemuth NJ**, Williams D, Mensch A, Cui Y, Richardson M, Rosenzweig Z, Orr G, Klaper RD. Hydrophobic quantum dot toxicity is ligand-dependent in the nematode *C. elegans*. Poster. 2019 Gordon Research Conference. Newry, ME.
- **Niemuth NJ**, Williams D, Richardson M, Rosenzweig Z, Klaper RD. Comparison of toxicity of DHLA, TOPO, and oleic-acid coated quantum dots and their ligands in the nematode *C. elegans*. Poster. 2018 Sustainable Nanotechnology Organization Conference. Alexandria, VA.

- **Niemuth NJ**, Williams D, Richardson M, Rosenzweig Z, Klaper RD. Novel comparison of toxicity of hydrophobic and hydrophilic quantum dots and their ligands using *C. elegans*. Poster. 2017 Gordon Research Conference. Stowe, VT.
- **Niemuth NJ**, Hang M, Hamers RJ, Zhang X, Murphy C, Klaper RD. Exploring impacts of complex nanomaterials using the nematode *C. elegans*. Poster. 2016 SETAC National Conference. Orlando, FL.
- **Niemuth NJ** and Klaper RD. Impacts of wastewater contaminant metformin on the reproductive system of fathead minnows (*Pimephales promelas*). Research talk. 2015 SETAC National Conference. Salt Lake City, UT.
- **Niemuth NJ**, Jordan RR, Crago JP, Klaper RD. Low-level exposure of common wastewater pharmaceutical reveals potential endocrine disrupting effects in fathead minnows (*Pimephales promelas*). Research talk. 2014 Midwest SETAC Conference. Chicago, IL.
- **Niemuth NJ**, Miller R, Jakob U. Quantitative Redox Proteomics in Tissues of Long-lived Mice. Research talk. 2011 Anachem/SAS Symposium. Detroit, MI.
- **Niemuth NJ**, Knoefler D, Diederich A, Jakob U. Investigating Tissue-specific Levels of Reactive Oxygen Species in *C. elegans* Aging. Poster. 2010 *C. elegans* topic meeting: Aging, Metabolism, Pathogenesis, Stress, and Small RNAs. Madison, WI.

- **Niemuth NJ**, Lieven CJ, Levin LA. *In Vitro* Characterization of Novel Neuroprotective Phosphine-Borane Complexes. Poster. 2009 ARVO Conference. Fort Lauderdale, FL.

## **Presentations to community**

---

- Klaper RD and **Niemuth NJ**. Impacts of metformin on the Great Lakes ecosystem. WUWM Lake Effect interview. 7 May 2015.
- **Niemuth NJ**. The Science of Snow. Sustainable Nano blog. 4 March 2016.

## **Research Skills**

---

### ***Molecular Biology***

- |   |  |
|---|--|
| • Mammalian and bacterial cell culture      | • DNA & RNA extraction and purification      |
| • Sterile technique                         | • PCR, qPCR, RNA-Seq                         |
| • Western blot and ELISA                    | • DNA-PAGE                                   |
| • Fluorescence <i>in situ</i> hybridization | • Protein mass spectrometry                  |
| • Bacterial transformation                  | • Plasmid and primer design and construction |
| • Fluorescence microscopy                   | • Metabolomics                               |

### ***Biochemistry***

- |                          |                               |
|--------------------------|-------------------------------|
| • Enzyme activity assays | • Differential thiol labeling |
|--------------------------|-------------------------------|

### ***Chemistry***

- Accurate solution prep and dilution
- Spectrophotometry
- Nanoparticle handling & characterization
- Electron paramagnetic resonance
- HPLC

### ***Biology***

- *P. promelas* culture and dissection
- *C. riparius* culture
- *C. elegans* handling and transformation
- Histology

### ***Statistics and data analysis***

- Parametric and non-parametric statistics
- BLAST, KEGG, DAVID, PantherDB
- SPSS, Sigma plot, GraphPad

### ***Communication***

- Conference presentation: oral, poster
- Science blogging
- Scientific writing
- Community outreach and demonstration
- Zoom, Teams, WebEx, GoToMeeting

### **Professional association**

---

- NSF Center for Sustainable Nanotechnology
- Society of Environmental Toxicology and Chemistry
- Sustainable Nanotechnology Organization
- Society of Toxicology

- American Association of the Advancement of Science

## Community Involvement

---

*Center for Sustainable*

Online

Jun 2020 – Feb 2021

*Nanotechnology*

Student-Administration Liaison

*NanoDays at Science Museum of*

Minneapolis, MN

Jan 2020

*Minnesota*

Community science demonstration